

General Disclaimer

One or more of the Following Statements may affect this Document

- This document has been reproduced from the best copy furnished by the organizational source. It is being released in the interest of making available as much information as possible.
- This document may contain data, which exceeds the sheet parameters. It was furnished in this condition by the organizational source and is the best copy available.
- This document may contain tone-on-tone or color graphs, charts and/or pictures, which have been reproduced in black and white.
- This document is paginated as submitted by the original source.
- Portions of this document are not fully legible due to the historical nature of some of the material. However, it is the best reproduction available from the original submission.

DOE/NASA/3303-3
NASA CR-168109
M.I.T. ASRL TR 197-4

Simplified Aeroelastic Modeling of Horizontal Axis Wind Turbines

(NASA-CR-168109) SIMPLIFIED AEROELASTIC
MODELING OF HORIZONTAL AXIS WIND TURBINES
Final Report (Massachusetts Inst. of Tech.)
231 p HC A11/MP A01

CSSL 10A

M83-21509

G3/44 Unclass
03176

John H. Wendell
Massachusetts Institute of Technology

September 1982



Prepared for
NATIONAL AERONAUTICS AND SPACE ADMINISTRATION
Lewis Research Center
Under Grant NSG-3303

for
U.S. DEPARTMENT OF ENERGY
Conservation and Renewable Energy
Division of Photovoltaic Energy Technology

DOE/NASA/3303-3
NASA CR-168109
M.I.T. ASRL TR 197-4

Simplified Aeroelastic Modeling of Horizontal Axis Wind Turbines

John H. Wendell
Aeroelastic and Structures Research Laboratory
Massachusetts Institute of Technology
Cambridge, Massachusetts 02139

September 1982

Prepared for
National Aeronautics and Space Administration
Lewis Research Center
Cleveland, Ohio 44135
Under Grant NSG-3303

for
U.S. DEPARTMENT OF ENERGY
Conservation and Renewable Energy
Division of Photovoltaic Energy Technology
Washington, D.C. 20545
Under Interagency Agreement DE-AI01-76ET20320

FOREWORD

This work was carried out in the Aeroelastic and Structures Research Laboratory, M.I.T., and was supported by NASA Lewis Research Center under Grant No. NSG-3303, "Development of a Methodology for Horizontal Axis Wind Turbines Dynamic Analysis". The NASA Technical Officer for this work was David C. Janetzke, who also provided data from his own work for Chapter 13. The principal investigator for the grant was Professor John Dugundji,

The present document constitutes a Ph.D. thesis by the author. The author wishes to acknowledge helpful discussions with Professors John Dugundji, Rene H. Miller, Manuel Martinez-Sanchez and Norman D. Ham who served on his doctoral committee.

PRECEDING PAGE BLANK NOT FILMED

TABLE OF CONTENTS

Chapter 1.	INTRODUCTION	1
Chapter 2.	MODELING TECHNIQUES FOR THE ISOLATED BLADE	9
Chapter 3.	EQUATIONS OF MOTION -- EQUIVALENT HINGE MODEL	12
3.1	Kinetic Energy of a General Rotor Blade	12
3.2	Nonlinear Equations of Motion	15
3.3	Linearized Equations	22
Chapter 4.	AERODYNAMIC LOADS -- EQUIVALENT HINGE MODEL	25
4.1	Relative Velocity of a General Rotor Blade	28
4.2	Equivalent Hinge Aerodynamic Moments	29
4.3	Linearized Moments	34
Chapter 5.	THE COMPLETE EQUIVALENT HINGE MODEL	37
5.1	Steady Equations	41
Chapter 6.	AEROELASTIC STABILITY OF THE EQUIVALENT HINGE MODEL	43
6.1	Classical Flutter and Divergence	45
6.2	Lag Instabilities	47

Chapter 7.	COMPARISON OF EQUIVALENT HINGE AND MODAL MODELS	52
Chapter 8.	MODELING TECHNIQUES FOR THE ROTOR-TOWER SYSTEM	57
Chapter 9.	EQUATIONS OF MOTION -- ROTOR-TOWER MODEL	60
9.1	Coordinate Systems	60
9.2	Kinetic Energy	65
9.3	Gravity Potential Energy	70
9.4	Strain Energy	71
9.5	Equations of Motion	72
Chapter 10.	AERODYNAMIC LOADS -- ROTOR-TOWER SYSTEM	87
10.1	Relative Velocity of the Blade	91
10.2	Pitch Rate of the Blade	94
10.3	Work of External Forces	94
10.4	Generalized Loads	97
Chapter 11.	HARMONIC BALANCE SOLUTION OF EQUATIONS WITH PERIODIC COEFFICIENTS	111
11.1	The Harmonic Balance Transform	113
11.2	Initial Conditions And Transient Response	121

ORIGINAL PAGE IS
OF POOR QUALITY

Chapter 12.	THE YAW-PITCH-TEETER MODEL	126
12.1	Reduction of Hub Coordinates	128
12.2	Equations of Motion	133
12.3	An Approximate Solution for Imbalance	139
Chapter 13.	AEROELASTIC BEHAVIOR OF THE YAW-PITCH-TEETER MODEL	143
13.1	Comparison of Two Models	143
13.2	Aeroelastic Stability Study	147
Chapter 14.	CONCLUSIONS	151
	REFERENCES	156
Appendix A.	MODAL MODEL SUMMARY	163
Appendix B.	MATRICES FOR PART II	167
Appendix C.	AERODYNAMIC INTEGRALS FOR PART II	171
Appendix D.	EIGENVALUES FOR MOD-2 CASES	175
Appendix E.	EIGENVECTORS FOR A MOD-2 CASE	181
	TABLES AND FIGURES FOR PART I	190
	TABLES AND FIGURES FOR PART II	206

LIST OF PRINCIPAL SYMBOLS

a	lift curve slope
B	$= \beta_t + \beta_p$, see sketch 9.2, p.71
C	lift deficiency function
C_{ij}	damping matrix coefficients
C_{do}	profile drag coefficient
c	chord
\bar{c}	$= c/L$
D	$= C_{do}/a$
d	drag per unit length
E	modulus of elasticity
e	undersling, see sketch 9.3, p. 73
e_A	distance aero center is forward of E.A.
e_H	blade root offset, see sketch 3.1, p. 21
e_I	distance C.G. is forward of E.A.
e_ξ, e_η	blade C.G. locations, see eq. (3.8)
e_1, e_2	blade C.G. locations. see eq. (3.9)
$\bar{e}_H, \bar{e}_\xi, \bar{e}_\eta$	nondimensional quantities, see eq. (3.21)
\bar{e}_A, \bar{e}_I	nondimensional quantities, $e_A/L, e_I/L$
g	gravity
H_V, H_W	blade mass integrals, see eq. (9.8)

$I_{\xi}, I_{\eta}, I_{\xi\eta}$
 I_1, I_2, I_{12}

blade moments of inertia, see eqs. (3.8), (3.9)

I_o

blade inertia about C.G., = $I_{\xi} - M_b e_I^2$

I_b, I_v, I_w
 I_{vw}, I_{xv}, I_{xw}

blade mass integrals, see eq. (9.8)

I_{xv}^*, I_{xw}^*
 I_b^*, I_b^{**}

blade mass integrals, see eq. (9.9)

I_{yn}, I_{pn}

nacelle moment of inertia in yaw and pitch

$\bar{I}_{\xi}, \bar{I}_{\xi\eta}, \bar{I}_o$

nondimensional quantities, see eqs. (3.21),
(6.1).

\bar{I}_y, \bar{I}_p

inertias, see eqs. (12.11) and (12.12)

$\hat{i} \hat{j} \hat{k}$

unit vectors along inertial axes X, Y, Z, see
sketches 3.1, 3.2, 9.1, pp. 21, 24, 70.

$\hat{i}_s \hat{j}_s \hat{k}_s$

unit vectors along shaft axes, X_s, Y_s, Z_s , see
sketches 9.1, 9.2, 9.3, pp. 70, 71, 73.

$\hat{i} \hat{j} \hat{k}$

unit vectors along undeformed blade axes
x, y, z, see sketches 3.1, 3.2, 9.2, 9.3,
pp. 21, 24, 71, 73.

K_{ij}

stiffness matrix coefficients

$K_v K_w K_{vw} K_t$

blade stiffnesses, see eqs. (9.13), (9.14)

$k_{\beta}, k_{\phi}, k_{\theta}$

blade hinge stiffnesses in flap, lag, pitch

$k_y k_p$

nacelle stiffness in yaw and pitch

L	Length of blade
L_i	aerodynamic integrals, see Appendix C
l_c, l_{nc}	circulatory and noncirculatory lift
l_n	nacelle length, see sketch 12.1, p. 136
\bar{l}_n	$= l_n/L$
M_b	blade mass
\bar{M}_b	$= M_b L^2 / I_b$
M_{ij}	mass matrix coefficients
m	mass of blade per unit length
m_{ea}	aerodynamic moment per unit length
P_i	external forces on wind turbine, see eqs. (10.14) to (10.25).
p	roots of characteristic equation, $= a + iv$
p_ξ, p_η	loads per unit length on blade, see sketches 4.1, 10.1, pp. 35, 97.
p_x, p_y, p_z	loads per unit length on blade, see sketch 10.2, p. 98.
Q_ξ, Q_ϕ, Q_ζ	generalized forces, see eqs. (4.10) to (4.13)
Q_i	external moments on wind turbine, see eqs. (10.14) to (10.25).
Q	generalized force
Q_0	steady-state generalized force
\tilde{Q}	perturbation generalized force

- q generalized coordinate
- q_v, q_w, q_θ generalized coordinates for blade, see eqs. (7.1), (9.6).
- $\left. \begin{array}{l} q_{ws}, q_{wa} \\ q_{vs}, q_{va} \end{array} \right\}$ symmetric and antisymmetric coordinates, see eqs. (9.15), (9.16).
- q_x, q_y, q_z translations of rotor hub, see sketch 9.1, p. 70.
- q_o, q_{s_m}, q_{c_m} harmonic balance coordinates, see eq. (11.7)
- q_ξ torsional moment per unit length on blade, see sketch 4.1, p. 35.
- R_v, R_w blade mass integrals, see eq. (9.8)
- S_b, S_v, S_w blade mass integrals, see eq. (9.8)
- S_b^* blade mass integral see eq. (9.9)
- $\bar{S}_b = S_b L / I_b$
- T kinetic energy
- $[T_1], [T_2]$ transformation matrices defined by eqs. (3.1), (3.6).
- $[T_X], [T_Y], [T_\psi], [T_B]$ transformation matrices defined by eq. (9.1)
- $[T_a], [T_b]$ transformation matrices defined by eqs. (9.1), (10.2)
- t time
- U relative wind velocity
- U_n, U_ζ relative wind components along n, ζ axes

CLAUD

U_x, U_y, U_z	relative wind components along x,y,z
u_{in}	wind inflow velocity in -z direction
u_{cr}	wind crossflow velocity in -Y direction
u, v, w	blade displacement in x,y,z directions, see sketch 9.2, p. 71.
V	potential energy
W	work done
X, Y, Z	fixed inertial axes, see sketches 3.1, 3.2, 9.1, pp. 21, 24, 70.
X_s, Y_s, Z_s	shaft axes, see sketches 9.1, 9.2, 9.3, pp. 70, 71, 73.
x, y, z	undeformed blade axes, see sketches 3.1, 3.2, 9.2, 9.3, pp. 21, 24, 71, 73.
α	angle of attack
β	flap angle, see sketch 3.2, p.24
β_p	precone angle, see sketches 3.1, 3.2, 9.2, 9.3, pp. 21, 24, 71, 73.
β_t	teeter angle, see sketch 9.2, p. 71
β_s	built-in, flap spring angle
β_0	steady-state flap angle
β'	perturbation flap angle about steady-state
γ	Locke number = $\rho a c L^4 / I_n$
$\gamma_v, \gamma_w, \gamma_\theta$	blade mode shapes, see eqs. (7.1), (9.6)

δ_v, δ_w	axial mode shapes, see eq. (9.6)
ϵ	small quantity
ζ	critical damping ratio
θ	blade pitch angle, see sketch 3.2, p. 24
θ_s	built-in, pitch spring angle
θ_o	steady-state pitch angle
$\tilde{\theta}$	perturbation pitch angle about steady-state
θ_b	built-in, distributed blade pretwist angle
$\hat{i}, \hat{y}, \hat{k}$	unit vectors along deformed blade axes ξ, η, ζ , see sketches 3.2, 10.1, pp. 24, 97.
λ	$= u_{in}/\Omega L$
μ	$= u_{cr}/\Omega L$
$\nu_\beta, \nu_\phi, \nu_\theta$	nondimensional frequency ratios ω_i/Ω in flap, lag, pitch, see eq. (3.21).
ν_γ, ν_p, ν_t	nondimensional frequency ratios ω_i/Ω in yaw, pitch, teeter, see eq. (12.12)
ξ, η, ζ	deformed blade axes, see sketches 3.2, 10.1, pp. 24, 97.
ρ	air density
τ	linear wind shear coefficient, see eq. (10.26)
ϕ	yaw alignment angle
ϕ	lag angle, see sketch 3.2, p. 24
ϕ_s	built-in, lag spring angle

- ϕ_0 steady-state lag angle
- $\tilde{\phi}$ perturbation lag angle about steady-state
- ϕ_X, ϕ_Y, ϕ_Z rotations of rotor hub, see sketch 9.1,
 p. 70.
- ϕ_p, ϕ_y nacelle pitch and yaw, see sketch 12.1,
 p. 136.
- ψ angular rotation coordinate of blade, see
 sketches 3.1, 9.2, pp. 21, 71. Note,
 $\psi = \Omega t.$
- Ψ $= \psi + \phi_Z$
- Ω rotation speed of wind turbine
- $\omega_\xi, \omega_\eta, \omega_\zeta$ angular rotation velocities of blade about
 ξ, η, ζ axes, see sketches 4.1, 10.1,
 pp. 35, 97.
- $\dot{(\)} \equiv \frac{d}{dt}$
- $\overset{\circ}{(\)} \equiv \frac{d}{d\psi}$

Rising energy prices over the last decade have made large wind energy conversion machines an attractive option for electric utilities. Still, such machines must be carefully designed to compete with the cost of energy from other resources. The capital cost, longevity, and maintenance costs of the machine determine the cost of wind energy produced, and these factors in turn are strongly influenced by the dynamic loads and vibrations of the structure. Thus, knowledge of the aeroelastic behavior of these machines is essential to reducing the cost of the energy they produce.

This thesis examines certain aspects of the aeroelastic modeling and behavior of the horizontal axis wind turbine, or HAWT. Some problems of HAWT aeroelasticity are simply new applications of rotary-wing aeroelasticity, while others are uniquely inherent to these systems. Wind turbines operate efficiently at relatively large thrust coefficients and high inflow angles, and gravity loads are important in some analyses. The rotor is subject to a sheared airflow due to the earth's boundary layer and the blades must pass through the tower wake if the rotor is downwind.

The first modern generation of large wind turbines is typified by the 100 kW NASA MOD-0 series [1]. The MOD-0 is characterized by:

- 1) Relatively stiff, cantilevered blades.
- 2) Rotor downwind of the tower.
- 3) Root pitch change mechanism and highly twisted blades.
- 4) Yaw drive and brake system to align the machine axis with the wind direction.

This configuration was also characterized initially by large dynamic overstresses, but subsequent measures taken reduced this problem substantially [2].

The 2.5 MW NASA MOD-2 wind turbine [3] embodies various advanced features intended among other things to reduce the cyclic loading of the blades:

- 1) More flexible blades with a teetering hub.
- 2) Rotor upwind of tower.
- 3) Tip pitch control and less severe blade twist.

In this machine, the upwind teetering rotor reduces the dynamic loads, but the MOD-2 has not been without dynamic problems.

A teetered, tip-controlled rotor has also been fitted to a MOD-0 wind turbine for evaluation of these proposals [4, 5]. This rotor was tested both upwind and downwind of the tower, and further tests with a more flexible tower are being conducted. Statistical data on blade bending moments, teeter response, and yaw moments are presented in these

references. Further proposals for advanced HAWTs include free yaw, more flexible tower, and soft drive train to isolate the rotor from the generator [6].

Although HAWT aeroelasticity is a relatively new field of study, a considerable body of literature exists. Brief reviews of the literature and methods of HAWT aeroelasticity are presented at appropriate junctures in this thesis. A good critical review has been presented by Friedmann [7]. See also his survey of rotary-wing aeroelasticity [8]. Literature in the related field of helicopter aeroelasticity has been extensively catalogued in a book by Johnson [9]. See also his study of proprotor aircraft dynamics [10].

Wind turbine aeroelasticity is conveniently divided into two areas of concern: stability and response. The designer's first task is to assure that the machine is free of aeroelastic and mechanical instabilities throughout the operating envelope. Nonlinear effects are important for the stability problem, and the equations of motion must be derived consistent with this fact. Generally, the equations of motion are then linearized about some equilibrium state of the system.

The designer's second task is to assure that the machine is structurally sound and will be long lived. The response of the wind turbine to the various unsteady inputs

such as gravity forcing, wind gusts, tower shadow, and wind shear must be calculated. Nonlinear effects are generally less important for the response problem.

The equations of motion and external load expressions of wind turbine systems are extremely complex. As the derivation of these equations progresses, it becomes apparent that some method must be used to sort out and keep only the most significant terms. Following the practice of rotary-wing aeroelasticity, an assumed ordering scheme for the various parameters and coordinates is usually established. This ordering scheme is based on typical wind turbine parameters and is therefore different from its rotary wing counterpart.

Many aspects of HAWT aeroelastic behavior can be studied by modeling an isolated blade with fixed hub. This implies that interactions with the tower motion or between blades are negligible, an acceptable assumption for the MOD-0 configuration. The isolated blade has important degrees of freedom in flapping out of the plane of rotation, lagging in the plane of rotation, and pitching about the blade axis.

Much less research has been done in modeling the rotor-tower system. The tower may have side-to-side and fore-and-aft bending, twisting about its vertical axis, yaw drive flexibility, and generator drive system degrees of freedom. The rotor may have a teeter or gimbal degree of

freedom. Each blade has flapping and lagging, but blade torsion has usually been neglected in examining rotor-tower interaction.

Both MOD-0 and MOD-2, and most other large wind turbines have two blades, a configuration forced by the economic considerations alluded to earlier. As a result, the equations of motion for the coupled rotor-tower system involve periodic coefficients which demand proper mathematical treatment.

There is a temptation to utilize the digital computer and numerical methods to construct an all-encompassing model of the HAWT system. In this way the issues of nonlinear terms, ordering schemes, and periodic coefficients may be sidestepped. Indeed, the equations of motion and external loads need not be derived explicitly. While this approach is useful in the final stages of design, it is unwieldy and expensive for initial design or basic research. The essential physics of a phenomenon may be overshadowed by lesser details of the model, and the source of a phenomenon may be untraceable.

An example of this approach is the MOSTAS computer code for wind turbines [11, 12, 13]. This is a very complete package which has roots in various helicopter codes. MOSTAS has been built up over the years to model most aspects of HAWT aeroelasticity and many different machine configurations.

A general review of MOSTAS has been made by Dugundji and Wendell [14]. Based on that study, eight specific recommendations were made. Four were suggestions to improve the MOSTAS package; four others were recommendations for further basic research. These four are summarized here with the original numbers in parentheses:

- 1) Develop simpler models to investigate the main origins of aeroelastic phenomena (1).
- 2) Examine aeroelastic and mechanical instabilities more closely, especially for the proposed more flexible systems (3).
- 3) Study teetering effects and propellor whirl type instabilities (4).
- 4) Look in detail at generator drive train interaction with other system components (7).

The two parts of this thesis address each of these four recommendations to a certain degree. The contents are summarized below.

Part I concerns modeling the isolated wind turbine blade of a MOD-0 type wind turbine. Modeling techniques are reviewed briefly, followed by a detailed development of a simple three degree of freedom equivalent hinge model of an isolated rotor blade for aeroelastic stability. This derivation introduces parameters, coordinate systems, and concepts of modeling such as linearization of nonlinear equations, ordering schemes, and unsteady aerodynamics, all of which are common to many of the modeling techniques. A

stability study which identifies the important parameters and phenomena is presented. Finally, the equivalent hinge model is compared to a simple modal model.

Thus, Part I addresses recommendation one, and, to some degree, recommendation two cited above. One criticism of the computer codes has been their inability to calculate stability boundaries [7]. This part of the thesis addresses that need with an extensive stability study.

Part II concerns modeling the coupled rotor-tower system of a MOD-2 type wind turbine. Models in the literature are reviewed, followed by the development of two building blocks for modeling the rotor-tower system. The first of these is the derivation of equations of motion and external load expressions for a two-bladed, teetering rotor on a flexible support. Blade bending modes in flap and lag are included, and hub degrees of freedom are used for generality. The final equations are in eleven degrees of freedom. The second building block is a general harmonic balance method to solve systems of second order ordinary differential equations with periodic coefficients. Stability, steady-state response, and transient response are included.

A simple three degree of freedom model with nacelle yaw, nacelle pitch, and rotor teeter demonstrates the use of these building blocks. Whirl flutter and divergence are

examined, and the effect of teeter, preconeing, and support stiffness is studied. Transient and forced response are calculated for several cases.

Thus, Part II addresses mainly recommendations one and three cited above. Some aspects of recommendation two are studied, and tools are developed for recommendation four. Thresher, Dugundji, Hohenemser, and Walton have reviewed the state of the art of HAWT structural dynamics analysis tools [15]. They reiterate the need for simple models and experimental measurements to validate the complex computer codes and to foresee dynamics problems. They also cite the need to study the effects of teetering and of more flexible systems. Dynamics problems encountered in full scale tests confirm these recommendations [12, 4, 5; see also 6].

In summary, this thesis aims to contribute to two general areas of HAWT aeroelasticity: modeling methodology and the understanding of structural dynamics problems.

Chapter 2.

MODELING TECHNIQUES FOR THE ISOLATED BLADE

The HAWT blade is essentially a rotating beam which is twisted and tapered. Usually, it does not have coincident center of gravity, shear center, or tension center, and it may have discontinuities in various properties. In addition, the blade may be precone and its root may be offset from the hub. Thus, there are complex structural and inertial couplings between torsion, bending in the plane of rotation, and bending out of the plane of rotation.

Houbolt and Brooks derived the linear differential equations of such a beam without precone [16]. In rotary-wing and HAWT aeroelasticity, it has been recognized that some nonlinear effects are important, and several researchers have derived related equations which include ordered nonlinear terms as well as precone [17, 18, 19, 20]. The most important nonlinear effects have been identified, although there is a current controversy about torsion-stretching coupling [21, 22].

The solution method of choice in these studies has been the Galerkin modal approach. Hodges and Ormiston developed the associated aerodynamic loads for stability of a uniform helicopter blade in hover [23]. They solved the equations using coupled rotating modes. Wendell developed aerodynamic

loads appropriate to wind turbine blades and used uncoupled, nonrotating modes to examine aeroelastic stability [20]. Kottapalli, et al., studied both stability and response of a wind turbine blade using uncoupled rotating modes [24]. Of special interest is their assertion that the equations for stability should be linearized about a time-dependent steady-state response of the wind turbine blade rather than a time-averaged steady position.

An alternate, mixed displacement and stress formulation of the equations of motion for a helicopter blade in hover has been advanced by Stephens, et al. [25]. They solved the nonlinear steady-state equations using a collocation method, and the linearized stability equations were solved by numerical integration techniques.

The finite element method has also been used to formulate the problem. Hodges has developed a method based on the Ritz approach [26], and Friedmann has developed a method based on the Galerkin approach [27]. Sivaneri and Chopra have presented an application of the method to a helicopter blade in hover [28]. The nonlinear steady-state equations were solved by iteration directly from the finite element analysis; the vibration modes were then calculated based on this steady-state deflection, and used for the stability analysis. Kamoulakos has applied a similar technique to HAWT rotor blades [29].

A simple model of a rotor blade which may be proposed is to replace the flexible, cantilevered blade with an equivalent articulated blade with springs at the root to represent the structural stiffness. This "equivalent hinge" model has been used extensively to study helicopter rotor blades [e.g. 30, 31, 32, 9].

Miller, et al., used an equivalent hinge model to study the aeroelastic stability of a wind turbine blade [33]. However, no ordering scheme was used to consistently retain nonlinear and higher-order terms. Chopra and Dugundji developed a nonlinear equivalent hinge model to study blade response and stability [34, 35]. This model was consistently derived, but ignores center of gravity and aerodynamic center offsets, and the feathering axis was assumed to be in the plane of rotation. Liebst used a derivative of this model to evaluate active control strategies for dynamic load alleviation [36].

The chapters that follow present a complete derivation of the equations of motion and aerodynamic loads, an aeroelastic stability study, and a comparison of the equivalent hinge and modal models. Nonlinear and higher-order terms are consistently derived, cross-sectional offsets are included, and the important distinction between blade preconing and feathering axis coning is maintained. Gravity, wind shear, and tower shadow effects are ignored for this simple stability study.

Chapter 3.

EQUATIONS OF MOTION -- EQUIVALENT HINGE MODEL

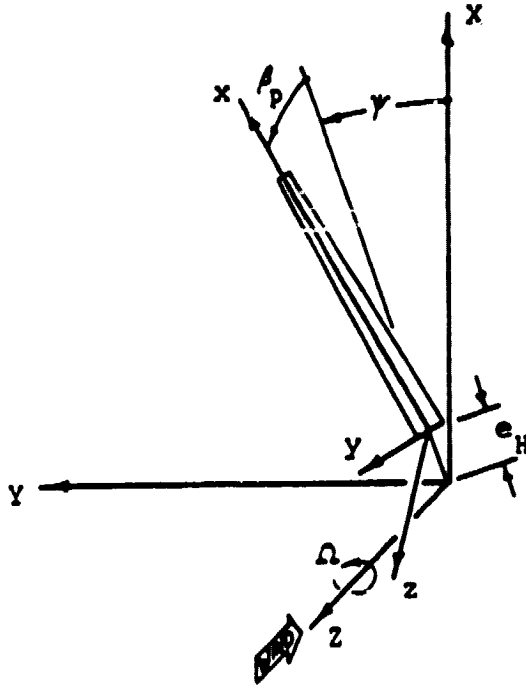
The equivalent hinge model is proposed as a simple approach to studying the aeroelastic stability of an isolated wind turbine blade. The model is useful for parameter studies and preliminary design. This chapter presents a derivation of the equations of motion without aerodynamic loads, which are derived in the next chapter.

Some nonlinear effects must be retained, but the goal is to create a simple model and to avoid over dressing the simple mechanism proposed. First, the nonlinear equations of motion are derived. Second, the equations are linearized in perturbations of the blade motion about a steady-state, deflected blade position. Finally, the equations of motion are simplified by applying an assumed ordering scheme for the parameters and the steady-state coordinates. An energy approach is followed in the derivation.

3.1 KINETIC ENERGY OF A GENERAL ROTOR BLADE

Two coordinate systems are used to describe the deformed position of the HAWT blade, as shown by Sketch 3.1. The $X Y Z$ system is fixed in space. The blade is located in the $x y z$ system which is rotating at a constant rate Ω so

that $\gamma = \Omega t$. The blade root is offset e_H from the hub axis and has a built-in precone angle β_p out of the plane of rotation.



Sketch 3.1 Inertial and Blade Coordinates

The unit vectors associated with the inertial system $X Y Z$ are $\hat{i} \hat{j} \hat{k}$ respectively, and those associated with the blade system $x y z$ are $\hat{i} \hat{j} \hat{k}$. The transformation between these unit vectors is

$$[\hat{i} \hat{j} \hat{k}] = [\hat{i} \hat{j} \hat{k}][T_1] \quad (3.1)$$

where $[T_1] =$

$$\begin{bmatrix} \cos\beta_p & 0 & \sin\beta_p \\ 0 & 1 & 0 \\ -\sin\beta_p & 0 & \cos\beta_p \end{bmatrix} \begin{bmatrix} \cos\gamma & \sin\gamma & 0 \\ -\sin\gamma & \cos\gamma & 0 \\ 0 & 0 & 1 \end{bmatrix}$$

In terms of the blade coordinates and the hub offset, the blade position components in the inertial system are then

$$\begin{aligned} X &= x \cos\beta_p \cos\gamma - y \sin\gamma - z \sin\beta_p \cos\gamma \\ &\quad + e_H \cos\gamma \\ Y &= x \cos\beta_p \sin\gamma + y \cos\gamma - z \sin\beta_p \sin\gamma \\ &\quad + e_H \sin\gamma \\ Z &= x \sin\beta_p + z \cos\beta_p \end{aligned} \quad (3.2)$$

The corresponding absolute velocity components are

$$\begin{aligned} \dot{X} &= (\dot{x} \cos\beta_p - \dot{z} \sin\beta_p - \Omega y) \cos\gamma \\ &\quad - (\dot{y} + \Omega x \cos\beta_p - \Omega z \sin\beta_p + \Omega e_H) \sin\gamma \\ \dot{Y} &= (\dot{x} \cos\beta_p - \dot{z} \sin\beta_p - \Omega y) \sin\gamma \\ &\quad - (\dot{y} + \Omega x \cos\beta_p - \Omega z \sin\beta_p + \Omega e_H) \cos\gamma \\ \dot{Z} &= \dot{x} \sin\beta_p + \dot{z} \cos\beta_p \end{aligned} \quad (3.3)$$

where $(\dot{}) = d/dt$.

The kinetic energy of the rotor blade is given by the integral over the blade of the kinetic energy of each particle dm

$$T = \int_{\text{blade}} \frac{1}{2} [(\dot{x})^2 + (\dot{y})^2 + (\dot{z})^2] dm \quad (3.4)$$

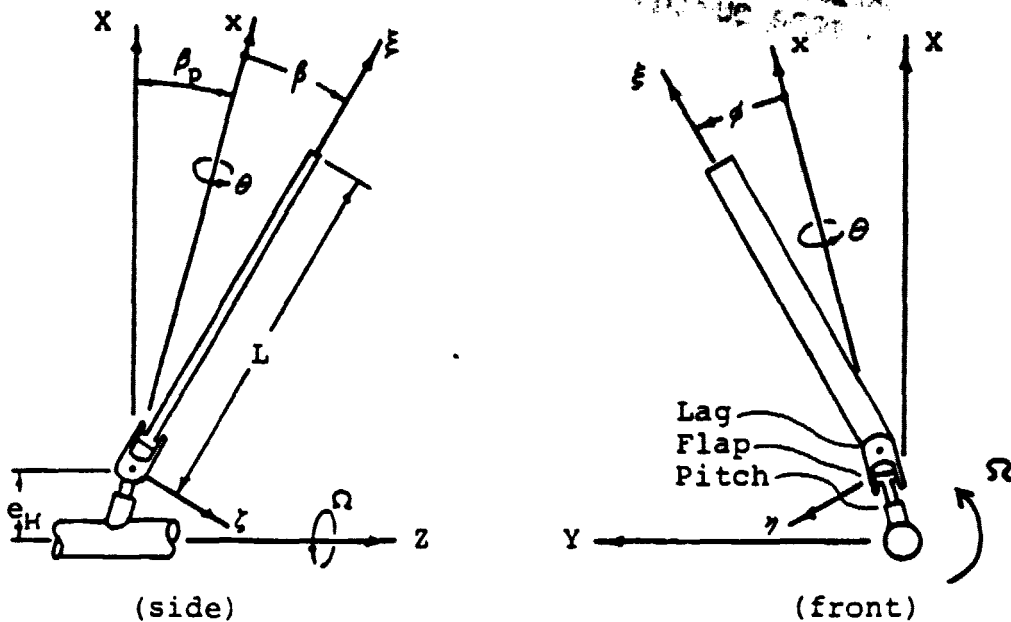
In terms of the blade coordinates this becomes

$$T = \int_{\text{blade}} \left\{ \frac{1}{2} [(\dot{x})^2 + (\dot{y})^2 + (\dot{z})^2] + \Omega[(x\dot{y} - \dot{x}y) \cos\beta_p + (y\dot{z} - \dot{y}z) \sin\beta_p + e_H \dot{y}] + \frac{1}{2} \Omega^2 [x^2 \cos^2\beta_p + y^2 + z^2 \sin^2\beta_p - 2xz \sin\beta_p \cos\beta_p + 2e_H x \cos\beta_p - 2e_H z \sin\beta_p + e_H^2] \right\} dm \quad (3.5)$$

This expression is valid for any coordinate scheme used to describe the deformation of the blade within the blade coordinate frame $x y z$, for example normal modes and generalized coordinates or equivalent hinge rotations.

3.2 NONLINEAR EQUATIONS OF MOTION

In the equivalent hinge model shown by Sketch 3.2, three degrees of freedom, and three hinge axes, are used to represent the HAWT blade: blade pitch θ about the pitch control axis; flapping β roughly perpendicular to the plane of rotation; and lagging ϕ roughly in the plane of rotation. Furthermore, the rotations are assumed to be in this same order. Spring moments about each axis represent the blade stiffnesses.



Sketch 3.2 The Equivalent Hinge Model

The deformed blade coordinate system ξ, η, ζ deflects with the blade. The transformation between the deformed blade unit vectors $\hat{i}, \hat{j}, \hat{k}$ and the undeformed blade unit vectors $\hat{i}, \hat{j}, \hat{k}$ is

$$[\hat{i} \ \hat{j} \ \hat{k}] = [\hat{i} \ \hat{j} \ \hat{k}][T_2] \quad (3.6)$$

where $[T_2] =$

$$\begin{bmatrix} \cos\phi & \sin\phi & 0 \\ -\sin\phi & \cos\phi & 0 \\ 0 & 0 & 1 \end{bmatrix} \begin{bmatrix} \cos\beta & 0 & \sin\beta \\ 0 & 1 & 0 \\ -\sin\beta & 0 & \cos\beta \end{bmatrix} \begin{bmatrix} 1 & 0 & 0 \\ 0 & \cos\theta & \sin\theta \\ 0 & -\sin\theta & \cos\theta \end{bmatrix}$$

Finally, the blade position components in terms of the deformed blade coordinates are

ORIGINAL PAGE IS
OF POOR QUALITY

$$\begin{aligned}
 x &= \xi \cos \beta \cos \phi - \eta \cos \beta \sin \phi - \zeta \sin \beta \\
 y &= \xi (\sin \phi \cos \theta - \sin \beta \cos \phi \sin \theta) \\
 &\quad + \eta (\cos \phi \cos \theta + \sin \beta \sin \phi \sin \theta) \\
 &\quad - \zeta \cos \beta \sin \theta \\
 z &= \xi (\sin \phi \sin \theta + \sin \beta \cos \phi \cos \theta) \\
 &\quad + \eta (\cos \phi \sin \theta - \sin \beta \sin \phi \cos \theta) \\
 &\quad - \zeta \cos \beta \sin \theta
 \end{aligned} \tag{3.7}$$

The associated velocity components are omitted for the sake of brevity.

To simplify the model, the blade is considered to be thin and untwisted, that is, approximately in the $\xi \eta$ plane. Then, $\zeta = 0$ and the following definitions can be made

$$\begin{aligned}
 \int_{\text{blade}} dm &= M_b & \int_{\text{blade}} \xi dm &= M_b e_\xi & \int_{\text{blade}} \eta dm &= M_b e_\eta \\
 \int_{\text{blade}} \xi^2 dm &= I_\eta & \int_{\text{blade}} \eta^2 dm &= I_\xi & \int_{\text{blade}} \xi \eta dm &= I_{\xi\eta}
 \end{aligned} \tag{3.8}$$

Furthermore, it is convenient to lump together the blade moments of inertia and products of inertia and make the following definitions

$$\begin{aligned}
 I_1 &= I_y \cos^2 \phi + I_z \sin^2 \phi - I_{yz} \sin 2\phi \\
 I_2 &= I_y \sin^2 \phi + I_z \cos^2 \phi + I_{yz} \sin 2\phi \\
 I_{12} &= (I_y - I_z) \sin 2\phi + I_{yz} \cos 2\phi \\
 e_1 &= e_z \cos \phi - e_y \sin \phi \\
 e_2 &= e_z \sin \phi + e_y \cos \phi
 \end{aligned}
 \tag{3.9}$$

These can be recognized as the corresponding inertial properties of the blade about a set of axes rotated an angle ϕ about the ζ axis. Note the useful properties:

$$\begin{aligned}
 dI_1/d\phi &= -2I_{12} & dI_2/d\phi &= 2I_{12} & dI_{12}/d\phi &= I_1 - I_2 \\
 I_1 + I_2 &= I_z + I_y & de_1/d\phi &= -e_2 & de_2/d\phi &= e_1
 \end{aligned}
 \tag{3.10}$$

The blade position components (3.7) are substituted into the general kinetic energy expression (3.5), and the above definitions are applied to yield

$$\begin{aligned}
 T = & \frac{1}{2} I_1 \dot{\beta}^2 + \frac{1}{2} (I_1 + I_2) \dot{\phi}^2 + \frac{1}{2} (I_2 + I_1 \sin^2 \beta) \dot{\theta}^2 \\
 & + I_{12} \cos \beta \dot{\beta} \dot{\theta} - (I_1 + I_2) \sin \beta \dot{\phi} \dot{\theta} \\
 & + \Omega \dot{\beta} [I_{12} (\sin \beta \cos \theta \cos \beta + \cos \beta \sin \beta_p) \\
 & \quad - I_1 \sin \theta \cos \beta_p - M_{b1} e_1 e_H \cos \beta \sin \theta] \\
 & + \Omega \dot{\phi} [(I_1 + I_2) (\cos \beta \cos \theta \cos \beta_p - \sin \beta \sin \beta_p) \\
 & \quad + M_{b1} e_1 e_H \cos \theta + M_{b2} e_2 e_H \sin \beta \sin \theta] \\
 & + \Omega \dot{\theta} [I_1 (\sin^2 \beta \sin \beta_p - \frac{1}{2} \sin 2\beta \cos \theta \cos \beta_p) \\
 & \quad + I_2 \sin \beta_p - I_{12} \cos \beta \sin \theta \cos \beta_p \\
 & \quad - M_{b1} e_1 e_H \sin \beta \cos \theta - M_{b2} e_2 e_H \sin \theta] \\
 & + \frac{1}{2} \Omega^2 [I_1 (\cos^2 \beta \cos^2 \beta_p + \sin^2 \beta \cos^2 \theta \sin^2 \beta_p \\
 & \quad + \sin^2 \beta \sin^2 \theta - \frac{1}{2} \sin 2\beta \cos \theta \sin 2\beta_p) \\
 & \quad + I_2 (\cos^2 \theta + \sin^2 \theta \sin^2 \beta_p \\
 & \quad - I_{12} (\sin \beta \sin 2\theta \cos^2 \beta_p + \cos \beta \sin \theta \sin 2\beta_p) \\
 & \quad - 2M_{b2} e_2 e_H \sin \theta \sin \beta_p \\
 & \quad + 2M_{b1} e_1 e_H (\cos \beta \cos \beta_p - \sin \beta \cos \theta \sin \beta_p)] \quad (3.11)
 \end{aligned}$$

As previously stated, spring moments are used to model the structural stiffnesses. The strain energy of the deflected springs is

$$V = \frac{1}{2} [k_\beta (\beta - \beta_s)^2 + k_\phi (\phi - \phi_s)^2 + k_\theta (\theta - \theta_s)^2] \quad (3.12)$$

where k_β , k_ϕ , and k_θ are the flap, lag, and pitch equivalent stiffnesses respectively, and the built-in angles β_s , ϕ_s , and θ_s allow for blade "droop", "trail", and "pitch

setting". To clarify, β_p is the built-in precone angle of the pitch axis, and β_s is the built-in droop angle of the blade in relation to the pitch axis.

The equations of motion are obtained by substituting the kinetic energy (3.11), and strain energy (3.12) into Lagrange's equations

$$\begin{aligned} \frac{d}{dt}\left(\frac{\partial T}{\partial \dot{\beta}}\right) - \frac{\partial T}{\partial \beta} + \frac{\partial V}{\partial \beta} &= Q_\beta \\ \frac{d}{dt}\left(\frac{\partial T}{\partial \dot{\phi}}\right) - \frac{\partial T}{\partial \phi} + \frac{\partial V}{\partial \phi} &= Q_\phi \\ \frac{d}{dt}\left(\frac{\partial T}{\partial \dot{\theta}}\right) - \frac{\partial T}{\partial \theta} + \frac{\partial V}{\partial \theta} &= Q_\theta \end{aligned} \quad (3.13)$$

where the Q_n s are applied moments about the three axes arising from external loads, generally functions of blade position and velocity. The β equation is

$$\begin{aligned} I_1 \ddot{\beta} + I_{12} \cos \beta \ddot{\theta} - \frac{1}{2} I_1 \sin 2\beta \dot{\theta}^2 - 2I_{12} \dot{\beta} \dot{\phi} + 2I_1 \cos \beta \dot{\phi} \dot{\theta} \\ + \Omega [2I_1 (\sin \beta \cos \theta \cos \beta_p + \cos \beta \sin \beta_p) + 2I_{12} \sin \theta \cos \beta_p] \dot{\phi} \\ - \Omega [I_1 (\cos \theta \cos \beta_p + \sin 2\beta \sin \beta_p - \cos 2\beta \cos \theta \cos \beta_p) \\ + 2I_{12} \sin \beta \sin \theta \cos \beta_p] \dot{\theta} \\ + \frac{1}{2} \Omega^2 [I_1 (\sin 2\beta \cos^2 \theta \cos^2 \beta_p - \sin 2\beta \sin^2 \beta_p + \cos 2\beta \cos \theta \sin 2\beta_p) \\ + I_{12} (\cos \beta \sin 2\theta \cos^2 \beta_p - \sin \beta \sin \theta \sin 2\beta_p) \\ + 2M_b e_1 e_H (\sin \beta \cos \beta_p + \cos \beta \cos \theta \sin \beta_p)] + k_\beta \beta \\ = k_\beta \beta_s + Q_\beta \end{aligned} \quad (3.14)$$

The ϕ equation is

$$\begin{aligned}
 & (I_1 + I_2)\ddot{\phi} - (I_1 + I_2)\sin\beta\ddot{\theta} + I_{12}\dot{\beta}^2 - I_{12}\cos^2\beta\dot{\theta}^2 - 2I_1\cos\beta\dot{\beta}\dot{\theta} \\
 & - \Omega[2I_1(\sin\beta\cos\theta\cos\beta_p + \cos\beta\sin\beta_p) + 2I_{12}\sin\theta\cos\beta_p]\dot{\beta} \\
 & - \Omega[2I_2\cos\beta\sin\theta\cos\beta_p + 2I_{12}(\cos^2\beta\sin\beta_p + \frac{1}{2}\sin 2\beta\cos\theta\cos\beta_p)]\dot{\theta} \\
 & + \frac{1}{2}\Omega^2[(I_1 - I_2)(\sin\beta\sin 2\theta\cos^2\beta_p + \cos\beta\sin\theta\sin 2\beta_p) \\
 & - 2I_{12}(\cos^2\beta\sin^2\beta_p + \sin^2\beta\cos^2\theta\cos^2\beta_p - \sin^2\theta\sin^2\beta_p \\
 & + \frac{1}{2}\sin 2\beta\cos\theta\sin 2\beta_p) + 2M_b e_1 e_H \sin\theta\sin\beta_p \\
 & + 2M_b e_2 e_H (\cos\beta\cos\beta_p - \sin\beta\cos\theta\sin\beta_p)] + k_\phi\phi \\
 & = k_\phi\phi_s + Q_\phi \tag{3.15}
 \end{aligned}$$

The θ equation is

$$\begin{aligned}
 & (I_1\sin^2\beta + I_2)\ddot{\theta} + I_{12}\cos\beta\ddot{\beta} - (I_1 + I_2)\sin\beta\ddot{\phi} \\
 & - I_{12}\sin\beta\dot{\beta}^2 + (I_1 - I_2)\cos\beta\dot{\beta}\dot{\phi} + 2I_{12}\cos^2\beta\dot{\phi}\dot{\theta} \\
 & + \Omega[I_1(\cos\theta\cos\beta_p + \sin 2\beta\sin\beta_p - \cos 2\beta\cos\theta\cos\beta_p) \\
 & + 2I_{12}\sin\beta\sin\theta\cos\beta_p]\dot{\beta} \\
 & + \Omega[2I_2\cos\beta\sin\theta\cos\beta_p + 2I_{12}(\cos^2\beta\sin\beta_p + \frac{1}{2}\sin 2\beta\cos\theta\cos\beta_p)]\dot{\phi} \\
 & + \frac{1}{2}\Omega[-I_1(\sin^2\beta\sin 2\theta\cos^2\beta_p + \frac{1}{2}\sin 2\beta\sin\theta\sin 2\beta_p) \\
 & + I_2\sin 2\theta\cos^2\beta + I_{12}(2\sin\beta\cos 2\theta\cos^2\beta_p + \cos\beta\cos\theta\sin 2\beta_p) \\
 & - 2M_b e_1 e_H \sin\beta\sin\theta\sin\beta_p + 2M_b e_2 e_H \cos\theta\sin\beta_p] + k_\theta\theta \\
 & = k_\theta\theta_s + Q_\theta \tag{3.16}
 \end{aligned}$$

Equations (3.14-16) are the complete nonlinear equations for large deflections and vibrations. The solution of these equations with all time derivatives set to zero is the steady state position of the rotating loaded blade, which will be designated $\beta_0, \phi_0, \theta_0$.

3.3

LINEARIZED EQUATIONS

For investigating small vibrations, the equations of motion are generally linearized in perturbations β , ϕ , θ about the steady position β_0 , ϕ_0 , θ_0 . The aeroelastic stability is very sensitive to the steady position due to the relatively large centrifugal effects [33]. Each equation takes the form

$$F(\ddot{\beta}, \ddot{\phi}, \ddot{\theta}, \dot{\beta}, \dot{\phi}, \dot{\theta}, \beta, \phi, \theta) = Q \quad (3.17)$$

Here, F represents the left hand side of the equation of motion, and Q the right hand. This form can be expanded in linear Taylor's series as follows

$$\begin{aligned} F_0 + (\partial F / \partial \ddot{\beta})_0 \ddot{\beta} + \dots + (\partial F / \partial \dot{\beta})_0 \dot{\beta} + \dots + (\partial F / \partial \theta)_0 \theta \\ = Q_0 + \tilde{Q} \end{aligned} \quad (3.18)$$

where the subscript $()_0$ denotes evaluation at the steady-state position: $\beta = \beta_0$, $\phi = \phi_0$, $\theta = \theta_0$. Note that the applied moment is expressed as a sum of a steady load Q_0 which is generally a function of the steady-state displacements and a perturbation load \tilde{Q} which is generally a function of the perturbations. By definition, the steady-state equation is

$$F_0(\beta_0, \phi_0, \theta_0) = Q_0(\beta_0, \phi_0, \theta_0) \quad (3.19)$$

Therefore the associated perturbation equation is

$$(\partial F / \partial \ddot{\beta})_0 \ddot{\beta} + \dots + (\partial F / \partial \dot{\phi})_0 \dot{\phi} + \dots + (\partial F / \partial \theta)_0 \theta = \ddot{Q} \quad (3.20)$$

The perturbation equations are further simplified by comparing and discarding higher order terms according to an ordering scheme which is reasonable for HAWTs. First define

$$\begin{aligned} \bar{I}_\beta &= I_\beta / I_\gamma & \bar{I}_{\beta\gamma} &= I_{\beta\gamma} / I_\gamma \\ \bar{e}_\beta &= M_b e_\beta L / I_\gamma & \bar{e}_\gamma &= M_b e_\gamma L / I_\gamma & \bar{e}_H &= e_H / L \\ v_\beta^2 &= k_\beta / \Omega^2 I_\gamma & v_\phi^2 &= k_\phi / \Omega^2 I_\gamma & v_\theta^2 &= k_\theta / \Omega^2 I_\beta \end{aligned} \quad (3.21)$$

where L is the blade length defined by Sketch 3.2. Then assume orders of magnitude

$$\begin{array}{ll} \bar{e}_\beta & O(\epsilon^0) \\ \beta_0, \beta_s, \beta_p, \theta_0, \theta_s & O(\epsilon^{1/2}) \\ e_H & O(\epsilon^1) \\ \rho_0, \rho_s, \bar{I}_{\beta\gamma}, \bar{e}_\gamma & O(\epsilon^{3/2}) \\ \bar{I}_\beta & O(\epsilon^2) \end{array}$$

These relative orders of magnitude are based on typical HAWT parameters. The steady-state deflections depend on the other parameters, and their order is determined by examining the steady equations (Section 5.1). From another perspective, the assumed orders of magnitude define the range of validity for the model.

The terms in each coefficient of the equations of motion are compared to one another, and terms which are smaller by one or more powers of ϵ are discarded to simplify the equations. Finally, the ordered perturbation equations are divided through by $\Omega^2 I_\gamma$. In these equations $(\dot{}) = d/d\gamma = (1/\Omega)d/dt$. The $\tilde{\beta}$ equation is

$$\begin{aligned} & \ddot{\tilde{\beta}} + (\bar{I}_{\xi\eta} + \phi_0) \ddot{\tilde{\theta}} + 2[(\beta_0 + \beta_p) + \theta_0] \dot{\tilde{\beta}} - 2\beta_0(\beta_0 + \beta_p) \dot{\tilde{\theta}} \\ & + [v_\phi^2 + 1 + \bar{e}_\xi \bar{e}_H - 2(\beta_0 + \beta_p)^2] \tilde{\beta} + \theta_0 \tilde{\beta} + [\bar{I}_{\xi\eta} + \phi_0 - (2\beta_0 + \beta_p)\theta_0] \tilde{\theta} \\ & = \tilde{Q}_\beta / \Omega^2 I_\gamma \end{aligned} \quad (3.22)$$

The $\tilde{\phi}$ equation is

$$\begin{aligned} & \ddot{\tilde{\phi}} - \beta_0 \ddot{\tilde{\theta}} - 2[(\beta_0 + \beta_p) + \theta_0] \dot{\tilde{\beta}} - 2(\bar{I}_{\xi\eta} + \phi_0)(\beta_0 + \beta_p) \dot{\tilde{\theta}} \\ & + \theta_0 \tilde{\beta} + [v_\phi^2 + \bar{e}_\xi \bar{e}_H - (\beta_0 + \beta_p)^2] \tilde{\phi} + (\beta_0 + \beta_p) \tilde{\theta} \\ & = \tilde{Q}_\phi / \Omega^2 I_\gamma \end{aligned} \quad (3.23)$$

The $\tilde{\theta}$ equation is

$$\begin{aligned} & (\bar{I}_{\xi\eta} + \phi_0) \ddot{\tilde{\beta}} - \beta_0 \ddot{\tilde{\phi}} + [\bar{I}_\xi + \beta_0^2 + 2\bar{I}_{\xi\eta} \phi_0 + \phi_0^2] \ddot{\tilde{\theta}} \\ & + 2\beta_0(\beta_0 + \beta_p) \dot{\tilde{\beta}} + 2(\bar{I}_{\xi\eta} + \phi_0)(\beta_0 + \beta_p) \dot{\tilde{\phi}} \\ & + [\bar{I}_{\xi\eta} + \phi_0 - (2\beta_0 + \beta_p)\theta_0] \tilde{\beta} + (\beta_0 + \beta_p) \tilde{\phi} \\ & + [\bar{I}_\xi (v_\theta^2 + 1) - e_\xi e_H - \beta_0(\beta_0 + \beta_p)] \tilde{\theta} \\ & = \tilde{Q}_\theta / \Omega^2 I_\gamma \end{aligned} \quad (3.24)$$

These are the important inertial terms for the equivalent hinge model of a HAWT blade.

Chapter 4.

AERODYNAMIC LOADS --
EQUIVALENT HINGE MODEL

Applied moments about the equivalent hinge axes which arise from aerodynamic forces are derived in this chapter, based upon unsteady aerodynamics and strip theory. The development of linearized aerodynamic loads is similar to the development of equations of motion in Chapter 3. First, expressions for the aerodynamic moments are derived which are nonlinear in the blade deflections. These expressions are then linearized in perturbations about the steady position, and simplified by using an assumed ordering scheme. Furthermore, the final linearized moments given assume quasisteady aerodynamics, a uniform inflow of air, and a uniform, untwisted blade.

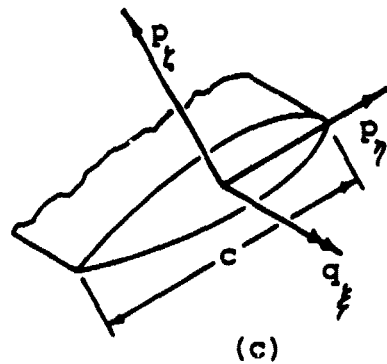
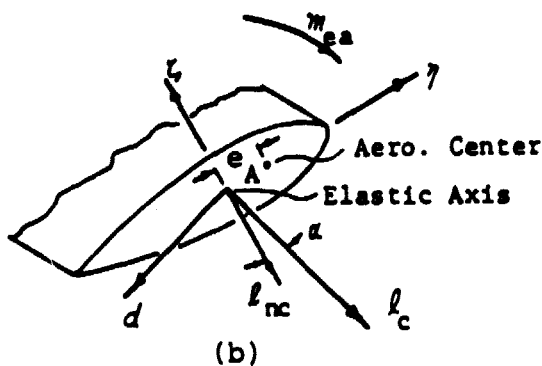
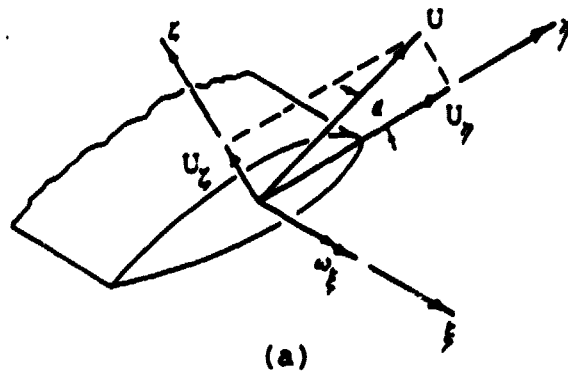
Theodorsen first developed an unsteady aerodynamic theory for a pitching, plunging airfoil in a uniform flow [37]. His theory used a lift deficiency function to represent the integrated influence of the shed wake. A rotary wing has a much more complex wake structure, but Loewy showed that its effect could be included by using a modified lift deficiency function [38]. These theories are not strictly applicable to a rotor which has chordwise motion of the blades, although they have been utilized.

Greenberg developed an unsteady aerodynamic theory for a pitching, plunging airfoil in a pulsating flow, thus extending Theodorsen's theory to helicopter rotors in forward flight [39]. Hodges and Ormiston adapted Greenberg's theory to study the flap-lag-torsion stability of a hovering rotor by using the pulsation to represent the lag motion [23].

Friedmann and Yuan modified several strip theories for use with rotary wings, including Theodorsen's and Greenberg's [40]. They compared the various theories with and without modification, and studied the quasisteady assumption. Recently, Johnson suggested a convenient grouping of terms in the lift and pitching moment expressions, which is used here [41, see also 42].

Pertinent velocity components of the blade axis relative to the inflowing air U_x and U_y , and the pitch rate ω , are shown in Sketch 4.1a. Expressions for these are derived later. U is the total velocity as shown. Also note definitions for the angle of attack α , the blade chord c , and the aerodynamic center offset e_A from the elastic axis.

ORIGINAL PAGE IS
OF POOR QUALITY



Sketch 4.1 Aerodynamic Nomenclature

The noncirculatory lift l_{nc} , the circulatory lift l_c , the drag d , and the pitching moment m_{ea} are defined by Sketch 4.1b. In terms of the present nomenclature, these distributed loads are

$$\begin{aligned}
 l_{nc} &= \frac{1}{8} \rho a c^2 [\dot{U}_z - (\frac{1}{4}c - e_A) \dot{\omega}_f] \\
 l_c &= \frac{1}{2} \rho a c C [U_z - (\frac{1}{2}c - e_A) \omega_f] U \\
 d &= \frac{1}{2} \rho c C_{d0} U^2 \\
 m_{ea} &= \frac{1}{2} \rho a c \left\{ \frac{1}{4}c \left[-(\frac{1}{4}c - e_A) \dot{U}_z + \frac{1}{4}c \omega_f U + \left(\frac{3}{32}c^2 - \frac{1}{2}c e_A + e_A^2 \right) \dot{\omega}_f \right] \right. \\
 &\quad \left. + s_A C [U_z - (\frac{1}{2}c - e_A) \omega_f] U \right\}
 \end{aligned} \tag{4.1}$$

where ρ is the air density, a is the lift curve slope $\partial C_l / \partial \alpha$, C is some lift deficiency function, and C_{d0} is the

profile drag coefficient. The resultant distributed loads of Sketch 4.1c are

$$\begin{aligned}
 q_x &= -m_{ea} \\
 p_y &= l_c \sin \alpha - d \cos \alpha \\
 p_z &= -l_{nc} - l_c \cos \alpha - d \sin \alpha
 \end{aligned}
 \tag{4.2}$$

All other components are zero. Since $\sin \alpha = U_z/U$ and $\cos \alpha = U_y/U$,

$$\begin{aligned}
 q_x &= \frac{1}{2} \rho a c \left\{ \frac{1}{4} c \left[\left(\frac{1}{4} c - e_A \right) \dot{U}_z - \frac{1}{4} c \omega_x U - \left(\frac{3}{32} c^2 - \frac{1}{2} c e_A + e_A^2 \right) \dot{\omega}_x \right] \right. \\
 &\quad \left. + e_A C [-U_z + \left(\frac{1}{2} c - e_A \right) \omega_x] U \right\} \\
 p_y &= \frac{1}{2} \rho a c \left\{ C [U_z^2 - \left(\frac{1}{2} c - e_A \right) \omega_x U_z] - D U_y U \right\} \\
 p &= \frac{1}{2} \rho a c \left\{ C [-U_z U_y + \left(\frac{1}{2} c - e_A \right) \omega_x U_z] \right. \\
 &\quad \left. - D U_z U + \frac{1}{4} c [-\dot{U}_z + \left(\frac{1}{4} c - e_A \right) \dot{\omega}_x] \right\}
 \end{aligned}
 \tag{4.3}$$

where $D = C_{d0}/a$. For small angles of attack α , U may be replaced by U_y wherever it appears here.

4.1 RELATIVE VELOCITY OF A GENERAL ROTOR BLADE

The relative velocity of the blade is the difference between the blade absolute velocity $\dot{x} \dot{y} \dot{z}$ and the inflow velocity of air at the turbine disk u_{in} , which is assumed to be in the $-z$ direction. That is,

$$\begin{pmatrix} U_x \\ U_y \\ U_z \end{pmatrix} = \begin{pmatrix} \dot{x} \\ \dot{y} \\ \dot{z} + u_{in} \end{pmatrix}
 \tag{4.4}$$

The absolute velocity components were expressed in terms of blade coordinates by equation (3.3). These are substituted into equation (4.4) and equation (3.1) is used to transform the relative velocities into the blade coordinate system.

$$\begin{aligned} U_x &= \dot{x} - \Omega y \cos\beta_p + u_{in} \sin\beta_p \\ U_y &= \dot{y} + \Omega x \cos\beta_p - \Omega z \sin\beta_p + \Omega e_H \\ U_z &= \dot{z} + \Omega y \sin\beta_p + u_{in} \cos\beta_p \end{aligned} \quad (4.5)$$

These relative velocity components, like the kinetic energy of a general rotor blade (3.5), are valid for any coordinates used to describe blade deformation within the x y z coordinate system.

4.2 EQUIVALENT HINGE AERODYNAMIC MOMENTS

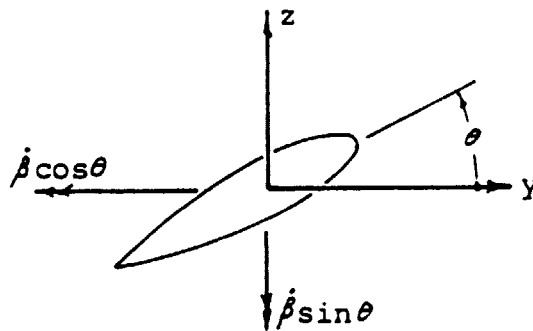
For the equivalent hinge model the position of the blade elastic axis is given by equation (3.7) with $\eta = 0$ and $\zeta = 0$.

$$\begin{aligned} x &= \ell \cos\beta \cos\phi \\ y &= \ell (\sin\phi \cos\theta - \sin\beta \cos\phi \sin\theta) \\ z &= \ell (\sin\phi \sin\theta + \sin\beta \cos\phi \cos\theta) \end{aligned} \quad (4.6)$$

These are substituted into equation (4.5), and equation (3.6) is used to transform the relative velocities into the deformed blade coordinate system. The pertinent components are

$$\begin{aligned}
 U_\eta = & \epsilon \dot{\phi} - \epsilon \sin\beta \dot{\theta} + \Omega \epsilon [-\sin\beta_p \sin\beta + \cos\beta_p \cos\beta \cos\theta] \\
 & + \Omega \epsilon_H [\cos\phi \cos\theta + \sin\beta \sin\phi \sin\theta] \\
 & + u_{in} [-\sin\beta_p \cos\beta \sin\phi + \cos\beta_p (\cos\phi \sin\theta - \sin\beta \sin\phi \cos\theta)]
 \end{aligned}
 \tag{4.7}$$

$$\begin{aligned}
 U_\zeta = & \epsilon \cos\phi \dot{\beta} + \epsilon \cos\beta \sin\phi \dot{\theta} - \Omega \epsilon_H \cos\beta \sin\theta \\
 & + \Omega \epsilon [\sin\beta_p \cos\beta \sin\phi - \cos\beta_p (\cos\phi \sin\theta - \sin\beta \sin\phi \cos\theta)] \\
 & + u_{in} [-\sin\beta_p \sin\beta + \cos\beta_p \cos\beta \cos\theta]
 \end{aligned}$$



Sketch 4.2 Resolution of Flap Angular Velocity

Four angular velocities contribute to the total angular velocity of the blade: $\dot{\phi}$ is about the ζ axis; $\dot{\beta}$ is broken down into components about the y and z axes as shown by Sketch 4.2; $\dot{\theta}$ is about the x axis; and Ω is about the z axis. These angular velocities are transformed to the deformed blade axis system using the transformations of equations (3.1) and (3.6), and they are added to give

$$\begin{pmatrix} u_x \\ u_y \\ u_z \end{pmatrix} = \begin{pmatrix} 0 \\ 0 \\ \dot{\phi} \end{pmatrix} + [T_2] \begin{pmatrix} \dot{\theta} \\ -\cos\theta \dot{\beta} \\ -\sin\theta \dot{\beta} \end{pmatrix} + [T_1] \begin{pmatrix} 0 \\ 0 \\ \Omega \end{pmatrix} \quad (4.8)$$

The only component required is

$$u_x = \Omega[\sin\beta_p \cos\beta \cos\phi + \cos\beta_p (\sin\phi \sin\theta + \sin\beta \cos\phi \cos\theta)] - \sin\phi \dot{\beta} + \cos\beta \dot{\theta} \quad (4.9)$$

The work of the external forces can be expressed both in terms of the equivalent hinge rotations, and in terms of blade motion as follows

$$\begin{aligned} \delta W &= Q_\beta \delta\beta + Q_\phi \delta\phi + Q_\theta \delta\theta \\ &= \int_0^L \{ q_x \delta a_x + p_\eta \delta \eta_{ea} + p_\zeta \delta \zeta_{ea} \} d\xi \quad (4.10) \end{aligned}$$

where η_{ea} and ζ_{ea} are the motions of the blade elastic axis in the η and ζ directions, and a_x is the rotation of the blade about the elastic axis ξ . These two families of variations are related in the same way as their corresponding velocities. First, set $\Omega = 0$ and $u_{in} = 0$ in equations (4.7) and (4.9).

$$\begin{aligned} U_\eta &= \xi \dot{\phi} - \xi \sin\beta \dot{\theta} \\ U_\zeta &= \xi \cos\phi \dot{\beta} + \cos\beta \cos\phi \dot{\theta} \\ U_x &= -\sin\phi \dot{\beta} + \cos\beta \cos\phi \dot{\theta} \end{aligned} \quad (4.11)$$

Then notice that

$$\begin{aligned} \delta\beta &= \dot{\beta} \delta t & \delta e_{\xi} &= u_{\xi} \delta t \\ \delta\phi &= \dot{\phi} \delta t & \text{and } \delta\eta_{ea} &= U_{\eta} \delta t \\ \delta\theta &= \dot{\theta} \delta t & \delta\zeta_{ea} &= U_{\zeta} \delta t \end{aligned}$$

Substitute these into equation (4.11) and write

$$\begin{aligned} \delta\eta_{ea} &= \xi \delta\phi - \xi \sin\beta \delta\theta \\ \delta\zeta_{ea} &= \xi \cos\phi \delta\beta + \xi \cos\beta \sin\phi \delta\theta \\ \delta e_{\xi} &= -\sin\phi \delta\beta + \cos\beta \cos\phi \delta\theta \end{aligned} \quad (4.12)$$

These expressions are substituted into the work expression (4.10) and coefficients of each variation are separately equated to give

$$\begin{aligned} Q_{\xi} &= \int_0^L [\xi \cos\phi p_{\xi} - \sin\phi q_{\xi}] d\xi \\ Q_{\phi} &= \int_0^L \xi p_{\eta} d\xi \\ Q_{\theta} &= \int_0^L [\xi \cos\beta \sin\phi p_{\zeta} - \xi \sin\beta p_{\eta} + \cos\beta \cos\phi q_{\xi}] d\xi \end{aligned} \quad (4.13)$$

Finally, the distributed loads (4.3) are substituted into equation (4.13).

$$\begin{aligned} Q_{\xi} &= \int_0^L \frac{1}{2} \rho a c \left\{ -\frac{1}{4} c [\xi \cos\phi + (\frac{1}{4} c - e_A) \sin\phi] \dot{U}_{\zeta} \right. \\ &\quad + \frac{1}{4} c \left[(\frac{1}{4} c - e_A) \xi \cos\phi + (\frac{3}{32} c^2 - \frac{1}{2} c e_A + e_A^2) \sin\phi \right] \dot{u}_{\xi} \\ &\quad + \left[C (\frac{1}{2} c - e_A) \xi \cos\phi + (\frac{1}{16} c^2 - \frac{1}{2} C c e_A + C e_A^2) \sin\phi \right] \omega_{\xi} U_{\eta} \\ &\quad \left. - [(C+D) \xi \cos\phi - C e_A \sin\phi] U_{\eta} U_{\zeta} \right\} d\xi \end{aligned} \quad (4.14)$$

ORIGINAL PAGE IS
OF POOR QUALITY

$$Q_p = \int_0^L \frac{1}{2} \rho a c \left\{ -C \left(\frac{1}{2} c - e_A \right) \epsilon \omega_p U_z + C \epsilon U_z^2 - D \epsilon U_z^2 \right\} d\epsilon \quad (4.15)$$

$$\begin{aligned} Q_o = \int_0^L \frac{1}{2} \rho a c \left\{ \frac{1}{4} c \left[-\epsilon \cos \beta \sin \phi + \left(\frac{1}{4} c - e_A \right) \cos \beta \cos \phi \right] \dot{U}_z \right. \\ + \frac{1}{4} c \left[\left(\frac{1}{4} c - e_A \right) \epsilon \cos \beta \sin \phi - \left(\frac{3}{32} c^2 - \frac{1}{2} c e_A + e_A^2 \right) \cos \beta \cos \phi \right] \dot{\omega}_p \\ + \left[C \left(\frac{1}{2} c - e_A \right) \epsilon \cos \beta \sin \phi - \left(\frac{1}{16} c^2 - \frac{1}{2} C e_A + C e_A^2 \right) \cos \beta \cos \phi \right] \omega_p U_z \\ + \left[C \left(\frac{1}{2} c - e_A \right) \epsilon \sin \beta \right] \omega_p U_z - \left[C \epsilon \sin \beta \right] U_z^2 + \left[D \epsilon \sin \beta \right] U_z^2 \\ \left. - \left[(C+D) \epsilon \cos \beta \sin \phi + C e_A \cos \beta \cos \phi \right] U_z U_z \right\} d\epsilon \quad (4.16) \end{aligned}$$

Equations (4.14-16) are the nonlinear aerodynamic moments for large blade deflections (although the angle of attack has been assumed small), given in terms of the velocities, pitch rate, and their derivatives. With all time derivatives set to zero, they are the steady aerodynamic moments, which will be designated Q_{p_0} , $Q_{\dot{\phi}_0}$, Q_{θ_0} . These steady moments are required to solve the steady part of equations (3.14-16) for the steady blade position β_0 , ϕ_0 , θ_0 . It is of interest that some effects of unsteady aerodynamics remain in these steady moments due to the steady pitch rate $\Omega[\sin \beta_p \dots]$ in equation (4.9). The resulting "apparent camber" terms are important for a precone rotor.

4.3 LINEARIZED MOMENTS

The aerodynamic moments are expanded in perturbations about the steady blade position in the same manner as the equations of motion.

$$Q = Q_0 + \tilde{Q} = Q_0 + (\partial Q / \partial \beta) \tilde{\beta} + \dots + (\partial Q / \partial \theta) \tilde{\theta} \quad (4.17)$$

Because of the multiplicity of aerodynamic terms, it is wise to establish the ordering scheme for aerodynamic parameters now, and apply it to eliminate terms as this expansion of aerodynamic moments proceeds.

The quasisteady assumption will be made, $C = 1$, and the blade will be approximated as being uniform along the span, with uniform inflow velocity. Actually, only an ideally twisted blade would have uniform inflow. A flat blade would not, but if θ_s is taken as the twist at $x/L = 0.75$, the aerodynamic coefficients are practically identical. Now, define

$$\begin{aligned} \lambda &= u_{in} / \Omega L & \bar{c} &= c / L \\ \gamma &= \rho a c L^4 / I_y & \bar{e}_A &= e_A / L \end{aligned} \quad (4.18)$$

Note that here the inflow angle λ and the lock number γ are defined in terms of the hinged length of the blade L . Then, assume orders of magnitude as before (Section 3.3)

ORIGINAL PAGE IS
OF POOR QUALITY

γ/β	$O(\epsilon^0)$
λ	$O(\epsilon^{\frac{1}{2}})$
\bar{c}	$O(\epsilon^{\frac{1}{2}})$
\bar{c}_A	$O(\epsilon^{\frac{1}{2}})$
$D (C_{d0}/a)$	$O(\epsilon^2)$

The velocities (4.7), the pitch rate (4.9), and their derivatives are substituted into equations (4.14-16), which are then expanded and ordered, and divided by $\Omega^2 I_y$ to give the linearized aerodynamic moments

$$\begin{aligned} \tilde{Q}_\beta / \Omega^2 I_y &= -\frac{1}{24} \gamma \bar{c} \ddot{\beta} - \frac{1}{8} \gamma \dot{\beta} - \frac{1}{24} \gamma (4\lambda - 3\theta_0) \dot{\beta} \\ &+ \left[\frac{1}{24} \gamma \beta_0 (4\lambda - 3\theta_0) - \frac{1}{8} \gamma \phi_0 + \frac{1}{24} \gamma \bar{c} + \frac{1}{6} \gamma (\frac{1}{2} \bar{c} - \bar{c}_A) \right] \ddot{\theta} \\ &+ \left[\frac{1}{24} \gamma (8\lambda - 3\theta_0) (\beta_0 + \beta_p) + \frac{1}{6} \gamma (\frac{1}{2} \bar{c} - \bar{c}_A) - \frac{1}{8} \gamma \phi_0 \right] \dot{\beta} - \frac{1}{8} \gamma (\beta_0 - \beta_p) \dot{\beta} \\ &+ \left[\frac{1}{8} \gamma + \frac{1}{3} \gamma \bar{c}_H - \frac{1}{16} \gamma \beta_p^2 - \frac{1}{16} \gamma (\beta_0 + \beta_p)^2 + \right. \\ &\quad \left. - \frac{1}{12} \gamma (3\lambda^2 - 8\lambda\theta_0 + 3\theta_0^2) \right] \ddot{\theta} \end{aligned} \quad (4.19)$$

$$\begin{aligned} \tilde{Q}_\phi / \Omega^2 I_y &= \frac{1}{12} \gamma (4\lambda - 3\theta_0) \dot{\beta} - \frac{1}{4} \gamma D \dot{\beta} \\ &+ \left[\frac{1}{12} \gamma \phi_0 (4\lambda - 3\theta_0) - \frac{1}{12} \gamma (\frac{1}{2} \bar{c} - \bar{c}_A) (3\lambda - 2\theta_0) \right] \ddot{\theta} \\ &+ \left[-\frac{1}{6} \gamma \lambda (\beta_0 + \beta_p) (3\lambda - 2\theta_0) - \frac{1}{12} \gamma (\frac{1}{2} \bar{c} - \bar{c}_A) (3\lambda - 2\theta_0) \right] \dot{\beta} \\ &+ \frac{1}{12} \gamma (4\lambda - 3\theta_0) (\beta_0 + \beta_p) \dot{\beta} - \frac{1}{12} \gamma (4\lambda - 3\theta_0) \ddot{\theta} \end{aligned} \quad (4.20)$$

$$\begin{aligned} \tilde{Q}_\theta / \Omega^2 I_y &= \left[-\frac{1}{12} \gamma \beta_0 (4\lambda - 3\theta_0) - \frac{1}{8} \gamma \phi_0 - \frac{1}{6} \gamma \bar{c}_A \right] \dot{\beta} \\ &+ \left[-\frac{1}{24} \gamma \phi_0 (4\lambda - 3\theta_0) - \frac{1}{12} \gamma \bar{c}_A (3\lambda - 2\theta_0) \right] \ddot{\theta} \\ &+ \left[-\frac{1}{32} \gamma \bar{c}^2 + \frac{3}{16} \gamma \bar{c} \bar{c}_A - \frac{1}{4} \gamma \bar{c}_A^2 + \frac{1}{24} \gamma \bar{c} \beta_0 (3\lambda - 2\theta_0) \right] \ddot{\theta} \\ &- \frac{1}{24} \gamma (6\lambda^2 - 8\lambda\theta_0 + 3\theta_0^2) \dot{\beta} - \frac{1}{24} \gamma (4\lambda - 3\theta_0) \dot{\beta} \\ &+ \left[\frac{1}{6} \gamma \bar{c}_A + \frac{1}{8} \gamma \phi_0 + \frac{1}{12} \gamma \beta_0 (4\lambda - 3\theta_0) \right] \ddot{\theta} \end{aligned} \quad (4.21)$$

21 3045 14100
YTH 14 1971

**ORIGINAL PAGE IS
OF POOR QUALITY**

These are the important aerodynamic moment terms for the equivalent hinge model of a HAWT blade.

ORIGINAL PAGE IS
OF POOR QUALITY

ORIGINAL PAGE IS
OF POOR QUALITY

Chapter 5. THE COMPLETE EQUIVALENT HINGE MODEL

This chapter summarizes the results of the preceding two, and presents the steady-state equations. When the linearized aerodynamic moments (4.19-21) are substituted into the linearized equations of motion (3.22-24) and subtracted from both sides, the complete perturbation equations take the form:

$$[M] \begin{Bmatrix} \ddot{\beta} \\ \ddot{\phi} \\ \ddot{\theta} \end{Bmatrix} + [C] \begin{Bmatrix} \dot{\beta} \\ \dot{\phi} \\ \dot{\theta} \end{Bmatrix} + [K] \begin{Bmatrix} \beta \\ \phi \\ \theta \end{Bmatrix} = \{0\} \quad (5.1)$$

The coefficient matrices of equation (5.1) are given on the following pages.

ORIGINAL PAGE IS
OF POOR QUALITY

20 3003
YUJADU
ORIGINAL
PAGE IS
OF POOR QUALITY

(5.2)

ORIGINAL PAGE IS
OF POOR QUALITY

$$[M] = \begin{bmatrix} 1 + \frac{1}{24}\gamma c & & & \\ & \bar{I}_{\xi\eta} + \phi_0 & & \\ & 0 & & \\ & & 1 & \\ & & & -\beta_0 \\ \bar{I}_{\xi\eta} + \phi_0 & & & \bar{I}_{\xi} + \beta_0^2 + 2\bar{I}_{\xi\eta}\phi_0 + \phi_0^2 \\ & & & -\beta_0 \end{bmatrix}$$

[C] =

$$-2\beta_0(\beta_0 + \beta_p) + \frac{1}{8}\gamma\phi_0 - \frac{1}{24}\gamma\bar{c}$$

$$- \frac{1}{24}\gamma\beta_0(4\lambda - 3\theta_0) - \frac{1}{6}\gamma(\frac{1}{2}\bar{c} - \bar{e}_A)$$

$$2(\beta_0 + \beta_p) + 2\theta_0$$

$$+ \frac{1}{24}\gamma(4\lambda - 3\theta_0)$$

$$\frac{1}{8}\gamma$$

$$-2(\bar{I}_{\beta\gamma} + \phi_0)(\beta_0 + \beta_p)$$

$$- \frac{1}{12}\gamma\beta_0(4\lambda - 3\theta_0)$$

$$+ \frac{1}{12}\gamma(\frac{1}{2}\bar{c} - \bar{e}_A)(3\lambda - 2\theta_0)$$

$C_{do}/4a$

$$-2(\beta_0 + \beta_p)$$

$$-2\theta_0$$

$$- \frac{1}{12}\gamma(4\lambda - 3\theta_0)$$

$$\frac{1}{32}\gamma\bar{c}^2 - \frac{3}{16}\gamma\bar{c}\bar{e}_A + \frac{1}{4}\gamma\bar{e}_A^2$$

$$- \frac{1}{24}\gamma\bar{c}\beta_0(3\lambda - 2\theta_0)$$

$$2(\bar{I}_{\beta\gamma} + \phi_0)(\beta_0 + \beta_p)$$

$$+ \frac{1}{24}\gamma\beta_0(4\lambda - 3\theta_0) + \frac{1}{12}\gamma\bar{e}_A(3\lambda - 2\theta_0)$$

$$2\beta_0(\beta_0 + \beta_p) + \frac{1}{8}\gamma\phi_0 + \frac{1}{6}\gamma\bar{e}_A$$

$$+ \frac{1}{12}\gamma\beta_0(4\lambda - 3\theta_0)$$

(5.3)

[K] =

$$\begin{aligned}
 & \nu_p^2 + 1 + \bar{e}_f \bar{e}_H - 2(\beta_0 + \beta_p)^2 \\
 & - \frac{1}{24} \gamma (\beta_0 + \beta_p) (8\lambda - 3\theta_0) \\
 & - \frac{1}{6} \gamma \left(\frac{1}{2} \bar{c} - \bar{e} \right) + \frac{1}{8} \gamma \beta_0 \\
 & \theta_0 + \frac{1}{8} \gamma (\beta_0 + \beta_p) \\
 & \nu_p^2 + \bar{e}_f \bar{e}_H - (\beta_0 + \beta_p)^2 \\
 & - \frac{1}{12} \gamma (\beta_0 + \beta_p) (4\lambda - 3\theta_0) \\
 & \theta_0 + \frac{1}{6} \gamma (\beta_0 + \beta_p) (3\lambda - 2\theta_0) \\
 & + \frac{1}{12} \gamma \left(\frac{1}{2} \bar{c} - \bar{e} \right) (3\lambda - 2\theta_0) \\
 & - (2\beta_0 + \beta_p) \theta_0 + \bar{I}_f \gamma + \phi_0 \\
 & + \frac{1}{24} \gamma (6\lambda^2 - 8\lambda\theta_0 + 3\theta_0^2) \\
 & - \frac{1}{8} \gamma - \frac{1}{3} \gamma \bar{e}_H + \frac{1}{16} \gamma \beta_p^2 + \frac{1}{16} \gamma (\beta_0 + \beta_p)^2 \\
 & + \frac{1}{12} \gamma (3\lambda^2 - 8\lambda\theta_0 + 3\theta_0^2) \\
 & (\beta_0 + \beta_p) \\
 & + \frac{1}{12} \gamma (4\lambda - 3\theta_0) \\
 & (\beta_0 + \beta_p) \\
 & + \frac{1}{24} \gamma (4\lambda - 3\theta_0) \\
 & \bar{I}_f (\nu_\theta^2 + 1) - \bar{e}_f \bar{e}_H \beta_0 \beta_p - \beta_0 (\beta_0 + \beta_p) \\
 & - \frac{1}{6} \gamma \bar{e}_A - \frac{1}{8} \gamma \phi_0 - \frac{1}{12} \gamma \beta_0 (4\lambda - 3\theta_0)
 \end{aligned}$$

(5.4)

5.1

STEADY EQUATIONS

The steady blade position β_0 is the solution of the equations of motion (3.14-16) including the applied aerodynamic moments (4.14-16), with all time derivatives zeroed. In their present form the equations of motion are quite complex and the steady aerodynamic moments more so. However, the trigonometric functions can be expanded and the ordering scheme applied to keep the most important terms.

Furthermore, the θ_0 equation need not be considered. This is because θ_0 will be prescribed for the desired power setting, which is related to λ and θ_0 as well as γ , \bar{c} , and C_{d0}/a . The power coefficient is not constant if any of these parameters is varied without adjusting the others. Also, γ and \bar{c} are not independent.

After some algebra, the ordered equation for β_0 is found to be quadratic, but uncoupled with ϕ_0 .

$$\begin{aligned}
 & [2\beta_p - \frac{1}{48}\gamma(8\lambda - 3\theta_0)]\beta_0^2 \\
 - & [\nu_\phi^2 + 1 + \bar{e}_\beta \bar{e}_H - 2\beta_p^2 - \theta_0^2 - \frac{1}{24}\gamma(8\lambda - 3\theta_0)\beta_p - \frac{1}{6}\gamma(\frac{1}{2}\bar{c} - \bar{e}_A)]\beta_0 \\
 + & [\nu_\phi^2 \beta_s - (1 + \bar{e}_\beta \bar{e}_H - \theta_0^2)\beta_p - \bar{I}_\beta \gamma \theta_0 - \frac{1}{24}\gamma(4\lambda - 3\theta_0)(1 - \beta_p^2) + \\
 & - \frac{1}{12}\gamma(3\lambda - 4\theta_0)\bar{e}_H + \frac{1}{6}\gamma(\frac{1}{2}\bar{c} - \bar{e}_A)\beta_p - \frac{1}{12}\gamma(3\lambda - 2\theta_0)\lambda\theta_0] \\
 & = 0
 \end{aligned} \tag{5.5}$$

The ordered equation for ϕ_0 is linear and dependent on β_0 .

$$\begin{aligned}
 & [\nu_\phi^2 - (\beta_0 + \beta_p)^2]\phi_0 = \\
 & [\nu_\phi^2 \beta_s + \bar{I}_\beta \gamma (\beta_0 + \beta_p)^2 - (\beta_0 + \beta_p)\theta_0 - \bar{e}_\gamma \bar{e}_H - \frac{1}{8}\gamma C_{d0}/a + \\
 & + \frac{1}{24}\gamma(6\lambda^2 - 8\lambda\theta_0 + 3\theta_0^2) - \frac{1}{12}\gamma(\beta_0 + \beta_p)^2(3\lambda - 2\theta_0)\lambda + \\
 & + \frac{1}{24}\gamma\beta_p^2(4\lambda - 3\theta_0)\theta_0 - \frac{1}{12}\gamma(\frac{1}{2}\bar{c} - \bar{e}_A)(\beta_0 + \beta_p)(3\lambda - 2\theta_0) + \\
 & - \frac{1}{6}\gamma(3\lambda - 2\theta_0)\theta_0 \bar{e}_H]
 \end{aligned} \tag{5.6}$$

In practice, θ_0 is prescribed, and these equations are solved sequentially for β_0 and ϕ_0 . After calculating the blade steady position, the stability of the blade is examined by extracting the eigenvalues of equation (5.1). These occur as complex conjugate pairs, $a_j \pm i\nu_j$ or as real roots a_j . Both the damping a_j and the frequency ν_j are expressed as ratios per revolution because nondimensional time $\gamma = \Omega t$ is used.

Chapter 6.

AEROELASTIC STABILITY
 OF THE EQUIVALENT HINGE MODEL

No complete parametric study is attempted due to the number of parameters, and the fact that any specific blade design can be easily studied as necessary. Rather, a standard case similar to the NASA MOD-0 wind turbine is used [1]. Two subcases are studied: a rotor precone downwind and a rotor without precone. Table 6.1 lists the parameters. (Tables and Figures appear together at the end of this thesis for convenient comparison to one another.) The effects of key parameters are examined in relation to the standard case by holding all parameters at their standard value except the parameters being plotted.

For the purposes of this section, the blade is assumed to be uniform. If I_0 is the pitching moment of inertia about the center of gravity and e_I is the distance the cross-section center of gravity is forward of the elastic axis, it can be shown that

$$\bar{I}_I = \bar{I}_0 + 3\bar{e}_I^2 \quad \bar{I}_{I, \gamma} = \frac{3}{2}\bar{e}_I \quad (6.1)$$

where

$$\bar{I}_0 = I_0/I, = I_0/\frac{1}{3}ML^2 \quad \bar{e}_I = e_I/L$$

These definitions allow direct comparison of \bar{e}_I to \bar{e}_A and to other studies.

Two representations of stability which appear often in the literature [e.g. 30, 9] are stability boundaries ($\sigma_j = 0$) on the plane of v_ϕ versus \bar{e}_I and on the plane of v_ϕ versus v_ϕ . Their advantage is that they show the interaction of two parameters and much information is conveyed by comparing two such plots with one other parameter changed. However, a shortcoming is that the strength of the instability is not indicated. Such information would be needed to assess a faulty blade design. Thus, plots of the damping ratio versus the parameter of interest, and root locus plots, are both useful as well.

Some general statements serve to introduce the discussion of aeroelastic stability trends and phenomena.

- 1) The flap damping is relatively large.
- 2) The lag damping is relatively small.
- 3) The pitch damping can approach zero under certain circumstances.
- 4) Lift couples flap to pitch in a strongly unsymmetric manner.

The resulting behavior divides the following discussion into two parts. First, classical flutter with frequency near v or classical divergence may occur. Second, a weak instability with frequency near v_ϕ may occur. The flap degree of freedom always remains well damped.

ORIGINAL PAGE IS
OF POOR QUALITY

6.1 CLASSICAL FLUTTER AND DIVERGENCE

Stability boundaries of the first type on the plane of v_0 versus \bar{e}_I , and on planes of v_0 versus related parameters \bar{e}_A and ρ_s , are adequate for the discussion of classical pitch-flap flutter and torsional divergence. For wind turbines the flexibility of the pitch change mechanism reduces the blade torsion natural frequency. The combined frequency ratio v_0 is important because of its connection with the cost of a wind turbine system.

Figure 6.1 defines the minimum v_0 required for stability of the preconed blade, which increases as the center of gravity is moved aft of the elastic axis. Figure 6.2 is the corresponding plot for the flat rotor. The $\bar{I}_{\xi\eta}$ (\bar{e}_I) coupling of pitch and flap in the mass matrix and the stiffness matrix can give rise to flutter or divergence respectively, although the divergence is not prominent here. The motivating force is the large unsymmetric lift term ($-\frac{1}{8}y$ in K_{13}) which couples flap to pitch but not pitch to flap. Note that the independent lag instability is insensitive to \bar{e}_I and completely enclosed within the flutter boundary for these cases.

Flutter also occurs when the elastic axis is moved back from the aerodynamic center as shown by Figure 6.3. Comparing Figures 6.1 and 6.3 shows that for $\bar{e}_I > -.005$ or $\bar{e}_A < 0.005$ their effects are similar. This again

demonstrates that what is important is the total distance that the center of gravity is aft of the aerodynamic center, at least for $\bar{e}_A - \bar{e}_I < \bar{c}/4$. When \bar{e}_A approaches $\bar{c}/6$, the pitch damping approaches zero. This gives the apparent asymptote of Figure 6.3 at $\bar{e}_A = 0.0066$. However, cases such as this do stretch the quasisteady assumption.

Inspection of the coefficients of the perturbation equations (5.1) shows the split personality of ϕ_0 which is proportional to ϕ_S and moves both the aerodynamic center and the center of gravity forward of the pitch axis. Figure 6.4 shows that, like a fixed wing, sweep forward gives divergence while sweep back gives flutter, at least if v_ϕ is low enough.

In all of these cases the flutter boundary encloses the boundary of the independent lag instability which proceeds at the lag frequency ratio v_ϕ . This suggests the idea of separating the three degree of freedom model into several two degree of freedom submodels. These would retain the steady blade position terms. Their advantage is that the new fourth order characteristic equation can be solved by hand calculation. The v_ϕ versus \bar{e}_I stability boundaries of Figure 6.1 were reproduced in Figure 6.5 by this technique with the pitch-flap and lag-pitch submodels. As could be expected, the flap-pitch flutter boundary compares

quite well. The lag-pitch instability boundary is not as good an approximation since the system is deprived of the flap damping.

6.2 LAG INSTABILITIES

Stability boundaries of the second type on the plane of v_ϕ versus v_β show the extent of unstable regions and how they are expanded by the various parameters, but must be supplemented by root locus plots showing the subtle interaction of the roots and the severity of the instabilities. The pitch frequency v_θ is still a key parameter, but so are β_p and β_s , λ and θ_0 .

Figure 6.6 clearly shows three regions of instability for the precone rotor. The familiar pitch-flap flutter and divergence is due to the increase in ϕ_0 as v_ϕ is reduced (see Figure 6.4). There is a region of flap-lag instability associated with the matched stiffness case $v_\phi = v_\beta$ which may occur when all three frequency ratios are reduced as in the case of an overspeeding rotor. The third region, near the v_ϕ ordinate, is of most interest. This "stiff in-plane" region is very sensitive to the parameters mentioned above.

The couplings are much more subtle than those of the flutter region:

- 1) β_0 couples ϕ and θ in the mass matrix.
- 2) $(\beta_0 + \beta_p)$ couples ϕ and θ in the stiffness matrix.
- 3) Coriolis terms couple β and ϕ .
- 4) There are unsymmetric damping terms due to λ and θ_0 .
- 5) There is unsymmetric stiffness coupling of ϕ and θ due to λ and θ_0 .

The last of these is associated with the torque component of the lift which is the prime mover of the lag-pitch instability.

The three degree of freedom character of these instabilities is emphasized by another look at the two degree of freedom submodels. In Figure 6.7 as before, the flutter boundary so calculated compares well with that of Figure 6.6. But while the flap-lag region is poorly represented, the lag-pitch submodel predicts no boundary at all.

Figure 6.8 corresponds to Figure 6.6 for the flat rotor with $\beta_p = 0$. Especially noteworthy is that the lag-pitch and flap-lag regions have merged. They are related in proceeding at the frequency v_ϕ .

Figure 6.9 shows the effect of increasing the inflow angle λ , which greatly enlarges the lag-pitch instability region. In this particular plot, the power coefficient is

not the same as that of Figure 6.6. A case such as this represents a situation where an increased inflow is not yet compensated by the pitch setting. This is the only type of variation presented in which the power is not held constant.

Halving the pitch frequency ratio v_p also enlarges this region as shown by Figure 6.10. This plot should again be compared to Figure 6.6.

Changing β_s can have a drastic effect on these stability boundaries, as Figure 6.11 demonstrates. Here the rotor blade has been drooped downwind on the precone rotor. This built-in flap angle has a direct influence on the steady flap angle β_0 . Part of the effects of β_p and of λ and θ_0 also come through the steady flap equation (5.5). The leading terms are

$$\beta_0 \sim [v_\beta^2 \beta_s - \beta_p - \frac{1}{24} \gamma (4\lambda - 3\theta_0)] / (1 + v_\beta^2) \quad (6.2)$$

The couplings of ϕ and θ are all influenced by β_0 which also increases the Coriolis coupling between ϕ and β .

The resulting complicated effect of β_s through β_0 is shown in Figure 6.12, a plot of the damping of the lag-pitch mode ϵ versus the built-in flap angle β_s . Had β_s been picked as $-.15$ or $-.05$, the lag-pitch instability region in Figure 6.11 would not have extended to the standard MOD-0 point at $v_\beta = 2.5$ and $v_\phi = 3.6$. The range of β_s which is unstable is small for negative β_s and the instability is a weak one, while positive β_s is generally destabilizing.

The complex interaction of parameters through the steady equations thwarts a more specific general statement about the lag-pitch instability.

To examine this instability more closely, root locus plots on the λ versus α plane are useful. Only the upper half plane will be shown, since the α axis is a line of symmetry. The three branches will be labeled conventionally as β , ϕ , and θ with respect for their origins, even though this may not always represent the nature of the corresponding eigenvector.

The preconed case of Figure 6.12 for the β_0 variation is replotted in this manner in Figure 6.13. The corresponding root locus for the flat rotor is presented in Figure 6.14. These plots show the ϕ branch crossing and recrossing the $\alpha = 0$ line in a relatively weak fashion. They clearly show the sympathetic participation of the β degree of freedom while the eigenvalue of the ϕ mode is dominated by ϕ and θ .

The migration of the roots as v_0 is reduced is plotted for both the preconed and flat rotor in Figures 6.15 and 6.16. In both cases, the θ branch (flutter) precedes the ϕ branch into the right half plane, though only slightly for the flat rotor. The θ branch also finishes near the lag frequency v_θ while the ϕ branch continues to retreat as v is reduced. It is the frequency of this branch which coalesces with that of the β branch. In fact both the ϕ

ORIGINAL PAGE IS
OF POOR QUALITY

and θ eigenvalues are dominated by the θ degree of freedom. The ϕ instability also can no longer be characterized as weak.

The similar root locus of Figure 6.17 for the preconed rotor but with $v_{\beta} = v_{\phi} = 2.5$ shows the weak nature of the flap-lag instability. The stability boundary is just less than $v_{\phi} = 5$, confirming Figure 6.10.

ORIGINAL PAGE IS
OF POOR QUALITY

Chapter 7. COMPARISON OF EQUIVALENT HINGE
 AND MODAL MODELS

To conclude the discussion of the equivalent hinge model, it is illuminating to compare and contrast it with a simple modal model derived by this author [20]. For convenience, this model is reviewed in Appendix A. The equations of motion of an isolated HAWT blade were reduced to a three degree of freedom modal model using Galerkin's method. One mode each was used for out-of-plane bending (w), inplane bending (v), and torsion (θ). Many details of the blade were modeled, including built-in twist, taper, and blade cross-section properties all varying along the span. All of these entered the equations as averages weighted by the mode shape functions.

The modal model is a three degree of freedom mathematical model of the blade. In contrast, the equivalent hinge model is a three degree of freedom mechanical analog of the blade, and the equations of motion derived here are those of this analog. Comparison of the two sets of equations reveals many differences, which this chapter will discuss. Their sources are:

- 1) The deflection shapes.
- 2) The coordinates.
- 3) Structural couplings.

Also, the modal model is less general, with a narrower ordering scheme. In particular, squares and products of the steady deflections such as β_0^2 and $\beta_0\theta_0$ appear in the equivalent hinge equations, but their counterparts do not appear in the modal equations.

In the modal model, the deflection of the elastic axis in the z and y directions, and the torsional deflection, respectively, are

$$\begin{aligned} w &= \gamma_w(x) q_w(t) \\ v &= \gamma_v(x) q_v(t) \\ \theta &= \gamma_\theta(x) q_\theta(t) \end{aligned} \quad (7.1)$$

where γ_n is the mode shape and q_n is the generalized coordinate. Whereas the deflection shapes for the modal model were taken as the nonrotating natural mode shapes, for the equivalent hinge model the deflection shapes are

$$\begin{aligned} \gamma_w = \gamma_v &= \begin{cases} x/L & 0 < x < L \\ 0 & \text{elsewhere} \end{cases} \\ \gamma_\theta &= \begin{cases} 1 & 0 < x < L \\ 0 & \text{elsewhere} \end{cases} \end{aligned} \quad (7.2)$$

That is, the blade is a straight line and all of the torsion is at the root. Many small differences between these models arise because the equivalent hinge deflection shapes weight spanwise averages of cross-section properties differently.

Modeling the blade with all torsion lumped at the root is justified for the common case where the root torsion predominates. In other cases a model with the pitch equivalent hinge outboard, such as one developed by Chopra may be more satisfactory [34].

The modal generalized coordinates were expressed as sums of steady deflections and perturbations in the same manner as the equivalent hinge coordinates. When the above deflection shapes were utilized, there is a straightforward relationship between the two coordinate sets. For the purposes of this chapter, this relationship can be expressed as

$$\begin{aligned} q_{w_0} &= \beta_0 \\ q_{v_0} &= \phi_0 - \beta_0 \theta_0 \\ q_0 &= \theta_0 \end{aligned} \quad (7.3)$$

and

$$\begin{aligned} \tilde{q}_w &= \tilde{\beta} + \theta_0 \tilde{\phi} + \phi_0 \tilde{\theta} \\ \tilde{q}_v &= \tilde{\phi} - \theta_0 \tilde{\beta} - \beta_0 \tilde{\theta} \\ \tilde{q}_\theta &= \tilde{\theta} \end{aligned} \quad (7.4)$$

Many apparent discrepancies between the equations dissolve when the deflection shapes (7.2) are substituted into the modal equations and these transformations are applied.

Structural couplings which arise in the modal model because of built-in twist and nonuniform cross-section stiffness properties do not arise in the equivalent hinge

model: Their mechanisms are not present. The most important structural coupling is between flap and lag bending. The form of the terms in the modal equations suggests that an average structural coupling angle θ_b can be used which is introduced into the equivalent hinge stiffness matrix (5.4) as follows

$$\begin{aligned}
 K_{\beta\beta} &= v_{\beta}^2 \cos^2 \theta_b + v_{\phi}^2 \sin^2 \theta_b + 1 + \dots \\
 K_{\beta\phi} &= (v_{\phi}^2 - v_{\beta}^2) \sin \theta_b \cos \theta_b + \theta_0 + \dots \\
 K_{\phi\beta} &= (v_{\phi}^2 - v_{\beta}^2) \sin \theta_b \cos \theta_b + \theta_0 + \dots \\
 K_{\phi\phi} &= v_{\phi}^2 \cos^2 \theta_b + v_{\beta}^2 \sin^2 \theta_b + e e_H + \dots
 \end{aligned} \tag{7.5}$$

This form was also used in reference [33]. The structural coupling angle θ_b can be approximated by the blade twist at one third span [29]. Similarly, the twist angle at three quarters span is generally taken as an approximate blade pitch setting θ_0 .

In principle, this comparison could be carried one step further by using it to relate the integrals of the modal model to the parameters of the equivalent hinge model. This would perhaps better define these parameters, but if such detailed information about the blade is known, it would probably be better to use the modal model.

The two models exhibit good numerical agreement, even though overall or typical section parameters are used to calculate equivalent hinge parameters. Both models have been applied to the MOD-0 wind turbine blade to demonstrate

21 30A 11 11 11
PAGE 12
ATTACHED

this point. The modal model results are taken from reference [20]. Figure 7.1 shows the effect of reducing the torsional stiffness of the control system, thus reducing ν . The two models predict the same minimum ν required, but give divergent results when the pitch frequency approaches the lag and flap frequencies. Figure 7.2 shows the effect of increasing the inflow angle λ , again without holding the power constant. Figure 7.3 shows the effect of changing the precone angle β_p .

The real usefulness of the equivalent hinge model is in understanding the effects of the various parameters and in simplifying the complex physics of the HAWT blade. This model can be used to test concepts, to begin design before details of a proposed blade are known, or to check the results of more complicated analyses. In short, the equivalent hinge model is a rotary-wing counterpart to the "typical section" of fixed-wing aeroelasticity.

Chapter 8.

MODELING TECHNIQUES FOR THE ROTOR-TOWER SYSTEM

The HAWT system is liable to various aeroelastic and mechanical instabilities and resonances which involve couplings between the main dynamic elements: the flexible tower, the yaw drive, the generator drive train, and the rotor consisting of several elastic blades and a hub of some configuration. Much less research has been presented for the rotor-tower system than for the isolated blade.

Several studies of mechanical instability and the effect of static imbalance without aerodynamics have been made. Dugundji developed such a model for a two-bladed rotor in connection with an experimental study [43]. He used an equivalent hinge representation with flap and lag for each blade, and two generalized coordinates for tower side-to-side and fore-to-aft motion. Sheu used a similar but more restricted model with blade lagging and tower side-to-side motion only [44]. He investigated ground resonance type instabilities for both two and three blades.

Several studies of aeroelastic stability and response have also been presented. Warmbrodt and Friedmann derived nonlinear equations of motion and loads for the rotor-tower system [45]. Galerkin's method was applied to study a MOD-0 type wind turbine with two blades. They used one lag and

one flap mode per blade, and one mode each for tower torsion, side-to-side bending, and fore-to-aft bending. Hultgren and Dugundji developed a similar linear model for the three-bladed case [46]. They studied mechanical stability and forced vibrations due to imbalance, gravity, and wind shear. Thresher, et al., examined the response of a three-bladed rigid rotor on a flexible tower to atmospheric turbulence [47]. Bousmann and Hodges presented an excellent experimental study of the aeromechanical stability of a three bladed hingeless rotor on a flexible pylon [48]. Bundas and Dugundji have conducted some experiments on the yaw behaviour of a model wind turbine with two blades [49].

Recently, Janetzke and Kaza presented an analytic rotor-tower model with a two-bladed teetering rotor applicable to the MOD-2 [50]. They used a teetering rotor, one flap mode for each blade, and a kind of equivalent pivot model of the tower nacelle with yaw and pitch degrees of freedom. Whirl flutter was investigated by numerically integrating the equations in time. This is quite similar to an approach used by Hall to study whirl flutter of a teetering proprotor [51].

Finally, it should be noted that various computer codes have been applied to the rotor-tower problem [e.g. 2, 12]. However, documentation of the theory used is generally poor, and very few parameter variations are given.

In the chapters that follow, a linear aeroelastic modeling methodology is developed for the MOD-2 type wind turbine. Equations of motion and loads are derived in closed form for a two-bladed teetering rotor with elastic blades on a flexible support. One lag and one flap mode are used for each blade, and six general hub degrees of freedom are assumed. A solution method for the resulting periodic coefficient equations is presented which is applicable to stability, steady-state response, and transient response calculations.

The methodology developed is demonstrated with a simple yaw, pitch and teeter model similar to that of Kaza and Janetzke. A limited study of the effect of imbalance is made. Whirl flutter and divergence, as well as other instabilities are examined, and the effect of teeter, precone, and support stiffness are discussed. Some steady-state and transient response results are presented.

Thus, while Part I mostly concerns the MOD-0 type wind turbine with cantilever blades, Part II mostly concerns the MOD-2 type with a teetering rotor. Flutter, divergence, and lag instabilities like those discussed in Part I are possible for the teetered rotor as well, but are modified by the interaction of the blades. For the helicopter case, Shamie and Friedmann have analyzed the flap-lag-torsion stability of a teetering rotor on a rigid support [52]. This problem is not addressed by this thesis.

A mathematical model of a teetering rotor on a flexible support, once derived, is a valuable building block for investigating HAWT aeroelasticity. The development presented here allows flap and lag modes for each blade, teetering motion of the rotor, and six general hub degrees of freedom -- eleven degrees of freedom in all. Thus, the new information given by this derivation is essentially a description of the interaction between rotor modes and hub motion. The hub degrees of freedom can then be used to match the rotor to any kind of tower or support model, from simple to complex. This approach is taken by other analyses as well [10, 11].

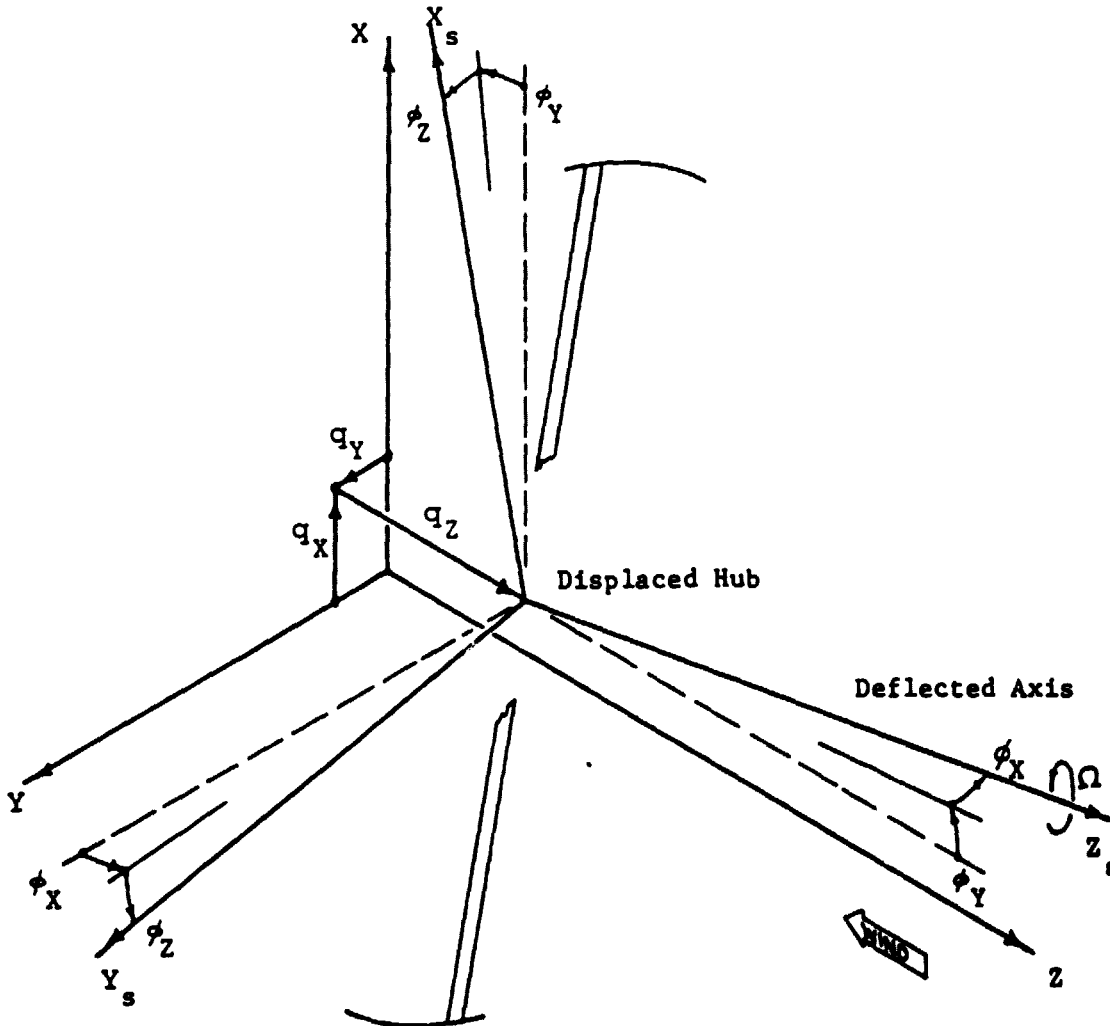
The equations of motion are derived in this chapter with gravity loads but without aerodynamic loads. The latter are developed in the following chapter. An energy approach similar to that of Part I is followed, but only linear terms will be obtained for the rotor-tower model.

9.1

COORDINATE SYSTEMS

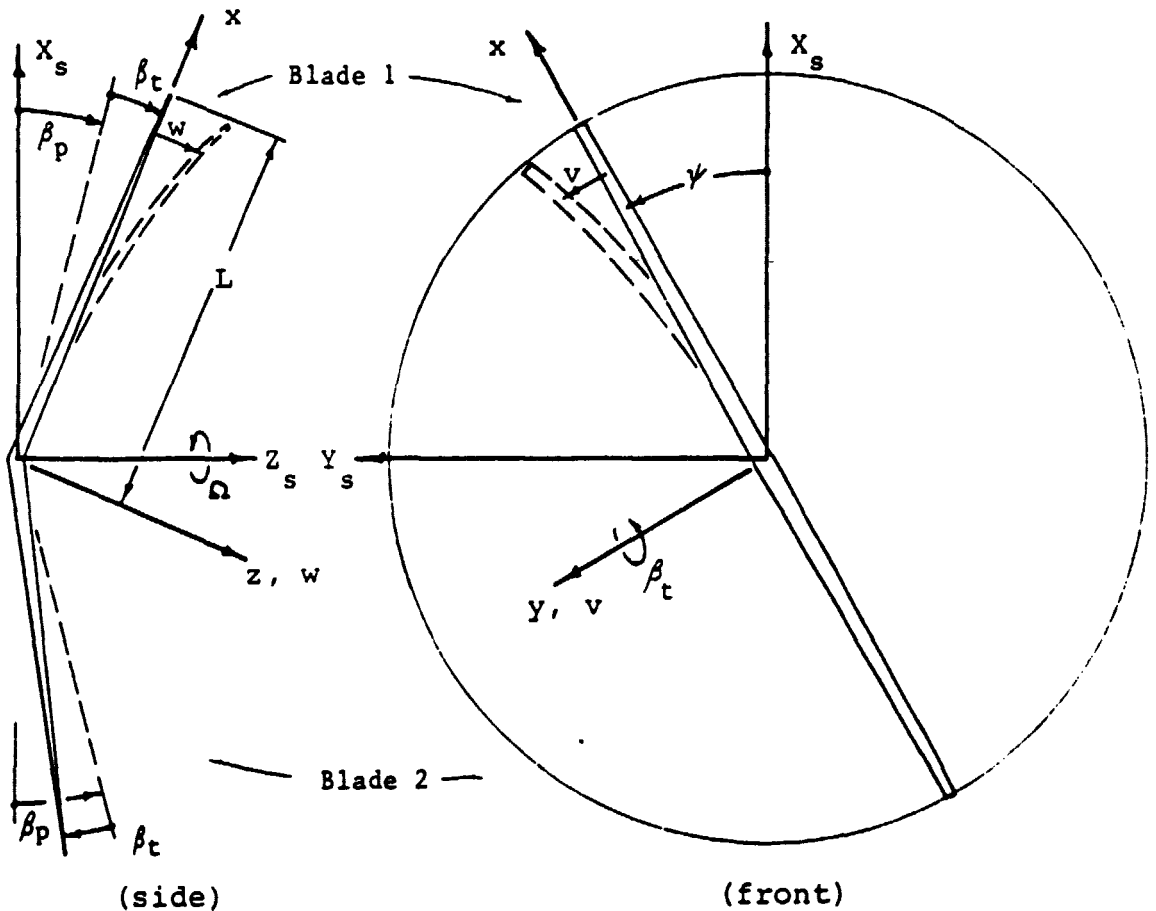
Three coordinate systems are used to describe the deflected position of a rotor blade as shown by Sketches 9.1 and 9.2. The inertial coordinate system $X Y Z$ is fixed in

space and has unit vectors $\hat{i} \hat{j} \hat{k}$. The shaft coordinate system $X_s Y_s Z_s$ ($\hat{i}_s \hat{j}_s \hat{k}_s$) defines the deflected position of the shaft axis and hub, but does not rotate. Finally, the blade coordinate system $x y z$ ($\hat{i} \hat{j} \hat{k}$) locates the rotating, teetering blade with x as the unbent position of the elastic axis. Elastic motion of the blade is described within this blade coordinate system.



Sketch 9.1 Inertial and Shaft Coordinates

Originally, the hub is at the $X Y Z$ origin, and the shaft axis is at the Z axis. The displaced hub is located by three Cartesian deflections q_X , q_Y , and q_Z , as shown by Sketch 9.1. The shaft axis Z_s is deflected in three rotations ϕ_X , ϕ_Y , and ϕ_Z about X , Y , and Z , respectively. Also, the rotor spins about Z_s at a constant rate Ω . This is not a restriction on the model however, since perturbations in rotation speed can be included in ϕ_Z .



Sketch 9.2

Shaft and Blade Coordinates

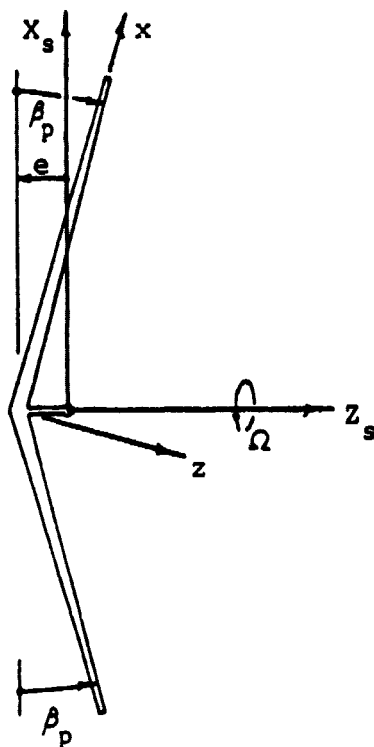
ORIGINAL PAGE IS
OF POOR QUALITY21 3044
10/10/72

Blade one is arbitrarily chosen as the reference blade in Sketch 9.2. The azimuth angle of blade one is $\gamma = \Omega t$. It should be noted that equations of motion and loads need be derived only for blade one. The results apply to blade two as well, but with $\gamma = \Omega t + \pi$ and $\beta_{t2} = -\beta_{t1}$ contributions from both blades are then summed as a final step in the derivation. The subscripts 1 and 2 are dropped from this point except where required for clarity.

The blades have an instantaneous teeter angle β_t in opposite directions, and a built-in precone angle β_p in the same direction as shown by Sketch 9.2. Both β_t and β_p are positive in the upwind direction for blade one.

As previously mentioned, elastic motion of the blade occurs in the x y z coordinate system: Flap bending w is in the z direction and lag bending v is in the y direction. The blade is also foreshortened by the bending, which gives rise to a deflection u in the x direction (not shown for clarity). Torsion and blade stretching are ignored in this analysis, because they are generally modes of much higher frequency for HAWTs.

To simplify Sketch 9.2, a small offset was omitted. A preconed rotor as shown is not balanced in teeter and flops forward under its own weight. Practical preconed rotors might counteract this by using a small undersling e as shown in Sketch 9.3. Thus, the teetering axis is actually situated in blade coordinates at $(e \sin \beta_p, 0, e \cos \beta_p)$.



Sketch 9.3 Rotor Undersling

To summarize, the displacements and rotations in going from the inertial system to the blade system are, in order of appearance:

Three Cartesian deflections q_x q_y q_z .

Three rotations ϕ_x ϕ_y ϕ_z .

Shaft rotation γ .

Precone β_p and teetering β_t .

Undersling e .

Elastic blade deflections u v w .

The rotations are taken in the order ϕ_y , then ϕ_x , then ϕ_z and γ , then β_p and β_t . Thus, the transformation between blade unit vectors and inertial unit vectors is

ORIGINAL PAGE IS
OF POOR QUALITY

$$[\hat{i} \ \hat{j} \ \hat{k}] = [\hat{i} \ \hat{j} \ \hat{k}][T_a] \quad (9.1)$$

where $[T_a] = [T_y][T_x][T_\psi][T_B] =$

$$\begin{bmatrix} \cos\phi_y & 0 & \sin\phi_y \\ 0 & 1 & 0 \\ -\sin\phi_y & 0 & \cos\phi_y \end{bmatrix} \begin{bmatrix} 1 & 0 & 0 \\ 0 & \cos\phi_x & -\sin\phi_x \\ 0 & \sin\phi_x & \cos\phi_x \end{bmatrix} \begin{bmatrix} \cos\psi & -\sin\psi & 0 \\ \sin\psi & \cos\psi & 0 \\ 0 & 0 & 1 \end{bmatrix} \begin{bmatrix} \cos B & 0 & -\sin B \\ 0 & 1 & 0 \\ \sin B & 0 & \cos B \end{bmatrix}$$

here, $\psi = \gamma + \phi_z$ and $B = \beta_t + \beta_p$ for convenience.

9.2

KINETIC ENERGY

With all this information, the radius vector in the inertial coordinate system can be written for a point x on the rotating, deflected blade. For blade one, it is

$$\begin{aligned} \vec{R} &= [\hat{i} \ \hat{j} \ \hat{k}] \begin{Bmatrix} x \\ y \\ z \end{Bmatrix} \\ &= [\hat{i} \ \hat{j} \ \hat{k}] \begin{Bmatrix} q_x \\ q_y \\ q_z \end{Bmatrix} + [\hat{i} \ \hat{j} \ \hat{k}] \begin{Bmatrix} u + x - e \sin\beta_p \\ v \\ w - e \cos\beta_p \end{Bmatrix} \end{aligned} \quad (9.2)$$

And, by substituting equation (9.1) in, this becomes

$$\vec{R} = [\hat{i} \ \hat{j} \ \hat{k}] \left\{ \begin{Bmatrix} q_x \\ q_y \\ q_z \end{Bmatrix} + [T_a] \begin{Bmatrix} u + x - e \sin\beta_p \\ v \\ w - e \cos\beta_p \end{Bmatrix} \right\} \quad (9.3)$$

The corresponding velocity vector is

$$\vec{v} = [\hat{i} \ \hat{j} \ \hat{k}] \left\{ \begin{array}{l} \dot{q}_x \\ \dot{q}_y \\ \dot{q}_z \end{array} \right\} + [\dot{T}_a] \left\{ \begin{array}{l} u+x-e\sin\beta_p \\ v \\ w - e\cos\beta_p \end{array} \right\} + [T_a] \left\{ \begin{array}{l} \dot{u} \\ \dot{v} \\ \dot{w} \end{array} \right\} \quad (9.4)$$

Recall that blade torsion is neglected in this analysis. Torsional moments are also assumed to have little effect on the blade bending or the other degrees of freedom, particularly when contributions from both blades are added. Specifically, torsional moments which arise from inertial sources are neglected by assuming that the blade is a long, slender beam with all its mass $m(x)$ concentrated along the elastic axis x . The kinetic energy of the blade is then

$$\begin{aligned}
 w &= \gamma_w(x)q_w(t) \\
 v &= \gamma_v(x)q_v(t) \\
 u &= -\frac{1}{2}\delta_v q_v^2 - \frac{1}{2}\delta_w q_w^2
 \end{aligned}
 \tag{9.6}$$

where

$$\delta_v = \int_0^x (\gamma'_v)^2 dx \quad \text{and} \quad \delta_w = \int_0^x (\gamma'_w)^2 dx$$

This form of elastic deformation and the various matrices are substituted into equation (9.5). With all quadratic terms, the kinetic energy of blade one is

$$\begin{aligned}
 T &= \frac{1}{2}M_b [(\dot{q}_x)^2 + (\dot{q}_y)^2 + (\dot{q}_z)^2] + \frac{1}{2}[I_v(\dot{q}_v)^2 + I_w(\dot{q}_w)^2] \\
 &- S_b^* [\dot{q}_x(\dot{\beta}_t \cos \gamma - \dot{\phi}_y) + \dot{q}_y(\dot{\beta}_t \sin \gamma - \dot{\phi}_x)] \\
 &+ S_b \cos \beta_p [\dot{\beta}_t + \dot{\phi}_x \sin \gamma - \dot{\phi}_y \cos \gamma] \dot{q}_z \\
 &+ \Omega S_b^* [\dot{q}_x \sin \gamma - \dot{q}_y \cos \gamma] \beta_t - \Omega S_b \cos \beta_p [\dot{q}_x \sin \gamma - \dot{q}_y \cos \gamma] \\
 &+ \Omega S_b \cos \beta_p [\dot{\phi}_x \cos \gamma + \dot{\phi}_y \sin \gamma] \dot{q}_z \\
 &- \Omega S_v [\dot{q}_x \cos \gamma + \dot{q}_y \sin \gamma] q_v + \Omega S_w \sin \beta_p [\dot{q}_x \sin \gamma - \dot{q}_y \cos \gamma] q_w \\
 &- S_w [\sin \beta_p (\dot{q}_x \cos \gamma + \dot{q}_y \sin \gamma) - \dot{q}_z \cos \beta_p] \dot{q}_w \\
 &+ \frac{1}{2} I_b^{**} [(\dot{\beta}_t)^2 + 2\dot{\beta}_t \dot{\phi}_x \sin \gamma - 2\dot{\beta}_t \dot{\phi}_y \cos \gamma + (\dot{\phi}_x)^2 + (\dot{\phi}_y)^2] \\
 &+ \frac{1}{2} I_b \cos^2 \beta_p [(\dot{\beta}_t)^2 + 2\dot{\beta}_t \dot{\phi}_x \sin \gamma - 2\dot{\beta}_t \dot{\phi}_y \cos \gamma + (\dot{\phi}_x)^2 \sin^2 \gamma + \\
 &\quad - 2\dot{\phi}_x \dot{\phi}_y \sin \gamma \cos \gamma + (\dot{\phi}_y)^2 \cos^2 \gamma] \\
 &- S_v [\dot{q}_x \sin \gamma - \dot{q}_y \cos \gamma] \dot{q}_v + \Omega I_b^{**} [\dot{\phi}_x \cos \gamma + \dot{\phi}_y \sin \gamma] \beta_t \\
 &- \Omega I_b \cos^2 \beta_p [(\dot{\phi}_x \cos \gamma + \dot{\phi}_y \sin \gamma) \beta_t + \dot{\phi}_y \dot{\phi}_x] \\
 &+ \Omega I_{xv}^* [\dot{\beta}_t + \dot{\phi}_x \sin \gamma - \dot{\phi}_y \cos \gamma] q_v \\
 &- \Omega I_b^* \cos \beta_p [\dot{\phi}_x \cos \gamma + \dot{\phi}_y \sin \gamma] + \frac{1}{2} \Omega^2 I_b \cos^2 \beta_p [1 - \beta_t^2] + \dots
 \end{aligned}$$

$$\begin{aligned}
 & + \Omega I_{xw}^* \sin \beta_p [\dot{\phi}_x \cos \gamma + \dot{\phi}_y \sin \gamma] q_w + 4 \Omega^2 I_b^{**} \beta_c^2 \\
 & - \Omega I_{xw}^* \cos^2 \beta_p [\dot{\phi}_x \cos \gamma + \dot{\phi}_y \sin \gamma] q_w - \Omega^2 I_b^* \cos \beta_p \beta_c \\
 & + 4 \Omega^2 I_v q_v^2 + 4 \Omega^2 I_v \sin^2 \beta_p q_w^2 + \Omega^2 I_{xw}^* \sin \beta_p \beta_c q_w \\
 & - \Omega^2 I_{xw}^* \sin \beta_p \cos \beta_p q_w - I_{xv}^* [\dot{\phi}_x \cos \gamma + \dot{\phi}_y \sin \gamma] \dot{q}_v \\
 & + I_{xw}^* [\dot{\beta}_c + \dot{\phi}_x \sin \gamma - \dot{\phi}_y \cos \gamma] \dot{q}_w - 4 \Omega^2 \cos^2 \beta_p [H_v q_v^2 + H_w q_w^2] \\
 & + \Omega I_{xv} \cos \beta_p \dot{q}_v - \Omega I_{xv}^* \beta_c \dot{q}_v + \Omega I_{vw} \sin \beta_p [q_v \dot{q}_w - \dot{q}_v q_w] \\
 & - \Omega S_b \cos \beta_p [\dot{q}_x \cos \gamma + \dot{q}_y \sin \gamma] \dot{\phi}_z - 2 \Omega I_b^* \cos \beta_p \dot{\phi}_z \beta_c \\
 & - S_b \cos \beta_p [\dot{q}_x \sin \gamma - \dot{q}_y \cos \gamma] \dot{\phi}_z + 4 I_b \cos^2 \beta_p (\dot{\phi}_z)^2 \\
 & + \Omega I_b^* \cos \beta_p [\dot{\phi}_x \sin \gamma - \dot{\phi}_y \cos \gamma] \dot{\phi}_z + \Omega I_b \cos^2 \beta_p \dot{\phi}_z \\
 & - I_b^* \cos \beta_p [\dot{\phi}_x \cos \gamma + \dot{\phi}_y \sin \gamma] \dot{\phi}_z + I_{xv} \cos \beta_p \dot{\phi}_z \dot{q}_v \\
 & - 2 \Omega I_{xw}^* \sin \beta_p \cos \beta_p \dot{\phi}_z \dot{q}_w
 \end{aligned}
 \tag{9.7}$$

In this equation, the following definitions are used:

$$\begin{aligned}
 M_b &= \int_0^L m dx \\
 S_b &= \int x m dx & S_v &= \int \gamma_v m dx & S_w &= \int \gamma_w m dx \\
 I_b &= \int x^2 m dx & I_v &= \int \gamma_v^2 m dx & I_w &= \int \gamma_w^2 m dx \\
 I_{vw} &= \int \gamma_v \gamma_w m dx & I_{xv} &= \int \gamma_v x m dx & I_{xw} &= \int \gamma_w x m dx \\
 R_v &= \int \delta_v m dx & R_w &= \int \delta_w m dx \\
 H_v &= \int \delta_v x m dx & H_w &= \int \delta_w x m dx
 \end{aligned}
 \tag{9.8}$$

and

$$\begin{aligned}
 S_b^* &= S_b \sin \beta_p - M_b e & I_b^* &= I_b \sin \beta_p - S_b e \\
 I_{xv}^* &= I_{xv} \sin \beta_p - S_v e & I_{xw}^* &= I_{xw} \sin \beta_p - S_w e \\
 I_b^{**} &= I_b^* \sin \beta_p - S_b^* e
 \end{aligned}
 \tag{9.9}$$

These latter definitions reduce to zero for the case with neither precone nor undersling.

9.3 GRAVITY POTENTIAL ENERGY

In this analysis gravity is assumed to act in the negative X direction. The effect of built-in rotor axis tilt is not included. The potential energy of the blade is

$$V = g \int_0^L X m dx \quad (9.10)$$

From equation (9.2) and equation (9.1), the height of a point x on the blade is given as

$$\begin{aligned} X = q_x + & [\cos\phi_x \cos B \cos \Psi + \sin\phi_y \sin\phi_x \cos B \sin \Psi + \\ & + \cos\phi_x \sin B](u+x-e \sin \beta_p) \\ & + [-\cos\phi_y \sin \Psi + \sin\phi_y \sin\phi_x] v \\ & + [-\cos\phi_y \sin B \cos \Psi - \sin\phi_y \sin\phi_x \sin B \sin \Psi + \\ & + \sin\phi_y \cos\phi_x \cos B](w-e \sin \beta_p) \end{aligned} \quad (9.11)$$

As with the kinetic energy, the potential energy is expanded in terms up to quadratic in the displacements and velocities. Thus, the potential energy of blade one is

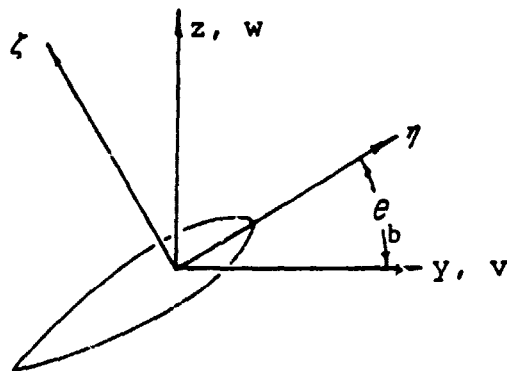
$$\begin{aligned} V = gM_b q + gS_b \cos \beta_p [\cos \gamma - \phi_2 \sin \gamma - \frac{1}{2} \phi_y^2 \cos \gamma + \beta_t \phi_y] \\ - \frac{1}{2} g \cos \beta_p \cos \gamma [R_v q_v^2 + R_w q_w^2] - gS_v [\sin \gamma + \phi_2 \cos \gamma] q_v \\ + gS_v [\cos \beta_p (\phi_y + \beta_t \cos \gamma) - \sin \beta_p (\cos \gamma - \phi_2 \sin \gamma)] q_w \\ + gS_b^* [\phi_y - \beta_t \cos \gamma + \beta_t \phi_2 \sin \gamma] \end{aligned} \quad (9.12)$$

**ORIGINAL PAGE IS
OF POOR QUALITY**

The spanwise integrals in this equation are defined as before (9.8-9).

9.4 STRAIN ENERGY

The elastic model of the blade is taken directly from reference [20] and is reviewed in Appendix A. However, only linear lag bending and flap bending are used; torsion and all nonlinear terms are ignored. A teeter spring is included, and structural coupling due to built-in twist of the blade $\theta_b(x)$ is allowed. Sketch 9.4 shows the principal axes defined by θ_b .



Sketch 9.4 Built-In Twist and Principal Axes

The strain energy of the blade is

$$U = \frac{1}{2}K_v q_v^2 + K_{vw} q_v q_w + \frac{1}{2}K_w q_w^2 + \frac{1}{2}K_t \theta_t^2 \quad (9.13)$$

Here, K_t is one half of the teeter spring rate, and the stiffness coefficients are defined as follows

$$\begin{aligned}
 K_v &= \int_0^L (EI_2 \cos^2 \theta_b + EI_1 \sin^2 \theta_b) (\gamma_v'')^2 dx \\
 K_{vw} &= \int_0^L (EI_2 - EI_1) \sin \theta_b \cos \theta_b (\gamma_v'' \gamma_w'') dx \\
 K_w &= \int_0^L (EI_2 \sin^2 \theta_b + EI_1 \cos^2 \theta_b) (\gamma_w'')^2 dx
 \end{aligned} \tag{9.14}$$

where

$$EI_2 = \int_{x\text{-sect}} E \eta^2 d\eta d\zeta \quad \text{and} \quad EI_1 = \int_{x\text{-sect}} E \zeta^2 d\eta d\zeta$$

9.5 EQUATIONS OF MOTION

With the kinetic energy (9.7), gravity potential energy (9.12), and internal strain energy (9.13) of the blade in hand, Lagrange's Equations are used to develop the equations of motion

$$\frac{d}{dt} \left(\frac{\partial T}{\partial \dot{q}_n} \right) - \frac{\partial T}{\partial q_n} + \frac{\partial V}{\partial q_n} - \frac{\partial U}{\partial q_n} = Q_n \tag{9.14}$$

where the q_n are the generalized coordinates q_x, q_y, \dots, q_w and the Q_n are corresponding generalized loads.

Lagrange's equations are applied first to blade one with $q_v = q_{v1}$, and $q_w = q_{w1}$ in T, V and U . Then they are applied to blade two with $q_v = q_{v2}$, $q_w = q_{w2}$, $\beta_c = -\beta_c$, and $\gamma = \gamma + \pi$. The contributions from both blades are added to give the equations of motion in eleven degrees of freedom:

ORIGINAL PAGE IS
OF POOR QUALITY

six hub deflections and rotations, teeter, lag bending of each blade, and flap bending of each blade. No contributions from the tower or other system components are yet included.

Some simplification is wrought by utilizing elastic modes for the complete rotor instead of separate modes for each blade. Consider the transformation

$$\begin{aligned}q_{ws} &= \frac{1}{2}[q_{w1} + q_{w2}] \\q_{wa} &= \frac{1}{2}[q_{w1} - q_{w2}]\end{aligned}\tag{9.15}$$

Then q_{ws} indicates motion symmetric about the rotor centerline and q_{wa} indicates antisymmetric. Opposite definitions must be used to give lag modes which are symmetric ("C" shaped) and antisymmetric ("S" shaped) in the usual sense.

$$\begin{aligned}q_{va} &= \frac{1}{2}[q_{v1} + q_{v2}] \\q_{vs} &= \frac{1}{2}[q_{v1} - q_{v2}]\end{aligned}\tag{9.16}$$

These sets of equations are multiblade coordinate transformations of a kind for two-bladed rotors. Their implications are made clear in Chapter 11.

The vector of generalized coordinates and the vector of corresponding generalized loads are defined as

$$\{q\} = \begin{Bmatrix} q_x \\ q_y \\ q_z \\ \phi_x \\ \phi_y \\ \phi_z \\ \beta_t \\ q_{va} \\ q_{vs} \\ q_{ws} \\ q_{wa} \end{Bmatrix} \quad \{Q\} = \begin{Bmatrix} P_x \\ P_y \\ P_z \\ Q_x \\ Q_y \\ Q_z \\ Q_t \\ P_{va} \\ P_{vs} \\ P_{ws} \\ P_{wa} \end{Bmatrix} \quad (9.17)$$

The equations of motion in these variables take the standard form

$$[M]\{\ddot{q}\} + [C]\{\dot{q}\} + [K]\{q\} = \{Q\} \quad (9.18)$$

The periodic-coefficient matrices of these equations are given on the following pages. For convenience in comparing them to the aerodynamic derivatives of Chapter 10, they are also given in individual coefficient form. These equations are left dimensional until the tower contributions can be added.

ORIGINAL PAGE IS
OF POOR QUALITY

(9.15)

$2M_b$	0	0	$2S_b^a$	0	$-2S_b^a \cos \beta$	0	$-2S_b^a \sin \beta$	0	$-2S_b^a \sin \beta \cos \beta$
0	$2M_b$	0	0	0	$-2S_b^a \sin \beta$	0	$2S_b^a \cos \beta$	0	$-2S_b^a \sin \beta \sin \beta$
0	0	$2M_b$	0	0	0	0	0	$2S_b^a \cos \beta$	0
0	$-2S_b^a$	$(1_b \cos^2 \beta_p (1 - \cos 2\beta) + 21_b^{aa})$	$-1_b \cos^2 \beta_p \sin 2\beta$	0	$(21_b \cos^2 \beta_p \sin \beta + 21_b^{aa} \sin \beta)$	0	$-21_b^a \cos \beta$	0	$(21_{xv} \cos^2 \beta_p \sin \beta + 21_{xv}^{aa} \sin \beta \cos \beta)$
$2S_b^a$	0	$-1_b \cos^2 \beta_p \sin 2\beta$	$(1_b \cos^2 \beta_p (1 + \cos 2\beta) + 21_b^{aa})$	0	$-(21_b \cos^2 \beta_p \cos \beta + 21_b^{aa} \cos \beta)$	0	$-21_b^a \sin \beta$	0	$-(21_{xv} \cos^2 \beta_p \cos \beta + 21_{xv}^{aa} \sin \beta \cos \beta)$
0	0	0	0	$21_b \cos^2 \beta_p$	0	$21_{xv} \cos \beta_p$	0	0	0
$-2S_b^a \cos \beta$	$-2S_b^a \sin \beta$	$(21_b \cos^2 \beta_p \sin \beta + 21_b^{aa} \sin \beta)$	$-(21_b \cos^2 \beta_p \cos \beta + 21_b^{aa} \cos \beta)$	0	21_b	0	0	0	$(21_{xv} \cos^2 \beta_p + 21_{xv}^{aa} \sin \beta)$
0	0	0	0	0	$21_{xv} \cos \beta_p$	0	21_v	0	0
$-2S_b^a \sin \beta$	$-2S_b^a \cos \beta$	$-21_{xv}^a \cos \beta$	$-21_{xv}^a \sin \beta$	0	0	0	0	21_v	0
0	0	$2S_b^a \cos \beta$	0	0	0	0	0	0	0
$-2S_b^a \sin \beta \cos \beta$	$-2S_b^a \sin \beta \sin \beta$	$(21_{xv} \cos^2 \beta_p \sin \beta + 21_{xv}^{aa} \sin \beta \cos \beta)$	$-(21_{xv} \cos^2 \beta_p \cos \beta + 21_{xv}^{aa} \sin \beta \cos \beta)$	0	$(21_{xv} \cos^2 \beta_p + 21_{xv}^{aa} \sin \beta)$	0	0	0	21_v

ORIGINAL PAGE 15
OF POOR QUALITY

$$\{Q\} = \begin{Bmatrix} -2gM_b \\ 0 \\ 0 \\ 0 \\ -2gS_b^* \\ 0 \\ 2gS_b^* \cos \psi \\ 0 \\ 2gS_v \sin \psi \\ -2\Omega^2 I_{xw} \sin \beta_p \cos \beta_p \\ 2gS_w \sin \beta_p \cos \psi \end{Bmatrix} \quad (9.22)$$

ORIGINAL PAGE IS
OF POOR QUALITY

$$M_{11} = 2M_b$$

$$M_{15} = 2S_b^*$$

$$M_{17} = -2S_b^* \cos y$$

$$M_{19} = -2S_v \sin y$$

$$M_{1,11} = -2S_w \sin \beta_p \cos y$$

$$M_{12} = M_{13} = M_{14} = M_{16} = M_{18} = M_{1,10} = 0$$

$$M_{22} = 2M_b$$

$$M_{24} = -2S_b^*$$

$$M_{27} = -2S_b^* \sin y$$

$$M_{29} = 2S_v \cos y$$

$$M_{2,11} = -2S_w \sin \beta_p \sin y$$

$$M_{21} = M_{23} = M_{25} = M_{26} = M_{28} = M_{2,10} = 0$$

$$M_{33} = 2M_b$$

$$M_{3,10} = 2S_w \cos \beta_p$$

$$M_{31} = M_{32} = M_{34} = M_{35} = 0$$

$$M_{36} = M_{37} = M_{38} = M_{39} = M_{3,11} = 0$$

$$M_{42} = M_{24}$$

$$M_{44} = I_b \cos^2 \beta_p (1 - \cos y) + 2I_b^{**}$$

$$M_{45} = -I_b \cos^2 \beta_p \sin 2y$$

$$M_{47} = 2(I_b \cos^2 \beta_p + I_b^{**}) \sin y$$

$$M_{49} = -2I_{xv}^* \cos y$$

$$M_{4,11} = 2(I_{xv} \cos^2 \beta_p + I_{xw}^* \sin \beta_p) \sin y$$

$$M_{41} = M_{43} = M_{46} = M_{48} = M_{4,10} = 0$$

21 APR 1964
 12-111111-111111

ORIGINAL PAGE IS
 OF POOR QUALITY

$$M_{51} = M_{15}$$

$$M_{54} = M_{45}$$

$$M_{55} = I_b \cos^2 \beta_p (1 + \cos 2\gamma) + 2I_b^{**}$$

$$M_{57} = -2(I_b \cos^2 \beta_p + I_b^{**}) \cos \gamma$$

$$M_{59} = -2I_{xv}^* \sin \gamma$$

$$M_{5,11} = -2(I_{xw} \cos^2 \beta_p + I_{xw}^* \sin \beta_p) \cos \gamma$$

$$M_{52} = M_{53} = M_{56} = M_{58} = M_{5,10} = 0$$

$$M_{66} = 2I_b \cos^2 \beta_p$$

$$M_{68} = 2I_{xv} \cos \beta_p$$

$$M_{61} = M_{62} = M_{63} = M_{64} = 0$$

$$M_{65} = M_{67} = M_{69} = M_{6,10} = M_{6,11} = 0$$

$$M_{71} = M_{17}$$

$$M_{72} = M_{27}$$

$$M_{74} = M_{47}$$

$$M_{75} = M_{57}$$

$$M_{77} = 2I_b$$

$$M_{7,11} = 2I_{xw} \cos^2 \beta_p + 2I_{xw}^* \sin \beta_p$$

$$M_{73} = M_{76} = M_{78} = M_{79} = M_{7,10} = 0$$

$$M_{86} = M_{68}$$

$$M_{88} = 2I_v$$

$$M_{81} = M_{82} = M_{83} = M_{84} = 0$$

$$M_{85} = M_{87} = M_{89} = M_{8,10} = M_{8,11} = 0$$

ORIGINAL PAGE IS
OF POOR QUALITY

$$M_{91} = M_{19}$$

$$M_{92} = M_{29}$$

$$M_{94} = M_{49}$$

$$M_{95} = M_{59}$$

$$M_{99} = 2I_v$$

$$M_{93} = M_{96} = M_{97} = M_{98} = M_{9,10} = M_{9,11} = 0$$

$$M_{10,3} = M_{3,10}$$

$$M_{10,10} = 2I_w$$

$$M_{10,1} = M_{10,2} = M_{10,4} = M_{10,5} = 0$$

$$M_{10,6} = M_{10,7} = M_{10,8} = M_{10,9} = M_{10,11} = 0$$

$$M_{11,1} = M_{1,11}$$

$$M_{11,2} = M_{2,11}$$

$$M_{11,4} = M_{4,11}$$

$$M_{11,5} = M_{5,11}$$

$$M_{11,7} = M_{7,11}$$

$$M_{11,11} = 2I_w$$

$$M_{11,3} = M_{11,6} = M_{11,8} = M_{11,9} = M_{11,10} = 0$$

(9.19)

$$C_{17} = 4NS_b^* \sin \gamma$$

$$C_{19} = -4NS_v \cos \gamma$$

$$C_{1,11} = 4NS_w \sin \theta_p \sin \gamma$$

$$C_{11} = C_{12} = C_{13} = C_{14} = C_{15} = C_{16} = C_{18} = C_{1,10} = 0$$

$$C_{27} = -4NS_b^* \cos \gamma$$

$$C_{29} = -4NS_v \sin \gamma$$

$$C_{2,11} = -4NS_w \sin \beta_p \cos \gamma$$

$$C_{21} = C_{22} = C_{23} = C_{24} = C_{25} = C_{26} = C_{28} = C_{2,10} = 0$$

$$C_{31} = C_{32} = C_{33} = C_{34} = C_{35} = 0$$

$$C_{36} = C_{37} = C_{38} = C_{39} = C_{3,10} = C_{3,11} = 0$$

$$C_{44} = 2NI_b \cos^2 \beta_p \sin 2\gamma$$

$$C_{45} = 2NI_b \cos^2 \beta_p (1 - \cos 2\gamma)$$

$$C_{47} = 4NI_b^{**} \cos \gamma$$

$$C_{49} = 4NI_{xv}^* \sin \gamma$$

$$C_{4,11} = 4NI_{xw}^* \sin \beta_p \cos \gamma$$

$$C_{41} = C_{42} = C_{43} = C_{46} = C_{48} = C_{4,10} = 0$$

$$C_{54} = -2NI_b \cos^2 \beta_p (1 + \cos 2\gamma)$$

$$C_{55} = -2NI_b \cos^2 \beta_p \sin 2\gamma$$

$$C_{57} = 4NI_b^{**} \sin \gamma$$

$$C_{59} = -4NI_{xv}^* \cos \gamma$$

$$C_{5,11} = 4NI_{xw}^* \sin \beta_p \sin \gamma$$

$$C_{51} = C_{52} = C_{53} = C_{56} = C_{58} = C_{5,10} = 0$$

$$C_{6,10} = -4NI_{xw} \sin \beta_p \cos \beta_p$$

$$C_{61} = C_{62} = C_{63} = C_{64} = C_{65} = 0$$

$$C_{66} = C_{67} = C_{68} = C_{69} = C_{6,11} = 0$$

ORIGINAL PAGE IS
OF POOR QUALITY

$$C_{74} = 4\Omega I_b \cos^2 \beta_p \cos \gamma$$

$$C_{75} = 4\Omega I_b \cos^2 \beta_p \sin \gamma$$

$$C_{79} = 4\Omega I_{xv}^*$$

$$C_{71} = C_{72} = C_{73} = C_{76} = C_{77} = C_{78} = C_{7,10} = C_{7,11} = 0$$

$$C_{8,10} = -4\Omega I_{xv} \sin \beta_p$$

$$C_{81} = C_{82} = C_{83} = C_{84} = C_{85} = 0$$

$$C_{86} = C_{87} = C_{88} = C_{89} = C_{8,11} = 0$$

$$C_{97} = -C_{79}$$

$$C_{9,10} = -4\Omega I_{xv} \sin \beta$$

$$C_{91} = C_{92} = C_{93} = C_{94} = 0$$

$$C_{95} = C_{96} = C_{98} = C_{99} = C_{9,11} = 0$$

$$C_{10,6} = -C_{6,10}$$

$$C_{10,8} = -C_{8,10}$$

$$C_{10,1} = C_{10,2} = C_{10,3} = C_{10,4} = 0$$

$$C_{10,5} = C_{10,7} = C_{10,9} = C_{10,10} = C_{10,11} = 0$$

$$C_{11,4} = 4\Omega I_{xw} \cos^2 \beta_p \cos \gamma$$

$$C_{11,5} = 4\Omega I_{xw} \cos^2 \beta_p \sin \gamma$$

$$C_{11,9} = -C_{9,11}$$

$$C_{11,1} = C_{11,2} = C_{11,3} = C_{11,6} = 0$$

$$C_{11,7} = C_{11,8} = C_{11,10} = C_{11,11} = 0$$

(9.20)

21 3140 100000
VTJAIN

$$K_{17} = 2\Omega^2 S_b^* \cos\gamma$$

$$K_{19} = 2\Omega^2 S_v \sin\gamma$$

$$K_{1,11} = 2\Omega^2 S_w \sin\beta_p \cos\gamma$$

$$K_{11} = K_{12} = K_{13} = K_{14} = K_{15} = K_{16} = K_{18} = K_{1,10} = 0$$

$$K_{27} = 2\Omega^2 S_b^* \sin\gamma$$

$$K_{29} = -2\Omega^2 S_v \cos\gamma$$

$$K_{2,11} = 2\Omega^2 S_w \sin\beta_p \sin\gamma$$

$$K_{21} = K_{22} = K_{23} = K_{24} = K_{25} = K_{26} = K_{28} = K_{2,10} = 0$$

$$K_{31} = K_{32} = K_{33} = K_{34} = K_{35} = 0$$

$$K_{36} = K_{37} = K_{38} = K_{39} = K_{3,10} = K_{3,11} = 0$$

$$K_{47} = 2\Omega^2 (I_b \cos^2 \beta_p - I_b^{**}) \sin\gamma$$

$$K_{49} = 2\Omega^2 I_{xv}^* \cos\gamma$$

$$K_{4,11} = 2\Omega^2 (I_{xw} \cos^2 \beta_p - I_{xw}^* \sin\beta_p) \sin\gamma$$

$$K_{41} = K_{42} = K_{43} = K_{44} = K_{45} = K_{46} = K_{48} = K_{4,10} = 0$$

$$K_{57} = -2\Omega^2 (I_b \cos^2 \beta_p - I_b^{**}) \cos\gamma$$

$$K_{59} = 2\Omega^2 I_{xv}^* \sin\gamma$$

$$K_{5,10} = 2gS_w \cos\beta_p$$

$$K_{5,11} = -2\Omega^2 (I_{xw} \cos^2 \beta_p - I_{xw}^* \sin\beta_p) \cos\gamma$$

$$K_{51} = K_{52} = K_{53} = K_{54} = K_{55} = K_{56} = K_{58} = 0$$

$$K_{67} = 2gS_b^* \sin\gamma$$

$$K_{69} = -2gS_v \cos\gamma$$

$$K_{6,11} = 2gS_w \sin\beta_p \sin\gamma$$

$$K_{61} = K_{62} = K_{63} = K_{64} = K_{65} = K_{66} = K_{68} = K_{6,10} = 0$$

$$K_{76} = K_{67}$$

$$K_{77} = 2K_t + 2\Omega^2 I_b \cos^2 \beta_p - 2\Omega^2 I_b^{**}$$

$$K_{7,10} = -2gS_v \cos \beta_p \cos \gamma$$

$$K_{7,11} = 2\Omega^2 I_{xv} \cos^2 \beta_p - 2\Omega^2 I_{xv}^* \sin \beta_p$$

$$K_{71} = K_{72} = K_{73} = K_{74} = K_{75} = K_{78} = K_{79} = 0$$

$$K_{88} = 2K_v + 2\Omega^2 H_v \cos^2 \beta_p - 2\Omega^2 I_v$$

$$K_{89} = -2gR_v \cos \beta_p \cos \gamma$$

$$K_{8,10} = 2K_{vw}$$

$$K_{81} = K_{82} = K_{83} = K_{84} = K_{85} = K_{86} = K_{87} = K_{8,11} = 0$$

$$K_{96} = K_{69}$$

$$K_{98} = K_{89}$$

$$K_{99} = K_{88}$$

$$K_{9,11} = 2K_{vw}$$

$$K_{91} = K_{92} = K_{93} = K_{94} = K_{95} = K_{97} = K_{9,10} = 0$$

$$K_{10,5} = K_{5,10}$$

$$K_{10,7} = K_{7,10}$$

$$K_{10,8} = K_{8,10}$$

$$K_{10,10} = 2K_w + 2\Omega^2 H_w \cos^2 \beta_p - 2\Omega^2 I_w \sin^2 \beta_p$$

$$K_{10,11} = -2gR_w \cos \beta_p \cos \gamma$$

$$K_{10,1} = K_{10,2} = K_{10,3} = K_{10,4} = K_{10,6} = K_{10,9} = 0$$

$$K_{11,6} = K_{6,11}$$

$$K_{11,7} = K_{7,11}$$

$$K_{11,9} = K_{9,11}$$

$$K_{11,10} = K_{10,11}$$

C-2

$$K_{11,11} = K_{10,10}$$

$$K_{11,1} = K_{11,2} = K_{11,3} = K_{11,4} = K_{11,5} = K_{11,8} = 0$$

(9.21)

$$P_x = -2gM_b$$

$$P_y = 0$$

$$P_z = 0$$

$$Q_x = 0$$

$$Q_y = -2gS_b^*$$

$$Q_z = 0$$

$$Q_t = 2gS_b^* \cos \gamma$$

$$P_{v_a} = 0$$

$$P_{v_s} = 2gS_v \sin \gamma$$

$$P_{w_s} = -2\Omega^2 I_{xw} \sin \beta_p \cos \beta_p$$

$$P_{w_a} = 2gS_w \sin \beta_p \cos \gamma$$

(9.22)

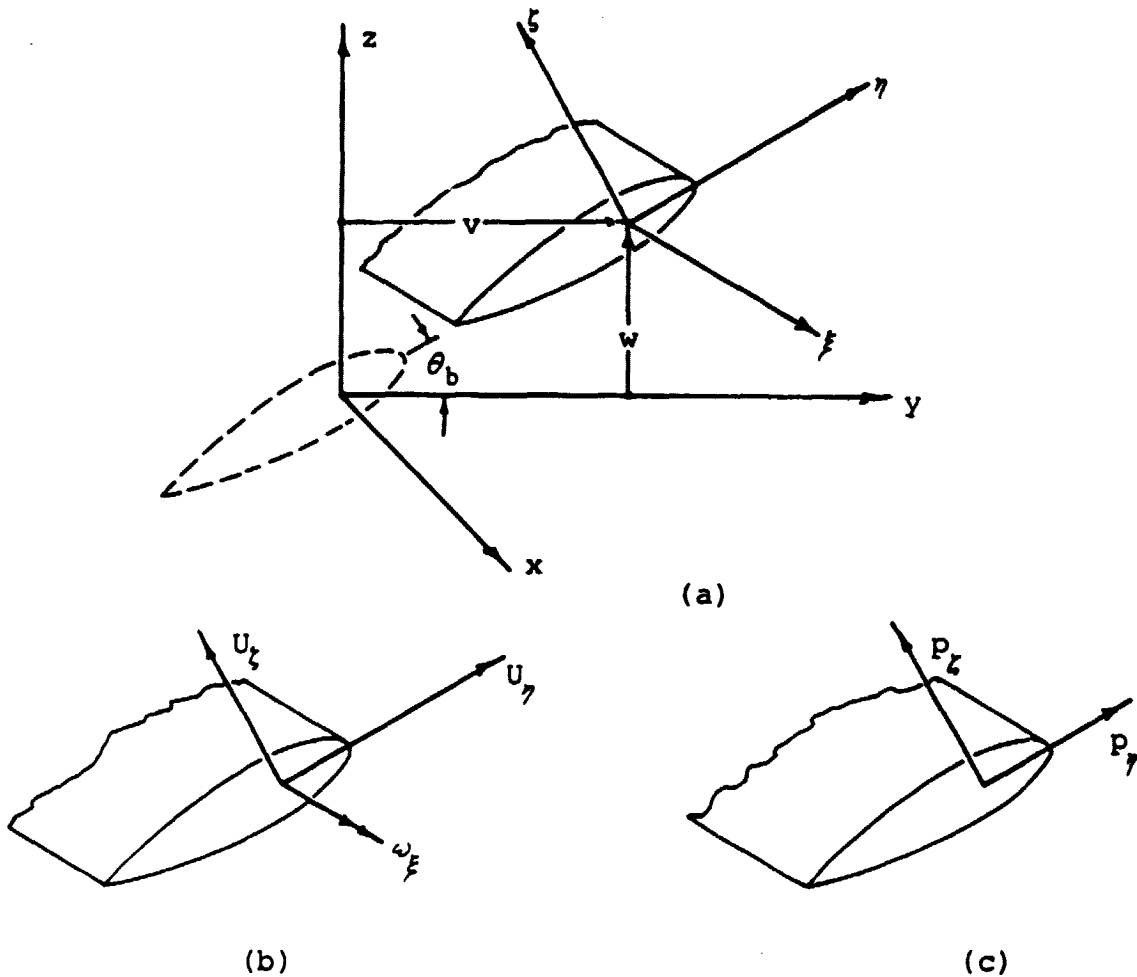
ORIGINAL PAGE IS
OF POOR QUALITY

Chapter 10.

AERODYNAMIC LOADS --
ROTOR-TOWER SYSTEM

Applied forces and moments which arise from aerodynamic forces on the blades are derived in this chapter in parallel fashion to Chapter 4. As with the rotor-tower equations of motion, torsion and torsional moments are neglected. This assumes that the aerodynamic center is at the elastic axis. The quasisteady assumption is made and apparent mass effects are ignored. However, preconing, blade twist and taper, wind shear, and crossflow over the rotor are included here. As in Chapter 9, the contribution of one blade is derived first. Then, loads from both blades are summed and the symmetric and antisymmetric coordinates are used.

A cross-section of the deflected blade is shown in Sketch 10.1a which defines the deformed blade coordinate system ξ, η, ζ . The corresponding unit vectors are $\hat{i}, \hat{j}, \hat{k}$. The blade has a built-in pretwist $\theta_b(x)$, followed by deflections v and w as before.



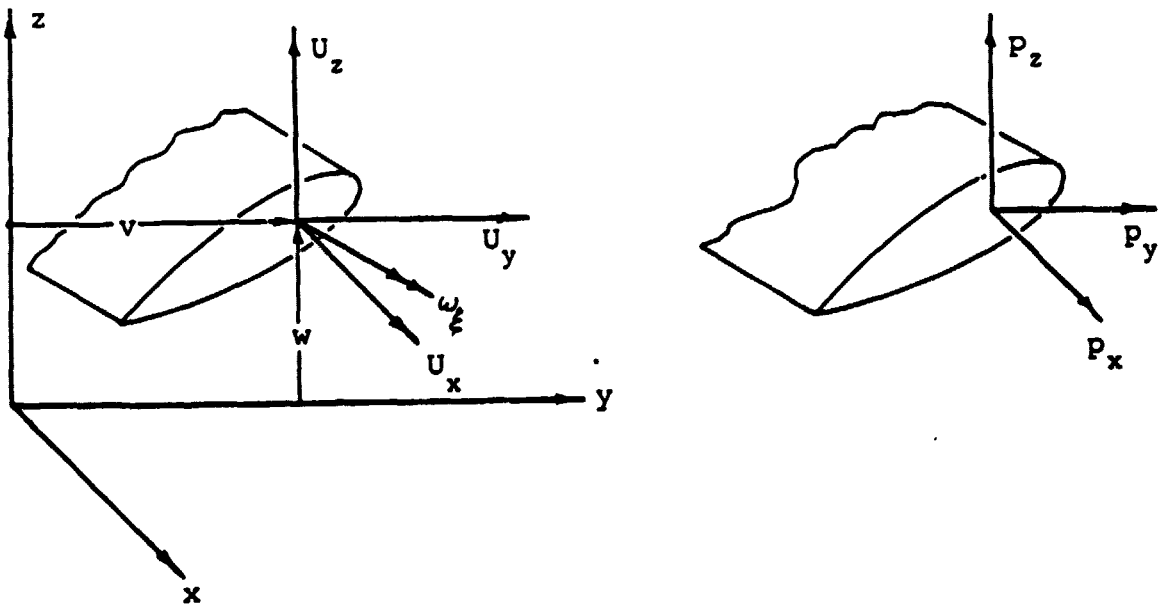
Sketch 10.1 Aerodynamic Nomenclature

Pertinent velocity components of the blade axis relative to the inflowing air U_η and U_ξ , and the pitch rate ω_ζ are reviewed in Sketch 10.1b. The distributed loads of interest here, p_η and p_ξ as shown in Sketch 10.1c, are distilled from equations (4.3) with the simplifications outlined above. They are

$$\begin{aligned}
 p_y &= \frac{1}{2} \rho a c \{ C [U_z^2 - c \omega_f U_z] - D U_y^2 \} \\
 p &= \frac{1}{2} \rho a c \{ C [-U_y U_z + c \omega_f U_y] - D U_y U_z \} \quad (10.1)
 \end{aligned}$$

where ρ is the air density, a is the lift curve slope, c is the blade chord at station x , C is some lift deficiency function, and $D = C_{d0}/a$.

It is actually more convenient to work with velocity and distributed load components in the $x y z$ system for this development. These are shown in Sketch 10.2a and b, respectively. Note that the pitch rate ω_f is retained in the deformed system; its transformation produces no simplification.



Sketch 10.2 Components in the $x y z$ System

The transformation between the deformed blade unit vectors $\hat{i} \hat{j} \hat{k}$ and the undeformed blade unit vectors $i j k$ is taken from reference [20]. It is

$$[\hat{i} \hat{j} \hat{k}] = [\hat{i} \hat{j} \hat{k}][T_b] \quad (10.2)$$

where $[T_b] =$

$$\begin{bmatrix} 1 & -v' & -w' \\ v' \cos \theta_b - w' \sin \theta_b & \cos \theta_b & -\sin \theta_b \\ v' \sin \theta_b + w' \cos \theta_b & \sin \theta_b & \cos \theta_b \end{bmatrix}$$

When this transformation is used for the velocities and distributed loads in equations (10.1), the distributed loads become

$$\begin{aligned} p_x = \frac{1}{2} \rho a c \{ & [-(C+D) \sin \theta_b \cos \theta_b w' - (C \sin^2 \theta_b - D \sin^2 \theta_b) v'] U_y^2 \\ & + (C+D) [\cos 2\theta_b w' + \sin 2\theta_b v'] U_y U_z \\ & + [(C+D) \sin \theta_b \cos \theta_b w' - (C \cos^2 \theta_b - D \sin^2 \theta_b) v'] U_z^2 \\ & - \frac{1}{2} c C [\sin \theta_b v' + \cos \theta_b w'] \omega_f U_y \\ & + \frac{1}{2} c C [\cos \theta_b v' - \sin \theta_b w'] \omega_f U_z \} \quad (10.3) \end{aligned}$$

$$\begin{aligned} p_y = \frac{1}{2} \rho a c \{ & 2[(C \sin^2 \theta_b + D) v' - D \sin \theta_b \cos \theta_b w'] U_x U_y \\ & - 2[C \sin \theta_b \cos \theta_b v' + (C + D \sin^2 \theta_b) w'] U_x U_z \\ & - D \cos \theta_b U_y^2 - (C+D) \sin \theta_b U_y U_z + C \cos \theta_b U_z^2 \\ & + \frac{1}{2} c C [\sin \theta_b v' + \cos \theta_b w'] \omega_f U_x - \frac{1}{2} c C \omega_f U_z \} \quad (10.4) \end{aligned}$$

$$\begin{aligned}
 p_z = & \frac{1}{2} \rho a c \{ 2[-C \sin \theta_b \cos \theta_b v' + (C + D \cos^2 \theta_b) w'] U_x U_y \\
 & + 2[(C \cos^2 \theta_b + D) v' + D \sin \theta_b \cos \theta_b w'] U_x U_z \\
 & + C \sin \theta_b U_y^2 - (C + D) \cos \theta_b U_y U_z - D \sin \theta_b U_z^2 \\
 & - \frac{1}{2} c C [\cos \theta_b v' + \sin \theta_b w'] \omega_{\dot{\beta}} U_x + \frac{1}{2} c C \omega_{\dot{\beta}} U_y \} \quad (10.5)
 \end{aligned}$$

Thus, the velocity components U_x , U_y , U_z , and the pitch rate $\omega_{\dot{\beta}}$ are required to formulate the distributed loads. For this purpose terms need be kept only up to linear in the displacements.

10.1 RELATIVE VELOCITY OF THE BLADE

The relative velocity of the blade U is the difference between the absolute velocity of the blade V and the velocity of the air at the turbine disk. An inflow velocity u_{in} in the $-Z$ direction and a crossflow velocity u_{cr} in the $-Y$ direction are assumed. The absolute velocity of the blade V is given in inertial coordinates by equation (9.4). The relative velocity in inertial coordinates is then

ORIGINAL PAGE IS
OF POOR QUALITY

$$\begin{aligned}
 U &= v + [\hat{i} \ \hat{j} \ \hat{k}] \begin{Bmatrix} 0 \\ u_{cr} \\ u_{in} \end{Bmatrix} = \\
 &= [\hat{i} \ \hat{j} \ \hat{k}] \left\{ \begin{Bmatrix} \dot{q}_x \\ \dot{q}_y + u_{cr} \\ \dot{q}_z + u_{in} \end{Bmatrix} + [\dot{T}_a] \begin{Bmatrix} u+x-e\sin\beta_p \\ v \\ w - e\cos\beta_p \end{Bmatrix} + [T_a] \begin{Bmatrix} \dot{u} \\ \dot{v} \\ \dot{w} \end{Bmatrix} \right\} \\
 & \hspace{15em} (10.6)
 \end{aligned}$$

This is transformed by equation (9.1) to give the relative velocity in blade coordinates

$$\begin{aligned}
 U &= [\hat{i} \ \hat{j} \ \hat{k}] \begin{Bmatrix} U_x \\ U_y \\ U_z \end{Bmatrix} \\
 &= [\hat{i} \ \hat{j} \ \hat{k}] \left\{ [T_a]^T \begin{Bmatrix} \dot{q}_x \\ \dot{q}_y + u_{cr} \\ \dot{q}_z + u_{in} \end{Bmatrix} + [T_a]^T [\dot{T}_a] \begin{Bmatrix} u+x-e\sin\beta_p \\ v \\ w - e\cos\beta_p \end{Bmatrix} + \begin{Bmatrix} \dot{u} \\ \dot{v} \\ \dot{w} \end{Bmatrix} \right\} \\
 & \hspace{15em} (10.7)
 \end{aligned}$$

Elements in the transformation matrix and in the product of the transformation matrix and its time derivative must be kept to adequate order to produce quadratic terms in equation (10.7), but only those quadratic terms which involve time derivatives of displacements. While only linear terms are required for the distributed load

expressions, these particular quadratic terms are required for the work expression in Section 10.3. The matrices are relegated to Appendix B. The required velocity components are then

$$\begin{aligned}
 U_x = & u_{in} \sin \beta_p + u_{cr} \cos \beta_p \sin \gamma + \cos \beta_p \cos \gamma \dot{q}_x + \cos \beta_p \sin \gamma \dot{q}_y \\
 & + \sin \beta_p \dot{q}_z + e \cos \beta_p \sin \gamma \dot{\phi}_x \\
 & - e \cos \beta_p \cos \gamma \dot{\phi}_y + e \cos \beta_p \dot{\beta}_t \quad (10.8)
 \end{aligned}$$

$$\begin{aligned}
 U_y = & \Omega x \cos \beta_p + u_{in} [\phi_x \cos \gamma + \phi_y \sin \gamma] + u_{cr} [\cos \gamma - \phi_z \sin \gamma] \\
 & - \Omega (x \sin \beta_p - e) \beta_t - \Omega \sin \beta_p v - [\sin \gamma + \phi_z \sin \gamma] \dot{q}_x \\
 & + [\cos \gamma - \phi_z \sin \gamma] \dot{q}_y + [\phi_x \cos \gamma + \phi_y \sin \gamma] \dot{q}_z \\
 & - [(x \sin \beta_p - e) (\cos \gamma - \phi_z \sin \gamma) + \beta_t x \cos \beta_p \cos \gamma + v \cos \beta_p \cos \gamma] \dot{\phi}_x \\
 & - [(x \sin \beta_p - e) (\sin \gamma + \phi_z \cos \gamma) + \beta_t x \cos \beta_p \sin \gamma + v \cos \beta_p \sin \gamma] \dot{\phi}_y \\
 & + [x \cos \beta_p - (x \sin \beta_p - e) \beta_t - v \sin \beta_p] \dot{\phi}_z + \dot{v} \quad (10.9)
 \end{aligned}$$

$$\begin{aligned}
 U_z = & - u_{cr} [\sin \beta_p \sin \gamma + (\phi_x + \phi_z \cos \gamma) \sin \beta_p + \beta_t \cos \beta_p \sin \gamma] \\
 & + u_{in} [\cos \beta_p - (\phi_x \sin \gamma - \phi_y \cos \gamma + \beta_t) \sin \beta_p] \\
 & + \Omega \sin \beta_p v - [\sin \beta_p \cos \gamma - \phi_z \sin \beta_p \sin \gamma + \beta_t \cos \beta_p \cos \gamma] \dot{q}_x \\
 & - [\sin \beta_p \sin \gamma + (\phi_x + \phi_z \cos \gamma) \sin \beta_p + \beta_t \cos \beta_p \sin \gamma] \dot{q}_y \\
 & + [\cos \beta_p - (\phi_x \sin \gamma - \phi_y \cos \gamma + \beta_t \sin \beta_p)] \dot{q}_z \\
 & + [(x - e \sin \beta_p) (\sin \gamma + \phi_z \cos \gamma) - v \cos \beta_p \cos \gamma] \dot{\phi}_x \\
 & - [(x - e \sin \beta_p) (\cos \gamma - \phi_z \sin \gamma) + v \cos \beta_p \sin \gamma] \dot{\phi}_y \\
 & - v \sin \beta_p \dot{\phi}_z + (x - e \sin \beta_p) \dot{\beta}_t + \dot{v} \quad (10.10)
 \end{aligned}$$

These expressions contain all necessary terms for the distributed loads (10.3-5) and for the work expression (10.1).

10.2

PITCH RATE OF THE BLADE

Various angular velocities as detailed in Chapter 9 contribute to the pitch rate ω_z . $\dot{\phi}_Y$ is about the Y axis, $\dot{\phi}_X$ is about the X axis following the ϕ_Y rotation, $\dot{\phi}_Z$ and Ω are about the Z axis, and \dot{v}' is about the z axis, all in the righthand sense. Finally, $\dot{\beta}_t$ and \dot{w}' are about the y axis in the opposite sense. Equation (9.1) is used to transform each of the angular velocities as required. The total angular velocity of a point on the blade elastic axis in the deformed coordinate system is

$$\begin{Bmatrix} \omega_x \\ \omega_y \\ \omega_z \end{Bmatrix} = [T_b]^T \left\{ [T_B]^T \left[[T_\Psi]^T \left([T_X]^T \begin{Bmatrix} 0 \\ \dot{\phi}_Y \\ 0 \end{Bmatrix} + \begin{Bmatrix} \dot{\phi}_X \\ 0 \\ 0 \end{Bmatrix} \right) + \begin{Bmatrix} 0 \\ 0 \\ \Omega + \dot{\phi}_Z \end{Bmatrix} \right] + \begin{Bmatrix} 0 \\ -\dot{\beta}_t - \dot{w}' \\ \dot{v}' \end{Bmatrix} \right\} \quad (10.11)$$

Linear terms are adequate in the expansion of the angular velocity. The only component required is

$$\begin{aligned} \omega_z = & \Omega \sin \beta_p + \Omega \cos \beta_p [\beta_t + \sin \theta_b v' + \cos \theta_b w'] \\ & + \cos \beta_p [\cos \gamma \dot{\phi}_X + \sin \gamma \dot{\phi}_Y] + \sin \beta_p \dot{\phi}_Z \end{aligned} \quad (10.12)$$

10.3

WORK OF EXTERNAL FORCES

The variation of work done by the aerodynamic forces can be expressed both in terms of blade deflections, and in terms of the generalized coordinates. In terms of variations of the blade elastic axis deflections it is

ORIGINAL PAGE IS
OF POOR QUALITY

$$\delta W = \int_{\text{blade span}} (P_x \delta x_{ea} + P_y \delta y_{ea} + P_z \delta z_{ea}) dx \quad (10.13)$$

where x_{ea} , y_{ea} , and z_{ea} are deflections of the elastic axis in the respective directions. In terms of variations of the generalized coordinates this is

$$\begin{aligned} \delta W = & P_x \delta q_x + P_y \delta q_y + P_z \delta q_z \\ & + Q_x \delta \phi_x + Q_y \delta \phi_y + Q_z \delta \phi_z \\ & + Q_c \delta \beta_c + P_v \delta q_v + P_w \delta q_w \end{aligned} \quad (10.14)$$

where the P_n and Q_n are the generalized loads of equation (9.14). Recall that $v = \gamma_v q_v$ and $w = \gamma_w q_w$; if more bending modes are required, more generalized loads would be used at this point.

Now, if the two sets of coordinate variations can be related, the generalized loads can be calculated. The variations are related through the velocities as in Chapter 4. Define the operator

$$\Lambda = \delta q_x (\partial / \partial q_x) + \delta q_y (\partial / \partial q_y) + \dots + \delta q_v (\partial / \partial q_v) \quad (10.15)$$

Then the relationship between the two sets is given by

$$\begin{aligned} \delta x_{ea} &= \Lambda \{U_x\} \\ \delta y_{ea} &= \Lambda \{U_y\} \\ \delta z_{ea} &= \Lambda \{U_z\} \end{aligned} \quad (10.16)$$

Equation (10.15) is applied to the velocity components

(10.8-10), and the result is substituted into the first work expression (10.13). Then, coefficients of each variation in the two work expressions are separately equated. The generalized loads which result are

$$P_X = \int \{p_x \cos \beta_p \cos \gamma - p_y [\sin \gamma + \phi_z \cos \gamma] - p_z [\sin \beta_p \cos \gamma + \phi_z \sin \beta_p \sin \gamma + \beta_t \cos \beta_p \cos \gamma]\} dx \quad (10.17)$$

$$P_Y = \int \{p_x \cos \beta_p \sin \gamma + p_y [\cos \gamma - \phi_z \sin \gamma] - p_z [\sin \beta_p \sin \gamma + \sin \beta_p (\phi_x + \phi_y \cos \gamma) + \beta_t \cos \beta_p \sin \gamma]\} dx \quad (10.18)$$

$$P_Z = \int \{p_x \sin \beta_p + p_y [\phi_x \cos \gamma + \phi_y \sin \gamma] + p_z [\cos \beta_p + \sin \beta_p (\phi_x \sin \gamma - \phi_y \cos \gamma + \beta_t)]\} dx \quad (10.19)$$

$$Q_X = \int \{p_y e \cos \beta_p \sin \gamma - p_y [(x - e \sin \beta_p)(\cos \gamma - \phi_z \sin \gamma) + \beta_t x \cos \beta_p \cos \gamma + w \cos \beta_p \cos \gamma] - p_z [v \cos \beta_p \cos \gamma + (x - e \sin \beta_p)(\sin \gamma + \phi_z \cos \gamma)]\} dx \quad (10.20)$$

$$Q_Y = \int \{-p_x e \cos \beta_p \cos \gamma - p_y [(x \sin \beta_p - e)(\sin \gamma + \phi_z \cos \gamma) + \beta_t x \cos \beta_p \sin \gamma + w \cos \beta_p \sin \gamma] - p_z [v \cos \beta_p \sin \gamma + (x - e \sin \beta_p)(\cos \gamma - \phi_z \sin \gamma)]\} dx \quad (10.21)$$

$$Q_Z = \int \{p_y [x \cos \beta_p - \beta_t (x \sin \beta_p - e) + w \sin \beta_p] - p_z v \sin \beta_p\} dx \quad (10.22)$$

$$Q_t = \int \{p_x e \cos \beta_p + p_z (x - e \sin \beta_p)\} dx \quad (10.23)$$

$$P_v = \int \{p_y \gamma_v\} dx \quad (10.24)$$

$$P_w = \int \{p_z \gamma_w\} dx \quad (10.25)$$

A note is in order at this point. Almost all of the expressions in this chapter are given in terms of v and w , in order to facilitate their expansion to include more bending modes. The last two equations are given in terms of γ_v and γ_w , and give generalized loads for these particular modes; entirely analogous expressions could be written for any additional modes. Then, each occurrence of v or w would be expanded in the appropriate modes. Here, a simple one mode model is used for each.

10.4 GENERALIZED LOADS

To recap, at this point the aerodynamic loads (10.17-25) are expressed in terms of the distributed loads (10.3-5). The distributed loads in turn are expressed in terms of the velocity components (10.8-10) and the pitch rate (10.12). This substitution process is too complex to be reported in detail here. Only an outline of the algebra and the results are given.

First, a simple form is assumed for the inflow and crossflow as follows

$$\begin{aligned} u_{in} &= \lambda \Omega L + r \Omega x \cos \beta_p \cos \gamma \\ u_{cr} &= \mu \Omega L \end{aligned} \quad (10.26)$$

where λ is the average inflow ratio, r is a linear wind

shear coefficient, and μ is the crossflow ratio. The use of mode shapes γ_v and γ_w , and the definitions of λ , r , and μ facilitate the integration of the generalized loads.

For a yaw alignment angle ϕ off the wind, momentum theory gives

$$\lambda = \left(\frac{1}{2}V\cos\phi - \frac{1}{16}\sigma a \right) + \left[\left(\frac{1}{2}V\cos\phi - \frac{1}{16}\sigma a \right)^2 + \frac{1}{12}\sigma a \theta \right]^{1/2} \quad (10.27)$$

and

$$\mu = V\sin\phi \quad (10.28)$$

where $V = v_\infty/\Omega L$ (at hub height), σ is the solidity (rotor planform area/disk area), and θ_0 is the reference pitch setting. If the reference chord length is c_0 , then the Lock number may be defined as $\gamma = \rho a c_0 L^4/I_b$.

Chopra has given a simple formula for the wind shear in terms of a power law exponent p [35]. Rearranged, this is

$$r = p\left(\lambda + \frac{1}{8}\sigma a\right)L/H \quad (10.29)$$

where H is the hub height and p is between 0.15 and 0.4 depending on the terrain.

Unlike the derivation of the equations of motion, this development of the aerodynamic loads requires an ordering scheme. Reasonable orders of magnitude for HAWTs are

ORIGINAL PAGE IS
OF POOR QUALITY

$$\begin{array}{ll}
 x/L, \gamma_v, \gamma_w, \dot{\gamma}_v, \dot{\gamma}_w, \gamma/B & O(\epsilon^0) \\
 \lambda, \theta_b & O(\epsilon^{1/2}) \\
 c/L, e/L, \beta_p, \tau, \mu & O(\epsilon^1)
 \end{array}$$

where ϵ is of the order of q_v/L . In any coefficient, only the largest terms and those one half order smaller are retained. Coefficients of like harmonics are also compared, and those more than one half order smaller are discarded. Also, all τ^2 , $\tau\mu$, and μ^2 terms are ignored, effectively eliminating higher harmonics of the airloads.

The contribution to the aerodynamic loads made by blade one is calculated by setting $q_v = q_{v1}$ and $q_w = q_{w1}$. Then, the contribution to the aerodynamic loads made by blade two is calculated by setting $q_v = q_{v2}$, $q_w = q_{w2}$, $\beta_t = -\beta_t$ and $\gamma = \gamma + \pi$. The contributions from both blades are added to give the eleven generalized loads. Here again, the multiblade coordinates (9.15,16) for symmetric and antisymmetric elastic rotor modes are used.

Finally, the generalized loads are substituted into the equations of motion (9.18). Many terms in the loads involve generalized coordinates or their time derivatives. These are subtracted from both sides of the equations and thus augment the C and K matrices. The remainder are added to the forcing vector Q.

These aerodynamic coefficients are given below with the degrees of freedom in the same order as in equation (9.18). In these coefficients, various aerodynamic integrals are used, L_n and D_n . These are defined in Appendix C. To aid in understanding the aerodynamic coefficients, they are arranged so that they are all equal to one for an idealized blade: flat, untwisted, uniform, and with $\gamma_v = \gamma_w = x/L$.

$$\begin{aligned}
 C_{11} &= \Omega I_b \gamma \left\{ \frac{1}{2} L_8 \lambda \theta_o [1 - \cos 2\gamma] - \frac{1}{4} (2L_7 \lambda + L_6 \theta_o) \beta_p \sin 2\gamma \right\} / L^2 \\
 C_{12} &= \Omega I_b \gamma \left\{ -\frac{1}{4} (6L_7 \lambda - 3L_6 \theta_o) \beta_p - \frac{1}{2} L_8 \lambda \theta_o \sin 2\gamma + \right. \\
 &\quad \left. + \frac{1}{4} (2L_7 \lambda + L_6 \theta_o) \beta_p \cos 2\gamma \right\} / L^2 \\
 C_{13} &= \Omega I_b \gamma \left\{ \frac{1}{2} (L_5 r - L_8 \mu \theta_o) \sin 2\gamma \right\} / L^2 \\
 C_{14} &= \Omega I_b \gamma \left\{ \frac{1}{2} (3L_5 \lambda - L_4 \theta_o) [1 - \cos 2\gamma] - \frac{1}{6} L_3 \beta_p \sin 2\gamma \right\} / L \\
 C_{15} &= \Omega I_b \gamma \left\{ \frac{1}{6} L_3 \beta_p [1 + \cos 2\gamma] - \frac{1}{6} (3L_5 \lambda - L_4 \theta_o) \sin 2\gamma \right\} / L \\
 C_{16} &= \Omega I_b \gamma \left\{ -\frac{1}{6} L_3 r \beta_p [1 + \cos 2\gamma] - \frac{1}{6} L_4 r \theta_o \sin 2\gamma \right\} / L \\
 C_{17} &= \Omega I_b \gamma \left\{ \frac{1}{3} (3L_5 \lambda - L_4 \theta_o) \sin \gamma - \frac{1}{3} L_3 \beta_p \cos \gamma \right\} / L \\
 C_{18} &= \Omega I_b \gamma \left\{ -\frac{1}{6} L_{12} r \beta_p [1 + \cos 2\gamma] - \frac{1}{6} L_{13} r \theta_o \sin 2\gamma \right\} / L^2 \\
 C_{19} &= \Omega I_b \gamma \left\{ -\frac{1}{2} L_{15} \lambda \theta_o \sin \gamma - \frac{1}{6} (3L_{14} \lambda - 4L_{13} \theta_o) \cos \gamma \right\} / L^2 \\
 C_{1,10} &= \Omega I_b \gamma \left\{ \frac{1}{12} (4L_{22} r - 3L_{25} \mu \theta_o) \sin 2\gamma \right\} / L^2 \\
 C_{1,11} &= \Omega I_b \gamma \left\{ \frac{1}{3} (3L_{24} \lambda - L_{23} \theta_o) \sin \gamma - \frac{1}{3} L_{22} \beta_p \cos \gamma \right\} / L^2 \\
 C_{21} &= \Omega I_b \gamma \left\{ \frac{1}{4} (6L_7 \lambda - 3L_6 \theta_o) \beta_p [1 + \cos 2\gamma] - \frac{1}{2} L_8 \lambda \theta_o \sin 2\gamma \right\} / L^2 \\
 C_{22} &= \Omega I_b \gamma \left\{ \frac{1}{2} L_8 \lambda \theta_o [1 + \cos 2\gamma] + \frac{1}{4} (2L_7 \lambda + L_6 \theta_o) \beta_p \sin 2\gamma \right\} / L^2 \\
 C_{23} &= \Omega I_b \gamma \left\{ -\frac{1}{2} (L_5 r - L_8 \mu \theta_o) [1 + \cos 2\gamma] \right\} / L^2 \\
 C_{24} &= \Omega I_b \gamma \left\{ -\frac{1}{6} L_3 \beta_p [1 - \cos 2\gamma] - \frac{1}{6} (3L_5 \lambda - L_4 \theta_o) \sin 2\gamma \right\} / L \\
 C_{25} &= \Omega I_b \gamma \left\{ \frac{1}{6} (3L_5 \lambda - L_4 \theta_o) [1 + \cos 2\gamma] + \frac{1}{6} L_3 \beta_p \sin 2\gamma \right\} / L \\
 C_{26} &= \Omega I_b \gamma \left\{ \frac{1}{6} L_4 r \theta_o [1 + \cos 2\gamma] - \frac{1}{6} L_3 r \beta_p \sin 2\gamma \right\} / L
 \end{aligned}$$

ORIGINAL PAGE IS
OF POOR QUALITY

$$\begin{aligned}C_{27} &= \Omega I_b \gamma \left\{ -\frac{1}{3} L_3 \rho_p \sin \gamma - \frac{1}{3} (3L_5 \lambda - L_4 \theta_0) \cos \gamma \right\} / L \\C_{28} &= \Omega I_b \gamma \left\{ \frac{1}{8} L_{13} r \theta_0 [1 + \cos 2\gamma] - \frac{1}{8} L_{12} r \rho_p \sin 2\gamma \right\} / L^2 \\C_{29} &= \Omega I_b \gamma \left\{ -\frac{1}{6} (3L_{14} \lambda - 4L_{13} \theta_0) \sin \gamma + \frac{1}{2} L_{15} \lambda \theta_0 \cos \gamma \right\} / L^2 \\C_{2,10} &= \Omega I_b \gamma \left\{ -\frac{1}{12} (4L_{22} r - 3L_{25} \mu \theta_0) [1 + \cos 2\gamma] \right\} / L^2 \\C_{2,11} &= \Omega I_b \gamma \left\{ -\frac{1}{3} L_{22} \rho_p \sin \gamma - \frac{1}{3} (3L_{24} \lambda - L_{23} \theta_0) \cos \gamma \right\} / L^2 \\C_{31} &= \Omega I_b \gamma \left\{ -\frac{1}{4} (L_5 r - 4L_8 \mu \theta_0) \sin 2\gamma \right\} / L^2 \\C_{32} &= \Omega I_b \gamma \left\{ \frac{1}{4} (L_5 r - 4L_8 \mu \theta_0) [1 + \cos 2\gamma] \right\} / L^2 \\C_{33} &= \Omega I_b \gamma \left\{ \frac{1}{2} L_5 \right\} / L^2 \\C_{34} &= \Omega I_b \gamma \left\{ \frac{1}{4} L_5 \mu \sin 2\gamma \right\} / L \\C_{35} &= \Omega I_b \gamma \left\{ -\frac{1}{4} L_5 \mu [1 + \cos 2\gamma] \right\} / L \\C_{36} &= \Omega I_b \gamma \left\{ \frac{1}{6} (3L_5 \lambda - 4L_6 \theta_0) \right\} / L \\C_{37} &= \Omega I_b \gamma \left\{ \frac{1}{2} L_5 \mu \cos \gamma \right\} / L \\C_{38} &= \Omega I_b \gamma \left\{ \frac{1}{6} (3L_{14} \lambda - 4L_{15} \theta_0) \right\} / L^2 \\C_{39} &= \Omega I_b \gamma \left\{ \frac{1}{3} (L_{12} r - 3L_{15} \mu \theta_0) \cos \gamma \right\} / L^2 \\C_{3,10} &= \Omega I_b \gamma \left\{ \frac{1}{3} L_{22} \right\} / L^2 \\C_{3,11} &= \Omega I_b \gamma \left\{ \frac{1}{2} L_{24} \mu \cos \gamma \right\} / L^2 \\C_{41} &= \Omega I_b \gamma \left\{ -\frac{1}{12} (3L_5 \lambda - 4L_4 \theta_0) [1 - \cos 2\gamma] - \frac{1}{6} L_3 \rho_p \sin 2\gamma \right\} / L \\C_{42} &= \Omega I_b \gamma \left\{ -\frac{1}{6} L_3 \rho_p [1 - \cos 2\gamma] + \frac{1}{12} (3L_5 \lambda - 4L_4 \theta_0) \sin 2\gamma \right\} / L \\C_{43} &= \Omega I_b \gamma \left\{ \frac{1}{4} L_5 \mu \sin 2\gamma \right\} / L \\C_{44} &= \Omega I_b \gamma \left\{ \frac{1}{8} L_1 [1 - \cos 2\gamma] \right\} \\C_{45} &= \Omega I_b \gamma \left\{ -\frac{1}{8} L_1 \sin 2\gamma \right\} \\C_{46} &= \Omega I_b \gamma \left\{ \frac{1}{24} (3L_1 r - 8L_4 \mu \theta_0) \sin 2\gamma \right\} \\C_{47} &= \Omega I_b \gamma \left\{ \frac{1}{4} L_1 \sin \gamma \right\} \\C_{48} &= \Omega I_b \gamma \left\{ \frac{1}{24} (3L_{10} r - 8L_{13} \mu \theta_0) \sin 2\gamma \right\} / L\end{aligned}$$

$$C_{4,9} = \Omega I_b \gamma \left\{ \frac{1}{6} (2L_{12} \lambda - 3L_{11} \theta_o) \sin \psi \right\} / L$$

$$C_{4,10} = \Omega I_b \gamma \left\{ \frac{1}{6} L_{22} \mu \sin 2\psi \right\} / L$$

$$C_{4,11} = \Omega I_b \gamma \left\{ \frac{1}{4} L_{20} \sin \psi \right\} / L$$

$$C_{51} = \Omega I_b \gamma \left\{ \frac{1}{6} L_3 \beta_p [1 + \cos 2\psi] + \frac{1}{12} (3L_5 \lambda - 4L_4 \theta_o) \sin 2\psi \right\} / L$$

$$C_{52} = \Omega I_b \gamma \left\{ -\frac{1}{12} (3L_5 \lambda - 4L_4 \theta_o) [1 + \cos 2\psi] + \frac{1}{6} L_3 \beta_p \sin 2\psi \right\} / L$$

$$C_{53} = \Omega I_b \gamma \left\{ -\frac{1}{4} L_5 \mu [1 + \cos 2\psi] \right\} / L$$

$$C_{54} = \Omega I_b \gamma \left\{ -\frac{1}{8} L_1 \sin 2\psi \right\}$$

$$C_{55} = \Omega I_b \gamma \left\{ \frac{1}{8} L_1 [1 + \cos 2\psi] \right\}$$

$$C_{56} = \Omega I_b \gamma \left\{ -\frac{1}{24} (3L_1 \tau - 8L_4 \mu \theta_o) [1 + \cos 2\psi] \right\}$$

$$C_{57} = \Omega I_b \gamma \left\{ -\frac{1}{4} L_1 \cos \psi \right\}$$

$$C_{58} = \Omega I_b \gamma \left\{ -\frac{1}{24} (3L_{10} \tau - 8L_{13} \mu \theta_o) [1 + \cos 2\psi] \right\} / L$$

$$C_{59} = \Omega I_b \gamma \left\{ -\frac{1}{6} (2L_{12} \lambda - 3L_{11} \theta_o) \cos \psi \right\} / L$$

$$C_{5,10} = \Omega I_b \gamma \left\{ -\frac{1}{6} L_{22} \mu [1 + \cos 2\psi] \right\} / L$$

$$C_{5,11} = \Omega I_b \gamma \left\{ -\frac{1}{4} L_{20} \cos \psi \right\} / L$$

$$C_{61} = \Omega I_b \gamma \left\{ \frac{1}{3} L_3 \beta_p [1 + \cos 2\psi] - \frac{1}{6} L_4 \tau \theta_o \sin 2\psi \right\} / L$$

$$C_{62} = \Omega I_b \gamma \left\{ \frac{1}{6} L_4 \tau \theta_o [1 + \cos 2\psi] + \frac{1}{3} L_3 \tau \beta_p \sin 2\psi \right\} / L$$

$$C_{63} = \Omega I_b \gamma \left\{ -\frac{1}{3} (3L_5 \lambda - L_4 \theta_o) \right\} / L$$

$$C_{64} = \Omega I_b \gamma \left\{ -\frac{1}{12} (3L_1 \tau - L_4 \mu \theta_o) \sin 2\psi \right\}$$

$$C_{65} = \Omega I_b \gamma \left\{ \frac{1}{12} (3L_1 \tau - 2L_4 \mu \theta_o) [1 + \cos 2\psi] \right\}$$

$$C_{66} = \Omega I_b \gamma \left\{ \frac{1}{3} L_4 \lambda \theta_o + \frac{1}{2} D_{1,do} / a \right\}$$

$$C_{67} = \Omega I_b \gamma \left\{ -\frac{1}{6} (3L_1 \tau - 2L_4 \mu \theta_o) \cos \psi \right\}$$

$$C_{68} = \Omega I_b \gamma \left\{ \frac{1}{3} L_{13} \lambda \theta_o \right\} / L$$

$$C_{69} = \Omega I_b \gamma \left\{ \frac{1}{4} L_{11} \tau \theta_o \cos \psi \right\} / L$$

$$C_{6,10} = \Omega I_b \gamma \left\{ -\frac{1}{12} (8L_{22} \lambda - 3L_{21} \theta_o) \right\} / L$$

$$C_{6,11} = \Omega I_b \gamma \left\{ -\frac{1}{6} (3L_{20} \tau - 2L_{23} \mu \theta_o) \cos \psi \right\} / L$$

$$C_{71} = \Omega I_b \gamma \left\{ -\frac{1}{6}(3L_5 \lambda - 2L_4 \theta_o) \sin \gamma - \frac{1}{3} L_3 \beta_p \cos \gamma \right\} / L$$

$$C_{72} = \Omega I_b \gamma \left\{ -\frac{1}{3} L_3 \beta_p \sin \gamma + \frac{1}{6}(3L_5 \lambda - 2L_4 \theta_o) \cos \gamma \right\} / L$$

$$C_{73} = \Omega I_b \gamma \left\{ \frac{1}{2} L_5 \mu \cos \gamma \right\} / L$$

$$C_{74} = \Omega I_b \gamma \left\{ \frac{1}{4} L_1 \sin \gamma \right\}$$

$$C_{75} = \Omega I_b \gamma \left\{ -\frac{1}{4} L_1 \cos \gamma \right\}$$

$$C_{76} = \Omega I_b \gamma \left\{ \frac{1}{12}(3L_1 \tau - 8L_4 \mu \theta_o) \cos \gamma \right\}$$

$$C_{77} = \Omega I_b \gamma \left\{ \frac{1}{4} L_1 \right\}$$

$$C_{78} = \Omega I_b \gamma \left\{ \frac{1}{12}(3L_{10} \tau - 8L_{13} \mu \theta_o) \cos \gamma \right\} / L$$

$$C_{79} = \Omega I_b \gamma \left\{ \frac{1}{6}(2L_{12} \lambda - 3L_{11} \theta_o) \right\} / L$$

$$C_{7,10} = \Omega I_b \gamma \left\{ \frac{1}{3} L_{22} \mu \cos \gamma \right\} / L$$

$$C_{7,11} = \Omega I_b \gamma \left\{ \frac{1}{4} L_{20} \right\} / L$$

$$C_{81} = \Omega I_b \gamma \left\{ \frac{1}{3} L_{12} \tau \beta_p [1 + \cos 2\gamma] - \frac{1}{6} L_{13} \tau \theta_o \sin 2\gamma \right\} / L^2$$

$$C_{82} = \Omega I_b \gamma \left\{ \frac{1}{6} L_{13} \tau \theta_o [1 + \cos 2\gamma] + \frac{1}{3} L_{12} \tau \beta_p \sin 2\gamma \right\} / L^2$$

$$C_{83} = \Omega I_b \gamma \left\{ -\frac{1}{3}(3L_{14} \lambda - L_{13} \theta_o) \right\} / L^2$$

$$C_{84} = \Omega I_b \gamma \left\{ -\frac{1}{12}(3L_{10} \tau - 2L_{11} \mu \theta_o) \sin 2\gamma \right\} / L$$

$$C_{85} = \Omega I_b \gamma \left\{ \frac{1}{12}(3L_{10} \tau - 2L_{13} \mu \theta_o) [1 + \cos 2\gamma] \right\} / L$$

$$C_{86} = \Omega I_b \gamma \left\{ \frac{1}{3} L_{13} \lambda \theta_o \right\} / L$$

$$C_{87} = \Omega I_b \gamma \left\{ -\frac{1}{6}(3L_{10} \tau - 2L_{13} \mu \theta_o) \cos \gamma \right\} / L$$

$$C_{88} = \Omega I_b \gamma \left\{ \frac{1}{3} L_{53} \lambda \theta_o + \frac{1}{2} D_3 C_{do} / a \right\} / L^2$$

$$C_{89} = \Omega I_b \gamma \left\{ \frac{1}{4} L_{51} \tau \theta_o \cos \gamma \right\} / L^2$$

$$C_{8,10} = \Omega I_b \gamma \left\{ -\frac{1}{12}(8L_{62} \lambda - 3L_{61} \theta_o) \right\} / L^2$$

$$C_{8,11} = \Omega I_b \gamma \left\{ -\frac{1}{6}(3L_{60} \tau - 2L_{63} \mu \theta_o) \cos \gamma \right\} / L^2$$

$$C_{91} = \Omega I_b \gamma \left\{ -\frac{1}{2} L_{15} \lambda \theta_o \sin \gamma + \frac{1}{3}(3L_{14} \lambda - L_{13} \theta_o) \beta_p \cos \gamma \right\} / L^2$$

$$C_{92} = \Omega I_b \gamma \left\{ \frac{1}{3}(3L_{14} \lambda - L_{13} \theta_o) \beta_p \sin \gamma + \frac{1}{2} L_{15} \lambda \theta_o \cos \gamma \right\} / L^2$$

$$C_{93} = \Omega I_b \gamma \left\{ -\frac{1}{6}(4L_{12} \tau - 3L_{15} \mu \theta_o) \cos \gamma \right\} / L^2$$

$$C_{94} = \Omega I_b \gamma \left\{ -\frac{1}{12} (8L_{12} \lambda - 3L_{11} \theta_o) \sin \gamma \right\} / L$$

$$C_{95} = \Omega I_b \gamma \left\{ \frac{1}{12} (8L_{12} \lambda - 3L_{11} \theta_o) \cos \gamma \right\} / L$$

$$C_{96} = \Omega I_b \gamma \left\{ \frac{1}{4} L_{11} \tau \theta_o \cos \gamma \right\} / L$$

$$C_{97} = \Omega I_b \gamma \left\{ -\frac{1}{12} (8L_{12} \lambda - 3L_{11} \theta_o) \right\} / L$$

$$C_{98} = \Omega I_b \gamma \left\{ \frac{1}{4} L_{51} \tau \theta_o \cos \gamma \right\} / L^2$$

$$C_{99} = \Omega I_b \gamma \left\{ \frac{1}{3} L_{53} \lambda \theta_o + \frac{1}{2} D_3 C_{d_o} / a \right\} / L^2$$

$$C_{9,10} = \Omega I_b \gamma \left\{ -\frac{1}{6} (3L_{60} \tau - 2L_{63} \mu \theta_o) \cos \gamma \right\} / L^2$$

$$C_{9,11} = \Omega I_b \gamma \left\{ -\frac{1}{12} (8L_{62} \lambda - 3L_{61} \theta_o) \right\} / L^2$$

$$C_{10,1} = \Omega I_b \gamma \left\{ -\frac{1}{6} (L_{22} \tau - 3L_{25} \mu \theta_o) \sin 2\gamma \right\} / L^2$$

$$C_{10,2} = \Omega I_b \gamma \left\{ \frac{1}{6} (L_{22} \tau - 3L_{25} \mu \theta_o) [1 + \cos 2\gamma] \right\} / L^2$$

$$C_{10,3} = \Omega I_b \gamma \left\{ \frac{1}{3} L_{22} \right\} / L^2$$

$$C_{10,4} = \Omega I_b \gamma \left\{ \frac{1}{6} L_{22} \mu \sin 2\gamma \right\} / L$$

$$C_{10,5} = \Omega I_b \gamma \left\{ -\frac{1}{6} L_{22} \mu [1 + \cos 2\gamma] \right\} / L$$

$$C_{10,6} = \Omega I_b \gamma \left\{ \frac{1}{6} (2L_{22} \lambda - 3L_{21} \theta_o) \right\} / L$$

$$C_{10,7} = \Omega I_b \gamma \left\{ \frac{1}{3} L_{22} \mu \cos \gamma \right\} / L$$

$$C_{10,8} = \Omega I_b \gamma \left\{ \frac{1}{6} (2L_{62} \lambda - 3L_{61} \theta_o) \right\} / L^2$$

$$C_{10,9} = \Omega I_b \gamma \left\{ \frac{1}{12} (3L_{60} \tau - 4L_{63} \mu \theta_o) \cos \gamma \right\} / L^2$$

$$C_{10,10} = \Omega I_b \gamma \left\{ \frac{1}{4} L_{70} \right\} / L^2$$

$$C_{10,11} = \Omega I_b \gamma \left\{ \frac{1}{3} L_{72} \mu \cos \gamma \right\} / L^2$$

$$C_{11,1} = \Omega I_b \gamma \left\{ -\frac{1}{6} (3L_{24} \lambda - 4L_{23} \theta_o) \sin \gamma - \frac{1}{3} L_{22} \beta_p \cos \gamma \right\} / L^2$$

$$C_{11,2} = \Omega I_b \gamma \left\{ -\frac{1}{3} L_{22} \beta_p \cos \gamma + \frac{1}{6} (3L_{24} \lambda - 4L_{23} \theta_o) \sin \gamma \right\} / L^2$$

$$C_{11,3} = \Omega I_b \gamma \left\{ \frac{1}{2} L_{24} \mu \cos \gamma \right\} / L^2$$

$$C_{11,4} = \Omega I_b \gamma \left\{ \frac{1}{4} L_{20} \sin \gamma \right\} / L$$

$$C_{11,5} = \Omega I_b \gamma \left\{ -\frac{1}{4} L_{20} \cos \gamma \right\} / L$$

$$C_{11,6} = \Omega I_b \gamma \left\{ \frac{1}{12} (3L_{20} \tau - 8L_{23} \mu \theta_o) \cos \gamma \right\} / L$$

ORIGINAL PAGE IS
OF POOR QUALITY

$$C_{11,7} = \Omega I_{b\gamma} \left\{ \frac{1}{4} L_{20} \right\} / L^2$$

$$C_{11,8} = \Omega I_{b\gamma} \left\{ \frac{1}{12} (3L_{60} \tau - 8L_{63} \mu \theta_0) \cos \psi \right\} / L^2$$

$$C_{11,9} = \Omega I_{b\gamma} \left\{ \frac{1}{6} (2L_{62} \lambda - 3L_{61} \theta_0) \right\} / L^2$$

$$C_{11,10} = \Omega I_{b\gamma} \left\{ \frac{1}{3} L_{72} \mu \cos \psi \right\} / L^2$$

$$C_{11,11} = \Omega I_{b\gamma} \left\{ \frac{1}{4} L_{70} \right\} / L^2$$

(10.30)

$$K_{14} = \Omega^2 I_{b\gamma} \left\{ -\frac{1}{4} (2L_7 \lambda - L_6 \theta_0) \lambda \beta_p [3 - \cos 2\psi] - \frac{1}{2} L_8 \lambda^2 \theta_0 \sin 2\psi \right\} / L$$

$$K_{15} = \Omega^2 I_{b\gamma} \left\{ -\frac{1}{2} L_8 \lambda^2 \theta_0 [1 - \cos 2\psi] + \frac{1}{4} (2L_7 \lambda - L_6 \theta_0) \lambda \beta_p \sin 2\psi \right\} / L$$

$$K_{16} = \Omega^2 I_{b\gamma} \left\{ \left[\frac{1}{4} (2L_7 \lambda - L_6 \theta_0) \tau - L_8 \lambda \mu \theta_0 \right] [1 + \cos 2\psi] + \right. \\ \left. + L_8 \lambda \mu \theta_0 + \frac{1}{4} L_5 \tau \beta_p \sin 2\psi \right\} / L$$

$$K_{17} = \Omega^2 I_{b\gamma} \left\{ -\frac{1}{6} (3L_5 \lambda - 2L_4 \theta_0) \cos \psi \right\} / L$$

$$K_{18} = \Omega^2 I_{b\gamma} \left\{ L_{37} \mu \theta_0^2 + \left[\frac{1}{2} (L_{35} \lambda - L_{36} \theta_0) \tau + L_{39} \lambda \mu \theta_0 \right] [1 + \cos 2\psi] + \right. \\ \left. + \left[\frac{1}{3} (L_{12} \beta_p + L_{34} \theta_0^2) \tau + L_{38} \lambda \mu \right] \sin 2\psi \right\} / L^2$$

$$K_{19} = \Omega^2 I_{b\gamma} \left\{ \frac{1}{3} (3L_{14} \lambda - L_{13} \theta_0) \beta_p \sin \psi + \right. \\ \left. + \frac{1}{3} (3L_{38} \lambda^2 - 3L_{36} \lambda \theta_0 + L_{34} \theta_0^2) \cos \psi \right\} / L^2$$

$$K_{1,10} = \Omega^2 I_{b\gamma} \left\{ -\frac{1}{4} L_{44} \tau - \frac{1}{2} (L_{47} \lambda - 2L_{46} \lambda - 2L_{45} \theta_0) \mu \right\} [1 + \cos 2\psi] / L^2$$

$$K_{1,11} = \Omega^2 I_{b\gamma} \left\{ -\frac{1}{6} (3L_{44} \lambda - 2L_{42} \theta_0) \cos \psi \right\} / L^2$$

$$K_{11} = K_{12} = K_{13} = 0$$

$$K_{24} = \Omega^2 I_{b\gamma} \left\{ -\frac{1}{6} (3L_5 \lambda - 2L_4 \theta_0) + \frac{1}{2} L_8 \lambda^2 \theta_0 [1 + \cos 2\psi] + \right. \\ \left. + \frac{1}{4} (2L_7 \lambda - L_6 \theta_0) \sin 2\psi \right\} / L$$

$$K_{25} = \Omega^2 I_{b\gamma} \left\{ -\frac{1}{4} (2L_7 \lambda - L_6 \theta_0) \lambda \beta_p [3 + \cos 2\psi] + \frac{1}{2} L_8 \lambda^2 \theta_0 \sin 2\psi \right\} / L$$

$$K_{26} = \Omega^2 I_{b\gamma} \left\{ -\frac{1}{4} L_5 \tau \beta_p [1 + \cos 2\psi] + \left[\frac{1}{4} (2L_7 \lambda - L_6 \theta_0) \tau - L_8 \lambda \mu \theta_0 \right] \sin 2\psi \right\} / L$$

$$K_{27} = \Omega^2 I_{b\gamma} \left\{ -\frac{1}{6} (3L_5 \lambda - 2L_4 \theta_0) \sin \psi \right\} / L$$

$$\begin{aligned}
 K_{28} &= \Omega^2 I_b \gamma \left\{ -\left[\frac{1}{3} (L_{12} \beta_p + L_{34} \theta_o^2) \tau + L_{38} \lambda \mu \right] [1 + \cos 2\gamma] + \right. \\
 &\quad \left. + \left[\frac{1}{2} (L_{35} \lambda - L_{36} \theta_o) \tau + L_{39} \lambda \mu \theta_o \right] \sin 2\gamma \right\} / L^2 \\
 K_{29} &= \Omega^2 I_b \gamma \left\{ \frac{1}{3} (3L_{38} \lambda^2 - 3L_{36} \lambda \theta_o + L_{34} \theta_o^2) \sin \gamma + \right. \\
 &\quad \left. - \frac{1}{3} (3L_{14} \lambda - L_{13} \theta_o) \beta_p \cos \gamma \right\} / L^2 \\
 K_{2,10} &= \Omega^2 I_b \gamma \left\{ -\frac{1}{4} L_{44} \tau - \frac{1}{2} (L_{47} \lambda - 2L_{46} \lambda - 2L_{47} \theta_o) \mu \right\} \sin 2\gamma / L^2 \\
 K_{2,11} &= \Omega^2 I_b \gamma \left\{ -\frac{1}{6} (3L_{44} \lambda - 2L_{42} \theta_o) \sin \gamma \right\} / L^2 \\
 K_{21} &= K_{22} = K_{23} = 0 \\
 K_{34} &= \Omega^2 I_b \gamma \left\{ -\frac{1}{2} L_5 \beta_p \mu + \left[\frac{1}{12} (3L_6 - 4L_4) \tau \theta_o - \frac{1}{2} L_8 \lambda \mu \theta_o \right] [1 + \cos 2\gamma] + \right. \\
 &\quad \left. - \frac{1}{12} (3L_5 + 2L_3) \tau \beta_p \sin 2\gamma \right\} / L \\
 K_{35} &= \Omega^2 I_b \gamma \left\{ \frac{1}{12} (3L_5 + 2L_3) \tau \beta_p [1 + \cos 2\gamma] + \right. \\
 &\quad \left. + \left[\frac{1}{12} (3L_6 - 4L_4) \tau \theta_o - \frac{1}{2} L_8 \lambda \mu \theta_o \right] \sin 2\gamma \right\} / L \\
 K_{37} &= \Omega^2 I_b \gamma \left\{ -\frac{1}{2} L_5 \mu \sin \gamma \right\} / L \\
 K_{38} &= \Omega^2 I_b \gamma \left\{ \frac{1}{3} L_{12} \beta_p - \frac{1}{4} L_{85} c \theta_o \right\} / L^2 \\
 K_{39} &= \Omega^2 I_b \gamma \left\{ -(2L_{38} \lambda - L_{36} \theta_o) \mu \sin \gamma + \frac{1}{6} (4L_{33} \tau \theta_o + 3L_{14} \mu \beta_p) \cos \gamma \right\} / L^2 \\
 K_{3,10} &= \Omega^2 I_b \gamma \left\{ -\frac{1}{6} [(6L_{44} + 6L_{43} + 3L_{24}) \lambda - (2L_{42} + L_{23}) \theta_o] \beta_p - \frac{1}{4} L_{87} c \right\} / L^2 \\
 K_{3,11} &= \Omega^2 I_b \gamma \left\{ -L_{43} \mu \sin \gamma - \frac{2}{3} L_{41} \tau \cos \gamma \right\} / L^2 \\
 K_{31} &= K_{32} = K_{33} = K_{36} = 0 \\
 K_{44} &= \Omega^2 I_b \gamma \left\{ -\frac{1}{6} L_3 \lambda \beta_p [1 - \cos 2\gamma] + \frac{1}{12} (3L_5 \lambda - 4L_4 \theta_o) \lambda \sin 2\gamma \right\} \\
 K_{45} &= \Omega^2 I_b \gamma \left\{ \frac{1}{12} (3L_5 \lambda - 4L_4 \theta_o) \lambda [1 - \cos 2\gamma] + \frac{1}{6} L_3 \lambda \beta_p \sin 2\gamma \right\} \\
 K_{46} &= \Omega^2 I_b \gamma \left\{ \frac{1}{6} L_3 \tau + \left[\frac{1}{6} L_3 \tau + \frac{1}{12} (3L_5 \lambda - 4L_4 \theta_o) \mu \right] \cos 2\gamma \right\} \\
 K_{47} &= \Omega^2 I_b \gamma \left\{ -\frac{1}{6} [2(2L_3 \beta_p - L_5 e) \lambda - 3(L_2 \beta_p - L_4 e) \theta_o + L_{80} c] \sin \gamma + \right. \\
 &\quad \left. + \frac{1}{6} (3L_5 \lambda - 2L_4 \theta_o) \lambda \cos \gamma \right\} \\
 K_{48} &= \Omega^2 I_b \gamma \left\{ -\left[\frac{1}{3} L_{12} \tau + \frac{1}{6} (3L_{14} \lambda - 2L_{13} \theta_o) \mu \right] [1 + \cos 2\gamma] + \right. \\
 &\quad \left. - \frac{1}{6} (3L_{35} \lambda - 2L_{33} \theta_o) \mu [1 - \cos 2\gamma] + \frac{1}{4} L_{30} \tau \theta_o \sin 2\gamma \right\} / L \\
 K_{49} &= \Omega^2 I_b \gamma \left\{ \frac{1}{4} L_{10} \beta_p \sin \gamma - \frac{1}{12} (4L_{12} \lambda - 3L_{11} \theta_o) \cos \gamma \right\} / L
 \end{aligned}$$

ORIGINAL PAGE IS
OF POOR QUALITY

$$K_{4,10} = \Omega^2 I_{b\gamma} \left\{ -\frac{1}{6}(2L_{41}\mu + L_{23}\tau\theta_0) [1 - \cos 2\gamma] - \frac{1}{4}L_{40}\tau \sin 2\gamma \right\} / L$$

$$K_{4,11} = \Omega^2 I_{b\gamma} \left\{ -\left[\frac{1}{6}(4L_{41}\lambda + 2L_{22}\lambda - 3L_{21}\theta_0) \beta_p + \frac{1}{4}L_{87}c + \frac{1}{6}(3L_{44}\lambda - 2L_{42}\theta_0) e \right] \sin \gamma + \frac{1}{6}(3L_{24}\lambda - 2L_{23}\theta_0) \lambda \cos \gamma \right\} / L$$

$$K_{41} = K_{42} = K_{43} = 0$$

$$K_{54} = \Omega^2 I_{b\gamma} \left\{ -\frac{1}{12}(3L_5\lambda - 4L_4\theta_0) \lambda [1 + \cos 2\gamma] + \frac{1}{6}L_3\lambda\beta_p \sin 2\gamma \right\}$$

$$K_{55} = \Omega^2 I_{b\gamma} \left\{ -\frac{1}{6}L_3\lambda\beta_p [1 + \cos 2\gamma] - \frac{1}{12}(3L_5\lambda - 4L_4\theta_0) \lambda \sin 2\gamma \right\}$$

$$K_{56} = \Omega^2 I_{b\gamma} \left\{ \left[\frac{1}{6}L_3\tau + \frac{1}{12}(3L_5\lambda - 4L_4\theta_0) \mu \right] \sin 2\gamma \right\}$$

$$K_{57} = \Omega^2 I_{b\gamma} \left\{ \frac{1}{6}(3L_5\lambda - 2L_4\theta_0) \lambda \sin \gamma + \frac{1}{6} [2(2L_3\beta_p - L_5e) \lambda - 3(L_2\beta_p - L_4e)\theta_0 + L_{80}c] \cos \gamma \right\}$$

$$K_{58} = \Omega^2 I_{b\gamma} \left\{ -\frac{1}{4}L_{30}\tau\theta_0 [1 + \cos 2\gamma] - \left[\frac{1}{3}L_{12}\tau + \frac{1}{6}(3L_{14}\lambda - 2L_{13}\theta_0) \mu + \frac{1}{6}(3L_{35}\lambda - 2L_{33}\theta_0) \mu \right] \sin 2\gamma \right\} / L$$

$$K_{59} = \Omega^2 I_{b\gamma} \left\{ -\frac{1}{12}(4L_{12}\lambda - 3L_{11}\theta_0) \sin \gamma - \frac{1}{4}L_{10}\beta_p \cos \gamma \right\} / L$$

$$K_{5,10} = \Omega^2 I_{b\gamma} \left\{ \frac{1}{4}L_{40}\tau [1 + \cos 2\gamma] + \frac{1}{6}(2L_{41}\mu - L_{23}\tau\theta_0) \sin 2\gamma \right\} / L$$

$$K_{5,11} = \Omega^2 I_{b\gamma} \left\{ \frac{1}{6}(3L_{24}\lambda - 2L_{23}\theta_0) \lambda \sin \gamma + \left[\frac{1}{6}(4L_{41}\lambda + 2L_{22}\lambda - 3L_{21}\theta_0) \beta_p + \frac{1}{6}(3L_{44}\lambda - 2L_{42}\theta_0) e + \frac{1}{4}L_{87}c \right] \cos \gamma \right\} / L$$

$$K_{51} = K_{52} = K_{53} = 0$$

$$K_{64} = \Omega^2 I_{b\gamma} \left\{ \frac{1}{3}L_4\lambda\tau\theta_0 [1 + \cos 2\gamma] \right\}$$

$$K_{65} = \Omega^2 I_{b\gamma} \left\{ \frac{1}{3}L_4\lambda\tau\theta_0 \sin 2\gamma \right\}$$

$$K_{67} = \Omega^2 I_{b\gamma} \left\{ \frac{1}{3}(3L_5\lambda - L_4\theta_0) \mu \sin \gamma + \frac{1}{6}L_{80}c \cos \gamma \right\}$$

$$K_{68} = \Omega^2 I_{b\gamma} \left\{ -\frac{1}{2}(2L_{12}\lambda - L_{11}\theta_0) \beta_p + \frac{1}{4}L_{85}c\lambda\theta_0 \right\} / L$$

$$K_{69} = \Omega^2 I_{b\gamma} \left\{ \frac{1}{3}(3L_{36}\lambda - 2L_{34}\theta_0) \mu\theta_0 \sin \gamma - \frac{1}{6} [(2L_{12} + 3L_{10}) \beta_p + 3L_{31}\theta_0^2] \tau \cos \gamma \right\} / L$$

$$K_{6,10} = \Omega^2 I_{b\gamma} \left\{ \frac{1}{6} [(6L_{43} + 3L_{24}) \lambda - 2L_{23}\theta_0] \beta_p + \frac{1}{4}L_{87}c\lambda \right\} / L$$

$$K_{6,11} = \Omega^2 I_{b\gamma} \left\{ L_{43}\lambda\mu \sin \gamma + \frac{1}{6}L_{86}c\tau \cos \gamma \right\} / L$$

$$K_{61} = K_{62} = K_{63} = K_{66} = 0$$

$$\begin{aligned}
 K_{74} &= \Omega^2 I_{by} \left\{ -\frac{1}{3} L_3 \lambda \beta_p \sin \gamma + \frac{1}{6} (3L_5 \lambda - 4L_4 \theta_0) \lambda \cos \gamma \right\} \\
 K_{75} &= \Omega^2 I_{by} \left\{ \frac{1}{6} (3L_5 \lambda - 4L_4 \theta_0) \lambda \sin \gamma + \frac{1}{3} L_3 \lambda \beta_p \cos \gamma \right\} \\
 K_{76} &= \Omega^2 I_{by} \left\{ -\frac{1}{6} (3L_5 \lambda - 4L_4 \theta_0) \mu \sin \gamma - \frac{1}{3} L_3 \mu \beta_p \cos \gamma \right\} \\
 K_{77} &= \Omega^2 I_{by} \left\{ -\frac{1}{6} [2(2L_3 \beta_p - L_5 e) \lambda - 3(L_2 \beta_p - L_4 e)] - \frac{1}{6} L_{80} c \right\} \\
 K_{78} &= \Omega^2 I_{by} \left\{ -\frac{1}{3} (3L_{35} \lambda - 2L_{33} \theta_0) \mu \sin \gamma + \left[\frac{1}{3} L_{12} \mu \beta_p + \frac{1}{2} L_{30} \tau \theta_0 \right] \cos \gamma \right\} / L \\
 K_{79} &= \Omega^2 I_{by} \left\{ \frac{1}{4} L_{10} \beta_p - \frac{1}{6} L_{84} c \theta_0 \right\} / L \\
 K_{7,10} &= \Omega^2 I_{by} \left\{ -\frac{2}{3} L_{41} \mu \sin \gamma - \frac{1}{2} L_{40} \tau \cos \gamma \right\} / L \\
 K_{7,11} &= \Omega^2 I_{by} \left\{ -\frac{1}{6} [(4L_{41} + 2L_{22}) \lambda - 3L_{21} \theta_0] \beta_p - \frac{1}{6} L_{86} c \right\} / L \\
 K_{71} &= K_{72} = K_{73} = 0 \\
 \\
 K_{84} &= \Omega^2 I_{by} \left\{ \frac{1}{3} L_{13} \lambda \tau \theta_0 [1 + \cos 2\gamma] \right\} / L \\
 K_{85} &= \Omega^2 I_{by} \left\{ \frac{1}{3} L_{13} \lambda \tau \theta_0 \sin 2\gamma \right\} / L \\
 K_{87} &= \Omega^2 I_{by} \left\{ \frac{1}{3} (3L_{14} \lambda - L_{13} \theta_0) \mu \sin \gamma + \frac{1}{6} L_{81} c \tau \cos \gamma \right\} / L \\
 K_{88} &= \Omega^2 I_{by} \left\{ -\frac{1}{12} (8L_{52} - 3L_{51} \theta_0) \beta_p + \frac{1}{4} L_{90} c \lambda \theta_0 \right\} / L^2 \\
 K_{89} &= \Omega^2 I_{by} \left\{ \frac{1}{3} [2L_{56} \lambda + (3L_{56} \lambda - 2L_{55} \theta_0) \theta_0] \mu \sin \gamma + \right. \\
 &\quad \left. -\frac{1}{2} (L_{50} \beta_p + L_{54} \theta_0^2) \tau \cos \gamma \right\} / L^2 \\
 K_{8,10} &= \Omega^2 I_{by} \left\{ \frac{1}{3} (3L_{69} \lambda - L_{63} \theta_0) \lambda \beta_p + \frac{1}{4} L_{93} c \lambda \right\} / L^2 \\
 K_{8,11} &= \Omega^2 I_{by} \left\{ L_{69} \lambda \mu \sin \gamma + \frac{1}{6} L_{92} c \tau \cos \gamma \right\} / L^2 \\
 K_{81} &= K_{82} = K_{83} = K_{86} = 0 \\
 \\
 K_{94} &= \Omega^2 I_{by} \left\{ \frac{1}{3} (3L_{14} \lambda - L_{13} \theta_0) \lambda \beta_p \sin \gamma + \frac{1}{2} L_{15} \lambda^2 \theta_0 \cos \gamma \right\} / L \\
 K_{95} &= \Omega^2 I_{by} \left\{ \frac{1}{2} L_{15} \lambda^2 \theta_0 \sin \gamma - \frac{1}{3} (3L_{14} \lambda - L_{13} \theta_0) \lambda \beta_p \sin \gamma \right\} / L \\
 K_{96} &= \Omega^2 I_{by} \left\{ -\frac{1}{2} L_{15} \lambda \mu \theta_0 \sin \gamma \right\} / L \\
 K_{97} &= \Omega^2 I_{by} \left\{ L_{14} \lambda^2 \beta_p - \frac{1}{3} (2L_{13} \beta_p - L_{15} e) \lambda \theta_0 + \frac{1}{4} L_{82} c \lambda \right\} / L \\
 K_{98} &= \Omega^2 I_{by} \left\{ \frac{1}{3} [2L_{52} \lambda + (3L_{56} \lambda - 2L_{55} \theta_0)] \mu \sin \gamma + \right. \\
 &\quad \left. -\frac{1}{2} (L_{50} \beta_p + L_{54} \theta_0^2) \tau \cos \gamma \right\} / L^2 \\
 K_{99} &= \Omega^2 I_{by} \left\{ -\frac{1}{12} (8L_{52} - 3L_{51} \theta_0) \beta_p + \frac{1}{4} L_{90} c \lambda \theta_0 \right\} / L^2
 \end{aligned}$$

$$K_{9,10} = \Omega^2 I_b \gamma \{ L_{69} \lambda \mu \sin \gamma + \frac{1}{6} L_{92} c r \cos \gamma \} / L^2$$

$$K_{9,11} = \Omega^2 I_b \gamma \{ \frac{1}{3} (3L_{69} \lambda - L_{63} \theta_0) \lambda \beta_p + \frac{1}{4} L_{93} c \lambda \} / L^2$$

$$K_{91} = K_{92} = K_{93} = 0$$

$$K_{10,4} = \Omega^2 I_b \gamma \{ \frac{1}{12} (4L_{22} \lambda - 3L_{21} \theta_0) r - \frac{1}{6} (2L_{22} \beta_p + 3L_{15} \lambda \theta_0) \mu - \frac{1}{8} r \beta_p \sin 2\gamma +$$

$$+ [\frac{1}{12} (4L_{22} \lambda - 3L_{21} \theta_0) r - \frac{1}{2} L_{15} \lambda \mu \theta_0] \cos 2\gamma \} / L$$

$$K_{10,5} = \Omega^2 I_b \gamma \{ \frac{1}{8} r \beta_p [1 + \cos 2\gamma] + [\frac{1}{12} (4L_{22} \lambda - 3L_{21} \theta_0) r +$$

$$- \frac{1}{2} L_{15} \lambda \mu \theta_0] \sin 2\gamma \} / L$$

$$K_{10,7} = \Omega^2 I_b \gamma \{ -\frac{1}{3} L_{22} \mu \sin \gamma \} / L$$

$$K_{10,8} = \Omega^2 I_b \gamma \{ \frac{1}{4} L_{60} \beta_p - \frac{1}{6} L_{91} c \theta_0 \} / L^2$$

$$K_{10,9} = \Omega^2 I_b \gamma \{ -\frac{1}{3} (3L_{67} \lambda - 2L_{66} \theta_0) \mu \sin \gamma +$$

$$+ (\frac{1}{2} L_{64} r \theta_0 + \frac{1}{3} L_{62} \mu \beta_p) \cos \gamma \} / L^2$$

$$K_{10,10} = \Omega^2 I_b \gamma \{ -\frac{1}{6} (4L_{74} \lambda + 2L_{72} \lambda - 3L_{71} \theta_0) \beta_p - \frac{1}{6} L_{94} c \} / L^2$$

$$K_{10,11} = \Omega^2 I_b \gamma \{ -\frac{2}{3} L_{74} \mu \sin \gamma - \frac{1}{2} L_{73} r \cos \gamma \} / L^2$$

$$K_{10,1} = K_{10,2} = K_{10,3} = K_{10,6} = 0$$

$$K_{11,4} = \Omega^2 I_b \gamma \{ -\frac{1}{3} L_{22} \lambda \beta_p \sin \gamma + \frac{1}{6} (3L_{24} \lambda - 4L_{23} \theta_0) \lambda \cos \gamma \} / L$$

$$K_{11,5} = \Omega^2 I_b \gamma \{ \frac{1}{6} (3L_{24} \lambda - 4L_{23} \theta_0) \lambda \sin \gamma - \frac{1}{3} L_{22} \lambda \beta_p \cos \gamma \} / L$$

$$K_{11,6} = \Omega^2 I_b \gamma \{ -\frac{1}{6} (3L_{24} \lambda - 4L_{23} \theta_0) \mu \sin \gamma - \frac{1}{3} L_{22} \mu \beta_p \cos \gamma \} / L$$

$$K_{11,7} = \Omega^2 I_b \gamma \{ -\frac{1}{6} [2(2L_{22} \beta_p - L_{24} e) \lambda - 3(L_{21} \beta_p - L_{23} e) \theta_0] - \frac{1}{6} L_{83} c \} / L$$

$$K_{11,8} = \Omega^2 I_b \gamma \{ -\frac{1}{3} (3L_{67} \lambda - 2L_{66} \theta_0) \mu \sin \gamma +$$

$$+ (\frac{1}{2} L_{64} r \theta_0 + \frac{1}{3} L_{62} \mu \beta_p) \cos \gamma \} / L^2$$

$$K_{11,9} = \Omega^2 I_b \gamma \{ \frac{1}{4} L_{60} \beta_p - \frac{1}{6} L_{91} c \theta_0 \} / L^2$$

$$K_{11,10} = \Omega^2 I_b \gamma \{ -\frac{2}{3} L_{74} \mu \sin \gamma - \frac{1}{2} L_{73} r \cos \gamma \} / L^2$$

$$K_{11,11} = \Omega^2 I_b \gamma \{ -\frac{1}{6} (4L_{74} \lambda + 2L_{72} \lambda - 3L_{71} \theta_0) \beta_p - \frac{1}{6} L_{94} c \} / L^2$$

$$K_{11,1} = K_{11,2} = K_{11,3} = 0$$

$$\begin{aligned}
 P_X &= \Omega^2 I_{b\gamma} \left\{ \frac{1}{4} L_5 \tau \beta_p [1 + \cos 2\gamma] - \left[\frac{1}{4} (2L_5 \lambda - L_6 \theta_0) \tau - \frac{1}{2} L_8 \lambda \mu \theta_0 \right] \sin 2\gamma \right\} / L \\
 P_Y &= \Omega^2 I_{b\gamma} \left\{ \left[\frac{1}{4} (2L_5 \lambda - L_6 \theta_0) \tau - \frac{1}{2} L_8 \lambda \mu \theta_0 \right] [1 + \cos 2\gamma] + \frac{1}{4} L_5 \tau \beta_p \sin 2\gamma \right\} / L \\
 P_Z &= \Omega^2 I_{b\gamma} \left\{ -\frac{1}{6} (3L_5 \lambda - 2L_4 \theta_0) \right\} / L \\
 Q_X &= \Omega^2 I_{b\gamma} \left\{ -\left[\frac{1}{6} L_{13} \tau + \frac{1}{12} (3L_5 \lambda - 4L_4 \theta_0) \mu \right] \sin 2\gamma \right\} \\
 Q_Y &= \Omega^2 I_{b\gamma} \left\{ \left[\frac{1}{6} L_{13} \tau + \frac{1}{12} (3L_5 \lambda - 4L_4 \theta_0) \mu \right] [1 + \cos 2\gamma] \right\} \\
 Q_Z &= \Omega^2 I_{b\gamma} \left\{ \frac{1}{6} (3L_5 \lambda - 2L_4 \theta_0) \lambda - \frac{1}{4} D_1 C_{d0} / a \right\} \\
 Q_t &= \Omega^2 I_{b\gamma} \left\{ -\left[\frac{1}{3} L_3 \tau + \frac{1}{6} (3L_5 \lambda - 4L_4 \theta_0) \mu \right] \cos \gamma \right\} \\
 P_v &= \Omega^2 I_{b\gamma} \left\{ \frac{1}{6} (3L_{14} \lambda - 2L_{13} \theta_0) \lambda - \frac{1}{4} D_2 C_{d0} / a \right\} / L \\
 P_v &= \Omega^2 I_{b\gamma} \left\{ \left[\frac{1}{3} (3L_{14} \lambda - L_{13} \theta_0) \tau - \frac{1}{2} L_{15} \lambda \mu \theta_0 \right] \cos \gamma \right\} / L \\
 P_w &= \Omega^2 I_{b\gamma} \left\{ -\frac{1}{12} (4L_{22} \lambda - 3L_{21} \theta_0) \right\} / L \\
 P_w &= \Omega^2 I_{b\gamma} \left\{ -\left[\frac{1}{3} L_{22} \tau + \frac{1}{6} (3L_{24} \lambda - 4L_{23} \theta_0) \mu \right] \cos \gamma \right\} / L
 \end{aligned}$$

(10.32)

Chapter 11. HARMONIC BALANCE SOLUTION OF EQUATIONS WITH PERIODIC COEFFICIENTS

The equations of motion and aerodynamic loads derived in the preceding chapters form a second order system of ordinary linear differential equations with periodic coefficients. A solution may be pursued using any of a number of techniques presented in the literature. Several of these are introduced briefly, followed by a detailed development of a general harmonic balance method useful for stability, steady-state response, and transient response calculations.

Perhaps the most straightforward approach is direct numerical integration of the equations beginning at some chosen initial conditions. Stability is determined by inspecting the result for growth or decay. In a stable case, the steady-state response is found if the calculation is carried far enough, or if the correct initial conditions happen to be chosen. This method ignores Floquet-Liapunov Theory [53, 54, 55] which reveals the mathematical form the solution must take. Floquet theory has spawned three general families of solution techniques:

- 1) Perturbation methods.
- 2) Calculation of the Floquet transition matrix by numerical integration.
- 3) Harmonic balance methods.

The perturbation method was first developed by Hsu [56]. These methods are limited to cases where the periodicity of coefficients can be expressed in terms of a small parameter. Inspection shows that this is not the case for the equations in question.

Calculation of the Floquet transition matrix can be accomplished by a number of numerical schemes [57, 58, 59, 60]. In general, integration proceeds over only one period in these methods. They come highly recommended for systems with many degrees of freedom.

Hill's method of infinite determinants is a classic harmonic balance method [55, 61]. Bolotin applied this method to problems of mechanical stability, but without the aid of the digital computer he sought only limited approximate solutions to the unwieldy determinants [55]. Recently, Takahashi has updated the harmonic balance method for the stability problem [62]. The method to be developed in this chapter is closely related to Takahashi's method and to a similar method used by Sheu [44]. Peters and Ormiston have derived a general harmonic balance operator for the steady-state response problem [63]. See also reference [64].

11.1 THE HARMONIC BALANCE TRANSFORM

The equations of motion and aerodynamic forces are in the general form

$$[M(\gamma)]\{\ddot{q}\} + [C(\gamma)]\{\dot{q}\} + [K(\gamma)]\{q\} = \{Q(\gamma)\} \quad (11.1)$$

where now $\gamma = \Omega t$ and $(\dot{}) = d/d\gamma$. The periodic coefficient matrices may be written as

$$M(\gamma) = M_0 + \sum_{n=1}^N (M_{s_n} \sin n\gamma + M_{c_n} \cos n\gamma) \quad (11.2)$$

$$C(\gamma) = C_0 + \sum_{n=1}^N (C_{s_n} \sin n\gamma + C_{c_n} \cos n\gamma) \quad (11.3)$$

$$K(\gamma) = K_0 + \sum_{n=1}^N (K_{s_n} \sin n\gamma + K_{c_n} \cos n\gamma) \quad (11.4)$$

$$Q(\gamma) = Q_0 + \sum_{n=1}^N (Q_{s_n} \sin n\gamma + Q_{c_n} \cos n\gamma) \quad (11.5)$$

Floquet theory gives the form of the solution as [55]

$$q = \exp(p\gamma) \left\{ \frac{1}{2} b_0 + \sum_{m=1}^{\infty} [a_m \sin m\gamma + b_m \cos m\gamma] \right\} \quad (11.6)$$

Here, the vectors b_0 , a_m and b_m are independent of time.

A more general solution form is [see 44]

$$q = \frac{1}{2}q_0(\gamma) + \sum_{m=1}^{\infty} [q_{s_m}(\gamma)\sin m\gamma + q_{c_m}(\gamma)\cos m\gamma] \quad (11.7)$$

Now, as indicated, the vectors q_0 , q_{s_m} and q_{c_m} are functions of time so that

$$\begin{aligned} \dot{q} = \frac{1}{2}\dot{q}_0 + \sum_{m=1}^{\infty} [(\dot{q}_{s_m} - m\dot{q}_{c_m})\sin m\gamma \\ + (\dot{q}_{c_m} + m\dot{q}_{s_m})\cos m\gamma] \end{aligned} \quad (11.8)$$

and

$$\begin{aligned} \ddot{q} = \frac{1}{2}\ddot{q}_0 + \sum_{m=1}^{\infty} [(\ddot{q}_{s_m} - 2m\dot{q}_{c_m} - m\dot{q}_{s_m})\sin m\gamma \\ + (\ddot{q}_{c_m} + 2m\dot{q}_{s_m} - m\dot{q}_{c_m})\cos m\gamma] \end{aligned} \quad (11.9)$$

Equations (11.2-5) and (11.7-9) are substituted into equation (11.1) and simplified using the following trigonometric identities.

$$\begin{aligned} \sin m\gamma \sin n\gamma &= \frac{1}{2}[\cos(m-n)\gamma - \cos(m+n)\gamma] \\ \sin m\gamma \cos n\gamma &= \frac{1}{2}[\sin(m-n)\gamma + \sin(m+n)\gamma] \\ \cos m\gamma \cos n\gamma &= \frac{1}{2}[\cos(m-n)\gamma + \cos(m+n)\gamma] \end{aligned} \quad (11.10)$$

The resulting double series equation is rearranged to expose the sum over harmonics, and the series are truncated at some harmonic, P. Because this equation in harmonic series must be satisfied for all time γ , the coefficients of each harmonic must balance independently. Thus, separate

equations can be written for constant terms (zeroth harmonic), for $\sin \gamma$ and $\cos \gamma$ terms (first harmonic), and so on, up to the Pth harmonic. Generally, it will not be possible to balance some terms of harmonic greater than P which occur in the sums; such terms are discarded.

This process transforms the periodic-coefficient system (11.1) into an approximate constant-coefficient system which is $2P + 1$ times larger. A new vector of coordinates is defined by stacking the harmonic coefficients,

$$\{\bar{q}\} = \begin{Bmatrix} q_0 \\ q_{s1} \\ q_{c1} \\ \vdots \\ \vdots \\ q_{cp} \end{Bmatrix} \quad (11.11)$$

Then, the transformed equations are given in the form

$$[\bar{M}]\{\ddot{\bar{q}}\} + [\bar{C}]\{\dot{\bar{q}}\} + [\bar{K}]\{\bar{q}\} = \{\bar{Q}\} \quad (11.12)$$

Each of the barred matrices is a matrix of smaller matrices. For periodic coefficients up to second harmonic ($N = 2$) and truncation at $P = 3$, these constant-coefficient barred matrices are given on the following pages. A pattern emerges which may be used to extend these matrices for $P > 3$.

[M] -

M_o	M_{s1}	M_{c1}	M_{s2}	M_{c2}	M_{s1}	M_{c2}	0	0
M_{s1}	$2M_o - M_{c2}$	M_{s2}	M_{c1}	M_{s1}	M_{c1}	$-M_{s1}$	M_{c2}	$-M_{s2}$
M_{c1}	M_{s2}	$2M_o + M_{c2}$	M_{s1}	M_{c1}	M_{c1}	M_{c1}	M_{c2}	M_{c2}
M_{s2}	M_{c1}	M_{s1}	$2M_o$	0	0	0	M_{c1}	$-M_{s1}$
M_{c2}	$-M_{s1}$	M_{c1}	M_{c1}	$2M_o$	$2M_o$	M_{s1}	M_{s1}	M_{c1}
0	M_{c2}	M_{s2}	M_{c1}	M_{s2}	M_{c1}	M_{s1}	$2M_o$	0
0	$-M_{s2}$	M_{c2}	$-M_{s1}$	M_{c1}	M_{c1}	M_{c1}	0	$2M_o$

(11.13)

[C] -

C_o	$C_{s_1} + 2M_{c_1}$	$C_{c_1} - 2M_{s_1}$	$C_{s_2} + 4M_{c_2}$	$C_{s_2} - 4M_{c_1}$	$C_{c_2} - 6M_{s_2}$	0
C_{s_1}	$2C_o - C_{c_2} + 2M_{s_2}$	$C_{s_2} + 2M_{c_2} - 4M_o$	$C_{c_1} - 4M_{s_1}$	$-C_{s_1} - 4M_{c_1}$	$C_{c_2} - 6M_{s_2}$	$-C_{s_2} - 6M_{c_2}$
C_{c_1}	$C_{s_2} + 2M_{c_2} + 4M_o$	$2C_o + C_{c_2} - 2M_{s_2}$	$C_{s_1} + 4M_{c_1}$	$C_{c_1} - 4M_{s_1}$	$C_{s_2} + 6M_{c_2}$	$C_{c_2} - 6M_{c_2}$
C_{s_2}	$C_{c_1} + 2M_{s_1}$	$C_{s_1} - 2M_{c_1}$	$2C_o$	$-8M_o$	$C - 6M$	$-C - 6M$
C_{c_2}	$-C_{s_1} + 2M_{c_1}$	$C_{c_1} + 2M_{s_1}$	$8M_o$	$2C_o$	$C_{s_1} + 6M_{c_1}$	$C_{c_2} - 6M_{s_2}$
0	$C_{c_2} + 2M_{s_2}$	$C_{s_2} - 2M_{c_2}$	$C_{c_1} + 4M_{s_1}$	$C_{s_1} - 4M_{c_1}$	$2C_o$	$-12M_o$
0	$-C_{s_2} + 2M_{c_2}$	$C_{c_2} + 2M_{s_2}$	$-C_{s_1} + 4M_{c_1}$	$C_{c_1} + 4M_{s_1}$	$12M_o$	$2C_o$

(11.14)

[K] =

K_o	$K_{s_1} + C_{c_1} - M_{s_1}$	$K_{c_1} - C_{s_1} - M_{c_1}$	$K_{s_2} + 2C_{c_2} - 4M_{s_2}$	$K_{c_2} - 2C_{s_2} - 4M_{c_2}$	0	0
K_{s_1}	$\{2K_o - 2M_o$ $- K_{c_2} + C_{s_2} + M_{c_2}\}$	$\{-2C_o$ $+ K_{s_2} + C_{c_2} - M_{s_2}\}$	$K_{c_1} - 2C_{s_1} - 4M_{c_1}$	$-K_{s_1} - 2C_{c_1} + 4M_{s_1}$	$K_{c_2} - 3C_{s_2} - 9M_{c_2}$	$-K_{s_2} - 3C_{c_2} + 9M_{s_2}$
K_{c_1}	$\{2C_o$ $+ K_{s_2} + C_{c_2} - M_{s_2}\}$	$\{2K_o - 2M_o$ $+ K_{c_2} - C_{s_2} - M_{c_2}\}$	$K_{s_1} + 2C_{c_1} - 4M_{s_1}$	$K_{c_1} - 2C_{s_1} - 4M_{c_1}$	$K_{s_2} + 3C_{c_2} - 9M_{s_2}$	$K_{c_2} - 3C_{s_2} - 9M_{c_2}$
K_{s_2}	$K_{c_1} + C_{s_1} - M_{c_1}$	$K_{s_1} - C_{c_1} - M_{s_1}$	$2K_o - 8M_o$	$-4C_o$	$K_{c_1} - 3C_{s_1} - 9M_{c_1}$	$-K_{s_1} - 3C_{c_1} + 9M_{s_1}$
K_{c_2}	$-K_{s_1} + C_{c_1} + M_{s_1}$	$K_{c_1} + C_{s_1} - M_{c_1}$	$4C_o$	$2K_o - 8M_o$	$K_{s_1} + 3C_{c_1} - 9M_{s_1}$	$K_{c_1} - 3C_{s_1} - 9M_{c_1}$
0	$K_{c_2} + C_{s_2} - M_{c_2}$	$K_{s_2} - C_{c_2} - M_{s_2}$	$K_{c_1} + 2C_{s_1} - 4M_{c_1}$	$K_{s_1} - 2C_{c_1} - 4M_{s_1}$	$2K_o - 18M_o$	$-6C_o$
0	$-K_{s_2} + C_{c_2} + M_{s_2}$	$K_{c_2} + C_{s_2} - M_{c_2}$	$-K_{s_1} + 2C_{c_1} + 4M_{s_1}$	$K_{c_1} + 2C_{s_1} - 4M_{c_1}$	$6C_o$	$2K_o - 18M_o$

(11.15)

ORIGINAL PAGE IS
OF POOR QUALITY

(11.16)

$$\left[\begin{array}{ccccccc} 2Q_0 & 2Q_{s1} & 2Q_{c1} & 2Q_{s2} & 2Q_{c2} & 2Q_{s3} & 2Q_{c3} \end{array} \right]$$

$$(\bar{Q}) =$$

These equations are solved using standard techniques for constant coefficient equations, and the periodic solution is reconstructed using equation (11.7). The equivalence of the two forms (11.6 and 11.7) may be seen by realizing that the solution must be in the form

$$\{\bar{q}\} = \{\bar{a}\} \exp(p\tau) \quad (11.17)$$

where \bar{a} is a vector of amplitudes. Thus, the stability of the periodic-coefficient system is approximately determined by examining the stability of the transformed equations. For a stable system, the steady-state response is simply

$$\{\bar{q}\} = [\bar{K}]^{-1} \{\bar{Q}\} \quad (11.18)$$

The steady-state periodic response is then determined from equation (11.7). It should be noted that it may be possible to calculate a steady response for unstable cases as well. The steady portion of the present method is analogous to the method of reference [63].

11.2 INITIAL CONDITIONS AND TRANSIENT RESPONSE

Application of the harmonic balance method to the transient response problem is somewhat more complicated. The initial conditions on q and \dot{q} are not sufficient to determine initial conditions on \bar{q} and $\dot{\bar{q}}$ because there are $2P + 1$ times as many. However, assuming that they can be established, standard techniques again apply and the response can be reconstructed using equation (11.7).

To review, the constant-coefficient equations can be recast in state vector form as

$$\{\ddot{\bar{x}}\} - [\bar{\Lambda}]\{\bar{x}\} = \{\bar{R}\} \quad (11.19)$$

where

$$\{\bar{x}\} = \begin{Bmatrix} \bar{q} \\ \dot{\bar{q}} \end{Bmatrix} \quad [\bar{\Lambda}] = \begin{bmatrix} 0 & 1 \\ -\bar{M}^{-1}\bar{K} & -\bar{M}^{-1}\bar{C} \end{bmatrix} \quad \{\bar{R}\} = \begin{Bmatrix} 0 \\ \bar{M}^{-1}\bar{Q} \end{Bmatrix}$$

The eigenvalues of the system p_j , and the corresponding eigenvectors \bar{v}_j are easily computed using standard eigenvalue routines. The general solution of equation (11.19) is a superposition of these solutions,

$$\{\bar{x}\} = [\bar{v}_1 \ \bar{v}_2 \ \dots \ \bar{v}_j \ \dots] \{c_j \exp(p_j \tau)\} \quad (11.20)$$

where the c_j are arbitrary constants which may be determined from the initial conditions $\bar{x}(0)$,

$$\{c_j\} = [\bar{v}_1 \ \bar{v}_2 \ \dots \ \bar{v}_j \ \dots]^{-1} \{\bar{x}(0)\} \quad (11.21)$$

Note that the second half of each eigenvector, which corresponds to the velocities, is no longer required once the initial conditions have been applied. The eigenvectors are partitioned in the same manner as q , that is

$$\{\bar{v}\} = \begin{Bmatrix} v_0 \\ v_{s1} \\ v_{c1} \\ \vdots \\ v_{cp} \end{Bmatrix} \quad (11.22)$$

Eigenvalues p_j occur as either complex conjugate root pairs or as real roots, and the corresponding eigenvectors likewise. Since the initial conditions are real numbers, it can be shown that the constants c_j also follow the same pattern. As a result, it is convenient to combine the contributions from conjugate pairs when reconstructing the periodic response. Consider a set of conjugate pairs:

Eigenvalue	$a + iv$	$a - iv$
Eigenvector	$\bar{u} + i\bar{w}$	$\bar{u} - i\bar{w}$
Constant	$a + ib$	$a - ib$

The combined contribution of such a generic conjugate pair to the response is

$$\begin{aligned} \Delta q = & \exp(\alpha \gamma) \{ (au_0 - bw_0) \cos \nu \gamma - (bu_0 + aw_0) \sin \nu \gamma \\ & + \sum_{n=1}^P [(-au_{s_n} + bw_{s_n} - bu_{c_n} - aw_{c_n}) \sin (\nu - n) \gamma \\ & + (au_{s_n} - bw_{s_n} - bu_{c_n} - aw_{c_n}) \sin (\nu + n) \gamma \\ & + (au_{c_n} - bw_{c_n} - bu_{s_n} - aw_{s_n}) \cos (\nu - n) \gamma \\ & + (au_{c_n} - bw_{c_n} + bu_{s_n} + aw_{s_n}) \cos (\nu + n) \gamma] \} \quad (11.23) \end{aligned}$$

Here, the imaginary part of the exponential in the solution has been expanded and combined with the harmonics in the solution. The contribution of a generic real root is simply

$$\Delta q = a \exp(\alpha \gamma) \{ \frac{1}{2} u_0 + \sum_{n=1}^P [u_{s_n} \sin n \gamma + u_{c_n} \cos n \gamma] \} \quad (11.24)$$

The question of initial conditions is answered by considering the implications of applying initial conditions to various harmonic coefficients. An initial condition applied to a zeroth harmonic coefficient (q_0 and \dot{q}_0) implies an initial displacement or disturbance. But any non-zero initial condition applied to a first or higher harmonic coefficient implies an on-going periodic motion, which would have to satisfy the equations of motion. Indeed, such is the case for a transient response which

begins at one steady-state condition and equilibrates again at a second. Except for this type of problem, the initial conditions are applied to q_0 and \dot{q}_0 as follows

$$\begin{aligned}\dot{q}_0(0) &= 2\dot{q}(0) \\ q_0(0) &= 2q(0)\end{aligned}\quad (11.25)$$

$$\dot{q}_{s1} = \dot{q}_{c1} = \dots = \dot{q}_{cp} = q_{s1} = \dots = q_{cp} = 0 \quad (11.25)$$

Several notes are in order at this point. In some cases, the constant-coefficient system (equation 11.11) may uncouple into several smaller subsystems. A rotor with two identical blades, as presented in the preceding chapters, has two such subsystems:

- 1) Even harmonics of support motion and of symmetric rotor modes with odd harmonics of antisymmetric rotor modes.
- 2) Odd harmonics of support motion and of symmetric rotor modes with even harmonics of antisymmetric rotor modes.

When elastic modes of the blades are included in the equations, these two sets are possible only if the multiblade coordinates are used (9.15 and 9.16).

For stability and transient response problems, it can be shown that the two sets become equivalent as the number of harmonics P goes to infinity. One form of the solution is included within the other, and it is tempting to drop one or the other of them. However, the two subsystems are not equivalent when the series are truncated at some finite P . The subsystems will generally have different orders and

different distributions of harmonics to the various degrees of freedom. The system may be partitioned and each subsystem studied separately, but each subsystem must be studied and the results must be combined. These points are illuminated in the application of the method in the following chapters.

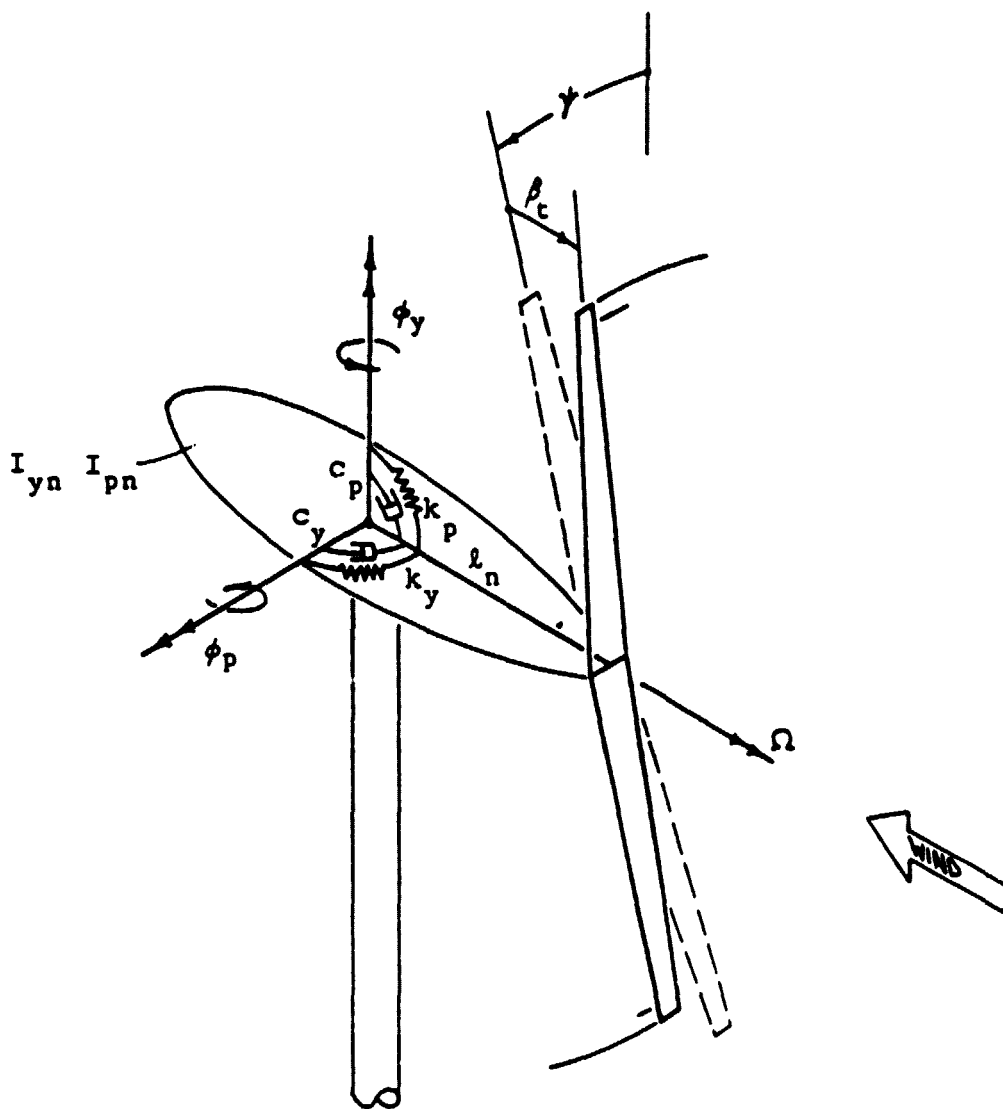
ORIGINAL PAGE IS
OF POOR QUALITY

Chapter 12. THE YAW-PITCH-TEETER MODEL

A simple rotor-tower model which may be proposed for a MOD-2 type wind turbine involves only yawing and pitching of the nacelle and teetering of the rotor. In this chapter, the model equations of motion are extracted from the eleven degree of freedom expressions derived in Chapters 9 and 10, and tower contributions are added. The equations are arranged to make use of the harmonic balance method described in Chapter 11. Also, the response of the yaw-pitch-teeter model to imbalance is calculated in closed form for a restricted case. In the next chapter, an aeroelastic stability study is presented for the complete yaw-pitch-teeter model.

Thus, the yaw-pitch-teeter model is developed with several aims. First of all, the development demonstrates the transformation or reduction of the six hub degrees of freedom to those chosen for the tower portion of a model. The same process would be used to extract other models, simple or complex, from the eleven degree of freedom parent. Secondly, the yaw-pitch-teeter model is used to give rudimentary results for aeroelastic stability and response. These will help explain the aeroelastic behavior of wind turbines with teetering rotors.

ORIGINAL PAGE IS
OF POOR QUALITY



Sketch 12.1 The Yaw-Pitch-Teeter Model

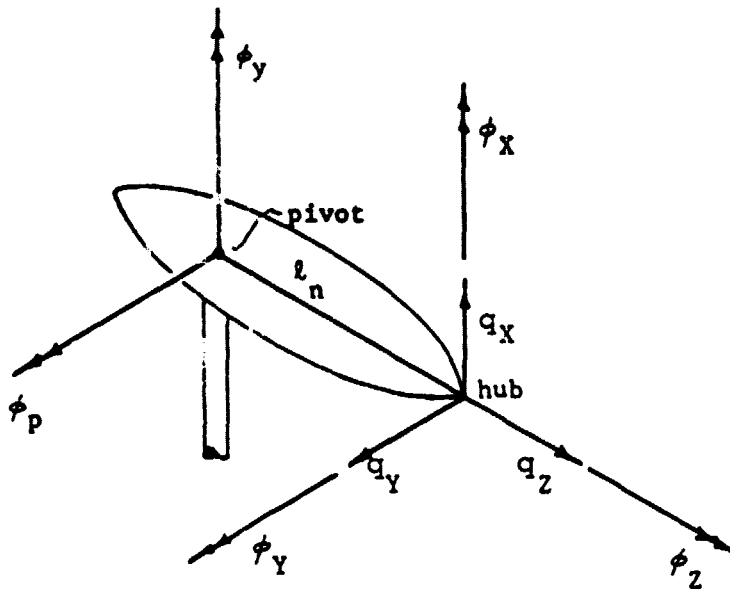
Sketch 12.1 gives a schematic of the proposed model. The elastic motions of the tower, yaw drive, and nacelle are represented by an equivalent pivot of the nacelle located a distance l_n downstream from the hub point. The nacelle has

degrees of freedom in yaw ϕ_y and in pitch ϕ_p which are constrained by springs k_y and k_p , and by dampers c_y and c_p as shown. It also has moments of inertia I_{yn} and I_{pn} about the respective axes.

The rotor has only the teeter degree of freedom β_t which is constrained by a spring $2k_t$, and a damper $2c_t$. It spins at a constant rate Ω and otherwise has all the attributes introduced in Chapters 9 and 10. Tip pitch control is a desirable feature, and it may be included through the aerodynamic integrals of Appendix C.

12.1 REDUCTION OF HUB COORDINATES

The first step in formulating the yaw-pitch-teeter model is to recognize the relationship between the six hub deflections and the tower deflections chosen, here ϕ_y and ϕ_p . This relationship is then used to transform the equations of motion and aerodynamic loads. Quadratic terms are required to transform the Q matrix, since this will produce terms which are moved to the K matrix.



Sketch 12.2 Hub and Tower Deflections

Both hub and tower deflections are shown in Sketch 12.2. These two sets are easily related by using the transformations of Chapter 9. The rotations are taken in the same order, that is ϕ_p then ϕ_y and then $\psi = \Omega t$. In this case ϕ_y and ϕ_p are analogous to ϕ_x and ϕ_y .

$$\begin{aligned}
 \phi_x &= \phi_y \\
 \phi_y &= \phi_p \\
 \phi_z &= 0
 \end{aligned}
 \tag{12.1}$$

The vector from the pivot to the hub is given in inertial coordinates as (see equation 9.1)

$$\tilde{\ell}_n = [T_Y][T_X] \begin{pmatrix} 0 \\ 0 \\ \ell_n \end{pmatrix} = \begin{pmatrix} \ell_n \cos \phi_y \sin \phi_p \\ -\ell_n \sin \phi_y \\ \ell_n \cos \phi_y \cos \phi_p \end{pmatrix} \quad (12.2)$$

Note that ϕ_y and ϕ_p are substituted here. This vector is also

$$\hat{\ell}_n = \begin{pmatrix} q_X \\ q_Y \\ \ell_n + q_Z \end{pmatrix} \quad (12.3)$$

Equations (12.2) and (12.3) are compared to give

$$\begin{aligned} q_X &= \ell_n \cos \phi_y \sin \phi_p & \approx & \ell_n \phi_p \\ q_Y &= -\ell_n \sin \phi_y & \approx & -\ell_n \phi_y \\ q_Z &= -\ell_n (1 - \cos \phi_y \cos \phi_p) & \approx & 0 \end{aligned} \quad (12.4)$$

The hub deflections q_X, \dots, q_Z are now all expressed in terms of the tower deflections ϕ_y and ϕ_p . The approximate expressions given last in equations (12.4) are adequate only to relate the coordinates.

The corresponding generalized loads can be related through the variation of the work done by them.

ORIGINAL PAGE IS
OF POOR QUALITY

$$Q_y \delta \phi_y + Q_p \delta \phi_p = P_x \delta q_x + P_y \delta q_y + \dots + Q_z \delta \phi_z \quad (12.5)$$

but

$$\begin{aligned} \delta q_x &= \ell_n \delta \phi_p & \delta \phi_x &= \delta \phi_y \\ \delta q_y &= -\ell_n \delta \phi_y & \delta \phi_y &= \delta \phi_p \\ \delta q_z &= -\ell_n (\phi_y \delta \phi_y + \phi_p \delta \phi_p) & \delta \phi_z &= 0 \end{aligned} \quad (12.6)$$

These are substituted into equation (12.5) and coefficients of $\delta \phi_y$ and $\delta \phi_p$ are separately equated to give

$$\begin{aligned} Q_y &= Q_x - \ell_n P_y - \ell_n \phi_y P_z \\ Q_p &= Q_y + \ell_n P_x - \ell_n \phi_p P_z \end{aligned}$$

These results could perhaps be written by inspection from Sketch 9.2, but the preceding method would be valuable for more complex models.

One way to use equations (12.1) and (12.4), and equation (12.7) is to set up transformations between the deflections and between the loads. Only the first seven of the eleven degrees of freedom are used in this model, $q_x \dots \beta_t$. These are related to ϕ_y , ϕ_p , and β_t by using (12.1) and (12.4).

$$\begin{Bmatrix} q_X \\ q_Y \\ q_Z \\ \phi_X \\ \phi_Y \\ \phi_Z \\ \beta_t \end{Bmatrix} = \begin{bmatrix} 0 & l_n & 0 \\ -l_n & 0 & 0 \\ 0 & 0 & 0 \\ 1 & 0 & 0 \\ 0 & 1 & 0 \\ 0 & 0 & 0 \\ 0 & 0 & 1 \end{bmatrix} \begin{Bmatrix} \phi_y \\ \phi_p \\ \beta_t \end{Bmatrix} \quad (12.8)$$

The corresponding loads are related by using (12.7).

$$\begin{Bmatrix} Q_y \\ Q_p \\ Q_t \end{Bmatrix} = \begin{bmatrix} 0 & -l_n & -l_n \phi_y & 1 & 0 & 0 & 0 \\ l_n & 0 & -l_n \phi_p & 0 & 1 & 0 & 0 \\ 0 & 0 & 0 & 0 & 0 & 0 & 1 \end{bmatrix} \begin{Bmatrix} P_X \\ P_Y \\ P_Z \\ Q_X \\ Q_Y \\ Q_Z \\ Q_t \end{Bmatrix} \quad (12.9)$$

Equation 12.8 is substituted into the equations of motion and aerodynamic terms, which are then premultiplied by the transformation of equation (12.9). This reduces the seven by seven equations to three by three. The terms $-l_n \phi_y$ and $-l_n \phi_p$ need not be used when M, C, and K are premultiplied, but they produce linear terms when Q is premultiplied. These are subsequently moved into K.

This is a convenient place to note an addition to the ordering scheme. A reasonable order of magnitude for HAWTs is

$$\ell_n/L \quad O(\epsilon^4)$$

Terms of differing magnitude are combined when the equations are reduced, and the ordering scheme must be applied to the aerodynamic terms as before in Section 10.1.

12.2 EQUATIONS OF MOTION

All that remains after reducing the hub degrees of freedom is to add the tower contributions to the equations of motion. These are very simple diagonal mass, damping, and stiffness terms. Without the rotor, the nacelle equations of motion are

$$\begin{aligned} I_{yn} \ddot{\phi}_y + c_y \dot{\phi}_y + k_y \phi_y &= 0 \\ I_{pn} \ddot{\phi}_p + c_p \dot{\phi}_p + k_p \phi_p &= gS_n \end{aligned} \quad (12.10)$$

All loads on the nacelle are ignored except for its mass imbalance S_n . It is assumed that the system is statically balanced so that $S_n + 2M_b \ell_n = 0$ and $S_b^* = 0$.

It is convenient to define total moments of inertia about the yaw and pitch axes which include the rotor mass

$$I_y = I_{yn} + 2M_b \ell_n^2 \quad I_p = I_{pn} + 2M_b \ell_n^2 \quad (12.11)$$

Further, the following nondimensional parameters are defined

$$\begin{aligned}
 \bar{M}_b &= M_b L^2 / I_b & \bar{S}_b &= S_b L / I_b \\
 \bar{I}_y &= I_y / 2I_b & \bar{I}_p &= I_p / 2I_b \\
 v_y^2 &= k_y / \Omega^2 I_y & \zeta_y &= \frac{1}{2} \sqrt{c_y^2 / k_y I_y} \\
 v_p^2 &= k_p / \Omega^2 I_p & \zeta_p &= \frac{1}{2} \sqrt{c_p^2 / k_p I_p} \\
 v_t^2 &= k_t / \Omega^2 I_b & \zeta_t &= \frac{1}{2} \sqrt{c_t^2 / k_t I_b} \\
 \bar{\ell}_n &= \ell_n / L & \bar{c} &= c / L
 \end{aligned} \tag{12.12}$$

The reduced equations of motion with aerodynamic terms and tower contributions are made nondimensional by dividing through by $2\Omega^2 I_b$, and all of the preceding definitions are applied. The equations are in the familiar form

$$[M] \begin{Bmatrix} \ddot{\phi}_y \\ \ddot{\phi}_p \\ \ddot{\beta}_t \end{Bmatrix} + [C] \begin{Bmatrix} \dot{\phi}_y \\ \dot{\phi}_p \\ \dot{\beta}_t \end{Bmatrix} + [K] \begin{Bmatrix} \phi_y \\ \phi_p \\ \beta_t \end{Bmatrix} = \{Q\} \tag{12.13}$$

where now $(\dot{}) = d/d\tau$. The coefficient matrices are given on the following pages in a form compatible with Chapter 11.

ORIGINAL PAGE IS
OF POOR QUALITY

[M] =

$$\begin{bmatrix} \bar{I}_y + \frac{1}{2} \cos^2 \beta_p + (1 - \bar{S}_b^2 / \bar{M}_b) \sin^2 \beta_p & 0 & 0 \\ 0 & \bar{I}_p + \frac{1}{2} \cos^2 \beta_p + (1 - \bar{S}_b^2 / \bar{M}_b) \sin^2 \beta_p & 0 \\ 0 & 0 & 1 \end{bmatrix}$$

$$+ \begin{bmatrix} 0 & 0 & 1 - (\bar{S}_b^2 / \bar{M}_b) \sin^2 \beta_p \\ 0 & 0 & 0 \\ 1 - (\bar{S}_b^2 / \bar{M}_b) \sin^2 \beta_p & 0 & 0 \end{bmatrix} \sin \gamma$$

$$+ \begin{bmatrix} 0 & 0 & 0 \\ 0 & 0 & -1 + (\bar{S}_b^2 / \bar{M}_b) \sin^2 \beta_p \\ 0 & -1 + (\bar{S}_b^2 / \bar{M}_b) \sin^2 \beta_p & 0 \end{bmatrix} \cos \gamma$$

$$+ \begin{bmatrix} 0 & -\frac{1}{2} \cos^2 \beta_p & 0 \\ -\frac{1}{2} \cos^2 \beta_p & 0 & 0 \\ 0 & 0 & 0 \end{bmatrix} \sin 2\gamma$$

$$+ \begin{bmatrix} -\frac{1}{2} \cos^2 \beta_p & 0 & 0 \\ 0 & \frac{1}{2} \cos^2 \beta_p & 0 \\ 0 & 0 & 0 \end{bmatrix} \cos 2\gamma \quad (12.14)$$

21 3049
YTUJ90

[c] =

$$\begin{bmatrix} \frac{1}{16}\gamma L_1 + 2\zeta_y \bar{I}_y \nu_y & \cos^2 \beta_p & 0 \\ -\cos^2 \beta_p & \frac{1}{16}\gamma L_1 + 2\zeta_p \bar{I}_p \nu_p & 0 \\ 0 & 0 & \frac{1}{8}\gamma L_1 + 2\zeta_c \nu_c \end{bmatrix}$$

$$+ \begin{bmatrix} 0 & 0 & \frac{1}{8}\gamma L_1 \\ 0 & 0 & 2(1 - \bar{S}_b^2 / \bar{M}_b) \sin^2 \beta_p \\ \frac{1}{8}\gamma L_1 & 2\cos^2 \beta_p & 0 \end{bmatrix} \sin \gamma$$

$$+ \begin{bmatrix} 0 & 0 & 2(1 - \bar{S}_b^2 / \bar{M}_b) \sin^2 \beta_p \\ 0 & 0 & -\frac{1}{8}\gamma L_1 \\ 2\cos^2 \beta_p & -\frac{1}{8}\gamma L_1 & 0 \end{bmatrix} \cos \gamma$$

$$+ \begin{bmatrix} \cos^2 \beta_p & -\frac{1}{16}\gamma L_1 & 0 \\ -\frac{1}{16}\gamma L_1 & -\cos^2 \beta_p & 0 \\ 0 & 0 & 0 \end{bmatrix} \sin 2\gamma$$

$$+ \begin{bmatrix} -\frac{1}{16}\gamma L_1 & -\cos^2 \beta_p & 0 \\ -\cos^2 \beta_p & \frac{1}{16}\gamma L_1 & 0 \\ 0 & 0 & 0 \end{bmatrix} \cos 2\gamma \quad (12.15)$$

ORIGINAL PAGE IS
OF POOR QUALITY

[K] =

$$\left[\begin{array}{ccc} \left\{ \bar{I}_y v^2 - \frac{1}{12} \gamma L_3 \lambda \beta_p \right. & \frac{1}{24} \gamma (3L_5 \lambda - 4L_4 \theta_o) \lambda & 0 \\ \left. - \frac{1}{12} \gamma (3L_5 \lambda - 2L_4 \theta_o) \bar{L}_n \right\} & & \\ - \frac{1}{24} \gamma (3L_5 \lambda - 4L_4 \theta_o) \lambda & \left\{ \bar{I}_p v^2 - \frac{1}{12} \gamma L_3 \lambda \beta_p \right. & 0 \\ & \left. - \frac{1}{12} \gamma (3L_5 \lambda - 2L_4 \theta_o) \bar{L}_n \right\} & \\ & & \{ v_t^2 + \cos 2\beta_p + (\bar{S}_b^2 / \bar{M}_b) \sin^2 \beta_p \\ & & - \frac{1}{12} \gamma [L_{80} \bar{c} + 3(L_3 \lambda - L_2 \theta_o) \beta_p \\ & & - (\bar{S}_b / \bar{M}_b) (2L_5 \lambda - 3L_4 \theta_o) \beta_p] \} \end{array} \right]$$

$$\left[\begin{array}{ccc} 0 & 0 & \{ \cos 2\beta_p + (\bar{S}_b^2 / \bar{M}_b) \sin^2 \beta_p \\ & & + \frac{1}{12} \gamma [(3L_5 \lambda - 2L_4 \theta_o) \bar{L}_n + \\ & & - L_{80} \bar{c} + 3(L_3 \lambda - L_2 \theta_o) \beta_p + \\ & & - (\bar{S}_b / \bar{M}_b) (2L_5 \lambda - 3L_4 \theta_o) \beta_p] \} \\ + & 0 & \frac{1}{12} \gamma (3L_5 \lambda - 4L_4 \theta_o) \lambda \quad \text{sin } \gamma \\ \left[- \frac{1}{6} \gamma L_3 \lambda \beta_p \right. & \left. \frac{1}{12} \gamma (3L_5 \lambda - 4L_4 \theta_o) \lambda \right. & \left. 0 \right] \end{array} \right]$$

$$\left[\begin{array}{ccc} 0 & 0 & \frac{1}{12} \gamma (3L_5 \lambda - 4L_4 \theta_o) \lambda \\ & & \{ -\cos 2\beta_p - (\bar{S}_b^2 / \bar{M}_b) \sin^2 \beta_p \\ + & 0 & - \frac{1}{12} \gamma [(3L_5 \lambda - 2L_4 \theta_o) \bar{L}_n + \\ & & - L_{80} \bar{c} + 3(L_3 \lambda - L_2 \theta_o) \beta_p + \\ & & - (\bar{S}_b / \bar{M}_b) (2L_5 \lambda - 3L_4 \theta_o) \beta_p] \} \quad \text{cos } \gamma + \\ \left[\frac{1}{12} \gamma (3L_5 \lambda - 4L_4 \theta_o) \lambda \right. & \left. \frac{1}{6} \gamma L_3 \lambda \beta_p \right. & \left. 0 \right] \end{array} \right]$$

$$\begin{aligned}
 & + \begin{bmatrix} \frac{1}{24}\gamma(3L_5\lambda - 4L_4\theta_0)\lambda & \frac{1}{12}\gamma L_3\lambda\beta_p & 0 \\ \frac{1}{12}\gamma L_3\lambda\beta_p & -\frac{1}{24}\gamma(3L_5\lambda - 4L_4\theta_0)\lambda & 0 \\ 0 & 0 & 0 \end{bmatrix} \sin 2\gamma \\
 & + \begin{bmatrix} \frac{1}{12}\gamma L_1\lambda\beta_p & -\frac{1}{24}\gamma(3L_5\lambda - 4L_4\theta_0)\lambda & 0 \\ -\frac{1}{24}\gamma(3L_5\lambda - 4L_4\theta_0)\lambda & -\frac{1}{12}\gamma L_3\lambda\beta_p & 0 \\ 0 & 0 & 0 \end{bmatrix} \cos 2\gamma
 \end{aligned}
 \tag{12.16}$$

{Q} =

$$\frac{1}{12}\gamma[2L_3\tau + (3L_5\lambda - 4L_4\theta_0)\mu]K \left\{ \begin{bmatrix} 0 \\ 1 \\ 0 \end{bmatrix} - \begin{bmatrix} 0 \\ 0 \\ 2 \end{bmatrix} \cos \gamma - \begin{bmatrix} 1 \\ 0 \\ 0 \end{bmatrix} \sin 2\gamma + \begin{bmatrix} 0 \\ 1 \\ 0 \end{bmatrix} \cos 2\gamma \right\}
 \tag{12.17}$$

ORIGINAL PAGE IS
 OF POOR QUALITY

12.3 AN APPROXIMATE SOLUTION FOR IMBALANCE

This section is a digression from the main development. The response of the yaw-pitch-teeter model to a small rotor imbalance is calculated in an approximate fashion. While the closed form solution presented is possible only for a restricted case, it is nonetheless of some interest. In this section only, the rotor is assumed to have no precone, no teeter spring or damper, and no aerodynamic loads. The in vacuo equations of motion are then

$$\begin{aligned}
 & \begin{bmatrix} \bar{I}_y + \frac{1}{2}(1-\cos 2\gamma) & -\frac{1}{2}\sin 2\gamma & \sin \gamma \\ -\frac{1}{2}\sin 2\gamma & \bar{I}_p + \frac{1}{2}(1+\cos 2\gamma) & -\cos \gamma \\ \sin \gamma & -\cos \gamma & 1 \end{bmatrix} \begin{Bmatrix} \ddot{\phi}_y \\ \ddot{\phi}_p \\ \ddot{\beta}_t \end{Bmatrix} \\
 & + \begin{bmatrix} 2\zeta_y \bar{I}_y v_y + \sin 2\gamma & 1-\cos 2\gamma & 0 \\ -1-\cos 2\gamma & 2\zeta_p \bar{I}_p v_p + \sin 2\gamma & 0 \\ 2\cos \gamma & 2\sin \gamma & 0 \end{bmatrix} \begin{Bmatrix} \dot{\phi}_y \\ \dot{\phi}_p \\ \dot{\beta}_t \end{Bmatrix} \\
 & + \begin{bmatrix} \bar{I}_y v_y^2 & 0 & \sin \gamma \\ 0 & \bar{I}_p v_p^2 & -\cos \gamma \\ 0 & 0 & 1 \end{bmatrix} \begin{Bmatrix} \phi_y \\ \phi_p \\ \beta_t \end{Bmatrix} = \{0\} \quad (12.18)
 \end{aligned}$$

Imagine a small imbalance mass m located on blade one at L_m . Besides adding negligible increments to the mass and moment of inertia terms, general imbalance terms are introduced which augment K and Q . These terms are quoted here without documentation. They can be derived from the kinetic and potential energy expressions (9.7 and 9.12) by

replacing M_b with m , S_b with $m\ell_m$, and i_b with $m\ell_m^2$ and applying Lagrange's equations and the transformations of this chapter. The resulting imbalance terms are

$$\Delta[K] = (\bar{s}g/\Omega^2 L) \begin{bmatrix} 0 & 0 & 0 \\ 0 & -\cos\gamma & 1 \\ 0 & 1 & \cos\gamma \end{bmatrix} \quad (12.19)$$

and

$$\Delta\{Q\} = \bar{s}\bar{\ell}_n \begin{Bmatrix} -\sin\gamma \\ \cos\gamma \\ 0 \end{Bmatrix} \quad (12.20)$$

where $\bar{s} = \tilde{m}\ell_m L/2I_b$.

These results demonstrate what occurs whenever the blades are dissimilar. Compare equation (12.19) with K in equation (12.18). The pattern of coupling between tower degrees of freedom and teetering discussed in Chapter 11 has broken down. However, the Mathieu type terms are very small compared to the other stiffness terms. A small amount of damping would eliminate any instability they may produce, and they are neglected henceforth.

The periodic excitation introduced by equation (12.20) is also small, but may produce resonances under some circumstances. These imbalance terms excite the opposite set of harmonics from those excited by the aerodynamic forcing terms (12.17).

ORIGINAL PAGE IS
 OF POOR QUALITY

An approximate solution to the in vacuo equations of motion (12.18) with imbalance forcing (12.20) is possible. First premultiply the equations by

$$[M]^{-1} = \begin{bmatrix} 1/\bar{I}_y & 0 & -\sin\gamma/\bar{I}_y \\ 0 & 1/\bar{I}_p & \cos\gamma/\bar{I}_p \\ -\sin\gamma/\bar{I}_y & \cos\gamma/\bar{I}_p & 1 + \sin^2\gamma/\bar{I}_y + \cos^2\gamma/\bar{I}_p \end{bmatrix} \quad (12.21)$$

For the restricted case of this section, ϕ_y and ϕ_p are completely uncoupled and the equations become simply

$$\begin{aligned} \ddot{\phi}_y + 2\zeta_y v_y \dot{\phi}_y + v_y^2 \phi_y &= -(\bar{s}\bar{\ell}_n/\bar{I}_y)\sin\gamma \\ \ddot{\phi}_p + 2\zeta_p v_p \dot{\phi}_p + v_p^2 \phi_p &= (\bar{s}\bar{\ell}_n/\bar{I}_p)\cos\gamma \end{aligned} \quad (12.22)$$

$$\begin{aligned} \ddot{\beta}_t + \dot{\beta}_t &= \frac{1}{2}\bar{s}\bar{\ell}_n \left[(1/\bar{I}_y + 1/\bar{I}_p) - (1/\bar{I}_y - 1/\bar{I}_p)\cos 2\gamma \right] \\ &\quad - 2\cos\gamma \dot{\phi}_y - 2\sin\gamma \dot{\phi}_p + v_y^2 \sin\gamma \phi_y - v_p^2 \cos\gamma \phi_p \end{aligned}$$

These equations are easily solved in sequence for ϕ_y and ϕ_p then β_t . If $\zeta_y = \zeta_p = 0$

$$\begin{aligned} \phi_y &= -a_y \sin\gamma \\ \phi_p &= a_p \cos\gamma \\ \beta_t &= [a_p + a_y] + [a_p - a_y]\cos 2\gamma \end{aligned} \quad (12.23)$$

where

$$\begin{aligned} a_y &= \bar{s}\bar{\ell}_n/[\bar{I}_y(v_y^2-1)] \\ a_p &= \bar{s}\bar{\ell}_n/[\bar{I}_y(v_y^2-1)] \end{aligned}$$

This response demonstrates an interesting mode of the

ALL INFORMATION CONTAINED
HEREIN IS UNCLASSIFIED
DATE 11-10-80 BY SP-5 BTJ/STW

system. As the hub follows the imbalance, it describes an ellipse with radii $a_y l_n$ and $a_p l_n$. The nacelle rotations are counteracted by the teetering in such a way that the tip path plane remains always the same.

The results of this section apply only for the rotor which has no airloads, is not preconed, and has no teeter spring or damper. However, the rotor-tower system would exhibit similar behavior if these attributes are not too large.

Chapter 13. AEROELASTIC BEHAVIOR
 OF THE YAW-PITCH-TEETER MODEL

Various aeroelastic instabilities of the teetering rotor-tower system are possible depending on the parameters of the machine and its operating condition. Several kinds of solutions of the yaw-pitch-teeter equations (12.13-17) are presented in this chapter for a range of parameters. First, transient response results are given for several unstable cases in the manner of Janetzke and Kaza [50]. The results of the present study are compared to theirs as a means to verify the yaw-pitch-teeter model. Second, a stability study is presented which displays the effects of some key parameters: support stiffness, damping, inflow angle, and preconing. Finally, the steady response to wind shear is briefly discussed.

In each solution, the NASA MOD-2 is used as a base case, and one or two parameters are changed at a time. The base case parameters are adapted from reference [50], and are given in Table 13.1. (Tables and Figures are placed at the end of this thesis for ready comparison.)

13.1 COMPARISON OF TWO MODELS

A more complete description of the model presented by Janetzke and Kaza is in order here to point out similarities

and differences [50]. The present model is physically similar to their model, although pitch is defined in the opposite sense. They used a flap bending mode for each blade in addition to the yaw, pitch, and teeter motions used here. They did not include preconing, but they did include a delta-three angle of the teetering axis. The present analysis assumes that the teetering axis is perpendicular to the blade axis.

The aerodynamics of reference [50] included nonlinear expressions for the lift and drag coefficient, and so were not given in explicit form. This was consistent with the solution technique used there, which was a straightforward numerical integration of the equations of motion. The aerodynamic forces were apparently calculated numerically at each time step.

The results presented by Janetzke and Kaza were transient response time histories, given an initial disturbance of the system. Stability was determined by examining these time histories for growth or decay, and the nature of the behavior was shown as well. The standard MOD-2 case was examined with and without damping; a case with reduced yaw stiffness, ($v_y = 2$) was examined without damping; and a case with both yaw and pitch stiffness reduced ($v_y = v_p = 2$) was examined with and without damping.

The stability of these same standard cases may be examined by applying the techniques of Chapter 11 to the yaw-pitch-teeter equations. The harmonic coefficient matrices (12.14-16) are calculated and substituted into the barred harmonic balance matrices (11.6-8). Then, the eigenvalues of this transformed system are extracted and examined. Roots are presented in Appendix D for all of the cases of reference [50]. The conclusions are the same for the two analyses, except that the present analysis predicts that the standard MOD-2 case without damping is slightly unstable ($\epsilon = .0015$). Reference [50] had this case as neutrally stable.

Appendix D gives the roots for the standard cases at three different truncations of the harmonic series: $P = 1$, $P = 2$, and $P = 3$. These results show the rapid convergence of the harmonic balance method for the stability problem. As P is increased, the real part of root converges and may repeat with an imaginary part which is different by an integer amount. The roots are also divided into the two sets discussed in Section 11.2. As P is increased, roots jump from set to set, but no new roots arise at $P = 3$.

Transient response time histories such as those in reference [50] can also be calculated using the techniques of Chapter 11. The eigenvalues and eigenvectors of the transformed system are calculated, and the initial

conditions applied (11.21). Then, the contributions of all conjugate pairs (11.23) and real roots (11.24) are added to give the transient response.

The two reduced stiffness cases without damping, both unstable, are arguably the most interesting and are used here to compare the two models. Appendix E presents the eigenvalues p_j , the eigenvectors v_j , and the combination constants c_j for the $v_y = 2$ case without damping. Figure 13.1 presents the transient response results from the present analysis for this case. The initial conditions and all other parameters are the same as those used by Janetzke and Kaza, whose results are given in Figure 13.2. These are transformed to match the conventions used here, the bending mode responses are omitted, and the scale is changed.

Figures 13.3 and 13.4 make the same comparison, but for the $v_y = v_p = 2$ case. Perhaps the most startling fact about these plots is that only harmonics up to the second are used ($P = 2$).

The initial conditions used in reference [50] are apparently designed to excite the forward whirl flutter mode of the system. The initial conditions used in the results of Figures 13.1 and 13.3 are placed on the zeroeth harmonic, based upon the guidelines of Chapter 11. If similar whirling initial conditions are used but placed on the second harmonic, an slightly different picture emerges. Figure 13.5 shows this result for the $v_y = v_p = 2$ case.

A number of unstable roots are given in Appendix D for the $v_y = v_p = 2$ case. A root with $\epsilon = 0.0104$ is largely responsible for the phenomena in Figure 13.3, and a root with $\epsilon = 0.0125$ is culpable in Figure 13.5. This points out a difficulty with using transient response histories to examine stability, since the initial conditions must be carefully chosen to assure excitation of the unstable modes of interest. Thus, transient response time histories are used here only for comparison to reference [50], and are not continued in the following stability study.

13.2 AEROELASTIC STABILITY STUDY

Both stability maps and plots of damping versus a parameter of interest are used in this section to give a rudimentary understanding of the aeroelastic stability of the model. Figure 13.6 shows the basic instability regions for different combinations of support stiffnesses. The locations of cases from the last section are shown. Generally, reducing either stiffness too much, or having them too close together can cause instability. This plot does not show the strength of the instability, and although the plot indicates that MOD-2 is unstable, a very small amount of damping suppresses the whole matched stiffness region.

Note also that a portion of the boundary was calculated with both $P = 2$ and $P = 3$. This is another check of the

convergence of the harmonic balance method. The periodic coefficients contain harmonics up to second, and it appears that $P = 2$ is adequate for these calculations.

The regions shown also must not be regarded necessarily as being one particular mode. Rather, many different roots (for $P = 2$ there are fifteen pairs) overlap to weave this pattern. This fact is demonstrated by Figure 13.7 which plots the real part σ of various roots which are active as the support stiffness is reduced along the line $v_y = v_p$. Here again, the branches are separated into the two sets discussed in Section 11.2. This plot shows the weak nature of the instability near the MOD-2 base case. Note also the very strong instability near $v_y = v_p = 1$.

A less confused and more rewarding picture of the instabilities involved is produced by decreasing the yaw stiffness while maintaining the pitch stiffness, as shown by Figure 13.8. Three general instability regions are shown: one at matched stiffness which is weak at least for this v_p ; another beginning around $v_y = 2$ which involves yaw and teeter as previously shown in Figure 13.1; and a divergence near $v_y = 1$. Figure 13.8 will be used as a basis for comparison in the following plots.

A reasonably small amount of damping applied equally to yaw and pitch suppresses the flutter instabilities as shown by Figure 13.9. Several of the roots from Figure 13.8 are completely off scale.

Increasing the inflow through the rotor disk is destabilizing to both the matched stiffness and reduced stiffness instabilities, as shown by Figure 13.10. This plot applies to the case of an increase in the inflow without a corresponding change of the pitch setting. A change in the inflow which is counteracted by the pitch controller so that the power output is constant has only a minor influence on the stability.

Finally, Figure 13.11 should be compared to Figure 13.8, which shows the effect of a practical amount of downwind precone on the stability. The matched stiffness instability is hardly affected, while the reduced stiffness instability is somewhat broader and more intense.

The divergence region is also broadened slightly by precone. This last observation is perhaps a little surprising, and it hints at the different nature of the freely teetering rotor. Precone would ordinarily stabilize the wind turbine in yaw, but this divergence involves teeter as well. In this regard, see reference [65]. Stiffening the teetering degree of freedom changes the aeroelastic behavior of the machine appreciably, as shown by Figure 13.12, which should be compared to Figure 13.6. Here, a large teetering spring has been applied, and the divergence boundary is at a much lower yaw stiffness.

ORIGINAL PAGE IS
OF POOR QUALITY

To conclude this discussion of aeroelastic behavior, Figure 13.13 is included. The steady response to wind shear ($r = .03$) is indicated for two cases of support stiffness with damping. The yaw and pitch response for the standard MOD-2 case is actually too small to be seen on this scale. The teeter response is the same for both the standard case and the $v_y = v_p = 2$ case.

As outlined in the introduction, this thesis has addressed four specific recommendations made in reference [14]. These same recommendations serve as an outline for these thoughts and are therefore repeated here.

- 1) Develop simpler models to investigate the main origins of aeroelastic phenomena (1).
- 2) Examine aeroelastic and mechanical instabilities more closely, especially for the proposed more flexible systems (3).
- 3) Study teetering effects and propellor whirl type instabilities (4).
- 4) Look in detail at generator drive train interaction with other system components (7).

Two simple aeroelastic models have been developed in accordance with 1) above. The first, a simple equivalent hinge model of an isolated rotor blade, was intended to meet some of the requirements of 2). The second, a simple rotor-tower model with a teetering rotor, was intended to fulfill some of the requirements of 3). In the process, a framework was established which facilitates the development of other simplified models, including possibly a model to address 4).

In Part I, an equivalent hinge model was proposed as a kind of typical section approach for the isolated HAWT blade. The blade was assumed to be rigid, but hinged near the root and constrained by springs. Three degrees of freedom were used: flapping out of the plane of rotation; lagging in the plane of rotation; and torsion about the pitch control axis. The model derived includes offsets of the center of gravity and the aerodynamic center, radial offset of the equivalent hinges from the hub, and both precone and droop angles of the blade.

First, the complete nonlinear equations of motion were derived, then they were linearized in perturbations about a steady-state blade position. The linearized equations were further simplified by applying an assumed ordering scheme reasonable for HAWTs. In particular, the ordering scheme allowed moderately large out of plane deflections, pitch setting, and inflow angle.

Quasisteady aerodynamic loads were derived in a similar process. Nonlinear aerodynamic loads were written assuming only that the angle of attack was small. These too were linearized and simplified as before. Finally, the nonlinear steady-state equations were written. The ordering scheme was also applied to these equations, which reduce to quadratic for flap deflection and linear for lag. The steady-state torsion is assumed to be prescribed by the power setting.

The resulting system of linearized equations and their associated steady-state equations were implemented on a digital computer. An extensive parameter variation was conducted using the NASA MOD-0 HAWT as a base case. The stability was also calculated for several two degree of freedom submodels extracted from the three degree of freedom system. These two degree of freedom models were acceptable for predicting flap-torsion flutter and flap-lag instability, but stiff inplane instabilities were only predicted by the three degree of freedom model. Finally, the model showed good agreement with results from a modal model previously derived by the author.

In Part II, several tools were first developed which have broad application to rotor-tower problems in HAWT aeroelasticity. An eleven degree of freedom linear model of a teetering rotor on a flexible support was derived using six hub degrees of freedom: three Cartesian deflections and three Euler rotations. The use of hub motions allows the rotor model to be adapted to any tower model chosen, from simple to complex.

Besides teetering, the rotor blades were modeled using symmetric and antisymmetric bending modes in both flap and lag bending; inextensional bending was assumed. Torsion of the blades and all torsional moments were neglected because of the high torsional stiffness which characterizes most

**ORIGINAL PAGE IS
OF POOR QUALITY**

HAWT blades. The rotor model derived includes preconing of the blades as well as a small undersling of the rotor, and the blades were assumed to be twisted and tapered.

The aerodynamics were again assumed to be quasisteady. Whereas the in vacuo equations of motion were derived without an assumed ordering scheme, the aerodynamic loads could not have been derived conveniently without one. Unlike some other analyses, the aerodynamic terms were derived in explicit form as coefficients of the equations.

Next, a harmonic balance method was developed to solve the equations of motion, which form a second order system with periodic coefficients. The method as outlined is useful for stability, transient response, and steady-state response calculations. The form of the harmonic balance method employed is quite convenient for small systems of equations, and the convergence has proven to be rapid. Thus, it would be useful as well for other problems with similar equations.

The model of a teetering rotor on a flexible support was intended to serve as a parent from which a number of simpler models could be extracted. This was demonstrated by developing a simple rotor-tower model which includes only nacelle yawing, nacelle pitching, and rotor teetering. The resulting equations of motion were solved using the harmonic

balance technique. Solutions were implemented with several computer programs for stability, transient response, and steady state response.

Transient response time histories were calculated for several cases taken from a study published by Janetzke and Kaza [50]. Their model included flap bending modes of the blades, but did not include preconing, and they solved the equations of motion by direct numerical integration using finite time steps. The comparison between their model and the simple rotor-tower model developed is very good, even though the harmonic balance was truncated at the second harmonic of the rotation speed for the present analysis.

The simple yaw-pitch-teeter model was used to examine the effect of key parameters on the whirl stability and divergence of a teetering HAWT. These included support stiffness, support damping, inflow increase due to a gust, and preconing. Finally, some implications of using a teetering rotor were investigated by including a teeter spring.

In summary, the thesis contributes to both the modeling methodology and the understanding of aeroelastic behavior of wind turbines. The general rotor model shows promise for the development of other models which can contribute to understanding new aeroelastic problems which may arise.

REFERENCES

- [1] Donham, R.E., Schmidt, J., and Linscott, B.S., "100-KW Hingeless Metal Wind Turbine Blade Design, Analysis, and Fabrication," 31st Annual National Forum of the American Helicopter Society, May 1975.
- [2] Linscott, B.S., Anderson, W.D., Glasgow, J., and Donham, R.E., "Experimental Data and Theoretical Analysis of an Operating 100 kW Wind Turbine," Paper 779273, 12th Intersociety Energy Conversion Engineering Conference, August 1977.
- [3] Adams, J., "Progress Report on MOD-2 Wind Turbine," 2nd DOE/NASA Wind Turbine Dynamics Workshop, NASA CP-2185, February 1981.
- [4] Glasgow, J.C., Miller, D.R., and Corrigan, R.D., "Comparison of Upwind and Downwind Rotor Operations of the DOE/NASA MOD-0 Wind Turbine," 2nd DOE/NASA Wind Turbine Dynamics Workshop, NASA CP-2185, February 1981.
- [5] Glasgow, J.C., and Miller, D.R., "Teetered, Tip-Controlled 100kW Wind-Turbine Rotor: Preliminary Test Results," Journal of Energy, Vol. 5, No. 5, pp. 257-262, September-October 1981.
- [6] Thresher, R.W., "Structural Dynamic Analysis of Wind Turbine Systems," 5th Biennial Wind Energy Conference and Workshop, NASA CP-635-1340, October 1981.
- [7] Friedmann, P.P., "Aeroelastic Stability and Response of Large Horizontal Axis Wind Turbines," Journal of Industrial Aerodynamics, Vol. 5, Nos. 3 and 4, pp. 373-402, May 1980.
- [8] Friedmann, P.P., "Recent Developments in Rotary-Wing Aeroelasticity," Journal of Aircraft, Vol. 14, No. 11, pp. 1027-1041, November 1977.
- [9] Johnson, W., Helicopter Theory, Princeton University Press, Princeton, N.J., 1980.
- [10] Johnson, W., "Dynamics of Tilting Proprotor Aircraft in Cruise Flight," NASA TN D-7677, 1974.

- [11] Hoffman, J.A., Dreier, M.E., Williamson, D.R., and Henninger, W.C., "Mathematical Methods Incorporated in the Wind Energy System Coupled Dynamics Analysis," Paragon Pacific, Inc., Report PPI-1014-7, January 1977.
- [12] Spera, D.A., "Comparison of Computer Codes for Calculating Dynamic Loads in Wind Turbines," 3rd Biennial Conference and Workshop on Wind Energy Conversion Systems, NASA TM-73773, September 1977.
- [13] Kaza, K.R.V., Janetzke, D.C., and Sullivan, T.L., "Evaluation of MOSTAS Computer Code for Predicting Dynamic Loads in Two-Bladed Wind Turbines," AIAA/ASME/ASCE/AHS 20th Structures, Structural Dynamics, and Materials Conference, Part 2, AIAA Paper 79-0733, 1979.
- [14] Dugundji, J., and Wendell, J.H., "General Review of the MOSTAS Computer Code for Wind Turbines," MIT ASRL TR-197-1, June 1981.
- [15] Thresher, D.W., Dugundji, J., Hohenesmer, K.H., and Walton, W.C., Jr., "Structural Dynamics Analysis Tools For Design of Large Wind Turbines: State of the Art Review," Wind Energy Projects Office, NASA Lewis Research Center, Cleveland, Ohio, September 1981.
- [16] Houbolt, J.C., and Brooks, G.W., "Differential Equations of Motion for Combined Flapwise Bending, and Torsion of Twisted Nonuniform Rotor Blades," NACA Report 1346, 1958.
- [17] Hodges, D.H., and Dowell, E.H., "Nonlinear Equations of Motion for the Elastic Bending and Torsion of Twisted Nonuniform Rotor Blades," NASA TN D-7818, 1974.
- [18] Rosen, A., and Friedmann, P., "Nonlinear Equations of Equilibrium for Elastic Helicopter or Wind Turbine Blades Undergoing Moderate Deformation," UCLA-ENG-7718, NASA CR-159478, June 1977.
- [19] Kaza, K.R.V., "Nonlinear Aeroelastic Equations of Motion of Twisted, Nonuniform, Flexible Horizontal-Axis Wind Turbine Blades," NASA-CR-159502, DOE/NASA/3139-1, 1979.
- [20] Wendell, J.H., "Aeroelastic Stability of Wind Turbine Rotor Blades," Wind Energy Conversion, Vol. X, ASRL TR-184-16, DOE COO-4131-T1, September 1978.

- [21] Hodges, D.H., Ormiston, R.A., and Peters, D.A., "On the Nonlinear Deformation Geometry of Euler-Bernouli Beams," NASA TP-1560, April 1980.
- [22] Hodges, D.H., "Torsion of Pretwisted Beams Due to Axial Loading," *Journal of Applied Mechanics*, Vol. 47, No. 2, pp. 393-397, June 1980. (Discussion, Vol. 48, No.3, pp. 679-681, September 1981.)
- [23] Hodges, D.H., and Ormiston, R.A., "Stability of Elastic Bending and Torsion of Uniform Cantilever Rotor Blades in Hover with Variable Structural Coupling," NASA TN D-8192, 1976.
- [24] Kottapalli, S.B.R., Friedmann, P.P., and Rosen, A., "Aeroelastic Stability and Response of Horizontal-Axis Wind Turbine Blades," *AIAA Journal*, Vol. 17, No. 12, pp. 1381-1389, December 1979.
- [25] Stephens, W.B., Hodges, D.H., Avila, J.H., and Kung, R-M., "Stability of Nonuniform Rotor Blades in Hover Using a Mixed Formulation," Paper 13, 6th European Rotorcraft and Powered Lift Aircraft Forum, September 1980.
- [26] Hodges, D.H., "Vibration and Response of Nonuniform Rotating Beams with Discontinuities," *Journal of the American Helicopter Society*, Vol. 24, No. 5, pp. 43-50, October 1979.
- [27] Friedmann, P.P., and Straub, F., "Application of the Finite Element Method to Rotary-Wing Aeroelasticity," *Journal of the American Helicopter Society*, Vol. 25, No. 1, pp. 36-44, January 1980.
- [28] Sivaneri, N.T., and Chopra, I., "Dynamic Stability of a Rotor Blade Using Finite Element Analysis," *AIAA Journal*, Vol. 20, No. 5, pp. 716-723, May 1982.
- [29] Kamoulakos, A., Stability Analysis of Flexible Wind Turbine Blades Using Finite Element Method, M.S. Thesis, M.I.T. Department of Aeronautics and Astronautics, August 1982.
- [30] Ham, N.D., "Helicopter Blade Flutter," AGARD Report No. 607, January 1973.
- [31] Bramwell, A.R.S., Helicopter Dynamics, Halsted Press, John Wiley and Sons, New York. N.Y., 1976.

- [32] Chopra, I., and Dugundji, J., "Non-Linear Dynamic Response of a Wind Turbine Blade," Journal of Sound and Vibration, Vol. 63, No. 2, pp. 265-286, March 1979.
- [33] Miller, R.H., Dugundji, J., Chopra, I., Sheu, D., and Wendell, J., "Dynamics of Horizontal Axis Wind Turbines," Wind Energy Conversion, Vol. III, MIT ASRL TR-184-9, DOE COO-4131-T1, September 1978.
- [34] Chopra, I., "Flap-Lag-Torsion Flutter Analysis of a Constant Lift Rotor," NASA CR-152244, January 1979.
- [35] Chopra, I., "Nonlinear Response of Wind Turbine Rotor," Wind Energy Conversion, Vol. VI, MIT ASRL TR-184-12, DOE COO-4131-T1, September 1978.
- [36] Liebst, B.S., A Pitch Control System for Large Scale Wind Turbines, Ph.D. Thesis, M.I.T. Department of Aeronautics and Astronautics, August 1981.
- [37] Theodorsen, T., "General Theory of Aerodynamic Instability and the Mechanism of Flutter," NACA Report 496, 1934.
- [38] Loewy, R.G., "A Two Dimensional Approximation to the Unsteady Aerodynamics of Rotary Wings," Journal of the Aeronautical Sciences, Vol. 24, No. 2, pp. 81-92 & 144, February 1957.
- [39] Greenberg, J.M., "Airfoil in Sinusoidal Motion in a Pulsating Stream," NACA TN 1326, 1947.
- [40] Friedmann, P.P., and Yuan, C., "Effect of Modified Strip Theories on Rotor Blade Aeroelastic Stability," AIAA Journal, Vol. 15, No. 7, pp. 923-940, July 1977.
- [41] Johnson, W., "Application of Unsteady Airfoil Theory to Rotary Wings," Journal of Aircraft, Vol. 17, No. 4, pp. 285-286, April 1980.
- [42] Kaza, K.R.V., and Kvaternik, R.G., "Application of Unsteady Airfoil Theory to Rotary Wings," Journal of Aircraft, Vol. 17, No. 7, pp. 604-605, July 1981.
- [43] Dugundji, J., "Some Dynamic Problems of Rotating Windmill Systems," Advances in Engineering Science, 13th Annual Meeting of the Society of Engineering Science, NASA CP-2001, Vol. 2, November 1976.

- [44] Sheu, D.L., "Effects of Tower Motion on the Dynamic Response of Windmill Rotor," Wind Energy Conversion, Vol. VII, ASRL TR-184-13, DOE COO-4131-T1, September 1978.
- [45] Warmbrodt, W., and Friedmann, P., "Formulation of the Aeroelastic Stability and Response Problem of Coupled Rotor/Support Systems," AIAA/ASME/ASCE/AHS 20th Structures, Structural Dynamics, and Materials Conference, Part 2, AIAA Paper 79-0732, 1979.
- [46] Hultgren, L.S., and Dugundji, J., "Dynamics of a Flexible Rotor-Tower System," ASRL TR-194-1, March 1979.
- [47] Thresher, R.W., Holley, W.E., Smith, W.E., Jafarey, N., and Lin, S-R., "Modeling the Response of Wind Turbines To Atmospheric Turbulence," DOE RLD/2227-81/2, 1981.
- [48] Bousmann, W.G., and Hodges, D.H., "An Experimental Study of Coupled Rotor-Body Aeromechanical Instability of Hingeless Rotors in Hover," Vertica, Vol. 3. Nos. 3/4, October 1979.
- [49] Bundas, D., and Dugundji, J., "Some Experiments on Yaw Stability of Wind Turbines with Various Coning Angles," MIT ASRL TR-197-2, July 1981.
- [50] Janetzke, D.C., and Kaza, K.R.V., "Whirl Flutter Analysis of a Horizontal-Axis Wind Turbine with a Two-Bladed Teetering Rotor," 2nd DOE/NASA Wind Turbine Dynamics Workshop, NASA CP-2185, February 1981.
- [51] Hall, W.E., Jr., "Prop-Rotor Stability at High Advance Ratios," Journal of the American Helicopter Society, Vol. 11, No. 2, pp. 11-26, April 1966.
- [52] Shamie, J., and Friedmann, P., "Aeroelastic Stability of Complete Rotors with Application to a Teetering Rotor in Forward Flight," Journal of Sound and Vibration, Vol. 53, No. 4, pp. 559-584, August 1977.
- [53] Caesari, L., Asymtotic Behavior and Stability Problems in Ordinary Differential Equations, 3rd Ed., Springer-Verlag, Berlin, Germany, 1970.
- [54] Yakubovich, V.A., and Starzhinskii, V.M., Linear Differential Equations With Periodic Coefficients, Vols. I and II, Halsted Press, John Wiley & Sons, New York, N.Y., 1975.

- [55] Bolotin, V.V., The Dynamic Stability of Elastic Systems, Holden-Day, Inc., San Francisco, Cal., 1964.
- [56] Hsu, C.S., "On the Parametric Excitation of a Dynamic System Having Multiple Degrees of Freedom," *Journal of Applied Mechanics*, Vol. 30, No. 3, September 1963.
- [57] Gaonkar, G.H., Simha Prasad, D.S., and Sastry, D., "On Computing Floquet Transition Matrices of Rotorcraft," Paper No. 25, 5th European Rotorcraft and Powered Lift Aircraft Forum, September 1979.
- [58] Friedmann, P.P., Hammond, C.E., and Woo, T-H., "Efficient Numerical Treatment of Periodic Systems with Application to Stability Problems," *International Journal for Numerical Methods in Engineering*, Vol. 11, No. 7, pp. 1117-1136, July 1977.
- [59] Friedmann, P.P., and Silverthorn, L.J., "Aeroelastic Stability of Periodic Systems With Application to Rotor Blade Flutter," *AIAA Journal*, Vol. 12, No. 11, pp. 1559-1565, November 1974.
- [60] Brosens, P.J., and Crandall, S.H., "Whirling of Unsymmetrical Rotors," *Journal of Applied Mechanics*, Vol. 28, Series E, No. 3, pp. 355-362, September 1961.
- [61] Peters, D.A., and Hohenemser, K.H., "Application of the Floquet Transition Matrix To Problems of Lifting Rotor Stability," *Journal of the American Helicopter Society*, Vol. 16, No. 2, pp. 25-33, April 1971.
- [62] Takahashi, K., "An Approach to Investigate the Instability of the Multiple-Degree-of-Freedom Parametric Dynamic Systems," *Journal of Sound and Vibration*, Vol. 78, No. 4, pp. 519-529, October 1981.
- [63] Peters, D.A., and Ormiston, R.A., "Flapping Response Characteristics of Hingeless Rotor Blades By A Generalized Harmonic Balance Method," NASA TN D-7856, 1975.
- [64] Kvaternik, R.G., and Walton, W.C., "A Formulation of Rotor-Airframe Coupling for the Design Analysis of Vibrations of Helicopter Airframes," NASA Reference Publication 1089 (FEDD), June 1982.
- [65] Miller, R.H., "On the Weathervaning of Wind Turbines," *Journal of Energy*, Vol. 5, No. 5, September-October 1979.

Appendix A. MODAL MODEL SUMMARY

The modal equations of reference [20] are reviewed here with some nomenclature changed to match that of Part I. Coordinate systems are the same except that, because the blade is twisted an angle $\theta_b(x)$, so are the principal axes η and ζ . The perturbation equations are

$$[M] \begin{Bmatrix} \ddot{q}_w \\ \ddot{q}_v \\ \ddot{q}_\theta \end{Bmatrix} + [C] \begin{Bmatrix} \dot{q}_w \\ \dot{q}_v \\ \dot{q}_\theta \end{Bmatrix} + [K] \begin{Bmatrix} q_w \\ q_v \\ q_\theta \end{Bmatrix} = \{0\} \quad (A.1)$$

Only the inertia and stiffness terms in the coefficient matrices of equation (A.1) are quoted below. Here, K_R is the torsional stiffness of the control system, ρ_b is the blade material density, E is the Young's modulus, and G is the shear modulus.

$$M_{ww} = (L^2/I_\eta) \int_0^L m \gamma_w^2 d\xi$$

$$M_{w\theta} = M_{\theta w} = (L/I_\eta) \int m e_I \cos \theta_b \gamma_\theta \gamma_w d\xi$$

$$M_{vv} = (L^2/I_\eta) \int m \gamma_v^2 d\xi$$

$$M_{v\theta} = -(L/I_\eta) \int m e_I \sin \theta_b \gamma_\theta \gamma_v d\xi$$

$$M_{\theta v} = M_{v\theta}$$

PRECEDING PAGE BLANK NOT FILMED

~~ORIGINAL PAGE IS
 OF POOR QUALITY~~

$$M_{\theta\theta} = (1/I_\gamma) \int m k_{m\gamma}^2 d\xi$$

$$M_{wv} = M_{vw} = 0$$

(A.2)

$$C_{wv} = 2(L^3/I_\gamma) \int m \gamma_v \delta_w d\xi q_{w_0} + 2\beta_p (L^2/I_\gamma) \int m \gamma_w \gamma_v d\xi + 2(L^2/I_\gamma) \int m e_I \sin\theta_b \gamma_w' \gamma_v d\xi$$

$$C_{vw} = -C_{wv}$$

$$C_{ww} = C_{vv} = C_{\theta\theta} = C_{w\theta} = C_{\theta w} = C_{v\theta} = C_{\theta v} = 0$$

(A.3)

$$K_{ww} = (L^2/\Omega^2 I_\gamma) \int (EI_2 \sin^2\theta_b + EI_1 \cos^2\theta_b) (\gamma_w'')^2 d\xi + 2(L^2/\Omega^2 I_\gamma) \int (EI_2 - EI_1) \sin\theta_b \cos\theta_b \gamma_\theta (\gamma_w'')^2 d\xi q_{\theta_0} + (1-\beta_p^2) (L^2/I_\gamma) \int m \xi \delta_w d\xi + e_H (L^2/I_\gamma) \int m \delta_w d\xi$$

$$K_{wv} = (L^2/\Omega^2 I_\gamma) \int (EI_2 - EI_1) \sin\theta_b \cos\theta_b \gamma_w'' \gamma_v'' d\xi + (L^2/\Omega^2 I_\gamma) \int (EI_2 - EI_1) (\cos^2\theta_b - \sin^2\theta_b) \gamma_\theta \gamma_w'' \gamma_v'' d\xi q_{\theta_0}$$

$$K_{vw} = K_{wv}$$

$$K_{w\theta} = (L/I_\gamma) \int m e_I \xi \cos\theta_b \gamma_\theta \gamma_w' d\xi - (L/\Omega^2 I_\gamma) \int E B_2 \theta_b' \sin\theta_b \gamma_\theta' \gamma_w'' d\xi + (L^2/\Omega^2 I_\gamma) \int (EI_2 - EI_1) (\cos^2\theta_b - \sin^2\theta_b) \gamma_\theta \gamma_w'' \gamma_v'' d\xi q_{v_0} + 2(L^2/\Omega^2 I_\gamma) \int (EI_2 - EI_1) \sin\theta_b \cos\theta_b \gamma_\theta (\gamma_w'')^2 d\xi q_{w_0}$$

$$K_{\theta w} = K_{w\theta}$$

$$K_{vv} = (L^2/\Omega^2 I_\gamma) \int (EI_2 \cos^2\theta_b + EI_1 \sin^2\theta_b) (\gamma_v'')^2 d\xi + 2(L^2/\Omega^2 I_\gamma) \int (EI_2 - EI_1) \sin\theta_b \cos\theta_b \gamma_\theta (\gamma_v'')^2 d\xi q_{\theta_0} + (1-\beta_p^2) (L^2/I_\gamma) \int m \xi \delta_v d\xi + e_H (L^2/I_\gamma) \int m \delta_v d\xi - (L^2/I_\gamma) \int m \gamma_v^2 d\xi$$

ORIGINAL PAGE IS
 OF POOR QUALITY

$$\begin{aligned}
 K_{v\theta} &= -(L/\Omega^2 I_\gamma) \int EB_2 \gamma'_\theta \gamma''_v d\xi + \\
 &\quad - 2(L^2/\Omega^2 I_\gamma) \int (EI_2 - EI_1) \sin\theta_b \cos\theta_b \gamma_\theta (\gamma''_v)^2 d\xi q_{v_0} + \\
 &\quad + (L^2/\Omega^2 I_\gamma) \int (EI_2 - EI_1) \sin\theta_b \cos\theta_b \gamma_\theta \gamma''_w \gamma''_v d\xi q_{w_0} + \\
 &\quad - (L/I_\gamma) \int m e_I \xi \sin\theta_b \gamma_\theta \gamma'_v d\xi + (L/I_\gamma) \int m e_I \sin\theta_b \gamma_\theta \gamma_v d\xi \\
 K_{\theta v} &= K_{v\theta} \\
 K_{\theta\theta} &= (K_R/\Omega^2 I_\gamma) \gamma_\theta^2(0) + (1/\Omega^2 I_\gamma) \int GJ_E (\gamma'_\theta)^2 d\xi + \\
 &\quad + (1/I_\gamma) \int m \xi \delta_\theta d\xi + (1/I_\gamma) \int m k_m^2 (\cos^2\theta_b - \sin^2\theta_b) \gamma_\theta^2 d\xi
 \end{aligned}
 \tag{A.4}$$

where

$$\delta_v = \int_0^\xi (\gamma'_v)^2 dx$$

$$\delta_w = \int_0^\xi (\gamma'_w)^2 dx$$

$$\delta_\theta = \int_0^\xi k_{A_b}^2 \theta' \gamma' dx$$

and

$$m = \int_{x\text{-sect}} \rho_b d\eta d\xi$$

$$e_I = (1/m) \int_{x\text{-sect}} \rho_b \eta d\eta d\xi$$

ORIGINAL PAGE IS
OF POOR QUALITY

$$k_m^2 = (1/m) \int \rho_b (\eta^2 + \zeta^2) d\eta d\zeta$$

$$k_A^2 = (1/EA) \int E (\eta^2 + \zeta^2) d\eta d\zeta$$

$$EA = \int E d\eta d\zeta$$

$$GJ = \int G (\eta^2 + \zeta^2) d\eta d\zeta$$

$$EI_1 = \int E \zeta^2 d\eta d\zeta$$

$$EI_2 = \int E \eta^2 d\eta d\zeta$$

$$EB_1 = \int E (\eta^2 + \zeta^2) (\eta^2 + \zeta^2 - k_A^2) d\eta d\zeta$$

$$EB_2 = \int E (\eta^2 + \zeta^2) \eta d\eta d\zeta$$

$$GJ_E = GJ + EB_1 (\theta'_b)^2$$

L. D. J. A. U.

Appendix B.

MATRICES FOR PART II

This appendix contains the transformation matrix (9.1), its time derivative matrix, and matrices which are products of either or both. All are expressed to adequate order for the expansion of the kinetic energy (9.5) and the blade relative velocity (10.7). The latter task is generally more demanding. A zero indicates that no terms significant to this study exist in that position of the matrix.

$$[\dot{T}_a]^T [T_a] =$$

$$\begin{bmatrix}
 0 & \{ \Omega(\cos\beta_p - \beta_t \sin\beta_p) + \dot{\phi}_2(\cos\beta_p - \beta_t \sin\beta_p) \\
 & -\dot{\phi}_X(\sin\beta_p \cos\psi - \phi_{2/2} \sin\beta_p \sin\psi + \beta_t \cos\beta_p \cos\psi) \\
 & -\dot{\phi}_Y(\sin\beta_p \sin\psi + \phi_X \cos\beta_p + \phi_{2/2} \sin\beta_p \cos\psi + \beta_t \cos\beta_p \sin\psi) \} \\
 \\
 \{-\Omega \cos\beta_p + \dot{\phi}_X \sin\beta_p \cos\psi \\
 + \dot{\phi}_Y \sin\beta_p \sin\psi - \dot{\phi}_2 \cos\beta_p \} & 0 \\
 \\
 \{-\dot{\phi}_X(\sin\psi + \phi_2 \cos\psi) \\
 + \dot{\phi}_Y(\cos\psi - \phi_2 \sin\psi) - \dot{\beta}_t \} & \{ \Omega(\sin\beta_p + \beta_t \cos\beta_p) + \dot{\phi}_2(\sin\beta_p + \beta_t \cos\beta_p) \\
 & -\dot{\phi}_X(\cos\beta_p \cos\psi - \phi_{2/2} \cos\beta_p \sin\psi - \beta_t \sin\beta_p \cos\psi) \\
 & -\dot{\phi}_Y(\cos\beta_p \sin\psi - \phi_X \sin\beta_p + \phi_2 \cos\beta_p \cos\psi - \beta_t \sin\beta_p \sin\psi) \} \\
 \\
 & \{ \dot{\phi}_X(\sin\psi + \phi_2 \cos\psi) \\
 & -\dot{\phi}_Y(\cos\psi - \phi_2 \sin\psi) + \dot{\beta}_t \} \\
 \\
 & (-\Omega \sin\beta_p + \dot{\phi}_X \cos\beta_p \cos\psi \\
 & + \dot{\phi}_Y \cos\beta_p \sin\psi - \dot{\phi}_2 \sin\beta_p) \\
 \\
 & 0
 \end{bmatrix}$$

$$(\sigma_x^2)^2 (\sigma_y^2)$$

$$\begin{aligned} & (\sigma_x^2 (\cos^2 \beta_p - \beta_c \sin^2 \beta_p - \beta_c^2 \cos^2 \beta_p) \\ & + \Delta 1 - \phi_x (\sin^2 \beta_p \cos^2 \beta_c - \beta_c^2 \sin^2 \beta_p \sin^2 \beta_c \cos^2 \beta_p \cos^2 \beta_c \cos^2 \beta_p) \\ & - \phi_y (\sin^2 \beta_p \sin^2 \beta_c \cos^2 \beta_c - 2 \phi_x \cos^2 \beta_p + \beta_c \sin^2 \beta_p \cos^2 \beta_c \cos^2 \beta_p \sin^2 \beta_c) \\ & + \phi_x^2 (2 \cos^2 \beta_p - 2 \beta_c \sin^2 \beta_p) \\ & + (\beta_c)^2 (\cos^2 \beta_p \sin^2 \beta_c + \sin^2 \beta_p) - \phi_x \beta_c \cos^2 \beta_p \sin^2 \beta_c \\ & - \phi_x \beta_c \sin^2 \beta_p \cos^2 \beta_c + 2 \phi_x \beta_c \sin^2 \beta_c \cos^2 \beta_p \cos^2 \beta_c \sin^2 \beta_p \\ & - \phi_x \beta_c \sin^2 \beta_p \sin^2 \beta_c \cos^2 \beta_c + (\beta_c)^2 \cos^2 \beta_p + (\beta_c)^2 \end{aligned}$$

$$\begin{aligned} & (\Delta 1 \phi_x \sin \beta_p \sin \gamma \\ & - \phi_y \sin \beta_p \cos \gamma \\ & + \beta_c \sin \beta_p) \\ & (\sigma_x^2 | - \beta_c \sin^2 \beta_p + \beta_c \cos^2 \beta_p - \beta_c^2 \sin^2 \beta_p) \\ & + \Delta 1 - \phi_x (\cos^2 \beta_p \cos^2 \beta_c - \beta_c^2 \cos^2 \beta_p \sin^2 \beta_c \sin^2 \beta_p \cos^2 \beta_p) \\ & - \phi_y (\cos^2 \beta_p \sin^2 \beta_c \sin^2 \beta_c + \beta_c \cos^2 \beta_p \cos^2 \beta_c - 2 \beta_c \sin^2 \beta_p \sin^2 \beta_c) \\ & - \phi_x^2 (\cos^2 \beta_p - 2 \beta_c \cos^2 \beta_p) \\ & + (\beta_c)^2 \sin^2 \beta_p \cos^2 \beta_c + \beta_c \sin^2 \beta_p \sin^2 \beta_c \\ & - \phi_x \beta_c \cos^2 \beta_p \cos^2 \beta_c + (\beta_c)^2 \sin^2 \beta_p \sin^2 \beta_c \\ & - \phi_x \beta_c \cos^2 \beta_p \sin^2 \beta_c \sin^2 \beta_c \sin^2 \beta_p \end{aligned}$$

σ_x^2

$$\begin{aligned} & \Delta 1 \phi_x \cos \beta_p \sin \beta_c \sin \gamma - \phi_y \cos \beta_p \cos \gamma + \beta_c \cos \beta_p \\ & (\sigma_x^2 |\sin^2 \beta_p + \beta_c \sin^2 \beta_p + \beta_c^2 \cos^2 \beta_p) \\ & + \Delta 1 \phi_x (\sin^2 \beta_p \cos^2 \beta_c - \beta_c^2 \sin^2 \beta_p \sin^2 \beta_c \cos^2 \beta_p \cos^2 \beta_c) \\ & + \phi_y (\sin^2 \beta_p \sin^2 \beta_c \sin^2 \beta_c + \beta_c \sin^2 \beta_p \cos^2 \beta_c + 2 \beta_c \sin^2 \beta_p \sin^2 \beta_c) \\ & + \phi_x^2 (2 \sin^2 \beta_p + 2 \beta_c \sin^2 \beta_p) \\ & + (\beta_c)^2 (\sin^2 \beta_p \sin^2 \beta_c + \cos^2 \beta_p) - \phi_x \beta_c \sin^2 \beta_p \sin^2 \beta_c \\ & + \phi_x \beta_c \sin^2 \beta_p \cos^2 \beta_c + 2 \phi_x \beta_c \sin^2 \beta_c \cos^2 \beta_p \cos^2 \beta_c \\ & + \phi_x \beta_c \sin^2 \beta_p \sin^2 \beta_c \cos^2 \beta_c + (\beta_c)^2 \sin^2 \beta_p + (\beta_c)^2 \end{aligned}$$

SYMMETRIC

Appendix C. AERODYNAMIC INTEGRALS

This appendix contains the integrals used in the aerodynamic terms of Chapter 10. Ordinarily, both the reference pitch setting θ_0 and the reference chord c_0 would be chosen at $x/L = 0.75$.

$$\begin{aligned}
 L_1 &= (4/c_0 L^4) \int_0^L Cc x^3 \cos \theta_b \, dx \\
 L_2 &= (4/c_0 L^4) \int Cc x^3 (\sin \theta_b / \theta_0) \, dx \\
 L_3 &= (3/c_0 L^3) \int Cc x^2 \cos \theta_b \, dx \\
 L_4 &= (3/c_0 L^3) \int Cc x^2 (\sin \theta_b / \theta_0) \, dx \\
 L_5 &= (2/c_0 L^2) \int Cc x \cos \theta_b \, dx \\
 L_6 &= (2/c_0 L^2) \int Cc x (\sin \theta_b / \theta_0) \, dx \\
 L_7 &= (1/c_0 L) \int Cc \cos \theta_b \, dx \\
 L_8 &= (1/c_0 L) \int Cc (\sin \theta_b / \theta_0) \, dx \\
 L_{10} &= (4/c_0 L^3) \int Cc \gamma_v x^2 \cos \theta_b \, dx \\
 L_{11} &= (4/c_0 L^3) \int Cc \gamma_v x^2 (\sin \theta_b / \theta_0) \, dx \\
 L_{12} &= (3/c_0 L^2) \int Cc \gamma_v x \cos \theta_b \, dx \\
 L_{13} &= (3/c_0 L^2) \int Cc \gamma_v x (\sin \theta_b / \theta_0) \, dx \\
 L_{14} &= (2/c_0 L) \int Cc \gamma_v \cos \theta_b \, dx \\
 L_{15} &= (2/c_0 L) \int Cc \gamma_v (\sin \theta_b / \theta_0) \, dx
 \end{aligned}$$

$$L_{20} = (4/c_o L^3) \int Cc\gamma_w x^2 \cos\theta_b dx$$

$$L_{21} = (4/c_o L^3) \int Cc\gamma_w x^2 (\sin\theta_b/\theta_o) dx$$

$$L_{22} = (3/c_o L^2) \int Cc\gamma_w x \cos\theta_b dx$$

$$L_{23} = (3/c_o L^2) \int Cc\gamma_w x (\sin\theta_b/\theta_o) dx$$

$$L_{24} = (2/c_o L) \int Cc\gamma_w \cos\theta_b dx$$

$$L_{25} = (2/c_o L) \int Cc\gamma_w (\sin\theta_b/\theta_o) dx$$

$$L_{30} = (4/c_o L^3) \int Cc\gamma'_v x^3 (\sin\theta_b \cos\theta_b/\theta_o) dx$$

$$L_{31} = (4/c_o L^3) \int Cc\gamma'_v x^3 (\sin^2\theta_b/\theta_o^2) dx$$

$$L_{32} = (3/c_o L^2) \int Cc\gamma'_v x^2 \cos^2\theta_b dx$$

$$L_{33} = (3/c_o L^2) \int Cc\gamma'_v x^2 (\sin\theta_b \cos\theta_b/\theta_o) dx$$

$$L_{34} = (3/c_o L^2) \int Cc\gamma'_v x^2 (\sin^2\theta_b/\theta_o^2) dx$$

$$L_{35} = (2/c_o L) \int Cc\gamma'_v x \cos^2\theta_b dx$$

$$L_{36} = (2/c_o L) \int Cc\gamma'_v x (\sin\theta_b \cos\theta_b/\theta_o) dx$$

$$L_{37} = (2/c_o L) \int Cc\gamma'_v x (\sin^2\theta_b/\theta_o^2) dx$$

$$L_{38} = (1/c_o) \int Cc\gamma'_v \cos^2\theta_b dx$$

$$L_{39} = (1/c_o) \int Cc\gamma'_v (\sin\theta_b \cos\theta_b/\theta_o) dx$$

$$L_{40} = (4/c_o L^3) \int Cc\gamma'_w x^3 dx$$

$$L_{41} = (3/c_o L^2) \int Cc\gamma'_w x^2 dx$$

$$L_{42} = (3/c_o L^2) \int Cc\gamma'_w x^2 (\sin 2\theta_b/2\theta_o) dx$$

$$L_{43} = (2/c_o L) \int Cc\gamma'_w x dx$$

$$L_{44} = (2/c_o L) \int Cc\gamma'_w x \cos 2\theta_b dx$$

$$L_{45} = (2/c_o L) \int Cc\gamma'_w x (\sin 2\theta_b/2\theta_o) dx$$

$$L_{46} = (1/c_o) \int Cc\gamma'_w dx$$

$$L_{47} = (1/c_o) \int Cc\gamma'_w \cos 2\theta_b dx$$

$$L_{50} = (4/c_o L^2) \int Cc\gamma_v^2 x \cos\theta_b dx$$

$$L_{51} = (4/c_o L^2) \int Cc\gamma_v^2 x (\sin\theta_b/\theta_o) dx$$

$$L_{52} = (3/c_o L) \int Cc\gamma_v^2 \cos\theta_b dx$$

$$L_{53} = (3/c_o L) \int Cc\gamma_v^2 (\sin\theta_b/\theta_o) dx$$

$$L_{54} = (4/c_o L^2) \int Cc\gamma_v' \gamma_v x^2 (\sin^2\theta_b/\theta_o^2) dx$$

$$L_{55} = (3/c_o L) \int Cc\gamma_v' \gamma_v x (\sin^2\theta_b/\theta_o^2) dx$$

$$L_{56} = (2/c_o) \int Cc\gamma_v' \gamma_v (\sin\theta_b \cos\theta_b/\theta_b) dx$$

$$L_{60} = (4/c_o L^2) \int Cc\gamma_v \gamma_w x \cos\theta_b dx$$

$$L_{61} = (4/c_o L^2) \int Cc\gamma_v \gamma_w x (\sin\theta_b/\theta_o) dx$$

$$L_{62} = (3/c_o L) \int Cc\gamma_v \gamma_w \cos\theta_b dx$$

$$L_{63} = (3/c_o L) \int Cc\gamma_v \gamma_w (\sin\theta_b/\theta_o) dx$$

$$L_{64} = (4/c_o L^2) \int Cc\gamma_v' \gamma_w x^2 (\sin\theta_b \cos\theta_b/\theta_o) dx$$

$$L_{65} = (3/c_o L) \int Cc\gamma_v' \gamma_w x \cos^2\theta_b dx$$

$$L_{66} = (3/c_o L) \int Cc\gamma_v' \gamma_w x (\sin\theta_b \cos\theta_b/\theta_o) dx$$

$$L_{67} = (2/c_o) \int Cc\gamma_v' \gamma_w \cos^2\theta_b dx$$

$$L_{68} = (3/c_o L) \int Cc\gamma_v \gamma_w' x dx$$

$$L_{69} = (2/c_o) \int Cc\gamma_v \gamma_w' dx$$

$$L_{70} = (4/c_o L^2) \int Cc\gamma_w^2 x \cos\theta_b dx$$

$$L_{71} = (4/c_o L^2) \int Cc\gamma_w^2 x (\sin\theta_b/\theta_o) dx$$

$$L_{72} = (3/c_o L) \int Cc\gamma_w^2 \cos\theta_b dx$$

$$L_{73} = (4/c_o L^2) \int Cc\gamma_w' \gamma_w x^2 dx$$

$$L_{74} = (3/c_o L) \int Cc\gamma_w' \gamma_w x dx$$

$$L_{80} = (3/c_o L^3) \int Cc^2 x^2 dx$$

$$L_{81} = (3/c_o L^2) \int Cc^2 \gamma_v x dx$$

$$L_{82} = (2/c_o^2 L) \int Cc^2 \gamma_v dx$$

$$L_{83} = (3/c_o^2 L^2) \int Cc^2 \gamma_w x dx$$

$$L_{84} = (3/c_o^2 L^2) \int Cc^2 \gamma_v' x^2 (\sin \theta_b / \theta_o) dx$$

$$L_{85} = (2/c_o^2 L) \int Cc^2 \gamma_v' x (\sin \theta_b / \theta_o) dx$$

$$L_{86} = (3/c_o^2 L^2) \int Cc^2 \gamma_w' x^2 \cos \theta_b dx$$

$$L_{87} = (2/c_o^2 L) \int Cc^2 \gamma_w' x \cos \theta_b dx$$

$$L_{90} = (2/c_o^2) \int Cc^2 \gamma_v' \gamma_v (\sin \theta_b / \theta_o) dx$$

$$L_{91} = (3/c_o^2 L) \int Cc^2 \gamma_v' \gamma_w x (\sin \theta_b / \theta_o) dx$$

$$L_{92} = (3/c_o^2 L) \int Cc^2 \gamma_v \gamma_w' x \cos \theta_b dx$$

$$L_{93} = (2/c_o^2) \int Cc^2 \gamma_v \gamma_w' \cos \theta_b dx$$

$$L_{94} = (3/c_o^2 L) \int Cc^2 \gamma_w' \gamma_w x \cos \theta_b dx$$

$$D_1 = (4/c_o L^4) \int cx^3 \cos \theta_b dx$$

$$D_2 = (4/c_o L^3) \int c \gamma_v x^2 \cos \theta_b dx$$

$$D_3 = (4/c_o L^2) \int c \gamma_v^2 x \cos \theta_b dx$$

Appendix D. EIGENVALUES FOR MOD-2 CASES

This appendix presents the eigenvalues calculated for the five MOD-2 standard cases of reference [50]. Eigenvalues from the first set discussed in Chapter 11 are given in the first column, and those from the second set are given in the second. The convergence of the harmonic balance method is demonstrated for each of these cases by giving the roots for truncation of the harmonic series at $P = 1$, $P = 2$, and $P = 3$.

STANDARD MOD-2 WITHOUT DAMPING
 $\nu_y = 7.77, \nu_p = 7.41, \zeta_y = \zeta_p = 0$

P = 1

-0.00001 ±	7.75776 i	-0.00278 ±	8.53409 i
-0.00000 ±	7.40553 i	-0.27690 ±	0.95124 i
-0.27673 ±	1.95111 i	-0.16108 ±	2.62089 i
-0.27709 ±	0.04890 i	0.00098 ±	6.51995 i
		-0.22098 ±	6.00436 i

P = 2

-0.00208 ±	9.52309 i	-0.00001 ±	8.89649 i
-0.00001 ±	7.75776 i	-0.00000 ±	8.34185 i
-0.00000 ±	7.40553 i	-0.00001 ±	6.87721 i
-0.22221 ±	6.97674 i	-0.00000 ±	6.33560 i
0.00146 ±	5.52122 i	-0.27673 ±	2.95111 i
-0.27691 ±	1.95124 i	-0.27691 ±	0.95123 i
-0.27690 ±	0.04875 i	-0.27709 ±	1.04891 i
-0.16103 ±	1.59245 i		

P = 3

-0.00001 ±	9.75776 i	-0.00208 ±	10.52309 i
-0.00000 ±	9.40553 i	-0.00001 ±	8.89649 i
-0.00001 ±	7.75776 i	-0.00000 ±	8.34185 i
-0.00000 ±	7.40553 i	-0.00001 ±	6.87721 i
-0.00001 ±	5.75775 i	-0.00000 ±	6.33560 i
-0.00000 ±	5.40553 i	-0.22221 ±	7.97674 i
-0.27691 ±	0.04876 i	0.00146 ±	4.52122 i
-0.27673 ±	3.95111 i	-0.27691 ±	2.95124 i
-0.27691 ±	1.95124 i	-0.27691 ±	0.95123 i
-0.27709 ±	2.04890 i	-0.27690 ±	1.04875 i
		-0.16103 ±	0.59245 i

ORIGINAL PAGE IS
OF POOR QUALITY

STANDARD MOD-2 WITH DAMPING
 $v_y = 7.77$, $v_p = 7.41$, $\zeta_y = \zeta_p = 0.01$

P = 1

-0.07768 ±	7.75737 i	-0.07788 ±	8.53374 i
-0.07410 ±	7.40516 i	-0.27690 ±	0.95124 i
-0.27673 ±	1.95111 i	-0.18084 ±	2.61980 i
-0.27709 ±	0.04890 i	-0.07416 ±	6.51962 i
		-0.24842 ±	6.00322 i

P = 2

-0.07730 ±	9.52272 i	-0.07764 ±	8.89611 i
-0.07768 ±	7.75737 i	-0.07414 ±	8.34148 i
-0.07410 ±	7.40516 i	-0.07765 ±	6.87683 i
-0.24952 ±	6.97564 i	-0.07413 ±	6.33523 i
-0.07377 ±	5.52084 i	-0.27673 ±	2.95110 i
-0.27691 ±	1.95124 i	-0.27691 ±	0.95123 i
-0.27690 ±	0.04875 i	-0.27709 ±	1.04891 i
-0.18071 ±	1.59136 i		

P = 3

-0.07768 ±	9.75737 i	-0.07730 ±	10.52272 i
-0.07410 ±	9.40516 i	-0.07764 ±	8.89611 i
-0.07768 ±	7.75737 i	-0.07414 ±	8.34148 i
-0.07410 ±	7.40516 i	-0.07765 ±	6.87683 i
-0.07768 ±	5.75737 i	-0.07413 ±	6.33523 i
-0.07410 ±	5.40516 i	-0.24952 ±	7.97564 i
-0.27691 ±	0.04876 i	-0.07377 ±	4.52084 i
-0.27673 ±	3.95111 i	-0.27691 ±	2.95124 i
-0.27691 ±	1.95124 i	-0.27691 ±	0.95123 i
-0.27709 ±	2.04890 i	-0.27690 ±	1.04875 i
		-0.18071 ±	0.59136 i

ORIGINAL PAGE IS
OF POOR QUALITY

YAW STIFFNESS, REDUCED WITHOUT DAMPING

$$\nu_y = 2.0, \nu_p = 7.41, \zeta_y = \zeta_p = 0$$

P = 1

-0.00000 ±	7.40552 i	-0.03208 ±	7.64394 i
0.00596 ±	1.95806 i	-0.01272 ±	5.49133 i
-0.28103 ±	1.95780 i	-0.23330 ±	3.23414 i
-0.27876 ±	0.04758 i	-0.27835 ±	0.95216 i
		0.12322 ±	0.00000 i

P = 2

-0.03390 ±	8.67816 i	-0.00000 ±	8.34673 i
-0.00000 ±	7.40552 i	-0.00000 ±	6.34439 i
-0.01321 ±	4.52008 i	-0.00045 ±	3.46171 i
-0.24415 ±	3.97586 i	-0.27534 ±	2.95392 i
0.00594 ±	1.95805 i	-0.00067 ±	1.26217 i
-0.28256 ±	1.95953 i	-0.27605 ±	0.95513 i
-0.27915 ±	0.04774 i	-0.27822 ±	1.04742 i
-0.09065 ±	1.25030 i		

P = 3

-0.00000 ±	9.40552 i	-0.00000 ±	8.34673 i
-0.00000 ±	7.40553 i	-0.03390 ±	9.67815 i
-0.00000 ±	5.40552 i	-0.00000 ±	6.34439 i
0.00596 ±	3.95808 i	-0.24415 ±	4.97586 i
-0.28103 ±	3.95780 i	-0.00045 ±	3.46166 i
0.00594 ±	1.95807 i	-0.01321 ±	3.52008 i
-0.28286 ±	1.95919 i	-0.27690 ±	2.95573 i
-0.27876 ±	2.04758 i	-0.00068 ±	1.26217 i
-0.28285 ±	0.04081 i	-0.27605 ±	0.95513 i
0.00594 ±	0.04194 i	-0.27860 ±	1.04758 i
		-0.09065 ±	2.25026 i

ORIGINAL PAGE IS
OF POOR QUALITY

YAW AND PITCH STIFFNESSES REDUCED WITHOUT DAMPING
 $\nu_y = 2.0, \nu_p = 2.0, \zeta_y = \zeta_p = 0$

P = 1

-0.27950 ± 0.04702 i	-0.16625 ± 3.26713 i
-0.28272 ± 1.96065 i	-0.12678 ± 2.82080 i
0.01037 ± 1.96065 i	-0.28603 ± 0.95799 i
-0.00198 ± 1.97835 i	0.01005 ± 0.85183 i
	-0.09175 ± 0.32810 i

P = 2

-0.00568 ± 3.97709 i	-0.00048 ± 3.51848 i
-0.29435 ± 3.97982 i	-0.27856 ± 2.95428 i
-0.28517 ± 1.96263 i	0.00421 ± 2.71537 i
0.01035 ± 1.96065 i	-0.00024 ± 1.28150 i
-0.00199 ± 1.97838 i	0.00349 ± 0.53595 i
-0.08900 ± 1.40584 i	-0.28016 ± 0.95583 i
-0.28434 ± 0.03866 i	-0.27901 ± 1.04660 i
0.01250 ± 0.02982 i	

P = 3

-0.28272 ± 3.96065 i	-0.00568 ± 4.97709 i
-0.00200 ± 3.97838 i	-0.29435 ± 4.97982 i
0.01039 ± 3.96067 i	-0.00048 ± 3.51841 i
0.01035 ± 1.96065 i	-0.28101 ± 2.95639 i
-0.00200 ± 1.97838 i	0.00417 ± 2.71531 i
-0.28527 ± 1.96253 i	-0.08900 ± 2.40583 i
-0.27950 ± 2.04702 i	-0.00021 ± 1.28147 i
-0.28527 ± 0.03747 i	0.00350 ± 0.53599 i
0.01034 ± 0.03936 i	-0.28016 ± 0.95583 i
-0.00198 ± 0.02165 i	0.00350 ± 0.53599 i
	0.01250 ± 1.02982 i

YAW AND PITCH STIFFNESSES REDUCED WITH DAMPING
 $\nu_y = 2.0, \nu_p = 2.0, \zeta_y = \zeta_p = 0.04$

P = 1

-0.27953 ±	0.04700 i	-0.21808 ±	3.27699 i
-0.28523 ±	1.96393 i	-0.19259 ±	2.80653 i
-0.06641 ±	1.95587 i	-0.28890 ±	0.95825 i
-0.08266 ±	1.97653 i	-0.06583 ±	0.84968 i
		-0.10447 ±	0.33195 i

P = 2

-0.08572 ±	3.97545 i	-0.08082 ±	3.51725 i
-0.33236 ±	3.97705 i	-0.27890 ±	2.95369 i
-0.28769 ±	1.96583 i	-0.07509 ±	2.71404 i
-0.06647 ±	1.95598 i	-0.08079 ±	1.27986 i
-0.08265 ±	1.97656 i	-0.07640 ±	0.53372 i
-0.10007 ±	1.40859 i	-0.27958 ±	0.95552 i
-0.28634 ±	0.03569 i	-0.27917 ±	1.04652 i
-0.06548 ±	0.03441 i		

P = 3

-0.28523 ±	3.96393 i	-0.08572 ±	4.97545 i
-0.08267 ±	3.97656 i	-0.33236 ±	4.97705 i
-0.06640 ±	3.95588 i	-0.08081 ±	3.51718 i
-0.28780 ±	1.96573 i	-0.28136 ±	2.95584 i
-0.06647 ±	1.95598 i	-0.07515 ±	2.71396 i
-0.08265 ±	1.97656 i	-0.10007 ±	2.40858 i
-0.27953 ±	2.04700 i	-0.07640 ±	0.53377 i
-0.28779 ±	0.03427 i	-0.08075 ±	1.27982 i
-0.06648 ±	0.04404 i	-0.27953 ±	0.95551 i
-0.08264 ±	0.02347 i	-0.28601 ±	1.03525 i
		-0.06548 ±	1.03440 i

ORIGINAL PAGE IS
OF POOR QUALITY

Appendix E. EIGENVECTORS FOR A MOD-2 CASE

This appendix contains the eigenvalues p_j , eigenvectors v_j , and combination constants c_j calculated for the $v_y = 2$ case of Figure 13.1. Only one half of each conjugate set is given. The eigenvalue is given first, followed by the associated eigenvector which is broken into harmonic parts. Finally, the combination constant is given at the bottom of the column. These constants were calculated with initial conditions placed on the zeroth harmonic coefficient as follows (in radians)

$$\begin{aligned} p_p &= 0.068 \\ p_j &= -.136 \end{aligned}$$

All other initial conditions were zero.

ORIGINAL PAGE IS
OF POOR QUALITY

p	-0.03390	8.67815 i

o	0.00081	-0.00104 i
	-0.00171	-0.00128 i
	0.00000	0.00000 i
s1	0.00000	-0.00000 i
	0.00000	0.00000 i
	-0.00744	-0.77072 i
c1	0.00000	-0.00000 i
	0.00000	0.00000 i
	0.77039	-0.00767 i
s2	-0.54368	0.02864 i
	-0.00000	-1.00000 i
	-0.00000	0.00000 i
c2	-0.02864	-0.54368 i
	1.00000	0.00000 i
	0.00000	-0.00000 i

c	-0.00001	0.00001 i

p	-0.00000	7.40552 i

o	0.00074	-0.00000 i
	1.00000	0.00000 i
	-0.00000	-0.00000 i
s1	0.00000	-0.00000 i
	-0.00000	0.00000 i
	-0.00583	-0.00072 i
c1	0.00000	-0.00000 i
	0.00000	0.00000 i
	0.50002	-0.00179 i
s2	0.00018	0.00018 i
	-0.00025	-0.00056 i
	-0.00000	0.00000 i
c2	0.00007	-0.00012 i
	0.00026	-0.00051 i
	0.00000	-0.00000 i

c	0.03401	0.00000 i

ORIGINAL PAGE IS
OF POOR QUALITY

p -0.00000 8.34673 i

o -0.00000 -0.00000 i
 0.00000 -0.00000 i
 -0.01692 0.94607 i

s1 0.00954 0.00024 i
 1.00000 -0.00000 i
 -0.00000 -0.00000 i

c1 0.00033 0.93706 i
 0.00053 0.94741 i
 0.00000 -0.00000 i

s2 0.00000 -0.00000 i
 0.00000 0.00000 i
 0.50007 -0.02524 i

c2 -0.00000 -0.00000 i
 -0.00000 0.00000 i
 0.01188 0.47400 i

c 0.00000 -0.00000 i

p -0.00000 6.34439 i

o -0.00000 0.00000 i
 0.00000 0.00000 i
 0.99866 0.01303 i

s1 0.00094 -0.02614 i
 -0.00073 0.93285 i
 -0.00000 -0.00000 i

c1 0.07845 0.00103 i
 1.00000 -0.00000 i
 -0.00000 0.00000 i

s2 0.00000 -0.00000 i
 -0.00000 0.00000 i
 -0.04402 0.46616 i

c2 -0.00000 0.00000 i
 -0.00000 0.00000 i
 0.49923 -0.00985 i

c -0.00000 -0.00000 i

ORIGINAL PAGE IS
OF POOR QUALITY

p	-0.01321	4.52008 i

0	0.00410	0.00473 i
	0.00106	-0.00090 i
	-0.00000	-0.00000 i
s1	-0.00000	0.00000 i
	-0.00000	-0.00000 i
	0.02073	0.84350 i
c1	-0.00000	-0.00000 i
	-0.00000	0.00000 i
	0.84629	-0.02336 i
s2	-0.68990	0.01434 i
	-0.00000	1.00000 i
	0.00000	0.00000 i
c2	0.01438	0.68993 i
	1.00000	-0.00000 i
	-0.00000	0.00000 i

c	0.00002	0.00001 i

p	-0.24415	3.97586 i

0	0.00420	0.00285 i
	-0.00052	0.00050 i
	-0.00000	-0.00000 i
s1	0.00000	0.00000 i
	-0.00000	-0.00000 i
	0.49543	0.03729 i
c1	-0.00000	0.00000 i
	-0.00000	-0.00000 i
	-0.03904	0.49773 i
s2	0.00001	-1.00000 i
	-0.00025	0.00842 i
	0.00000	-0.00000 i
c2	1.00000	-0.00000 i
	-0.00843	-0.00025 i
	0.00000	-0.00000 i

c	-0.00004	-0.00005 i

ORIGINAL PAGE 13
OF POOR QUALITY.

p	0.00594	1.95805 i

o	1.00000	0.00000 i
	0.00052	-0.00019 i
	0.00000	-0.00000 i
s1	-0.00000	-0.00000 i
	-0.00000	-0.00000 i
	-0.74625	-0.03842 i
c1	-0.00000	0.00000 i
	0.00000	-0.00000 i
	0.00498	-0.25452 i
s2	0.00466	0.00662 i
	-0.00046	-0.00008 i
	0.00000	-0.00000 i
c2	-0.00659	0.00477 i
	-0.00039	0.00006 i
	0.00000	0.00000 i

c	-0.00269	0.03305 i

p	-0.28256	1.95953 i

o	-0.09115	-0.06131 i
	0.00082	0.00069 i
	0.00000	0.00000 i
s1	-0.00000	-0.00000 i
	0.00000	0.00000 i
	0.04296	-0.96580 i
c1	-0.00000	-0.00000 i
	0.00000	-0.00000 i
	1.00000	-0.00000 i
s2	-0.00990	0.01208 i
	-0.00021	-0.00043 i
	0.00000	0.00000 i
c2	-0.01209	-0.00991 i
	0.00051	-0.00022 i
	-0.00000	0.00000 i

c	-0.02576	0.00321 i

ORIGINAL PAGE IS
OF POOR QUALITY

p	-0.27915	0.04774 i

o	-0.02050	0.02340 i
	0.00077	0.00064 i
	0.00000	-0.00000 i
s1	-0.00000	-0.00000 i
	0.00000	-0.00000 i
	0.04161	-0.98270 i
c1	-0.00000	0.00000 i
	-0.00000	-0.00000 i
	1.00000	-0.00000 i
s2	0.00357	-0.00187 i
	-0.00065	-0.00086 i
	0.00000	-0.00000 i
c2	0.00177	0.00345 i
	0.00090	-0.00067 i
	-0.00000	0.00000 i

c	0.00041	-0.00509 i

p	-0.00045	3.46171 i

o	0.00000	0.00000 i
	0.00000	0.00000 i
	-0.07248	0.74632 i
s1	-0.00221	-0.75562 i
	-0.00037	-0.00482 i
	0.00000	-0.00000 i
c1	1.00000	0.00000 i
	-0.02647	0.00015 i
	0.00000	0.00000 i
s2	0.00000	-0.00000 i
	0.00000	0.00000 i
	-0.59104	0.14121 i
c2	0.00000	0.00000 i
	0.00000	-0.00000 i
	-0.16022	-0.46922 i

c	-0.00000	0.00000 i

ORIGINAL PAGE IS
OF POOR QUALITY

p	-0.27534	2.95392 i

o	-0.00000	-0.00000 i
	0.00000	-0.00000 i
	0.01762	-0.00429 i
s1	-0.01690	0.00698 i
	0.00033	0.00038 i
	-0.00000	-0.00000 i
c1	-0.01244	-0.02383 i
	-0.00009	0.00103 i
	0.00000	-0.00000 i
s2	-0.00000	0.00000 i
	-0.00000	0.00000 i
	1.00000	0.00000 i
c2	-0.00000	-0.00000 i
	-0.00000	0.00000 i
	0.00366	0.99770 i

c	0.00000	0.00000 i

p	-0.09065	1.25030 i

o	0.00602	-0.02858 i
	-0.00058	-0.00007 i
	0.00000	0.00000 i
s1	0.00000	-0.00000 i
	0.00000	0.00000 i
	0.29449	0.47728 i
c1	-0.00000	-0.00000 i
	0.00000	-0.00000 i
	-0.46408	0.29915 i
s2	1.00000	-0.00000 i
	0.00163	-0.02834 i
	0.00000	-0.00000 i
c2	0.00001	0.99999 i
	0.02834	0.00164 i
	0.00000	-0.00000 i

c	0.00007	0.00018 i

ORIGINAL PAGE IS
OF POOR QUALITY

p	-0.00067	1.26217	i

0	-0.00000	0.00000	i
	0.00000	-0.00000	i
	1.00000	0.00000	i
s1	-0.80329	-0.14241	i
	-0.00007	-0.00007	i
	-0.00000	0.00000	i
c1	-0.07444	0.39271	i
	0.00182	-0.00801	i
	-0.00000	-0.00000	i
s2	-0.00000	0.00000	i
	0.00000	0.00000	i
	-0.00660	-0.26469	i
c2	-0.00000	-0.00000	i
	-0.00000	0.00000	i
	-0.31905	-0.15022	i

c	0.00000	0.00000	i

p	-0.27605	0.95513	i

0	-0.00000	0.00000	i
	-0.00000	0.00000	i
	1.00000	0.00000	i
s1	-0.01742	-0.01847	i
	-0.00034	0.00002	i
	0.00000	-0.00000	i
c1	-0.01443	0.00256	i
	0.00071	-0.00003	i
	0.00000	0.00000	i
s2	-0.00000	-0.00000	i
	-0.00000	-0.00000	i
	0.01789	0.00208	i
c2	0.00000	-0.00000	i
	-0.00000	-0.00000	i
	-0.01054	0.00095	i

c	0.00000	-0.00000	i

ORIGINAL PAGE IS
OF POOR QUALITY

21 3047 IAVIINO
YTIJAUO 9004 10

	-0.27822	1.04742 i
	-0.00000	0.00000 i
0	-0.00000	-0.00000 i
	0.04326	-0.01527 i
	-0.02479	0.00863 i
s1	0.00038	0.00034 i
	0.00000	0.00000 i
	-0.00781	0.00231 i
c1	-0.00016	0.00036 i
	-0.00000	0.00000 i
	0.00000	-0.00000 i
s2	-0.00000	-0.00000 i
	1.00000	0.00000 i
	0.00000	0.00000 i
c2	0.00000	0.00000 i
	-0.01346	0.99952 i
	-0.00000	-0.00000 i
c	-0.00000	-0.00000 i

ORIGINAL PAGE IS
OF POOR QUALITY

Table 6.1 STANDARD MOD-0 BLADE PARAMETERS

$\beta_s = 0$	$\beta_p = -.1$	$\rho_s = 0$
$\bar{I}_o = 0.001$	$\bar{e}_I = 0$	$\bar{e}_H = 0$
$v_{\beta} = 2.5$	$v_{\rho} = 3.6$	$v_{\theta} = 10$
$\gamma = 12$	$\lambda = 0.1$	$\theta_o = 0$
$\bar{c} = 0.04$	$\bar{e}_A = 0$	$D = .002$

ORIGINAL PAGE IS
OF POOR QUALITY

SI 3015
11/14/67

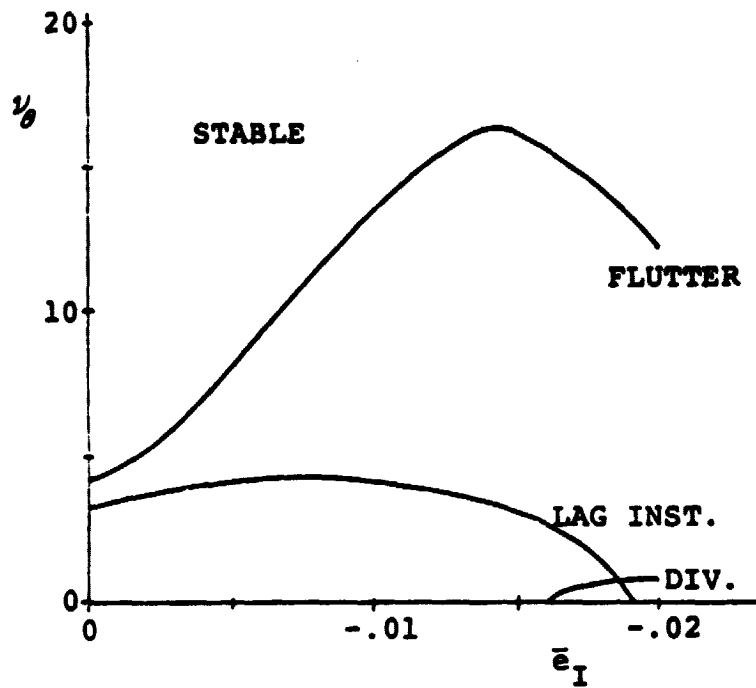


Figure 6.1 ν_θ vs \bar{e}_I Stability Boundaries, Preconed Rotor

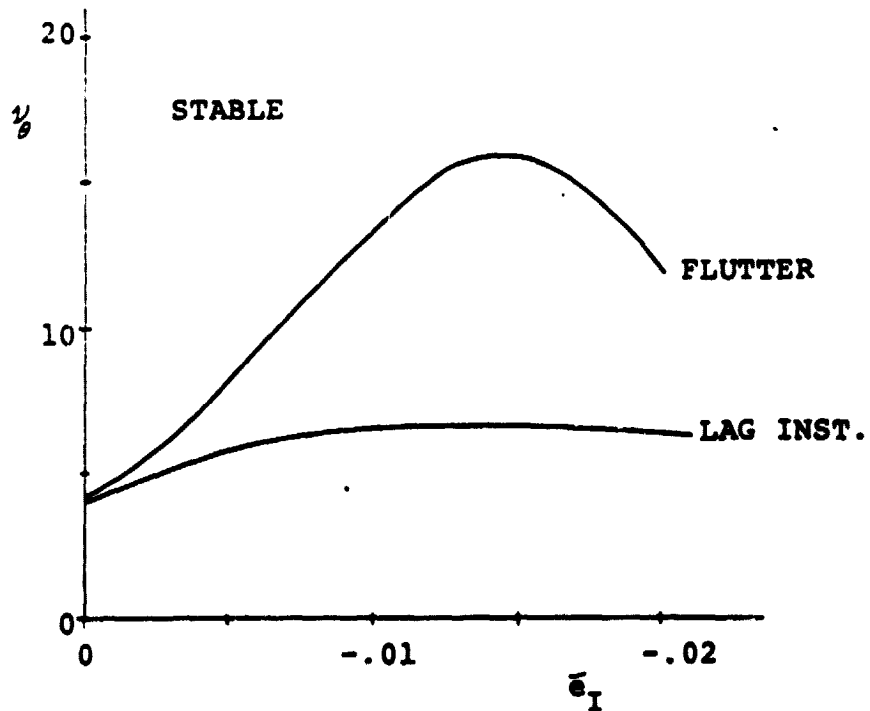


Figure 6.2 ν_θ vs \bar{e}_I Stability Boundaries, Flat Rotor

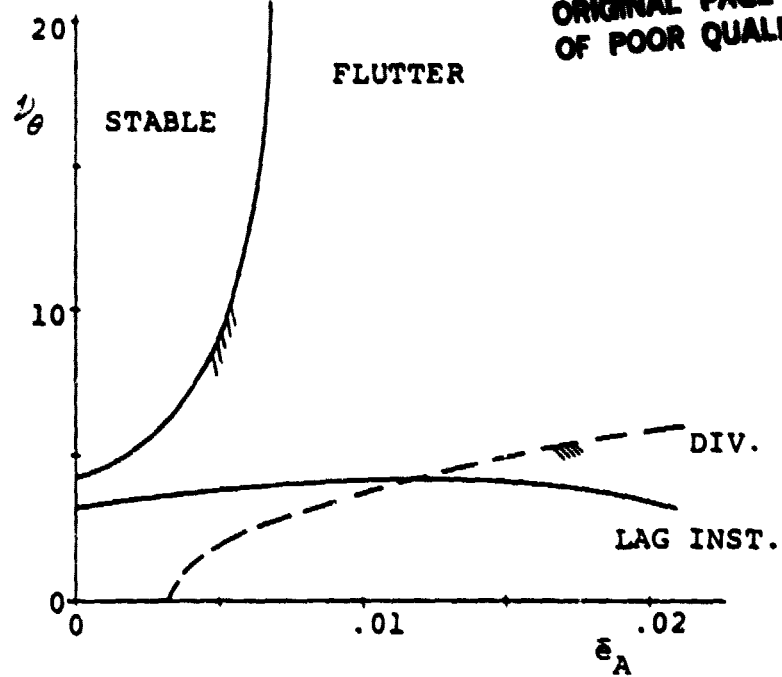


Figure 6.3 ν_θ vs. $\bar{\epsilon}_A$ Stability Boundaries, Preconed Rotor

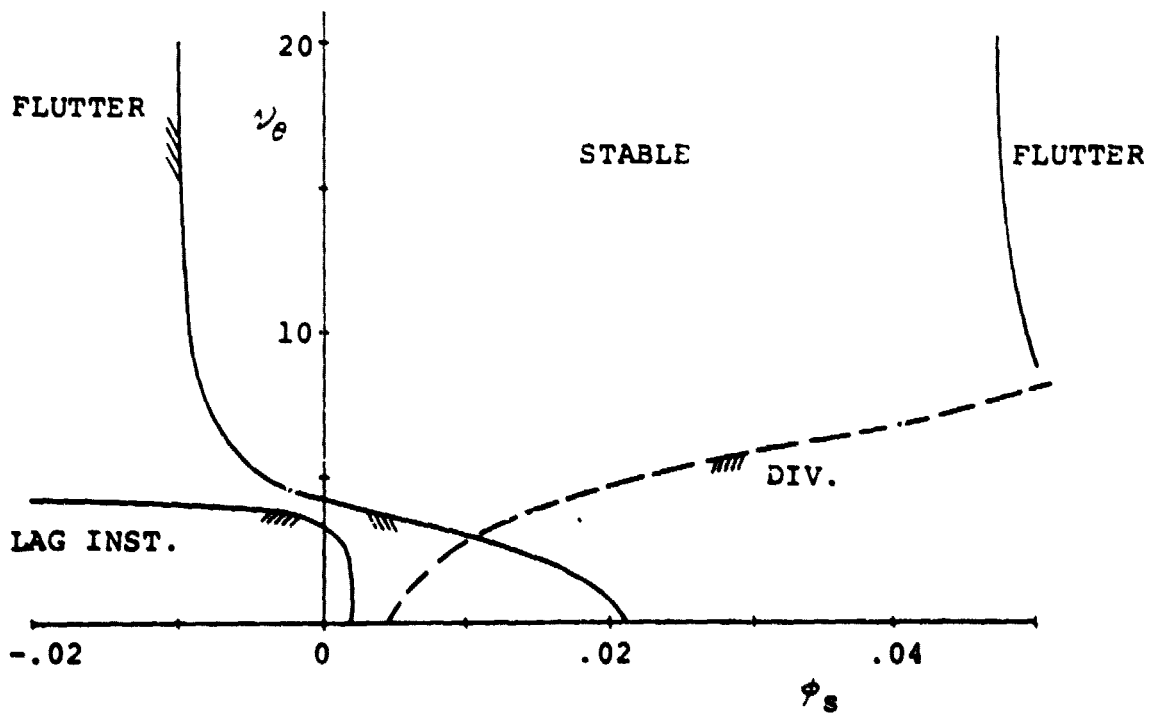


Figure 6.4 ν_θ vs ϕ_s Stability Boundaries, Preconed Rotor

ORIGINAL PAGE IS
OF POOR QUALITY

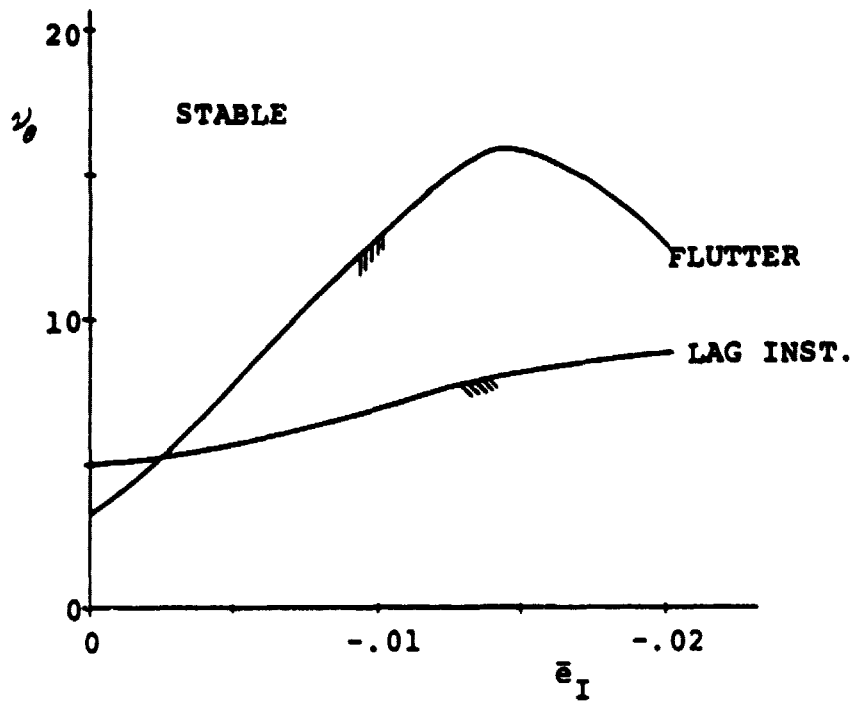


Figure 6.5 ν_θ vs \bar{e}_I Stability Boundaries, Preconed Rotor, From 2 dof Submodels

ORIGINAL PAGE IS OF POOR QUALITY

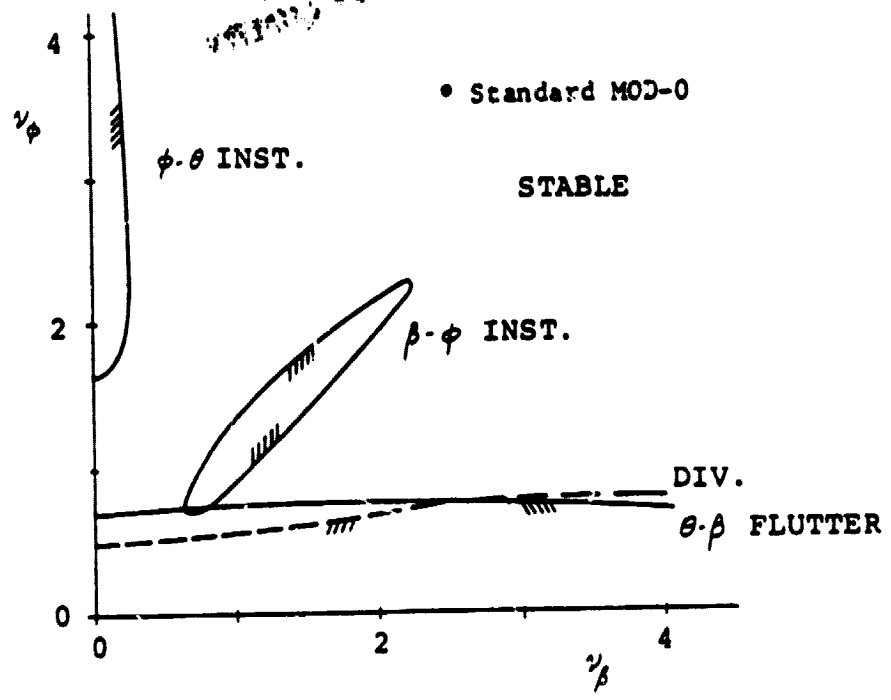


Figure 6.6 ν_ϕ vs ν_β Stability Boundaries, Preconed Rotor

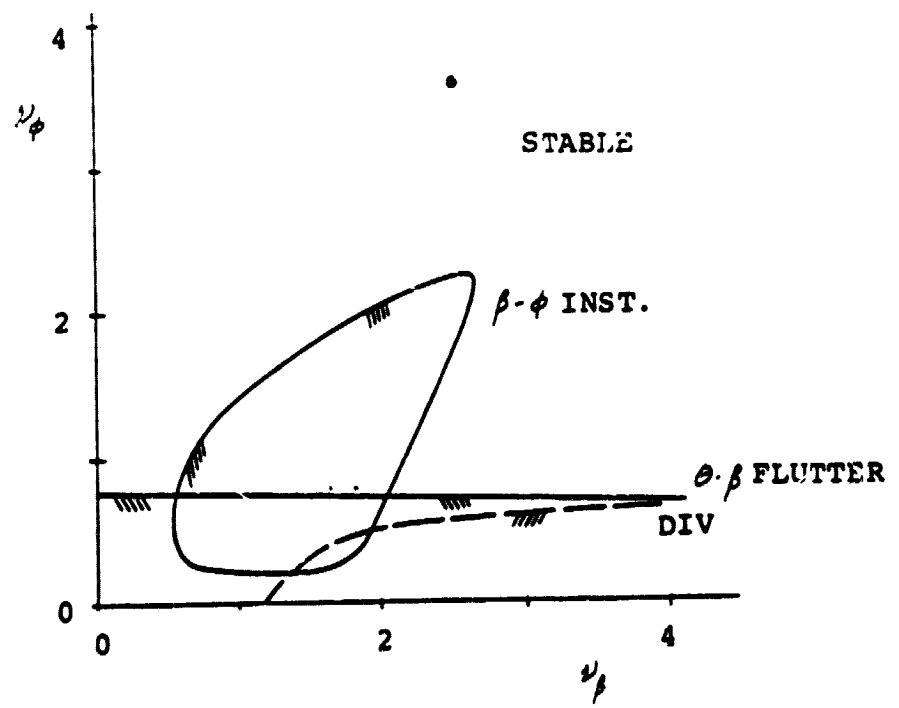


Figure 6.7 ν_ϕ vs ν_β Stability Boundaries, Preconed Rotor, From 2 dof Submodels

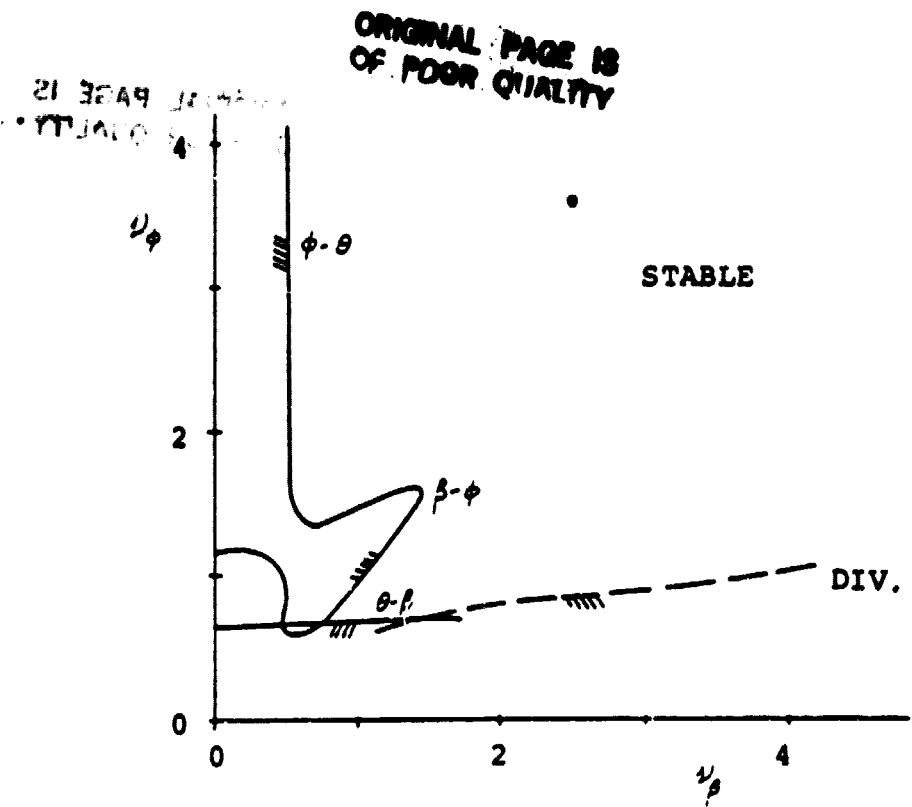


Figure 6.8 ν_ϕ vs ν_β Stability Boundaries, Flat Rotor

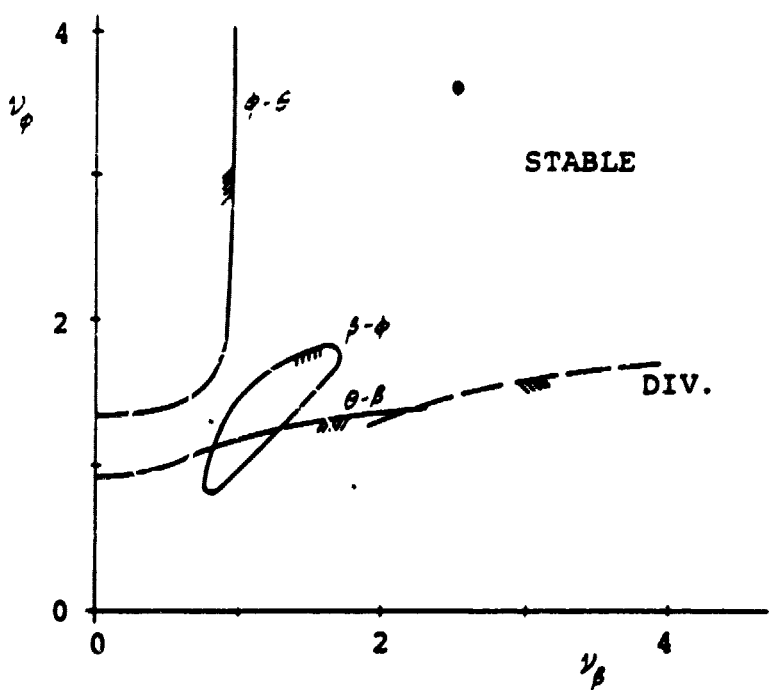


Figure 6.9 ν_ϕ vs ν_β Stability Boundaries with $\lambda = 0.2$, Precone Rotor

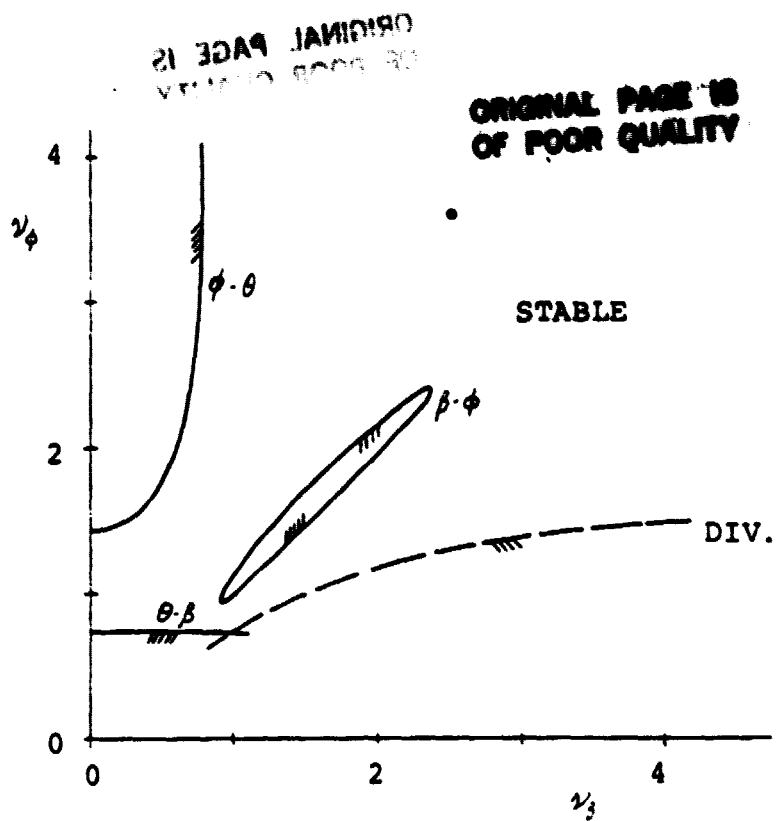


Figure 6.10 ν_ϕ vs ν_β Stability Boundaries with $\nu_\epsilon = 5$,
Preconed Rotor

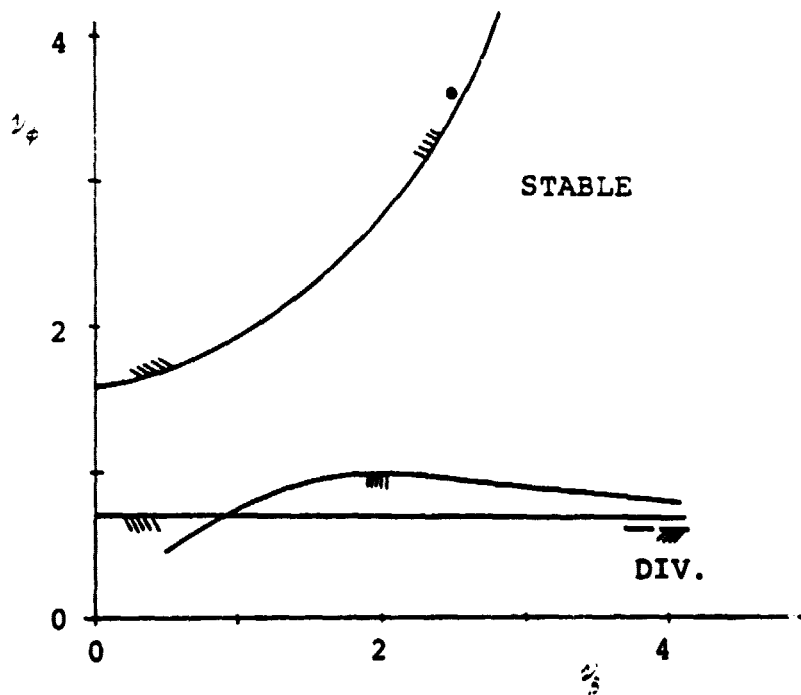


Figure 6.11 ν_ϕ vs ν_β Stability Boundaries with $\beta_s = -0.1$,
Preconed Rotor

ORIGINAL PAGE IS
OF POOR QUALITY

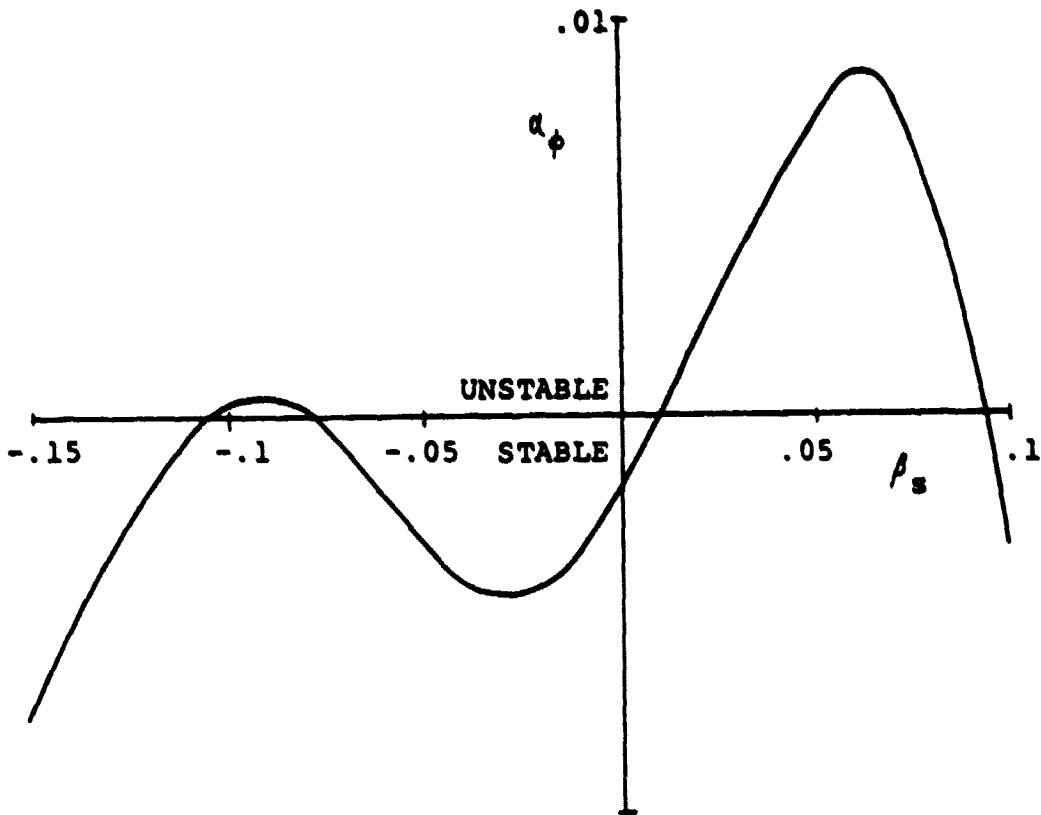


Figure 6.12 Lag Damping vs β_s , Preconed Rotor

ORIGINAL PAGE IS
OF POOR QUALITY

ORIGINAL PAGE IS
OF POOR QUALITY

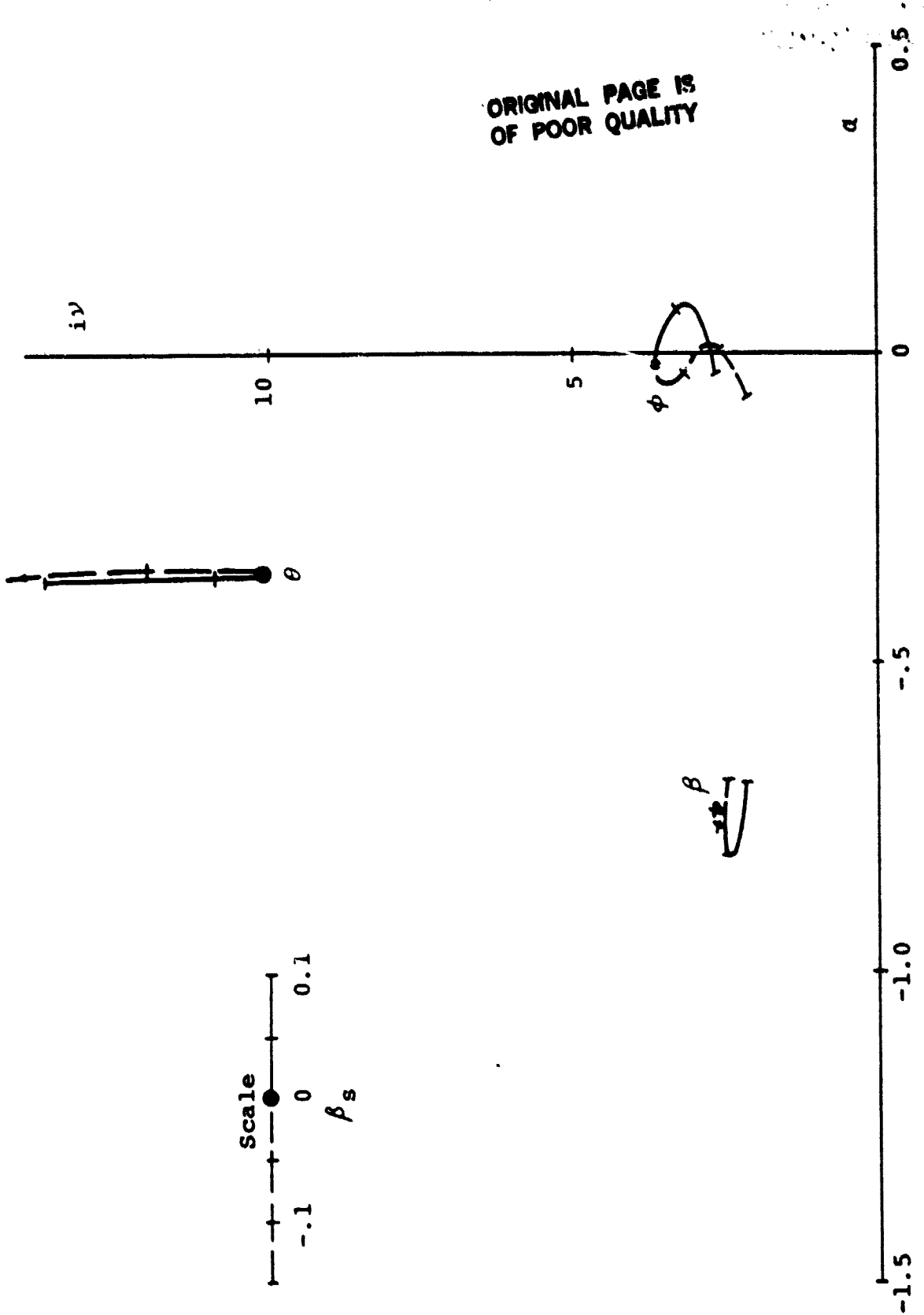


Figure 6.13 Root Locus Plot for Parameter β_s , Preconed Rotor

ORIGINAL PAGE IS
OF POOR QUALITY

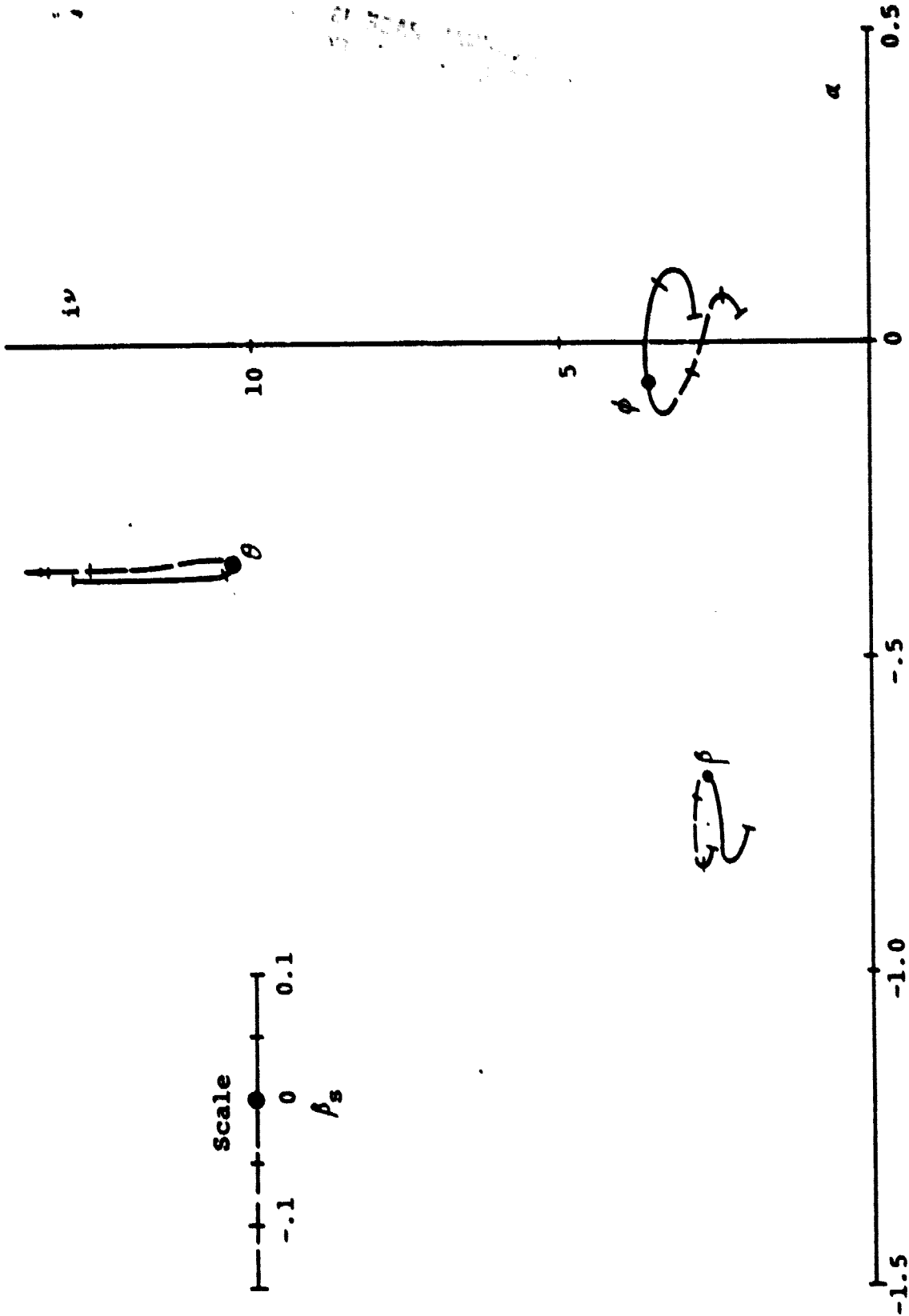


Figure 6.14 Root Locus Plot for Parameter β_s , Flat Rotor

ORIGINAL PAGE IS
OF POOR QUALITY

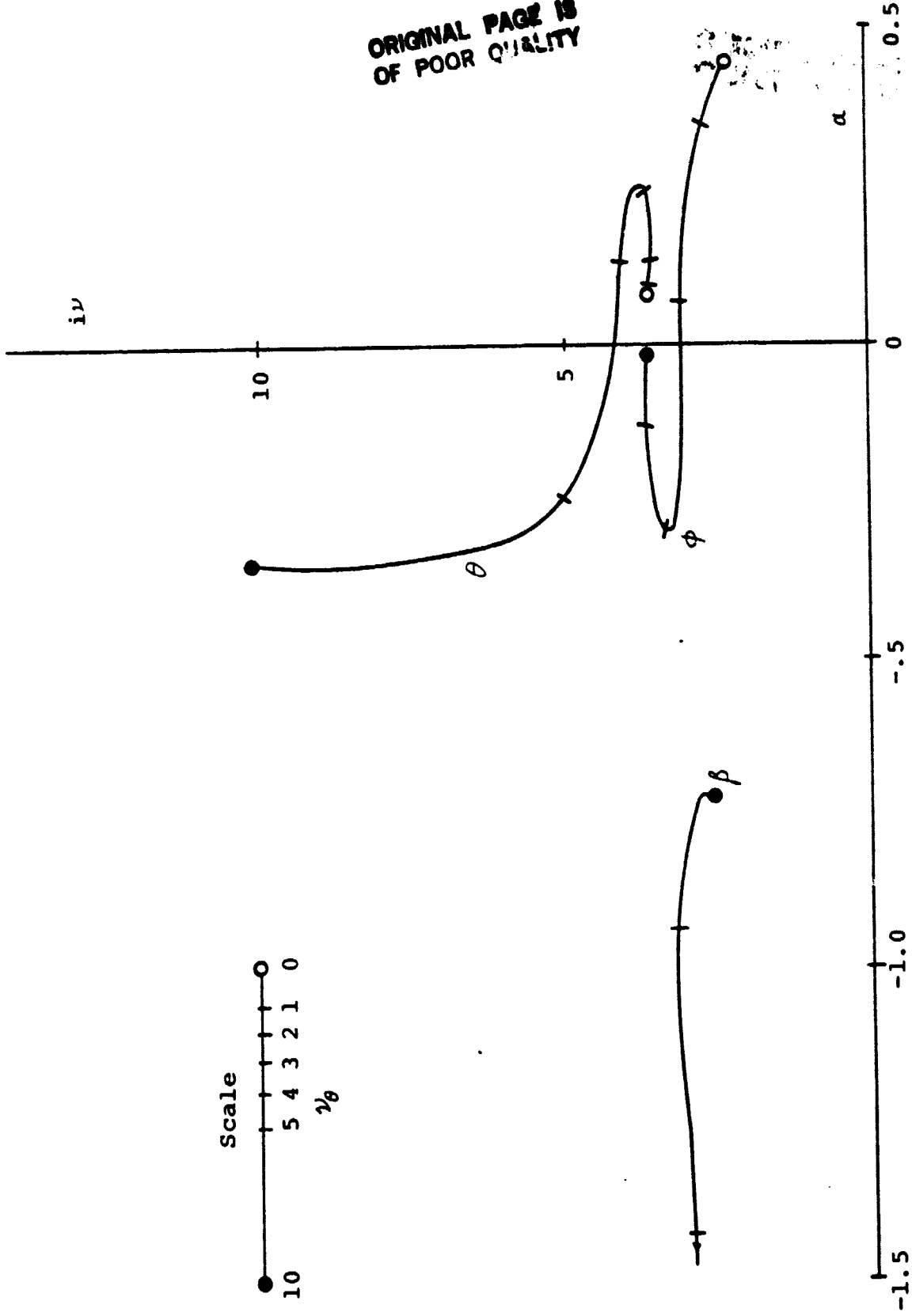


Figure 6.15 Root Locus Plot for ν_θ , Preconed Rotor

ORIGINAL PAGE IS
OF POOR QUALITY

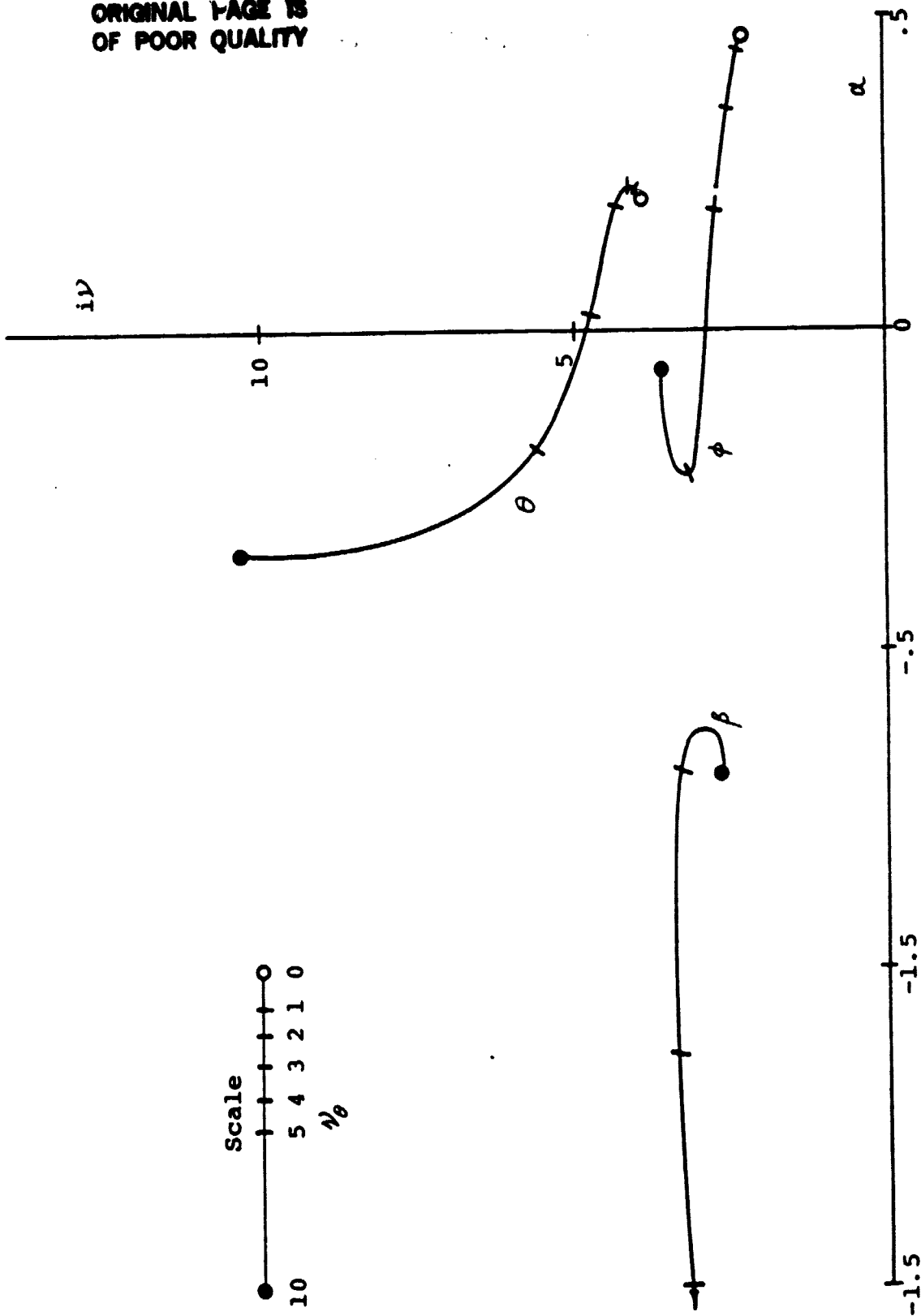


Figure 6.16 Root Locus Plot for $1/\theta$, Flat Rotor

ORIGINAL PAGE IS
OF POOR QUALITY

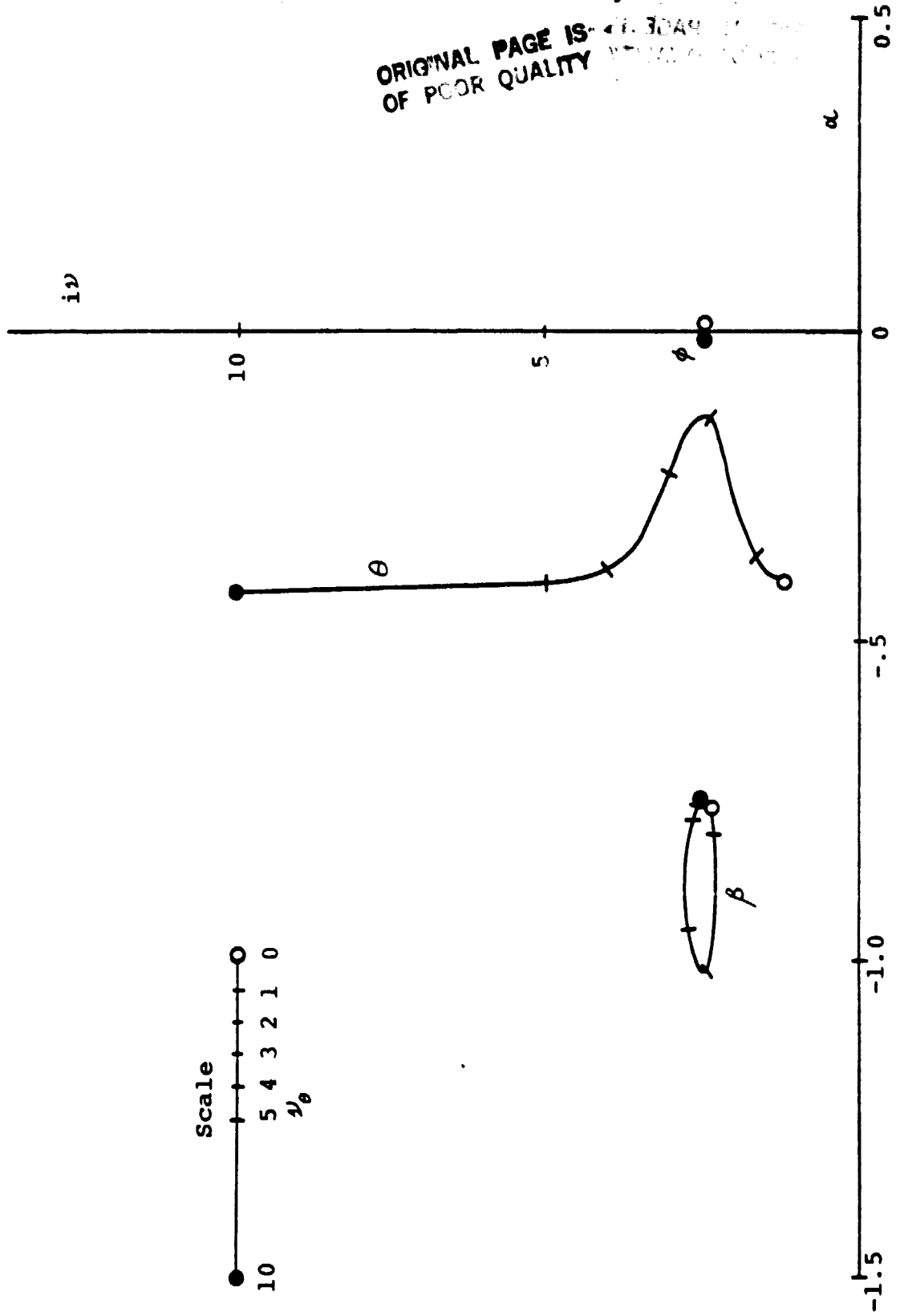


Figure 6.17 Root Locus Plot for $\gamma_\theta = \gamma_\beta = 2.5$, Precone Rotor

ORIGINAL PAGE IS
OF POOR QUALITY

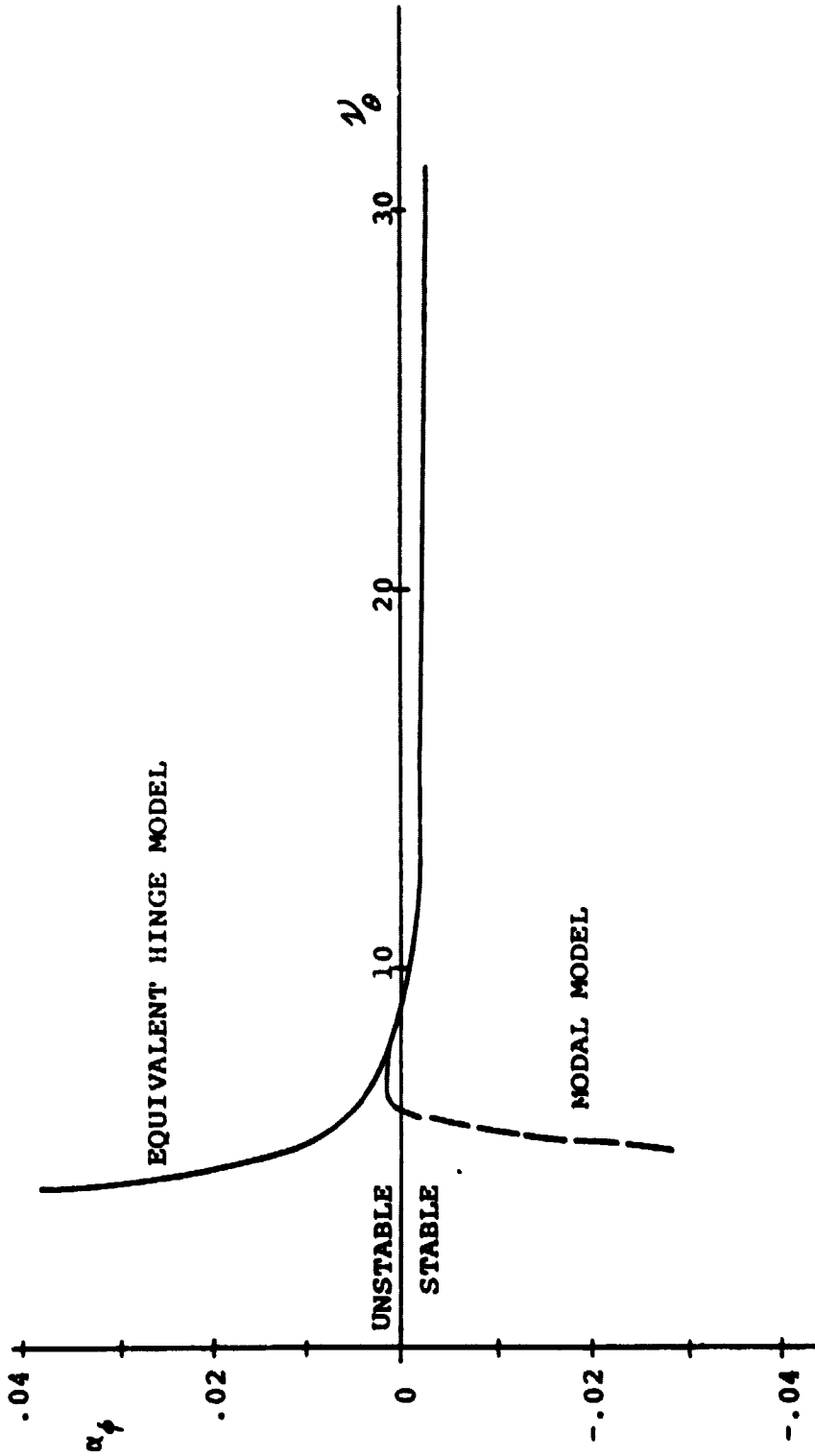


Figure 7.1 Lag Mode Damping vs ν_θ , MOD-0 Case of Reference [20]

ORIGINAL PAGE IS
OF POOR QUALITY

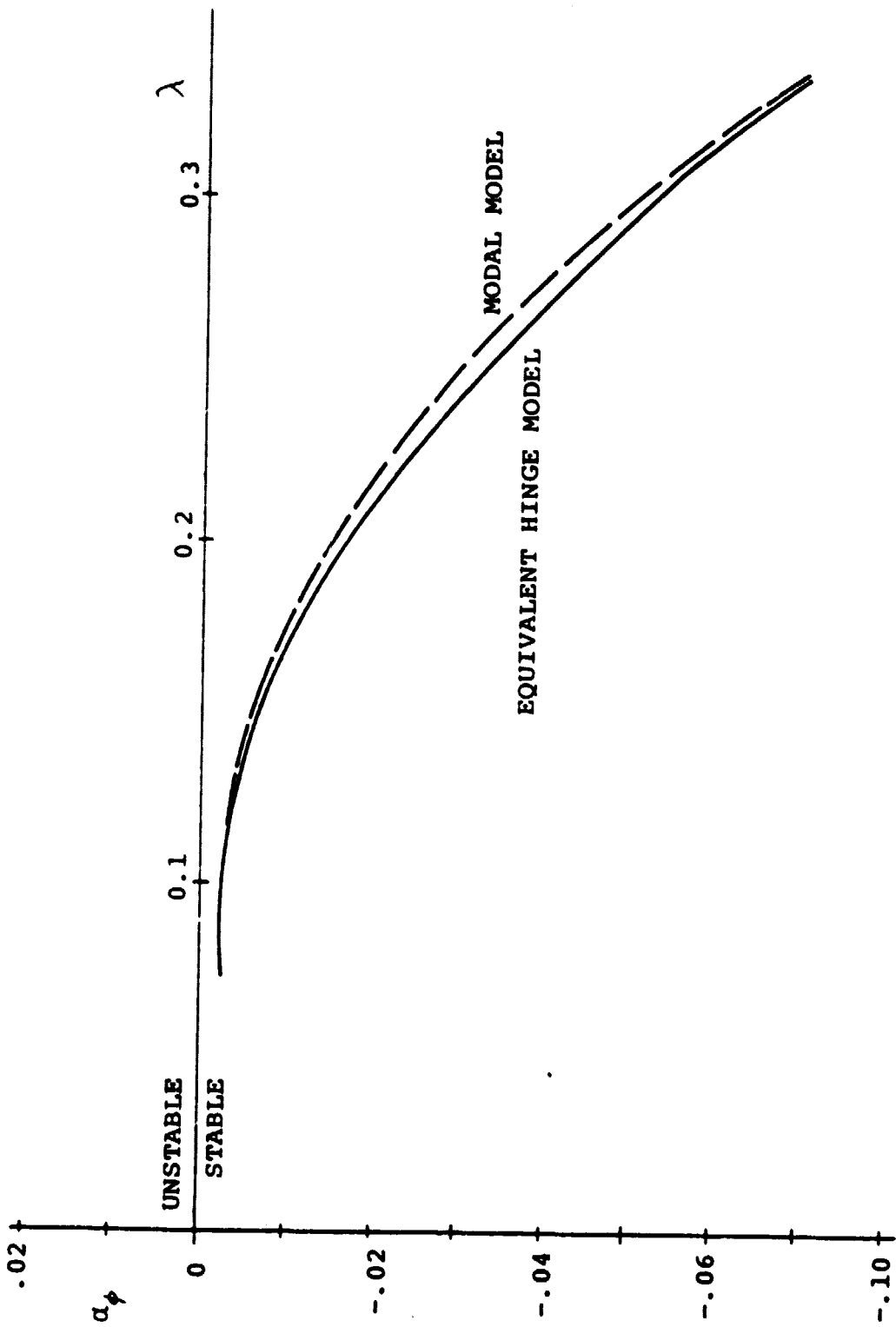


Figure 7.2 Lag Mode Damping vs λ , MOD-0 Case of Reference [20]

ORIGINAL PAGE IS
OF POOR QUALITY

QUALITY
PAGE 13

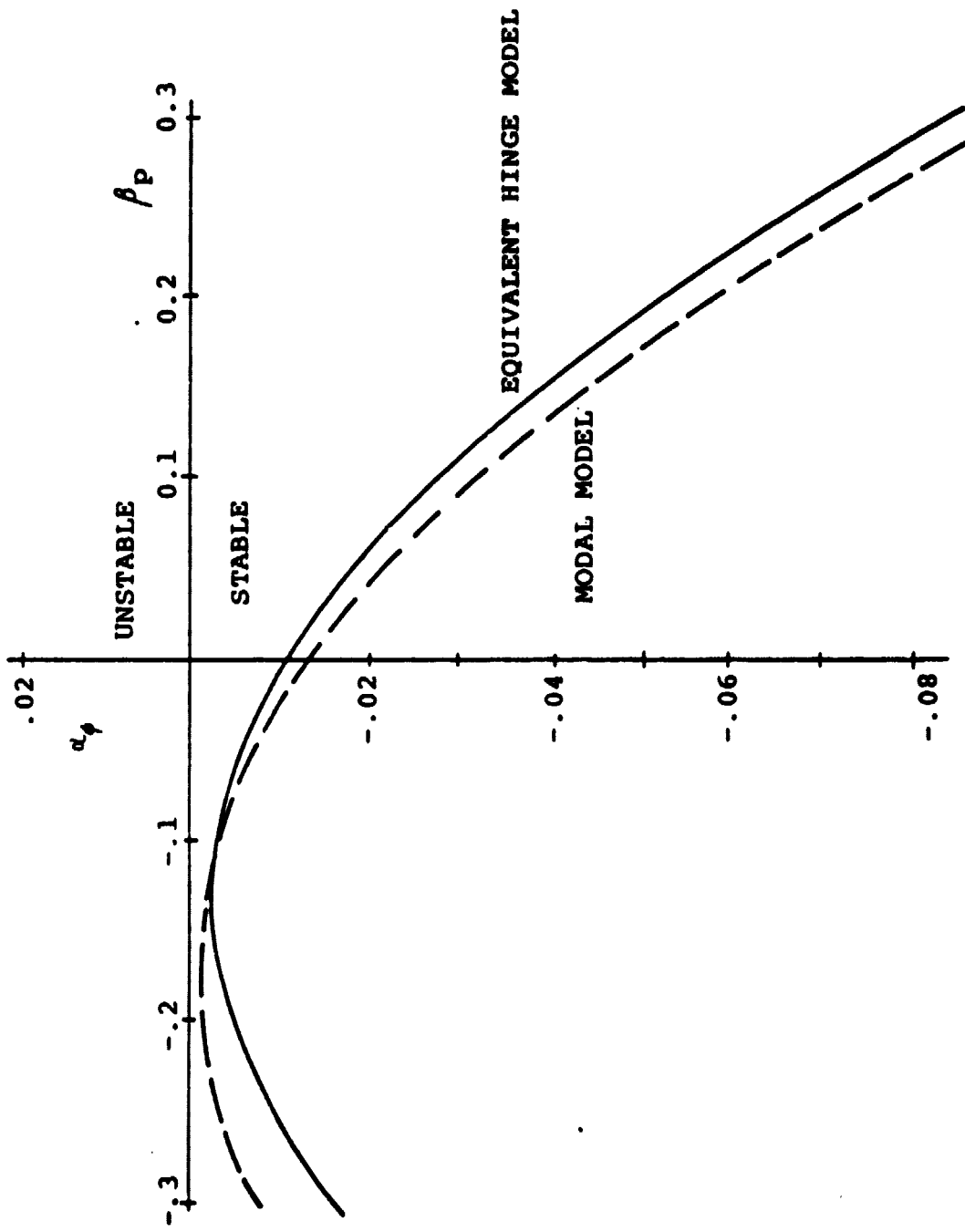


Figure 7.3 Lag Mode Damping vs β_p , MOD-0 Case of Reference [20]

Table 13.1

STANDARD MOD-2 PARAMETERS

$\bar{M}_b = 5.512$	$\bar{S}_b = 1.805$	$A_p = 0$
$\bar{I}_y = 0.1619$	$\bar{I}_p = 0.3502$	$\bar{L}_n = 0.1597$
$v_y = 7.767$	$v_p = 7.41$	$v_t = 0$
$\zeta_y = 0$	$\zeta_p = 0$	$\zeta_t = 0$
$\gamma = 4.777$	$\lambda = 0.129$	$A_c = -.0524$
$\bar{c} = 0.047$	$r = 0.03$	$\mu = 0$
$L_1 = 0.9275$	$\theta_o L_2 = 0.0951 + 0.6312\theta_c$	
$L_3 = 0.9787$	$\theta_o L_4 = 0.1059 + 0.5529\theta_c$	
$L_5 = 1.0248$	$L_{80} = 1.0139$	

Here, θ_c is the tip pitch control setting.

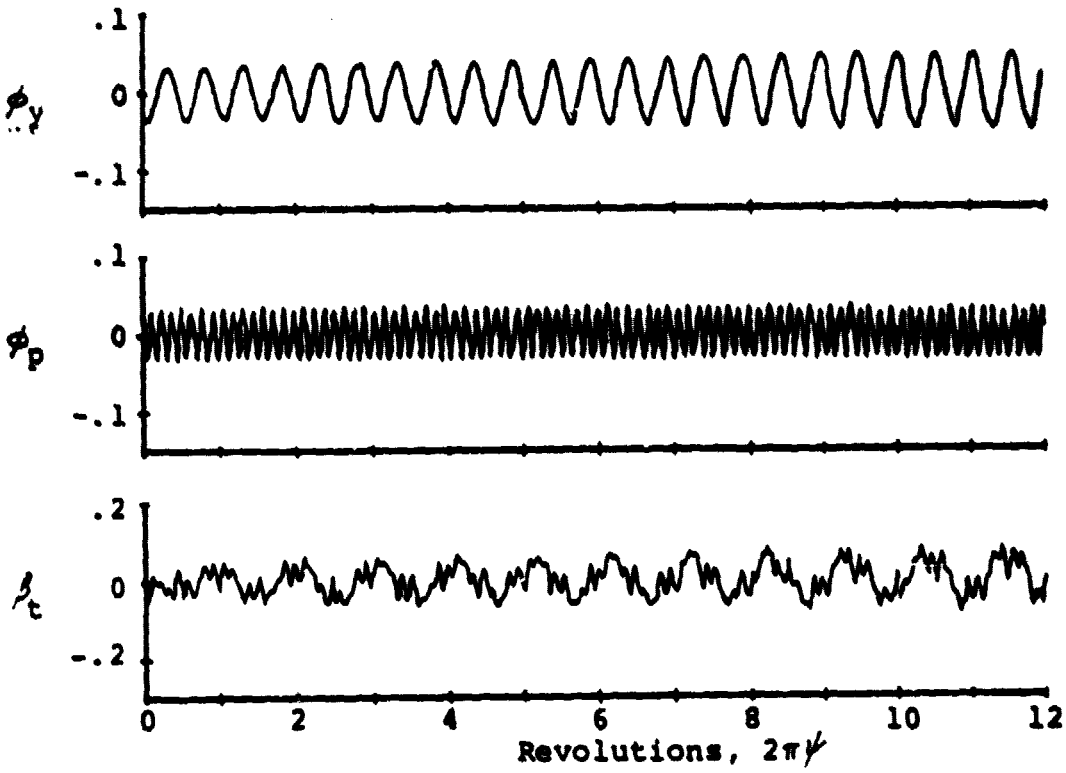


Figure 13.1 Present Analysis Transient Response for $\nu_y = 2$

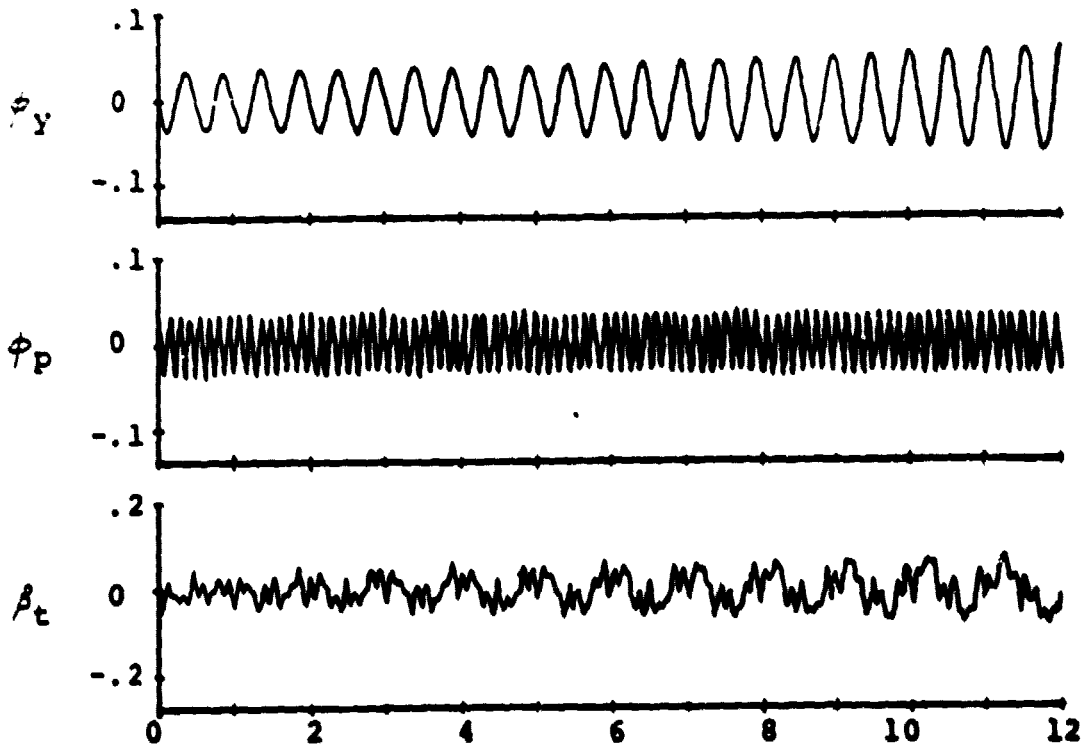


Figure 13.2 Transient Response from Reference [50] for $\nu_y = 2$

21 5049 JAN 1950

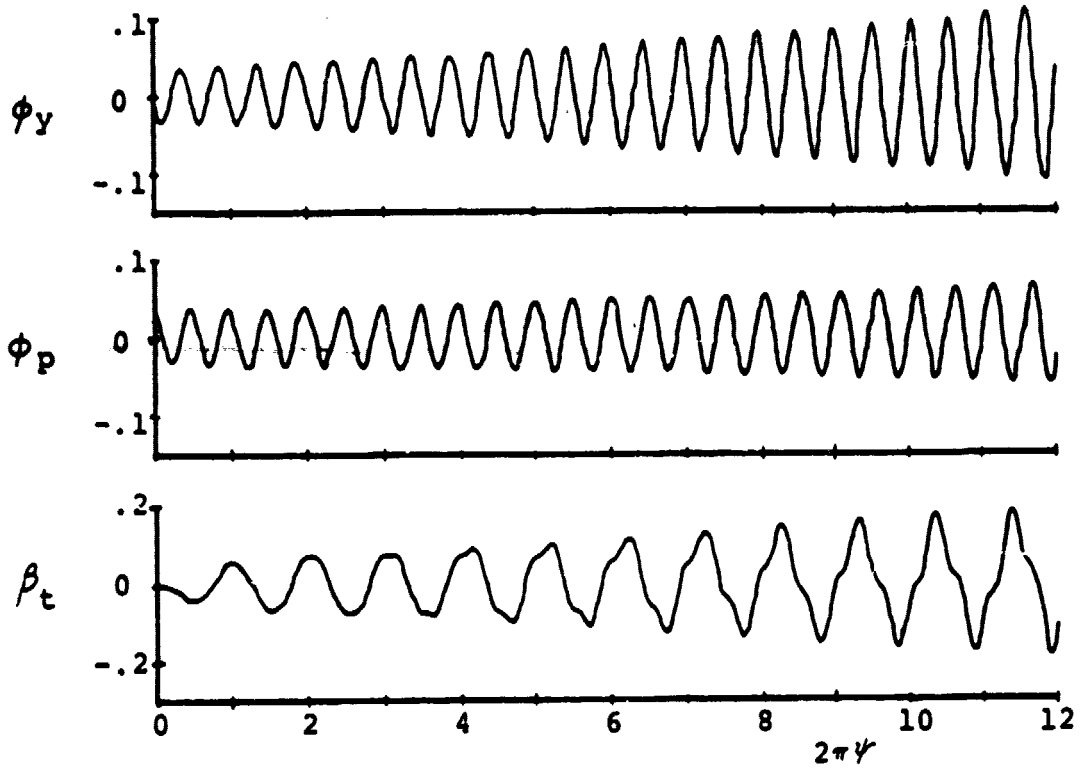


Figure 13.3 Present Analysis Transient Response, $\nu_y = \nu_p = 2$

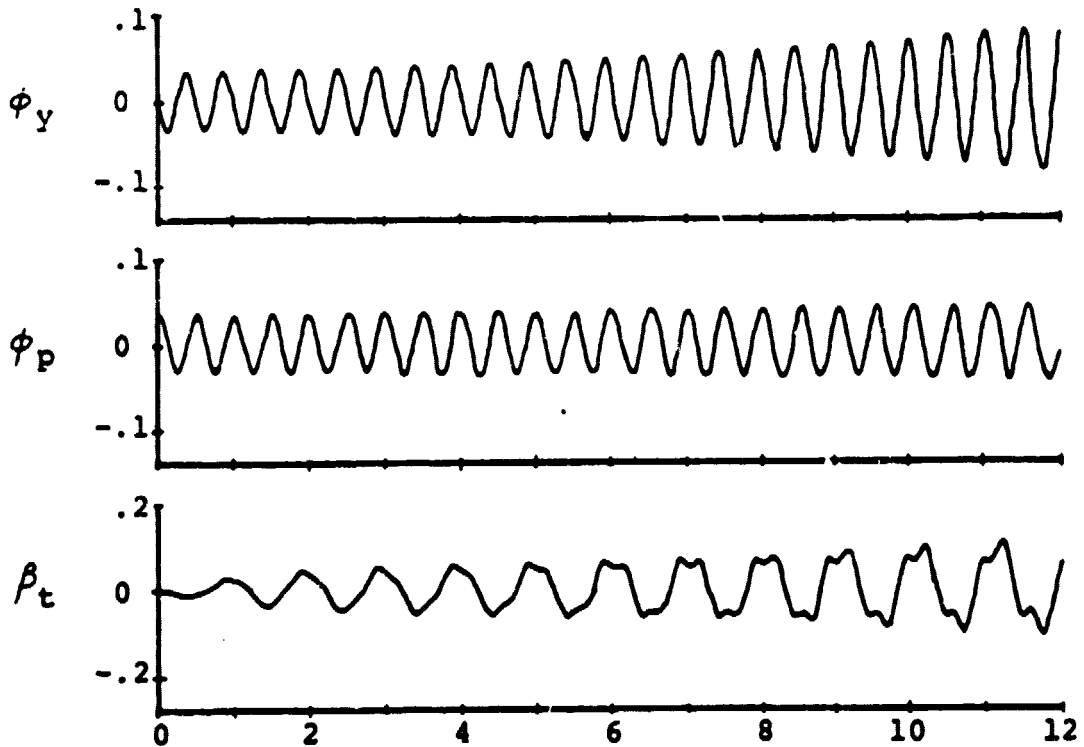


Figure 13.4 Transient Response from [50], $\nu_y = \nu_p = 2$

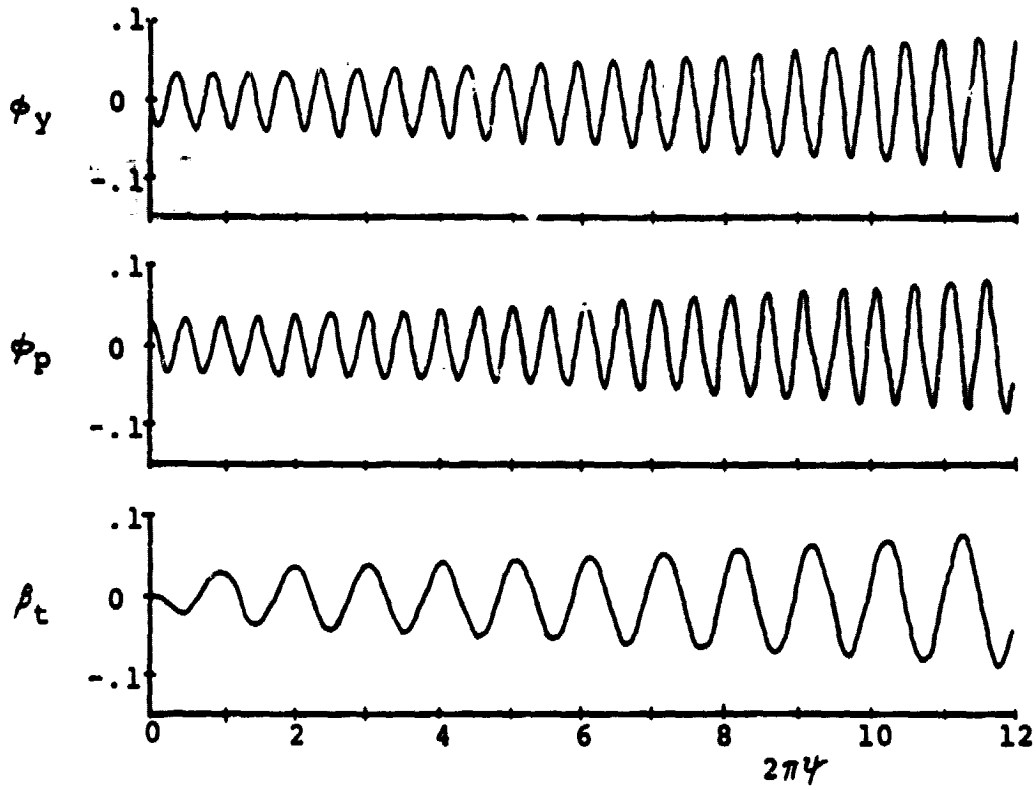


Figure 13.5 Present Analysis Transient Response,
 $\nu_y = \nu_p = 2$ with Alternate Initial Conditions

ORIGINAL PAGE IS
OF POOR QUALITY

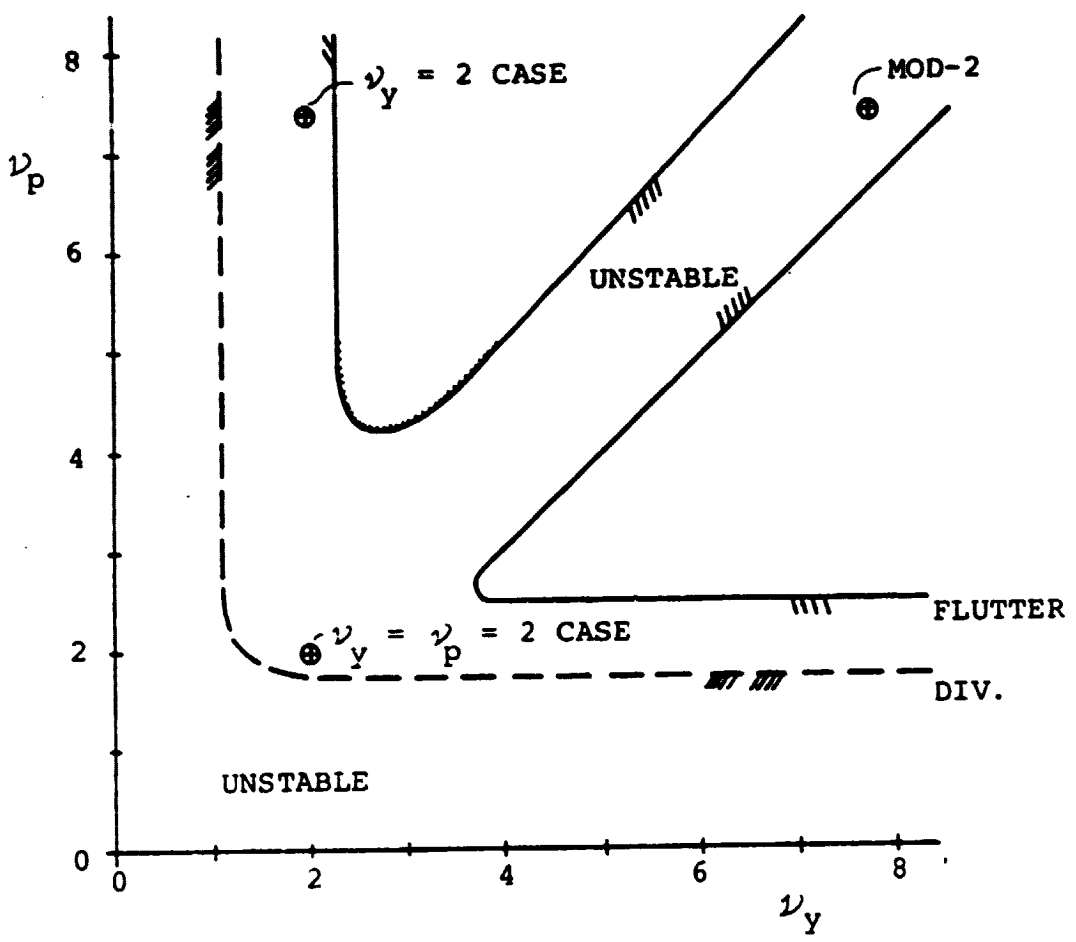


Figure 13.6 ν_y vs ν_p Stability Map for MOD-2 Without Damping
 ——— P = 2 P = 3

ORIGINAL PAGE IS
OF POOR QUALITY

Seven more highly damped
modes ($\alpha \approx .3$) omitted.

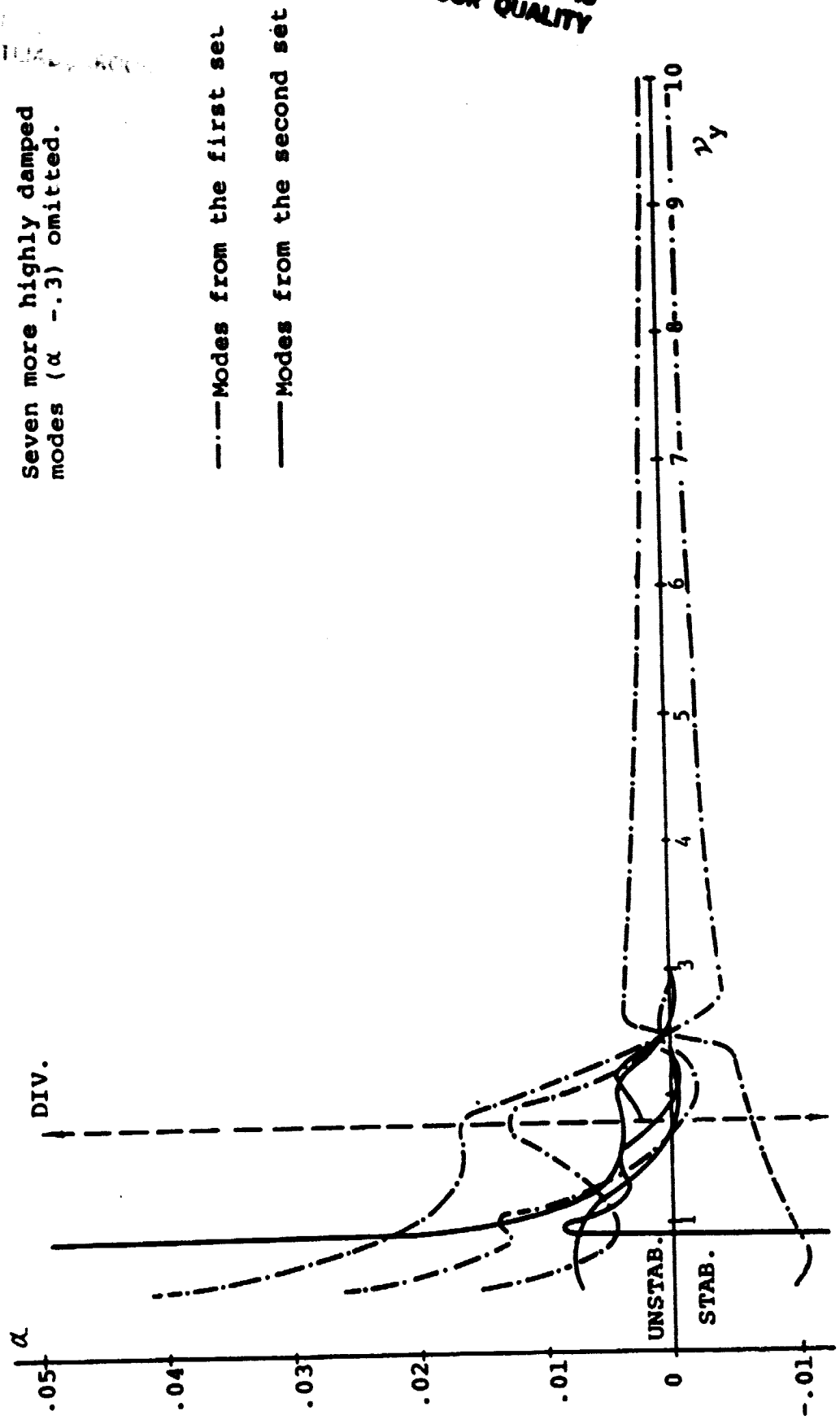


Figure 13.7 Damping of various Modes vs ν_y for $\nu_p = \nu_y$, $\zeta_y = \zeta_p = 0$, Standard Parameters

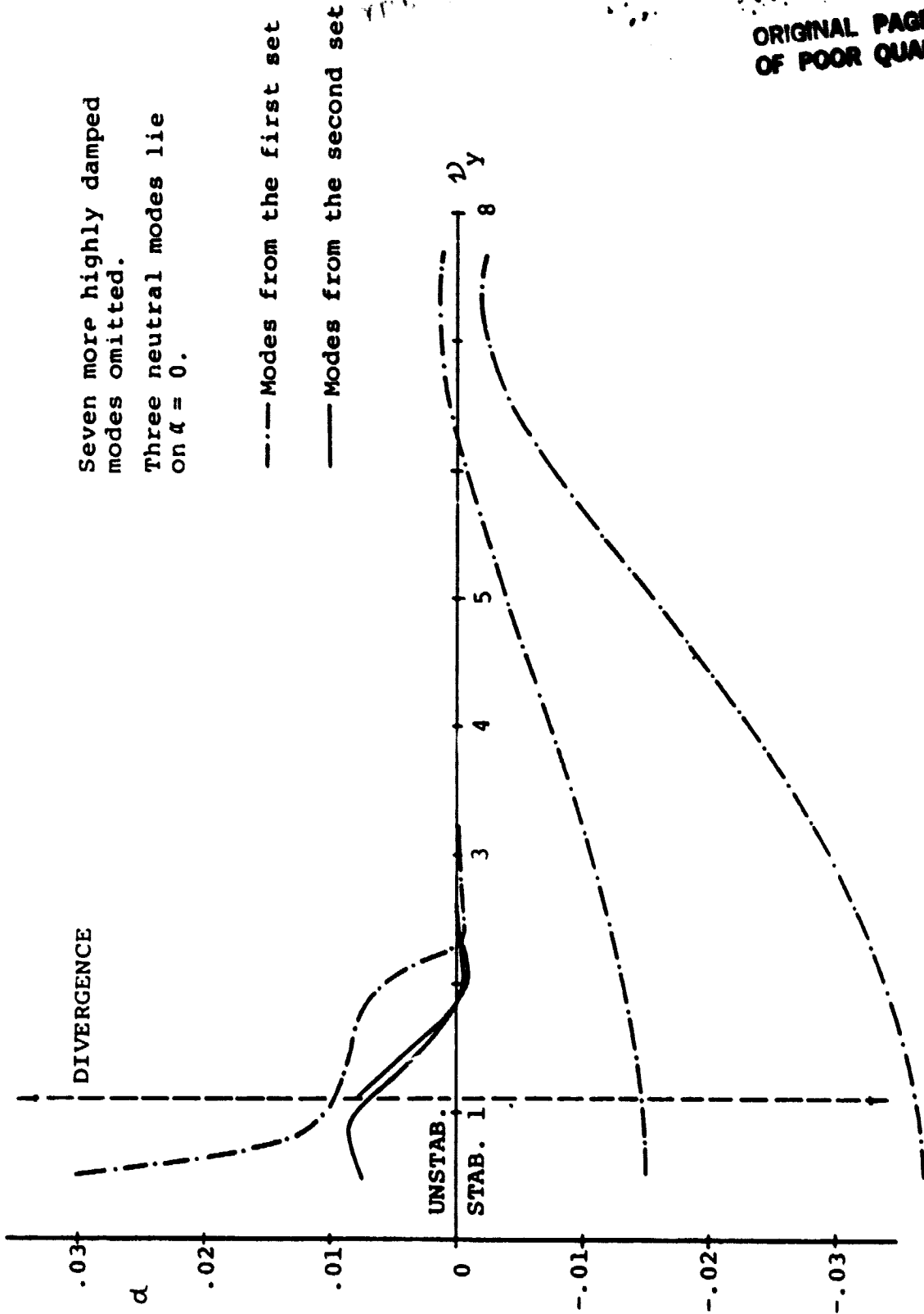


Figure 13.8 Damping of Various Modes vs ν_y for $\nu_p = 7.41$ and $\zeta_y = \zeta_p = 0$

ORIGINAL MANUSCRIPT
OF POOR QUALITY

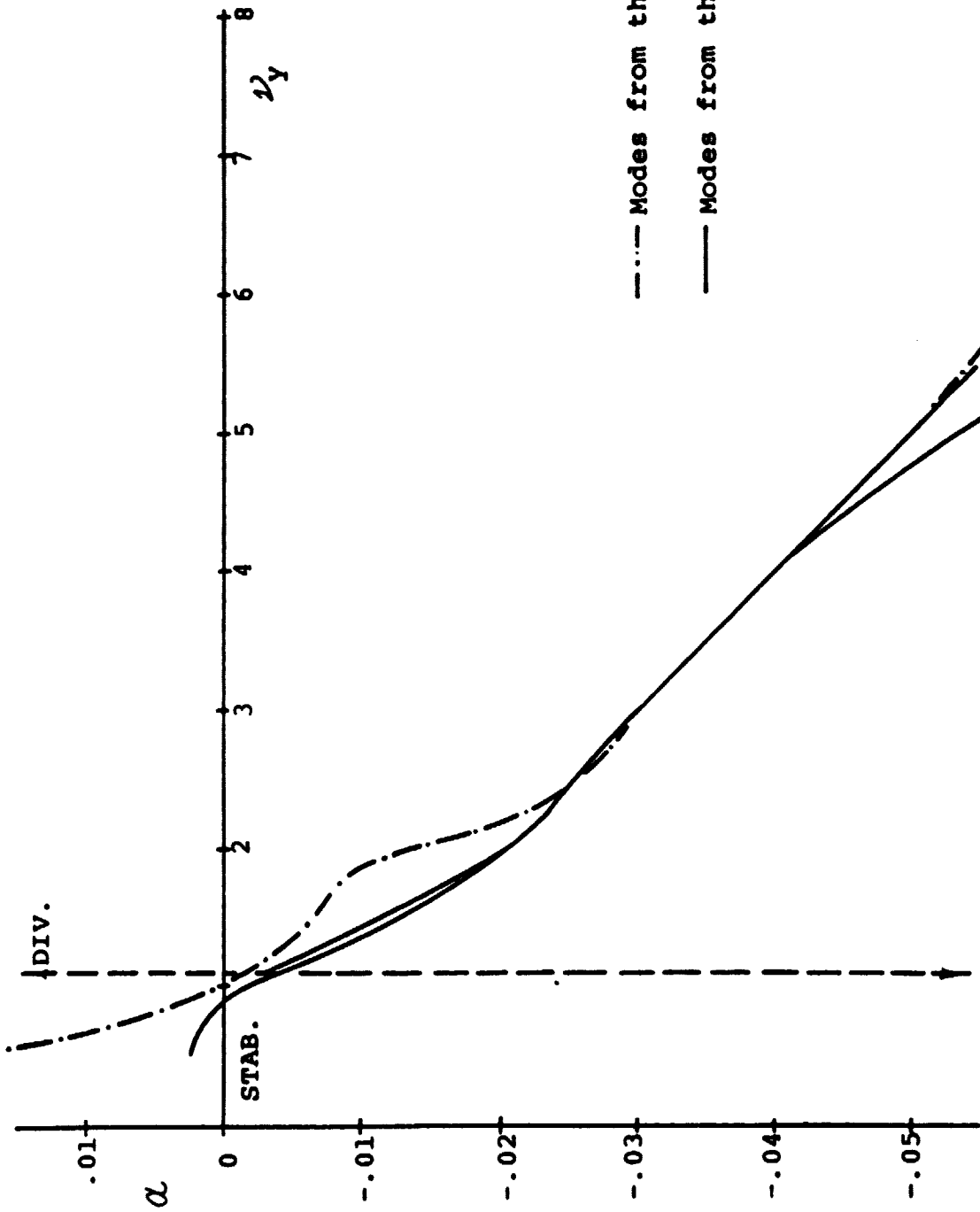
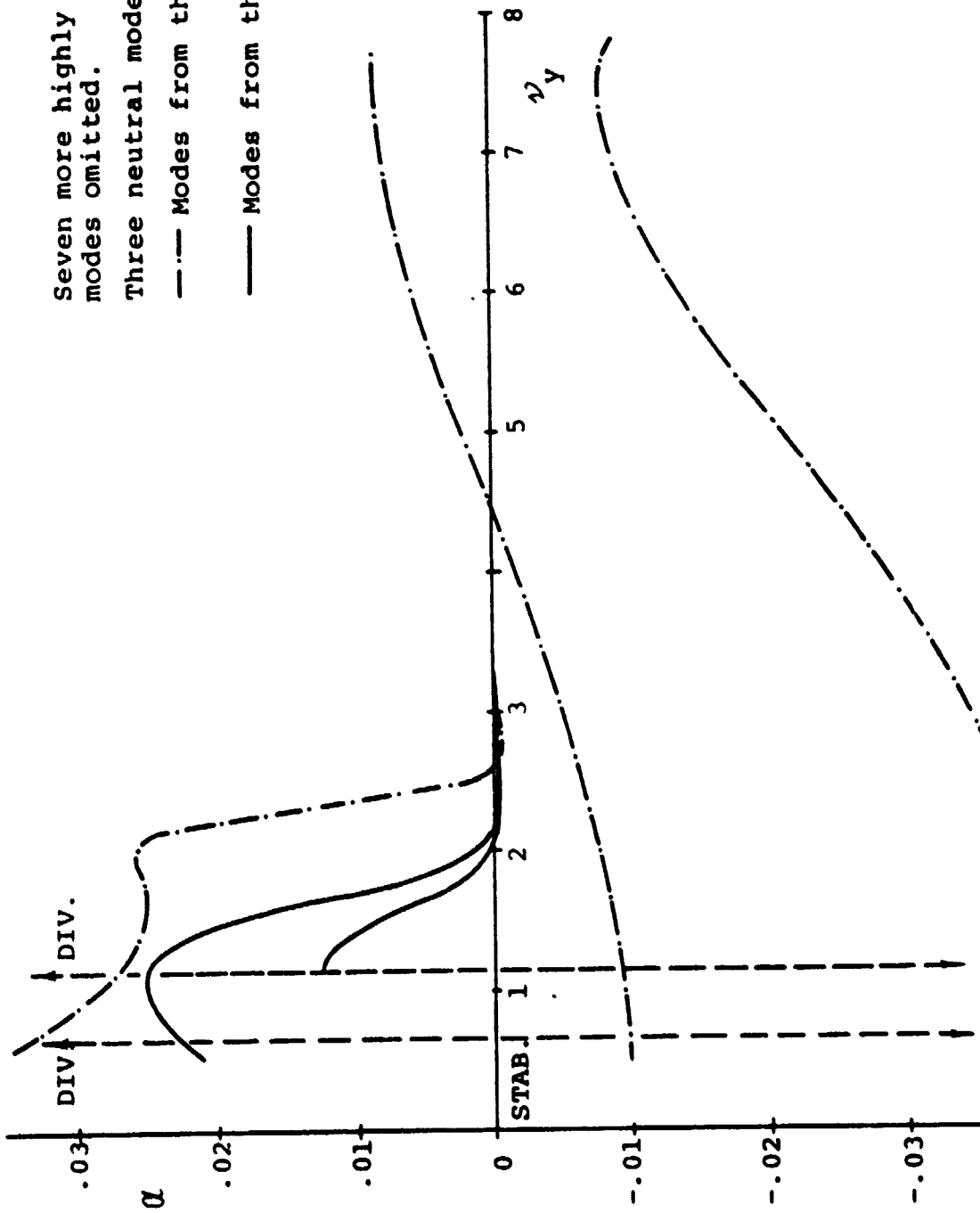


Figure 13.9 Damping of Various Modes vs ν_y for $\zeta_y = \zeta_p = 0.01$, $\nu_p = 7.41$



Seven more highly damped modes omitted.
 Three neutral modes lie on $\alpha = 0$.

--- Modes from the first set

— Modes from the second set

ORIGINAL PAGE IS OF POOR QUALITY

Figure 13.10 Damping of Various Modes vs ν_y for $\lambda = .25$, $\nu_p = 7.41$, $\zeta_y = \zeta_p = 0$

ORIGINAL PAGE IS
OF POOR QUALITY

Seven more highly damped
modes omitted.

Two neutral modes lie on $\alpha = 0$.

--- Modes from the first set

— Modes from the second set

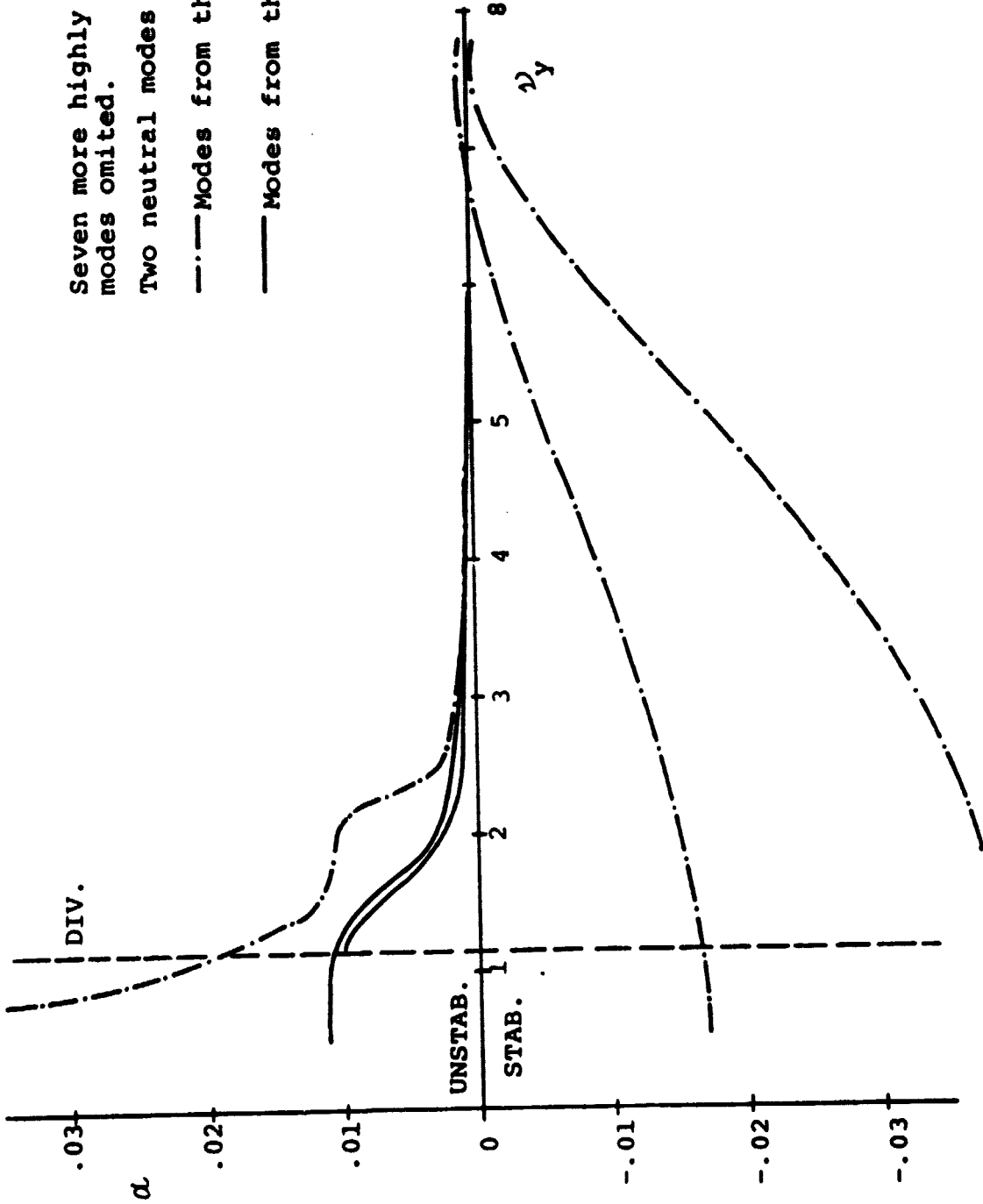


Figure 13.11 Damping of Various Modes vs ν_y for $\beta_p = -.15$, $\nu_p = 7.41$, $\zeta_y = \zeta_p = 0$

ORIGINAL PAGE IS
OF POOR QUALITY

ORIGINAL PAGE IS
OF POOR QUALITY

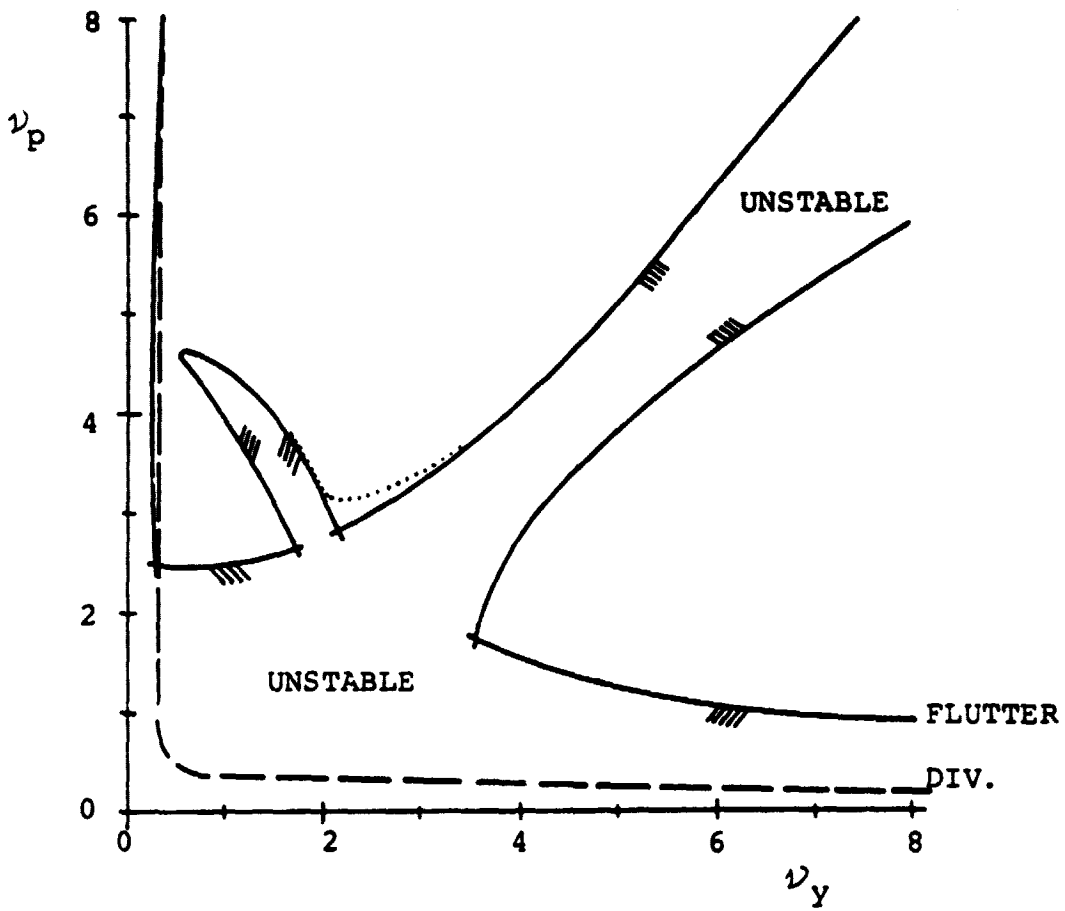
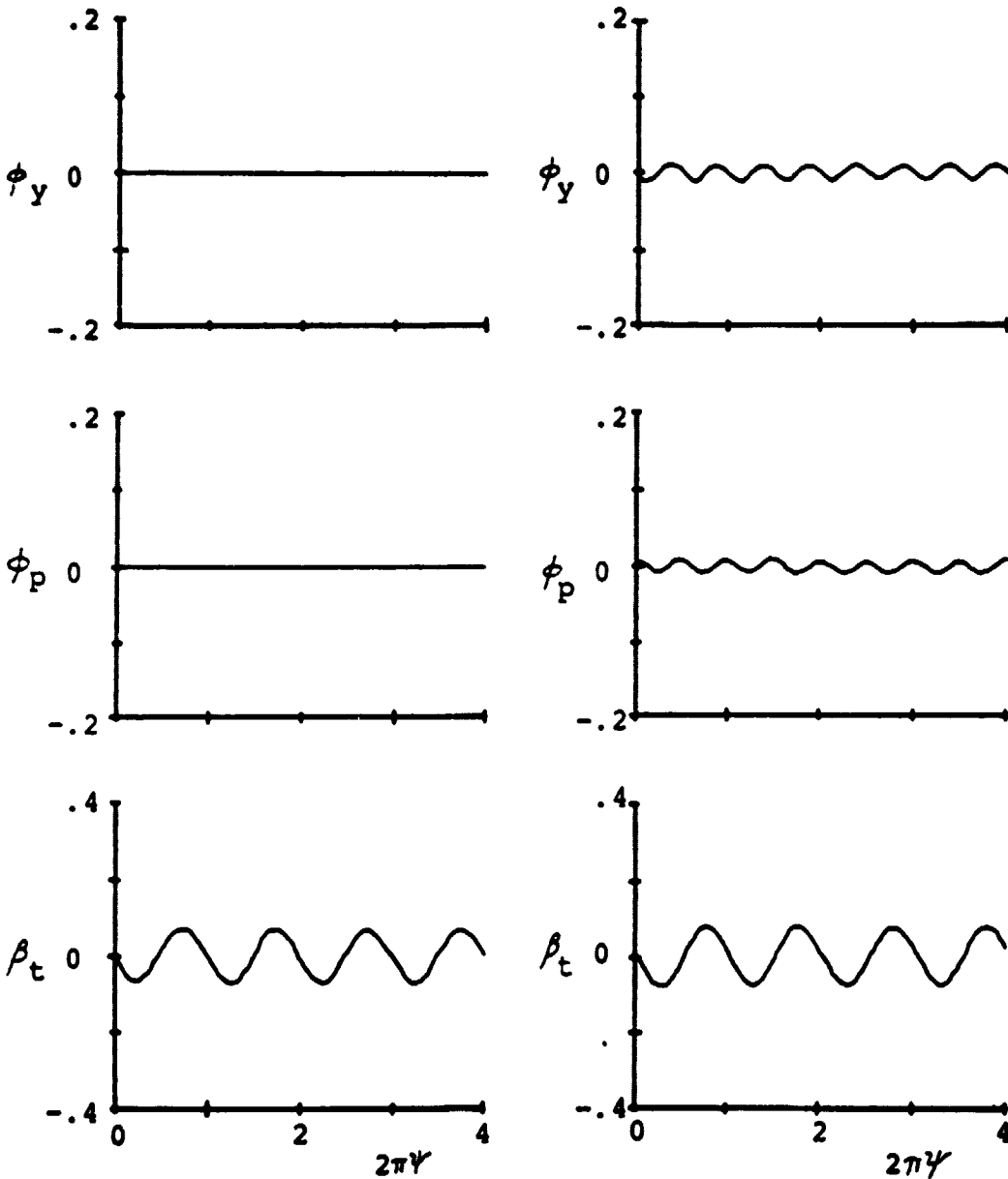


Figure 13.12 ν_y vs ν_p Stability Map for $\nu_t = 10, \zeta_y = \zeta_p = 0$

— $P = 2$ $P = 3$

ORIGINAL PAGE IS
OF POOR QUALITY



MOD-2 CASE, $\zeta_y = \zeta_p = .01$ $\nu_y = \nu_p = 2$, $\zeta_y = \zeta_p = .04$

Figure 13.13 Steady Response to Wind Shear, $\tau = .03$